The sources and sinks of thiols, reduced sulphur substances, and humic-like substances in hydrothermal waters

Thesis submitted in accordance with the requirements of the University of Liverpool for the degree of

Doctor in Philosophy

By

Gemma Portlock

March 2023

Faculty of Science and Engineering

School of Environmental Sciences

Department of Earth, Ocean and Ecological Sciences

Declaration of Authorship

I hereby declare that the research presented in this thesis titled 'The sources and sinks of reduced sulphur substances and humic-like compounds in hydrothermal waters' is a product of my own work. The material presented in this thesis has not been presented for any other degree or qualification.

Gemma Portlock

March 2023

Acknowledgment

My PhD has been one of the most challenging things I have ever done, but the experience has been invaluable. I would not have made it through if it wasn't for the incredible support that I have received. Firstly, I thank my supervisors, Pascal Salaün and Hannah Whitby. I am truly grateful for your support and encouragement during my PhD. I would also like to thank my former supervisor Alessandro Tagliabue.

Thank you to all my old and new friends for being there through the good and the tough times. Special mentions go to Ed Doherty and Jack Walker for helping me with R. Thank you to the members of the Stitch 'n' b*tch group. I have some wonderful memories with you all, and a shout out to Jessie Foest for teaching us how to knit. I want to thank Millie Goddard-Dwyer for being an ear to listen whenever I needed to talk about voltammetry or humic substances. Thank you to Alice Lowry for being an excellent gym buddy and a truly wonderful friend. I am thankful to have gone through my PhD with you. A special shout-out goes to Daniela König (you know why).

Finally, I would like to thank my parents for always being my biggest supporters and believing in me.

Dedicated to

Mary Cassells White

3rd April 1925 – 5th May 2022

Abstract

The Western Tropical South Pacific (WTSP) Ocean has some of the most active zones for submarine volcanic activity in the world. In particular, the Lau Basin has intense hydrothermal activity due to the fast convergence of the Tonga–Kermadec arc and the basins spreading centre. Within the Lau Basin are many shallow hydrothermal vents, these vents can be a source of metals. The fluids from these vents are directly released into the photic layer, which can be either beneficial or detrimental to the surface communities. Reduced sulphur substances (RSS), humics and sulphides have been shown to play essential roles in the cycling of trace metals.

Intercomparison of three electroanalytical methods used for the quantification of electroactive humic substances (eHS) found that in open ocean samples all three methods (eHS-Fe, eHS-Cu and eHS-Mo) appear to be sensitive to the same fraction of eHS. Comparison of two methods (eHS-Mo and eHS-Fe) across French GEOTRACES TONGA (shallow hydroThermal sOurces of trace elemeNts: potential impacts on biological productivity and the bioloGicAl carbon pump) cruise transect, showed discrepancies in the eHS concentrations. However, this transect was conducted in a highly dynamic region and is not representative of most oceanographic regions. Scanned stripping voltammetry (pseudopolarography) showed differences between marine humics and the river-derived SRFA standard.

Species-specific RSS (thioacetamide-like (TA-like), glutathione-like (GSH-like compounds) and electroactive humic substances (eHS) were quantified in the GEOTRACES TONGA transect. Concentrations of TA-like compounds (48 to 984 nM), GSH-like compounds (0.61 to 6.23 nM), and eHS (11.47 to 134 $\mu g.L^{-1}$ eq SRFA) were measured by cathodic stripping voltammetry (CSV). In the hydrothermal plume at PANAMAX, there were elevated concentrations of eHS, GSH-like and TA-like compounds. Sulphide was also present at PANAMAX. Elevated concentrations of TA-like compounds were found in the Melanesian waters. Cathodic pseudopolarography profiles of marine samples were used for the qualitative analysis of RSS and eHS.

The minicosm experiments were designed to understand the impact of hydrothermal fluids on surface communities in the WTSP. In these experiments, different volumes of hydrothermal fluids were mixed with surface water and the communities' response was monitored. Here we compare the concentration and speciation of humics, RSS and copper over the course of the experiment and assess if these are directly or indirectly produced by the mixing of hydrothermal fluids with surface waters. We show that the concentration of eHS, TA-like and GSH-like compounds increase with the addition of hydrothermal fluids. Cathodic pseudopolarography profiles of eHS found that the addition of hydrothermal fluids affected the nature of the eHS.

Publications and contribution

Included in thesis (In prep)

Portlock, G., Salaün, P., Dulaquais, G., Fourrier, P., Riso, R., Omanovic, D., Guieu, C., Bonnet, S., Whitby, H, Humic substances in the Western Tropical South Pacific: an intercomparison of electrochemical techniques. To be submitted to Marine Chemistry.

Portlock, G., Whitby, H., Tilliette, C., Bonnet, S., Guieu, G., Salaün, P, Distribution and behaviour of reduced sulphur substances and humic-like substances in the oligotrophic and hydrothermal waters of the Western South Tropical Pacific. To be submitted to Frontiers Research Topic 'Hydrothermal and submarine volcanic activity: Impacts on ocean chemistry and plankton dynamics'.

Portlock, G., Tilliette, C., Bonnet, S., Guieu, G., Gonzalez-Santana, D., Whitby, H., Salaün, P, The impact of shallow hydrothermal fluids on the production of reduced sulphur substances and humic-like substances. An incubation study. To be submitted to Frontiers Research Topic 'Hydrothermal and submarine volcanic activity: Impacts on ocean chemistry and plankton dynamics'.

Contributions to other journal articles

Tilliette, C., Gazeau, F., **Portlock, G**., Bonnet, S., Guigue, C., Leblond, N., Lory, C., Marie, D., Montanes, M., Pulido-, E., Sarthou, G., Tedetti, M., Vorrath, M., Whitby, H., Guieu, C., 2023. Influence of shallow hydrothermal fluids release on the functioning of phytoplankton communities. Front. Mar. Sci. (accepted).

Eikelboom, M., Wang, Y., **Portlock, G**., Gourain, A., Gardner, J., Bullen, J., Lewtas, P., Carriere, M., Alvarez, A., Kumar, A., O'Prey, S., Tölgyes, T., Omanović, D., Bhowmick, S., Weiss, D., Salaün, P., Voltammetric determination of inorganic arsenic in groundwaters from Mexico and India in near-neutral pH buffer solutions. Anal. Chim. Acta. (submitted).

Contents

Chapter 1

Introduction

1.1. Importance of hydrothermal vents in ocean chemistry

The earth's lithosphere comprises of seven major and many minor plates. These plates meet at plate boundaries. Over time, the plates move and collide, resulting in various geological features. Mid-ocean ridges occur along divergent boundaries. This is where two tectonic plates are moving away from each other (Lin et al., 1990). Arc/back-arc spreading areas occur along convergent boundaries. This is where two or more tectonic plates collide, and one slides underneath the other through a process known as subduction (Lin et al., 1990) which causes the formation of a trench and a ridge. During the splitting or subduction of the plates, magma from the earth's core moves to the surface or just below the seafloor. Seawater permeates through cracks and porous rocks in the seafloor. The heat from the magma induces chemical reactions in the seawater, which can remove oxygen, magnesium, sulphates, and other chemicals from the fluid. The fluids also become hotter and more acidic, which causes metals to leach out of the surrounding rocks/sediment. The fluids then rise to the surface through a fissure in the seafloor, forming hydrothermal vents (German and Seyfried, 2014) (Figure 1.1).

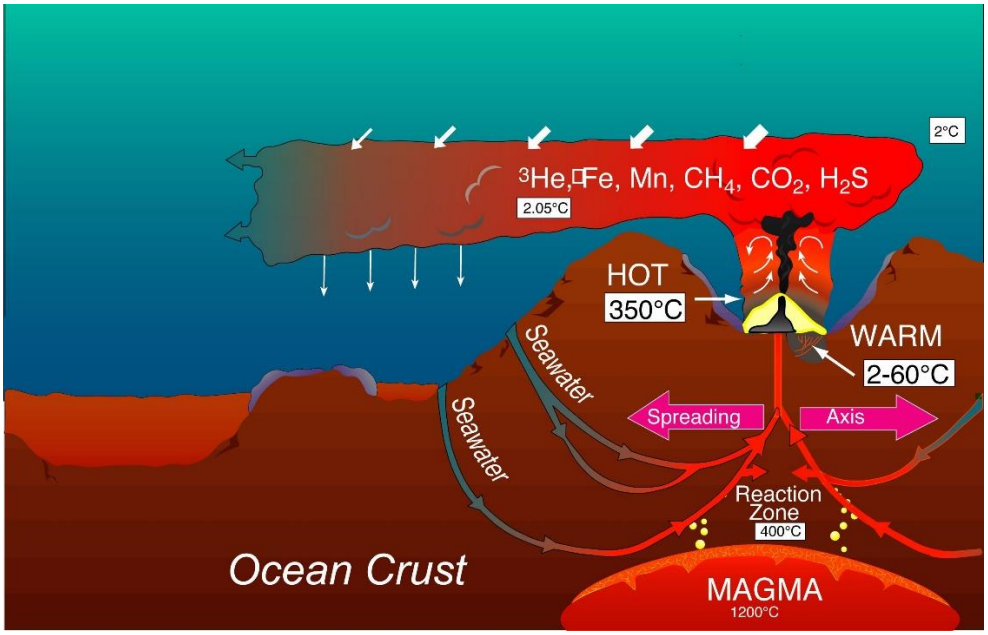

Figure 1.1. *Diagram of hydrothermal vent circulation, resulting in a hydrothermal plume. Figure 1 was obtained from the Schmidt Ocean Institute (Schmidt Ocean Institute, n.d.).*

The first observation of a hydrothermal vent was in 1977 at the Galápagos Rift (Ballard, 1977). Since then, increasing numbers of hydrothermal vents have been found worldwide (Beaulieu and Szafrański, 2020) (Figure 1.2). They have been of interest to scientists as they are a source of heat and chemicals (German and Seyfried, 2014). When hydrothermal fluids are released, they can be hot (>400 °C) (Foustoukos and Seyfried, 2007; Koschinsky et al., 2008; Zhang et al., 2017). The seawater around the vent is cool, and this causes the hydrothermal fluids to rise. The rising hydrothermal fluids are referred to as the buoyant plume. When the plume has cooled, it no longer rises and is then referred to as the neutrally buoyant or non-buoyant plume, which is still chemically different from the surrounding seawater. At this stage, the plume can be transported thousands of kilometres away from the vent (Fitzsimmons et al., 2017; Gartman and Findlay, 2020; Resing et al., 2015).

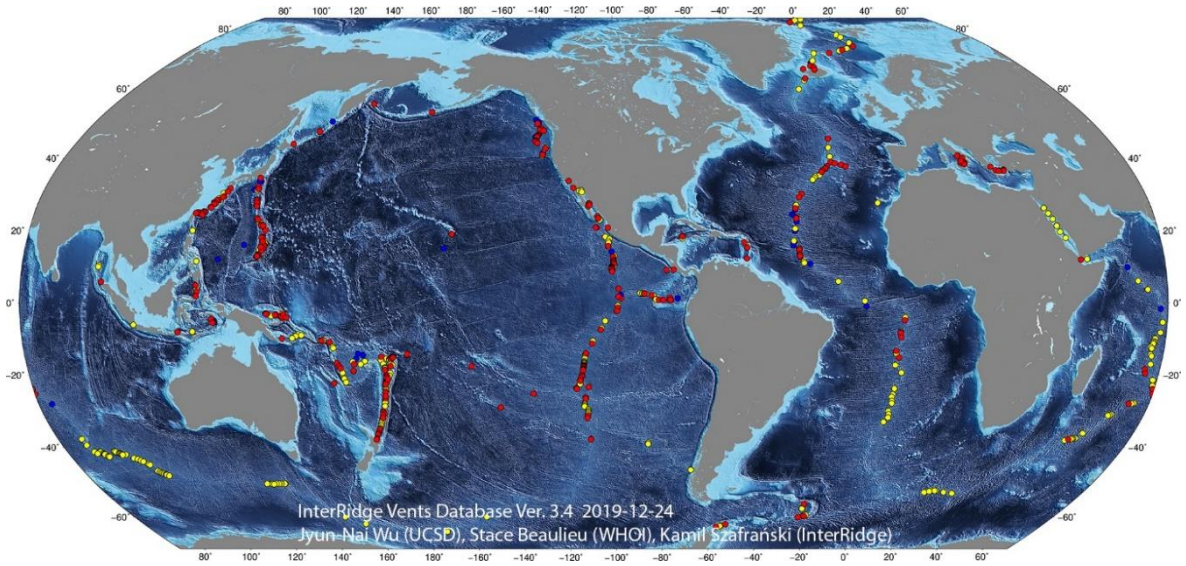

Figure 1.2. *Global map of submarine hydrothermal vent fields. This dataset was completed on 25 March 2020 and includes a total of 721 vent fields, with 666 confirmed to be active (red) or inferred active (yellow) and 55 inactive (blue). Figure obtained from (Beaulieu and Szafrański, 2020).*

Fluids released from hydrothermal vents are enriched with metals (Figure 1.3) (Kilinkhammer et al., 1977; Resing et al., 2015). In the hydrothermal plumes, chemical reactions can occur, which can result in the removal of metals by either precipitation or scavenging (Bruland et al., 2014; Feely et al., 1996; Gartman and Findlay, 2020), leaving trace amounts in seawater. Trace metals are important in marine environments as some are bio-essential nutrients for marine microbes (Aparicio-González et al., 2012; Lohan and Tagliabue, 2018). Therefore, understanding metal's input and removal process from hydrothermal vents is essential for understanding marine biogeochemical cycles. However, this can be tricky as the composition of metals in hydrothermal fluids can vary between different sites. Hydrothermal vent-fluid composition in arc/back-arc spreading areas is more diverse compared to in mid-ocean ridges, this is due to the subduction of the tectonic plate (Araoka et al., 2016; Ishibashi and Urabe, 1995; Wang et al., 2023). As it stands, no two vents have yet been found to have exactly the same composition (German and Seyfried, 2014).

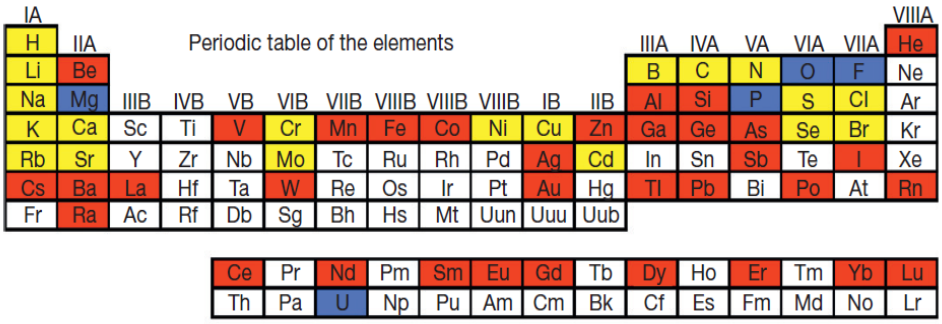

Figure 1.3. *Periodic table that shows which elements are enriched (red), and depleted (blue) in hydrothermal fluids. Some elements have shown to be both enriched and depleted (yellow) at different hydrothermal site. Figure obtained from (German and Seyfried, 2014).*

1.2. Hydrothermal vents in the Western Tropical South Pacific

The Western Tropical South Pacific (WTSP) is an oceanographic region that has some of the most extensive hydrothermal activity on the earth (Baker et al., 2019; German et al., 2006; Pelletier et al., 1998). The intense hydrothermal activity is due to the subduction of the Pacific plate under the Australian plate, creating the Tonga–Kermadec arc (Figure 1.4A). It is one of the fastest subduction zones in the world, but the convergence rate differs between the north and south of the arc. The northern part of the arc is converging at a faster rate (24 $cm.yr^{-1}$ (Bevis et al., 1995; Smith and Price, 2006)) than the south (7.2 $cm.yr^{-1}$ (Parson and Wright, 1996)). The Tonga–Kermadec arc is comprised of the Tonga–Kermadec ridge and trench. It is approximately 2550 km long and is located between New Zealand and Tonga (Smith and Price, 2006). It is the second deepest trench in the world (~10,800 m deep) (Britannica, 2018; NOAA, 2021). The arc is divided into two segments by the Louisville Seamount Chain (Figure 1.4A). The northern segment is named the Tonga Trench/Ridge, and the southern segment is called the Kermadec Trench/Ridge. West of the Tonga–Kermadec ridge are two back-arc basins, the Lau Basin and the Havre Trough (Karig, 1970a, 1970b).

The Lau Basin is a shallow basin located between the Tonga ridge and the Lau ridge, with a maximum depth of 3.4 km deep and an average depth of 2.25 km (Hawkins, 1995) (Figure 1.4B). It has been the

focus of research as it has intense hydrothermal activity due to the fast convergence of the Tonga–Kermadec arc and the spreading centre of the Lau Basin (Baker et al., 2019; Crawford et al., 2003; Zellmer and Taylor, 2001). The fluids released from hydrothermal vents in the Lau Basin are enriched in metals compared to other hydrothermal vents (Donval et al., 1991). In recent years, multiple research cruises have visited the Lau Basin to investigate this area (Guieu and Bonnet, 2019; Hannington and Kopp, 2018; Langmuir, 2004; Moutin, 2015; Resing, 2012, 2010, 2009, 2008; Rubin, 2017). From these cruises it has was found that the waters in the Lau Basin are phosphorus-rich and nitrogen-poor (Bonnet et al., 2018; Caffin et al., 2018) and there was high input of dissolved iron (dFe) from the hydrothermal activity (Guieu et al., 2018; Tilliette et al., 2022; Wang et al., 2022). The combination of these factors have led diazotrophs to bloom extensively and is likely why the Lau Basin is a hotspot for N_2 fixation (Bonnet et al., 2018, 2017).

The Lau Basin is characterised by both deep-water and shallow hydrothermal vents. Shallow hydrothermal vents are similar to deep hydrothermal vents with regards to fluid formation and inner structure, but they differ due to the depth, being <200 m deep (Zhang et al., 2020). Due to their shallow depth, the buoyant hydrothermal plumes is able to reach the surface waters (Zhang et al., 2020). The material produced from shallow hydrothermal plumes is believed to be fresher and more labile compared to deep mid ocean ridges vents (Hawkes et al., 2014). The influx of metals can have biogeochemical consequences on the surface communities. Even though shallow hydrothermal vents are more likely to have significant impact on primary production they have received less attention compared to deep hydrothermal vents in their role in ocean biogeochemistry (Guieu et al., 2018; Zhang et al., 2020).

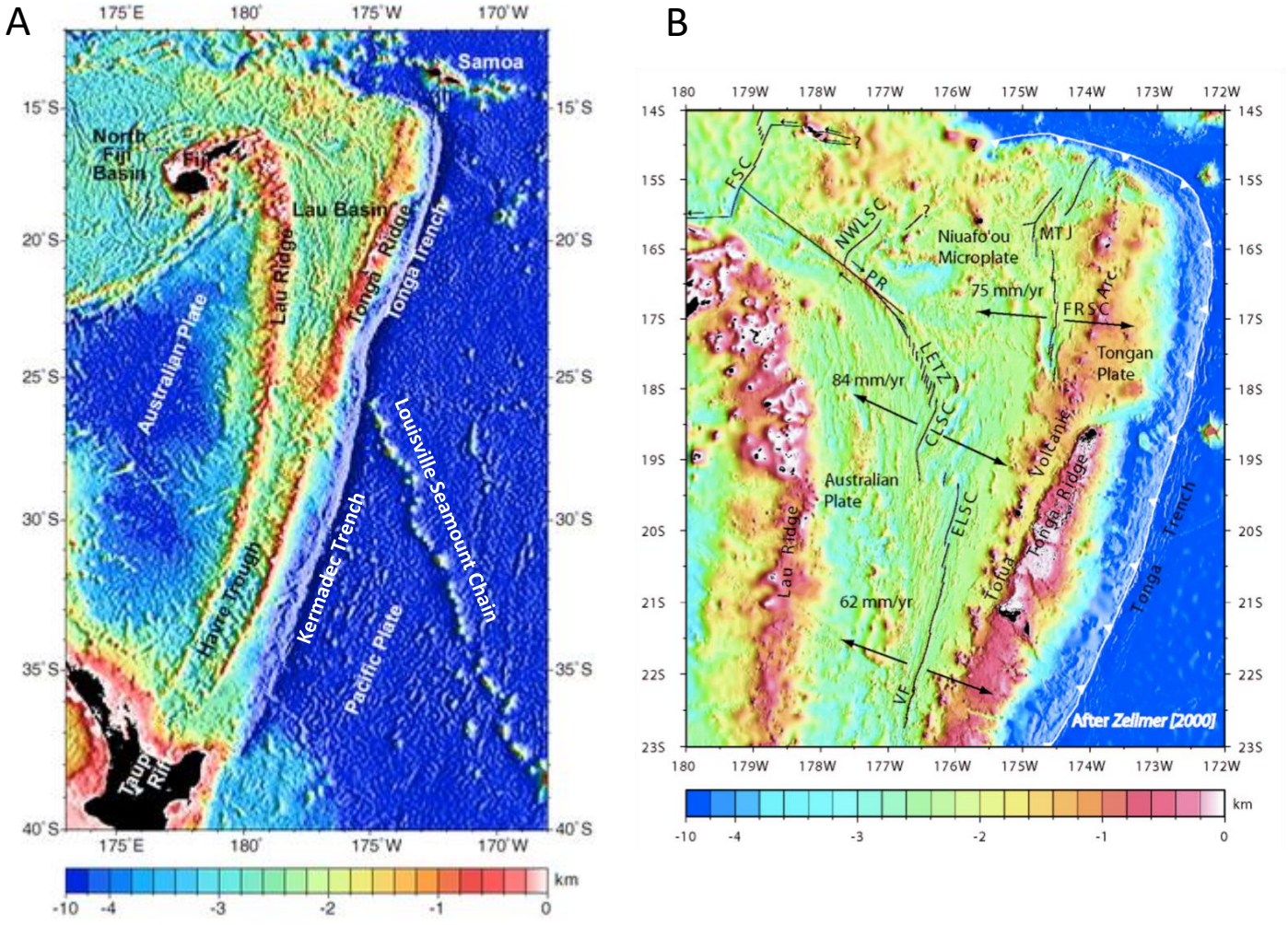

Figure 1.4. *(A) Bathymetric map Tonga–Kermadec arc. Colour gradient is the depth (km), islands are shown in black. Figure obtained from (Zellmer and Taylor, 2001). (B) Bathymetric map of the Lau Basin. Black lines show the spreading centre and the rate at which they are spreading. Arrows show the direction of the spreading. Figure obtained from (Reysenbach, 2015).*

1.3. Trace metal speciation

Metal speciation refers to the form in which the metal is present (Bartlett and Norwood, 2013). In marine environments, trace metal speciation is important as it can determine a metal's bioavailability or toxicity to marine microbes (Hirose, 2006). Iron (Fe) and Copper (Cu) are two trace metals that have been extensity researched due to their importance to marine microbes. Fe is one of the most crucial trace metals in marine environments. It is required by marine microbes for processes such as nitrate uptake, nitrogen fixation, photosynthesis and respiration (Geider and La Roche, 1994; Sutak et al.,

2020). Despite being one of the most abundant elements on the earth, seawater concentrations of dissolved Fe are low. This is because Fe is primarily present in the form Fe(III), which has a very low solubility in seawater at natural pH (Liu and Millero, 2002).

Cu can be both an essential micronutrient and a toxicant to marine microbes. It is involved in many metabolic processes, such as respiration and photosynthesis, and is important in the nitrogen cycle (Jacquot et al., 2014; Laporte et al., 2020; Lewis, 1991). However, not all Cu present in the ocean can be taken up by microbes. Its bioavailability is influenced by the Cu species present (Crecelius et al., 1982; Lewis, 1991; Manaban and Smith, 1973). Excess Cu in its free bioavailable form (Cu(II)) can act as a potent toxicant as it can hinder metabolic functions, such as inhibition of reproduction and oxidative damage to tissue macromolecules, including DNA, proteins and lipids (Ercal et al., 2002; Posacka et al., 2017; Xu et al., 2018).

A ligand is a molecule or ion that binds to a central metal atom forming a coordination complex, thus governing the speciation of trace metals. In marine waters, the percentage of metals bound with ligands can vary (Bruland, 1992, 1989), but >99% of Fe and Cu in seawater is bound to ligands (Buck et al., 2018, 2015; Gerringa et al., 2015; Jacquot and Moffett, 2015). Ligands are vital as they can help stabilise trace metals in the dissolved phase as well govern trace metal bioavailability. When bound to ligands, Fe solubility increases, resulting in higher concentrations of dissolved Fe in seawater than what would be expected due to its low solubility in marine waters (Buck and Bruland, 2007; Kuma et al., 1998; Millero, 1998). When Cu is bound to ligands, it can prevent the formation of Cu(II), thus reducing toxicity (Moffett et al., 2012; Oldham et al., 2014). Therefore, understanding the distribution of ligands is crucial to understand the biogeochemical cycles and bioavailability of trace metals.

1.4. Sulphides

Sulphide is an inorganic anion of sulphur that mainly occurs in marine environments in the form of hydrogen sulphide (H_2S), bisulphide (HS^-) and sulphide (S^{2-}) (Millero, 1986). In marine environments, they can be present across a wide range of concentrations (pM to µM) (Cotte et al., 2018; He et al., 2002; Hsu-kim et al., 2008; Luther and Tsamakis, 1989). They mainly occur in anoxic marine environments (Al-Farawati, 1999; Baciu et al., 2015), because they are unstable in oxygenated aquatic systems due to their rapid oxidation in the presence of oxygen (O_2), hydrogen peroxide (H_2O_2) and iodate (IO_3^-), (Jøgensen, 1978) hence they were not regarded as an environmentally significant species. The predominant species of sulphide is dependent on environmental conditions. In seawater at pH 8 the dominant species of sulphide is HS^-, whereas at pH values below 7, HS^- is converted to H_2S (pKa, 6.98) (Al-zuhair et al., 2008; Goldhaber and Kaplan, 1975; Olson and Straub, 2015). In the presence of dissolved oxygen, sulphur is present in the form of SO_4^{2-} (Cline and Richards, 1969).

Sulphides can enter marine environments when organism breakdown (Treude et al., 2009), as a by-product from bacterial processes (Al-Farawati and van den Berg, 1997; Colon et al., 2007; Lawrence et al., 2002), aerosols (Elliott et al., 1987; Nault et al., 2021; Radford-Knęry and Cutter, 1994), sediments (Jorgensen and Fenchel, 1974), and hydrothermal vents (Dias et al., 2010; Olson, 2019). Hydrothermal vents can release large quantities of sulphides (Hsu-kim et al., 2008; Shaw et al., 2021; Yücel et al., 2011). They have a high affinity for metal ions and form stable complexes (Dyrssen, 1988; Luther W. et al., 2001; Plavšić et al., 2011; Theberge et al., 1997; Yücel et al., 2011; Zhang and Millero, 1994), for example Cu and Fe (Dyrssen, 1988; Luther W. et al., 2001; Plavšić et al., 2011; Theberge et al., 1997; Yücel et al., 2011). When sulphides are released from hydrothermal vents, they react with the metals in the fluids. These complexes can stay present in oxic water for months (Dyrssen, 1988), but can also precipitate, which can lead to the formation of massive sulphide deposits at the seafloor (Findlay et al., 2019). The Lau Basin has some of the largest sulphide deposits (Hannington et al., 2011).

1.5. Thiols and other reduced sulphur substances

Thiols are organic sulphur compounds that contain a –SH functional group and they tend to be of low weight <1000 Daltons (Da) (Tang et al., 2001) (Figure 1.5). In addition to having a –SH functional group, thiols can also be abundant in nitrogen and oxygen functionality (van Laer et al., 2013). Thiols are produced by marine microbes (Kawakami et al., 2006; Leal et al., 1999), they are strong nucleophiles and therefore are involved in many biochemical processes (Lopachin and Gavin, 2017). Thiols are part a wider group of reduced sulphur substances (RSS). RSS are a group of compounds that possess a reduced sulphur function group. This group includes compounds such as thioureas and thioamides (Figure 1.5).

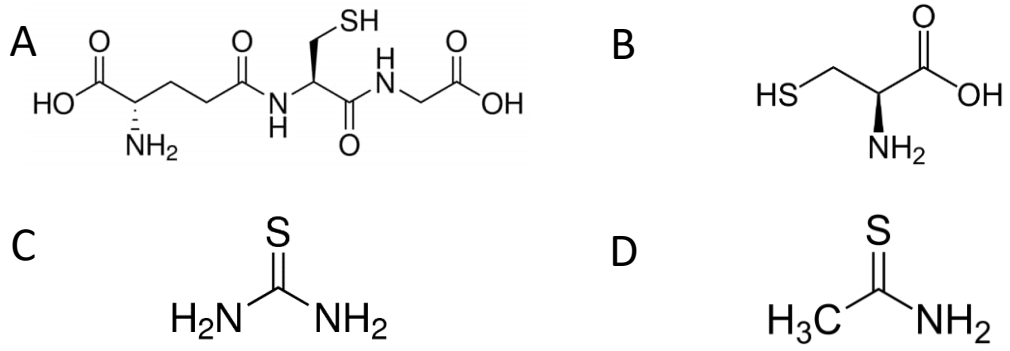

Figure 1.5. *Chemical structures of reduced sulphur substances. Glutathione (A) and cysteine (B) are thiol compounds. Thiourea (C) and thioacetamide (D) are thioamide compounds.*

Thiols and RSS act as an antioxidant against reactive oxygen species (ROS) (Pandey et al., 2013; Ulricha and Jakoba, 2019). ROS are highly reactive oxygen species that include radicals (e.g. hydroxyl radicals (OH·)) and nonradicals (e.g., hydrogen peroxide (H_2O_2)) (Madkour, 2020a; Morris et al., 2022; Schieber and Chandel, 2014). ROS are damaging to marine microbes as they can cause oxidative stress, which can lead to cell death (Madkour, 2020b). Thiols/RSS are able to remove ROS by accepting their unpaired electron (McLeay et al., 2017; Morelli and Scarano, 2004)(Equation 1).

$$R\text{-}SH + [O] \rightarrow R\text{-}SOH + H_2O \qquad \text{Equation 1.}$$

ROS can be induced in multiple different ways in the marine environment. Aerobic organisms produce ROS as a byproduct of photosynthesis, photorespiration and oxidative phosphorylation (Apel and Hirt, 2004; Diaz and Plummer, 2018; Mullineaux et al., 2018). ROS can also be produced during exposure to metals (Briffa et al., 2020).

As well as acting as an antioxidant against ROS, thiols and RSS can complex with metals, which can either inhibit metal toxicity or help with uptake (Dupont and Ahner, 2005; Huang et al., 2018; Mironov & Tsvelodub, 1996; Navarrete et al., 2019; Rea et al., 2004; Steffens, 1990). Due to their abundance in marine environments, thiols are one of the most extensively studied RSS, with particular interest with their role as a metal ligand. In metal stressed environments, marine microbes have been found to produce increased levels of thiols (Bjørklund et al., 2019; Kumar et al., 2021; Pál et al., 2018), in order to reduce metal toxicity. Leal et al., (1998) showed that thiols are able to complex with Cu^{+} to stabilise it this oxidation state, therefore preventing the formation of Cu(II) (Leal and van den Berg, 1998). In environments of low trace metal concentrations, microbes have been found to produce thiols to help with the uptake of metals. For example, in low nickel (Ni) environments, *Prorocentrum donghaiense* Lu have been found to exude thiols to help with the uptake of Ni (Huang et al., 2018).

Several types of RSS have been detected in marine waters including glutathione (GSH), cysteine (Cys), γ-glutamylcysteine (γ-Glu-Cys), cysteinyl- arginine (Arg–Cys), cysteinyl- glutamine (Gln–Cys) and thiourea-like (Dupont et al., 2006; Dupont and Ahner, 2005; Tang et al., 2005; Whitby et al., 2018). Thioamides are not known to be present in marine environments, but they have been observed in estuarine and river waters (Marie et al., 2017, 2015; Superville et al., 2013). The concentration and distribution of RSS can vary throughout the ocean. Thiol compounds are the most common type of RSS found in marine environments. The common thiols found are Cys, γ-Glu-Cys and GSH (Dupont et al., 2006; Gao and Guéguen, 2018; Hu et al., 2006; Swarr et al., 2016; Tang et al., 2000). While some thiols like GSH are found in almost all natural waters, other thiols have only been found in specific areas, which could be because their concentration is too low for current detection methods or that

they are absent. It is thought that the reason for the variety of thiols that are present in marine systems could be due to the different microbes being exposed to different metals and local environmental factors. Ahner et al., (2002) exposed several species of eukaryotic phytoplankton to Cd and Cu. When exposed to these elements, some phytoplankton species produced γ-Glu-Cys and Cys (Ahner et al., 2002). Leal et al., 1999, exposed *Emiliania huxleyi* to Cu. In their study, they found that the RSS glutathione and a thioacetamide-like compound were produced. Similarly, Dupont et al., (2005) found that when *Emiliania huxleyi* were exposed to Cu the primary thiols that were released Arg–Cys, Gln–Cys, and Cys. However, in the presence of Cd, *Emiliania huxleyi* released these thiols and GSH. When exposed to high zinc (Zn) concentrations, the primary thiol that was synthesised was γ-Glu-Cys (Dupont and Ahner, 2005). HPLC analysis carried out by Tang et al., (2000) showed the presence of unidentified thiols in marine settings (Tang et al., 2000).

1.6. Humic substances

Humic substances (HS) originate from the decomposition of organic matter and are among the most widely distributed organic materials on the earth. They are an ill-defined group of refractory heterogeneous organic compounds with varying molecular weight, polarity and composition. In marine waters, HS can account for approximately 50% of the dissolved organic carbon (DOC) (Fourrier et al., 2022; Zigah et al., 2017). They can enter marine systems through microbial production, decay, photooxidation of triglycerides and fatty acids (Ferrari et al., 1996; Kieber et al., 1997; Lorenzo et al., 2007; Sarma et al., 2018; Whitby et al., 2020b), aerosols (Krivácsy et al., 2008), land/rivers (Krachler et al., 2015; Muller, 2018), deep-sea sediment (Dulaquais et al., 2018; Shigemitsu et al., 2021) and hydrothermal vents (Yang et al., 2012). In an area like the Lau Basin, hydrothermal vents may contribute a significant portion to the HS pool. Hydrothermal vents can be a source of HS either from active production from autochthonous microbial communities (Sarma et al., 2018) or through the alteration of dissolved organic matter (DOM) (Shao et al., 2022). As the Lau Basin also contain many

shallow hydrothermal vents, the metals released from these vents may impact the biology and therefore affect the production of HS.

HS can be subdivided into two fractions: humic acids (HA), which precipitate below pH 2 and fulvic acids (FA), which are soluble at all pH (Aiken et al., 1985). HA are larger molecules that FA and molecular weights approximately range from 1000 to greater than 10,000 Daltons (Da), whereas FA are smaller, ranging from 500 to 2000 Da Averett et al., 1994; Qin et al., 2016; Thurman et al., 1982). HA tend to be more aromatic than FA (Sharma and Anthal, 2007) while FA have a higher oxygen content compared to HA (Ritchie and Michael Perdue, 2003; Schellekens et al., 2017). Marine HS tend to be aliphatic, have few or no aromatic protons and are carboxyl rich (Esteves et al., 2009; Harvey et al., 1983; Hertkorn et al., 2006).

HS act as ligands for a wide range of trace metals (Mantoura et al., 1978), including Fe and Cu, forming relatively strong complexes (Muller and Batchelli, 2013; Yang and van den Berg, 2009). HS can be the dominant ligand for Cu in coastal waters (Muller and Batchelli, 2013). The conditional stability constants are a measure of how tightly a ligand binds to a metal ion (Vraspir & Butler, 2009). For Cu-HS complexes ($\log K_{CuLi,Cu(II)}$) the conditional stability constants are reported to range from 10 to 12 (Kogut and Voelker, 2001; Whitby and van den Berg, 2015) and overlap with thiols, although the latter demonstrate a wider range and stronger Cu-complexes ($\log K_{CuLi,Cu(II)}$ range from 11 to 16) (Leal and van den Berg, 1998; Walsh and Ahner, 2013; Whitby et al., 2017).

For Fe, HS are one of the most important ligands (Hassler et al., 2017; Laglera and van den Berg, 2009), helping to keep Fe in a dissolved form. HS can account for up to 80% of Fe-binding ligands but this can vary depending on the region (Hassler et al., 2020; Laglera et al., 2019; Slagter et al., 2019; Whitby et al., 2020a). HS have a variety of different moieties that trace metals could bind to, but it has been suggested that carboxylic and phenolic groups are the main functional groups responsible for complexing metals (Aeschbacher et al., 2012; Fourrier et al., 2022; Heerah and Reader, 2022).

Fe, Cu, Zn, cobalt (Co) and aluminium (Al) have been found to bind to HS through the same functional group (Yang and van den Berg 2009), causing competition between those metals. Cu can actively compete with Fe and displace it when it is bound to HS (Abualhaija et al., 2015). This shows that the organic speciation of a metal is not only dependent on its concentration and the concentration of the ligand(s) involved in its complexation, but it is also on the concentration of competing metals, that are often unknown. The origin and age of HS can affect its ability to bind with metals. A study in the Mediterranean suggested that HS can remain in mesopelagic waters for ~18 years (Dulaquais et al., 2018). During this, time HS evolve and change through processes like remineralization. This increases humic aromaticity and the density of binding sites (Williford et al., 2021) which can affect metal binding capacity. This metal binding capacity allows us to estimate how much of the metal could be bound to HS. For Fe, increased aromaticity and Fe-binding capacity appear positively related (Kikuchi et al., 2017). Currently, we do not know how hydrothermal environments affect HS and their role in metal speciation.

1.7. Aim and structure of thesis

The Lau Basin has some of the most intense hydrothermal activity in the world and hosts both deep- and shallow-water hydrothermal vents. Shallow vents have received less attention than deep hydrothermal vents, but they are likely to have a significant impact on primary production. The release of various metals, metal-complexants and of fresher and more labile organic material could be either beneficial or detrimental to surface communities. Understanding the distribution of metal-binding ligands in this region is important because they control trace metal bioavailability. In this thesis, I aim to assess the role of shallow hydrothermal vents in the supply and cycling of RSS, sulphide and humic substances, which have been shown to play important roles in the cycling of key trace metals, notably Cu and Fe.

This thesis has three specific aims that are addressed in chapters 2 to 4, as outlined below.

1. Humic substances in the Western Tropical South Pacific: an intercomparison of electrochemical techniques. (Chapter 2)

This chapter aims to compare the three published cathodic stripping voltammetry (CSV) methods for the quantification of electroactive humic concentrations (eHS). These are the Mo method (Pernet-Coudrier et al., 2013), the Cu method (Whitby and van den Berg, 2015) and the Fe method (Laglera et al., 2007; Sukekava et al., 2018). This chapter aims to see if the separate methods are sensitive to the same fraction of HS in a dynamic region including hydrothermally-influenced waters, where HS composition could be distinct. In addition, scanned stripping voltammetry (pseudopolarography), was used to compare pseudopolarograms of marine humics to the commonly-used terrestrial standard, to see if the standard was representative of the humics within the different sample types.

2. Distribution and behaviour of RSS and humic-like substances in the oligotrophic and hydrothermal waters of the Western South Tropical Pacific. (Chapter 3)

The TONGA cruise took place in the Western South Tropical Pacific Ocean. The cruise aimed to investigate two active shallow (< 500 m) hydrothermal sites. I investigated the distribution of eHS and two different types of RSS, glutathione-like (GSH-like) and thioacetamide-like (TA-like)) in the hydrothermally-influenced Lau Basin, Melanesian Basin and the oligotrophic South Pacific Gyre. Pseudopolarography of RSS and eHS (surface and deep) were performed to see if there were differences between sites and depths compared to standards and to determine if sulphide was present.

3. The impact of shallow hydrothermal fluids on the production of RSS-like compounds and humic-like substances. An incubation study (Chapter 4)

Two incubation studies were carried out during the TONGA 2019 cruise in order to understand the impact of shallow hydrothermal venting on the plankton communities and biogeochemical functioning. In these experiments, surface water was mixed with water of hydrothermal origin in different ratios. I assess if shallow hydrothermal vents can be an indirect source of RSS and humic substances. Cathodic pseudopolarography was used to see if hydrothermal fluids influenced the humic and material produced and degraded by microbial communities. I also compared Cu pseudopolarograms with/without hydrothermal fluids and at the start/end of the minicosms.

Annex - Voltammetric detection and speciation of RSS, sulphide and copper in seawater

The annex at the end of this thesis provides the reader with background information about the electrochemical behaviour of RSS and sulphides present in marine waters when detected using a mercury electrode, as well as information about the electrochemical behaviour of copper when using a gold electrode. This annex also provides background information/theory about the technique stripping scanned voltammetry (pseudopolarography).

1.8. References

Abualhaija, M.M., Whitby, H., van den Berg, C.M.G., 2015. Competition between copper and iron for humic ligands in estuarine waters. Mar. Chem. 172, 46–56. https://doi.org/10.1016/J.MARCHEM.2015.03.010

Aeschbacher, M., Graf, C., Schwarzenbach, R.P., Sander, M., 2012. Antioxidant properties of humic substances. Environ. Sci. Technol. 46, 4916–4925. https://doi.org/10.1021/es300039h

Ahner, B.A., Wei, L., Oleson, J.R., Ogura, N., 2002. Glutathione and other low molecular weight thiols in marine phytoplankton under metal stress. Mar. Ecol. Prog. Ser. 232, 93–103. https://doi.org/10.3354/meps232093

Aiken, G.R., McKnight, D.M., Wershaw, R.L., MacCarthy, P., 1985. An introduction to humic substances in soil, sediment, and water. Humic Subst. Soil, Sediment, Water Geochemistry, Isol. Charact. 1–9.

Al-Farawati, R., van den Berg, C.M.G., 1997. The determination of sulfide in seawater by flow-analysis with voltammetric detection. Mar. Chem. 57, 277–286. https://doi.org/10.1016/S0304-

4203(97)00014-5

Al-Farawati, R.C.M.G. van den B., 1999. Metal-sulfide complexation in seawater. Mar. Chem. 63, 331–352. https://doi.org/10.1016/S0304-4203(98)00056-5

Al-zuhair, S., El-naas, M.H., Al-hassani, H., 2008. Sulfate inhibition effect on sulfate reducing bacteria. J. Biochem. Technol. 1, 39–44.

Aparicio-González, A., Duarte, C.M., Tovar-Sánchez, A., 2012. Trace metals in deep ocean waters: A review. J. Mar. Syst. 100–101, 26–33. https://doi.org/10.1016/j.jmarsys.2012.03.008

Apel, K., Hirt, H., 2004. REACTIVE OXYGEN SPECIES: Metabolism, Oxidative Stress, and Signal Transduction. Annu. Rev. Plant Biol. 55, 373–399. https://doi.org/10.1146/annurev.arplant.55.031903.141701

Araoka, D., Nishio, Y., Gamo, T., Yamaoka, K., Kawahata, H., 2016. Lithium isotopic systematics of submarine vent fluids from arcand back-arc hydrothermal systems in the western Pacific. Geochemistry, Geophys. Geosystems 17, 3835–3853. https://doi.org/10.1002/2016GC006355.Received

Baciu, A., Ardelean, M., Pop, A., Pode, R., Manea, F., 2015. Simultaneous voltammetric/amperometric determination of sulfide and nitrite in water at BDD electrode. Sensors (Switzerland) 15, 14526–14538. https://doi.org/10.3390/s150614526

Baker, E.T., Walker, S.L., Massoth, G.J., Resing, J.A., 2019. The NE Lau Basin: Widespread and abundant hydrothermal venting in the back-arc region behind a superfast subduction zone. Front. Mar. Sci. 6, 1–15. https://doi.org/10.3389/fmars.2019.00382

Ballard, R.D., 1977. The discovery of hydrothermal vents. Oceanus 20. 3.

Bartlett, A.J., Norwood, W., 2013. Encyclopedia of Aquatic Ecotoxicology, Encyclopedia of Aquatic Ecotoxicology. https://doi.org/10.1007/978-94-007-5704-2

Beaulieu, S.E., Szafrański, K.M., 2020. InterRidge Global Database of Active Submarine Hydrothermal Vent Fields Version 3.4. [WWW Document]. PANGAEA. URL https://vents-data.interridge.org/

Bevis, M., Taylort, F.W., Schutzt, B.E., Recy, J., L, B., Helu, S., Singh, R., Kendrick, E., Stowentt, J., Taylor, B., 1995. Geodetic observations of very rapid convergence and back-arc extension at the Tonga arc 249–251.

Bjørklund, G., Crisponi, G., Nurchi, V.M., Cappai, R., Djordjevic, A.B., Aaseth, J., 2019. A review on coordination properties of thiol-containing chelating agents towards mercury, cadmium, and lead. Molecules 24, 1–32. https://doi.org/10.3390/molecules24183247

Bonnet, S., Caffin, M., Berthelot, H., Grosso, O., Benavides, M., Helias-Nunige, S., Guieu, C., Stenegren, M., Foster, R.A., 2018. In-depth characterization of diazotroph activity across the western tropical South Pacific hotspot of N2 fixation (OUTPACE cruise). Biogeosciences 15, 4215–4232. https://doi.org/10.5194/bg-15-4215-2018

Bonnet, S., Caffin, M., Berthelot, H., Moutin, T., 2017. Hot spot of N2 fixation in the western tropical South Pacific pleads for a spatial decoupling between N2 fixation and denitrification. Proc. Natl. Acad. Sci. U. S. A. 114, E2800–E2801. https://doi.org/10.1073/pnas.1619514114

Briffa, J., Sinagra, E., Blundell, R., 2020. Heavy metal pollution in the environment and their toxicological effects on humans. Heliyon 6, e04691. https://doi.org/10.1016/j.heliyon.2020.e04691

Britannica, 2018. Tonga Trench [WWW Document]. Encycl. Br. URL

https://www.britannica.com/place/Tonga-Trench

Bruland, K.W., 1992. Complexation of cadmium by natural organic ligands in the central North Pacific. Limnol. Oceanogr. 37, 1008–1017. https://doi.org/10.4319/lo.1992.37.5.1008

Bruland, K.W., 1989. Complexation of zinc by by natural organic ligands in the central North Pacific. Limnol. Oceanogr. 34, 269–285. https://doi.org/10.4319/lo.1992.37.5.1008

Bruland, K.W., Middag, R., Lohan, M.C., 2014. Controls of Trace Metals in Seawater, in: The Oceans and Marine Geochemistry. Elsevier Ltd., pp. 19–51. https://doi.org/10.1016/B978-0-08-095975-7.00602-1

Buck, K.N., Bruland, K.W., 2007. The physicochemical speciation of dissolved iron in the Bering Sea, Alaska. Limnol. Oceanogr. 52, 1800–1808. https://doi.org/10.4319/lo.2007.52.5.1800

Buck, K.N., Sedwick, P.N., Sohst, B., Carlson, ~, 2018. Organic complexation of iron in the eastern tropical South Pacific: Results from US GEOTRACES Eastern Pacific Zonal Transect (GEOTRACES cruise GP16). Mar. Chem. 201, 229–241. https://doi.org/10.1016/j.marchem.2017.11.007

Buck, K.N., Sohst, B., Sedwick, P.N., 2015. The organic complexation of dissolved iron along the U.S. GEOTRACES (GA03) North Atlantic Section. Deep. Res. Part II Top. Stud. Oceanogr. 116, 152–165. https://doi.org/10.1016/j.dsr2.2014.11.016

Caffin, M., Moutin, T., Ann Foster, R., Bouruet-Aubertot, P., Michelangelo Doglioli, A., Berthelot, H., Guieu, C., Grosso, O., Helias-Nunige, S., Leblond, N., Gimenez, A., Alexandra Petrenko, A., De Verneil, A., Bonnet, S., 2018. N2 fixation as a dominant new N source in the western tropical South Pacific Ocean (OUTPACE cruise). Biogeosciences 15, 2565–2585. https://doi.org/10.5194/bg-15-2565-2018

Cline, J.D., Richards, F.A., 1969. Oxygenation of hydrogen sulfide in seawater at constant salinity, temperature, and pH. Environ. Sci. Technol. 3, 838–843. https://doi.org/10.1021/es60032a004

Colon, M., Iglesias, M., Hidalgo, M., 2007. Development of a new method for sulfide determination by vapor generator-inductively coupled plasma-mass spectrometry. Spectrochim. Acta - Part B At. Spectrosc. 62, 470–475. https://doi.org/10.1016/j.sab.2007.04.004

Cotte, L., Omanović, D., Waeles, M., Laës, A., Cathalot, C., Sarradin, P.M., Riso, R.D., 2018. On the nature of dissolved copper ligands in the early buoyant plume of hydrothermal vents. Environ. Chem. 15, 58–73. https://doi.org/10.1071/EN17150

Crawford, W.C., Hildebrand, J.A., Dorman, L.M., Webb, S.C., 2003. Tonga Ridge and Lau Basin crustal structure from seismic refraction data Tonga Ridge and Lau Basin crustal structure from seismic refraction data. J. Geophys. Res. Atmos. 108. https://doi.org/10.1029/2001JB001435

Crecelius, E.A., Hardy, J.T., Gibson, C.I., Schmidt, R.L., Apts, C.W., Gurtisen, J.M., Joyce, S.P., 1982. Copper bioavailability to marine bivalves and shrimp: Relationship to cupric ion activity. Mar. Environ. Res. 6, 13–26. https://doi.org/10.1016/0141-1136(82)90004-6

Dias, D., do Nascimento, P.C., Jost, C.L., Bohrer, D., de Carvalho, L.M., Koschinsky, A., 2010. Voltammetric determination of low-molecular-weight sulfur compounds in hydrothermal vent fluids-studies with hydrogen sulfide, methanethiol, ethanethiol and propanethiol. Electroanalysis 22, 1066–1071. https://doi.org/10.1002/elan.200900472

Diaz, J.M., Plummer, S., 2018. Production of extracellular reactive oxygen species by phytoplankton: past and future directions. J. Plankton Res. 40, 655–666. https://doi.org/10.1093/plankt/fby039

Donval, J.P., Erzinger, J., Foucher, J.P., 1991. Hydrothermal activity and metallogenesis in the Lau back-arc basin. Nature 349, 778–781. https://doi.org/10.1038/349778a0

Dulaquais, G., Waeles, M., Gerringa, L.J.A., Middag, R., Rijkenberg, M.J.A., Riso, R., 2018. The Biogeochemistry of Electroactive Humic Substances and Its Connection to Iron Chemistry in the North East Atlantic and the Western Mediterranean Sea. J. Geophys. Res. Ocean. 123, 5481–5499. https://doi.org/10.1029/2018JC014211

Dupont, C.L., Ahner, B.A., 2005. Effects of copper, cadmium, and zinc on the production and exudation of thiols by Emiliania huxleyi. Limnol. Oceanogr. 50, 508–515. https://doi.org/10.4319/lo.2005.50.2.0508

Dupont, C.L., Moffett, J.W., Bidigare, R.R., Ahner, B.A., 2006. Distributions of dissolved and particulate biogenic thiols in the subartic Pacific Ocean. Deep. Res. Part I Oceanogr. Res. Pap. 53, 1961–1974. https://doi.org/10.1016/j.dsr.2006.09.003

Dyrssen, D., 1988. Sulfide complexation in surface seawater. Mar. Chem. 24, 143–153. https://doi.org/10.1016/0304-4203(88)90045-X

Elliott, S., Lu, E., F.S. Rowland, 1987. Physical chemistry in seawater. Geophys. Res. Letts 14, 131–134. http://doi.org/10.1029/GL014i002p00131

Ercal, N., Gurer-Orhan, H., Aykin-Burns, N., 2002. Toxic Metals and Oxidative Stress Part I: Mechanisms Involved in Me-tal induced Oxidative Damage. Curr. Top. Med. Chem. https://doi.org/10.2174/1568026013394831.

Esteves, V.I., Otero, M., Duarte, A.C., 2009. Comparative characterization of humic substances from the open ocean, estuarine water and fresh water. Org. Geochem. 40, 942–950. https://doi.org/10.1016/j.orggeochem.2009.06.006

Feely, R.A., Baker, E.T., Marumo, I.K., Urabe, T., Ishibashl, J., Gendron, J., Lebon, G.T., Okamura, K., 1996. Hydrothermal plume particles and dissolved phosphate over the superfast-spreading southern East Pacific Rise 60, 2297–2323. https://doi.org/10.1016/S0967-0637(02)00086-9

Ferrari, G.M., Dowell, M.D., Grossi, S., Targa, C., 1996. Relationship between the optical properties of chromophoric dissolved organic matter and total concentration of dissolved organic carbon in the southern Baltic Sea region. Mar. Chem. 55, 299–316. https://doi.org/10.1016/S0304-4203(96)00061-8

Findlay, A.J., Estes, E.R., Gartman, A., Yücel, M., Kamyshny, A., Luther, G.W., 2019. Iron and sulfide nanoparticle formation and transport in nascent hydrothermal vent plumes. Nat. Commun. 10, 1–7. https://doi.org/10.1038/s41467-019-09580-5

Fitzsimmons, J.N., John, S.G., Marsay, C.M., Ho, C.L., Nicholas, S.L., Toner, B.M., German, C.R., Sherrell, R.M., 2017. Iron persistence in a distal hydrothermal plume supported by dissolved–particulate exchange. Nat. Geosci. 10, 195–201. https://doi.org/10.1038/NGEO2900

Fourrier, P., Dulaquais, G., Guigue, C., Giamarchi, P., Sarthou, G., Whitby, H., Riso, R., 2022. Characterization of the vertical size distribution, composition and chemical properties of dissolved organic matter in the (ultra)oligotrophic Pacific Ocean through a multi-detection approach. Mar. Chem. 240, 104068. https://doi.org/10.1016/j.marchem.2021.104068

Foustoukos, D.I., Seyfried, W.E., 2007. Fluid Phase Separation Processes in Submarine Hydrothermal Systems. Rev. Mineral. Geochemistry 65, 213–239. https://doi.org/10.2138/rmg.2007.65.7

Gao, Z., Guéguen, C., 2018. Distribution of thiol, humic substances and colored dissolved organic matter during the 2015 Canadian Arctic GEOTRACES cruises. Mar. Chem. 203, 1–9. https://doi.org/10.1016/j.marchem.2018.04.001

Gartman, A., Findlay, A.J., 2020. Impacts of hydrothermal plume processes on oceanic metal cycles

and transport. Nat. Geosci. 13, 396–402. https://doi.org/10.1038/s41561-020-0579-0

Geider, R.J., La Roche, J., 1994. The role of iron in phytoplankton photosynthesis, and the potential for iron-limitation of primary productivity in the sea. Photosynth. Res. 39, 275–301. https://doi.org/10.1007/BF00014588

German, C.R., Baker, E.T., Connelly, D.P., Lupton, J.E., Resing, J., Prien, R.D., Walker, S.L., Edmonds, H.N., Langmuir, C.H., 2006. Hydrothermal exploration of the Fonualei Rift and Spreading Center and the Northeast Lau Spreading Center. Geochemistry, Geophys. Geosystems 7, 1–15. https://doi.org/10.1029/2006GC001324

German, C.R., Seyfried, W.E., 2014. Hydrothermal Processes, 2nd ed, The Oceans and Marine Geochemistry. Elsevier Ltd. https://doi.org/10.1016/B978-0-08-095975-7.00607-0

Gerringa, L.J.A., Rijkenberg, M.J.A., Schoemann, V., Laan, P., de Baar, H.J.W., 2015. Organic complexation of iron in the West Atlantic Ocean. Mar. Chem. 177, 434–446. https://doi.org/10.1016/j.marchem.2015.04.007

Goldhaber, M.B., Kaplan, I.R., 1975. Apparent dissociation constants of hydrogen sulfide in chloride solutions. Mar. Chem. 3, 83–104. https://doi.org/10.1016/0304-4203(75)90016-X

Guieu, C., Bonnet, S., 2019. TONGA 2019 cruise, R/V L'Atalante [WWW Document]. https://doi.org/https://doi.org/10.17600/18000884

Guieu, C., Bonnet, S., Petrenko, A., Menkes, C., Chavagnac, V., Desboeufs, K., Maes, C., Moutin, T., 2018. Iron from a submarine source impacts the productive layer of the Western Tropical South Pacific (WTSP). Nat. Sci. Reports 1–9. https://doi.org/10.1038/s41598-018-27407-z

Hannington, M., Jamieson, J., Monecke, T., Petersen, S., Beaulieu, S., 2011. The abundance of seafloor massive sulfide deposits. Geology 39, 1155–1158. https://doi.org/10.1130/G32468.1

Hannington, M., Kopp, H., 2018. ARCHIMEDES [WWW Document]. URL https://www.oceanblogs.org/so267/about/

Harvey, G. r., Tokar, J. m., Boran, D., Chesal, L.A., 1983. The structure of marine fulvic and humic acids. Mar. Biol. 12, 119–132. https://doi.org/10.1016/0304-4203(83)90075-0

Hassler, C., Cabanes, D., Blanco-Ameijeiras, S., Sander, S.G., Benner, R., 2020. Importance of refractory ligands and their photodegradation for iron oceanic inventories and cycling. Mar. Freshw. Res. 71, 311–320. https://doi.org/10.1071/MF19213

Hassler, C.S., van den Berg, C.M.G., Boyd, P.W., 2017. Toward a regional classification to provide a more inclusive examination of the ocean biogeochemistry of iron-binding ligands. Front. Mar. Sci. 4. https://doi.org/10.3389/fmars.2017.00019

Hawkes, J.A., Connelly, D.P., Rijkenberg, M.J.A., Achterberg, E.P., 2014. The importance of shallow hydrothermal island arc systems in ocean biogeochemistry. Geophys. Res. Lett. 41, 749–1078. https://doi.org/10.1002/2013GL058817.Received

Hawkins, J.W., 1995. The Geology of the Lau Basin, in: Backarc Basins: Tectonics and Magmatism, Plenum Press, New York. pp. 63–64.

He, Y., Zheng, Y., Locke, D.C., 2002. Differential pulse cathodic stripping voltammetric determination of nanomolar levels of dissolved sulfide applicable to field analysis of groundwater. Anal. Chim. Acta 459, 209–217. https://doi.org/10.1016/S0003-2670(02)00132-0

Heerah, K.M., Reader, H.E., 2022. Towards the identification of humic ligands associated with iron transport through a salinity gradient. Sci. Rep. 12, 1–11. https://doi.org/10.1038/s41598-022-

19618-2

Hertkorn, N., Benner, R., Frommberger, M., Schmitt-Kopplin, P., Witt, M., Kaiser, K., Kettrup, A., Hedges, J.I., 2006. Characterization of a major refractory component of marine dissolved organic matter. Geochim. Cosmochim. Acta 70, 2990–3010. https://doi.org/10.1016/j.gca.2006.03.021

Hirose, K., 2006. Chemical speciation of trace metals in seawater: a review. Anal. Sci. 22, 1055–1063. https://doi.org/10.2116/analsci.22.1055

Hsu-kim, H., Mullaugh, K.M., Tsang, J.J., Yucel, M., Iii, G.W.L., 2008. Formation of Zn- and Fe-sulfides near hydrothermal vents at the Eastern Lau Spreading Center : implications for sulfide bioavailability to chemoautotrophs. Geochem. Trans. 14, 1–14. https://doi.org/10.1186/1467-4866-9-6

Hu, H., Mylon, S.E., Benoit, G., 2006. Distribution of the thiols glutathione and 3-mercaptopropionic acid in Connecticut lakes. Limnol. Oceanogr. 51, 2763–2774. https://doi.org/10.4319/lo.2006.51.6.2763

Huang, X.G., Li, S. xing, Liu, F.J., Lan, W.R., 2018. Regulated effects of Prorocentrum donghaiense Lu exudate on nickel bioavailability when cultured with different nitrogen sources. Chemosphere 197, 57–64. https://doi.org/10.1016/j.chemosphere.2018.01.014

Ishibashi, J., Urabe, T., 1995. Hydrothermal Activity Related to Arc-Backarc Magmatism in the Western Pacific, in: Backarc Basins. Springer, Boston, MA, pp. 451–495. https://doi.org/10.1007/978-1-4615-1843-3_13

Jacquot, J.E., Horak, R.E.A., Amin, S.A., Devol, A.H., Ingalls, A.E., Armbrust, E.V., Stahl, D.A., Moffett, J.W., 2014. Assessment of the potential for copper limitation of ammonia oxidation by Archaea in a dynamic estuary. Mar. Chem. 162, 37–49. https://doi.org/10.1016/j.marchem.2014.02.002

Jacquot, J.E., Moffett, J.W., 2015. Copper distribution and speciation across the International GEOTRACES Section GA03. Deep Sea Res. Part II Top. Stud. Oceanogr. 116, 187–207. https://doi.org/10.1016/J.DSR2.2014.11.013

Jensen, W.B., 1978. The Lewis Acid-Base Definitions: A Status Report. Chem. Rev. 78. https://doi.org/10.1021/cr60311a002

Jøgensen, M.H.H.K.I.B.B., 1978. Mechanisms of hydrogen sulfide release from coastal marine sediments to the atmosphere. Limnol. Oceanogr. 1, 68–76.

Jorgensen, B.B., Fenchel, T., 1974. The sulfur cycle of a coastal marine sediment. Mar. Biol. 24, 189–201.

Karig, D.E., 1970a. Kermadec arc — New Zealand tectonic confluence. New Zeal. J. Geol. Geophys. 13, 5–294. https://doi.org/10.1080/00288306.1970.10428203

Karig, D.E., 1970b. Ridges and basins of the Tonga-Kermadec Island Arc System. J. Geophys. Res. 75. https://doi.org/10.1029/JB075i002p00239

Kawakami, S.K., Gledhill, M., Eric, P., 2006. Production of phytochelatins and glutathione by marine phytoplankton in response to metal stress 989, 975–989. https://doi.org/10.1111/j.1529-8817.2006.00265.x

Kieber, R.J., Hydro, L.H., Seaton, P.J., 1997. Photooxidation of triglycerides and fatty acids in seawater: Implication toward the formation of marine humic substances. Limnol. Oceanogr. 42, 1454–1462. https://doi.org/10.4319/lo.1997.42.6.1454

Kikuchi, T., Fujii, M., Terao, K., Jiwei, R., Lee, Y.P., Yoshimura, C., 2017. Correlations between

aromaticity of dissolved organic matter and trace metal concentrations in natural and effluent waters: A case study in the Sagami River Basin, Japan. Sci. Total Environ. 576, 36–45. https://doi.org/10.1016/j.scitotenv.2016.10.068

Kilinkhammer, G., Bender, R., Weiss, F., 1977. Hydrothermal manganese in the Galapagos Rift Solar influence on North. Nature 269, 319–320. https://doi.org/https://doi.org/10.1038/269319a0

Kogut, M.B., Voelker, B.M., 2001. Strong copper-binding behavior of terrestrial humic substances in seawater. Environ. Sci. Technol. 35, 1149–1156. https://doi.org/10.1021/es0014584

Koschinsky, A., Garbe-Schönberg, D., Sander, S., Schmidt, K., Gennerich, H.H., Strauss, H., 2008. Hydrothermal venting at pressure-temperature conditions above the critical point of seawater, 5°S on the Mid-Atlantic Ridge. Geology 36, 615–618. https://doi.org/10.1130/G24726A.1

Krachler, R., Krachler, R.F., Wallner, G., Hann, S., Laux, M., Cervantes Recalde, M.F., Jirsa, F., Neubauer, E., von der Kammer, F., Hofmann, T., Kepplera, B.K., 2015. River-derived humic substances as iron chelators in seawater. Mar. Chem. 174, 85–93. https://doi.org/10.1016/j.marchem.2015.05.009

Krivácsy, Z., Kiss, G., Ceburnis, D., Jennings, G., Maenhaut, W., Salma, I., Shooter, D., 2008. Study of water-soluble atmospheric humic matter in urban and marine environments. Atmos. Res. 87, 1–12. https://doi.org/10.1016/j.atmosres.2007.04.005

Kuma, K., Katsumoto, A., Nishioka, J., Matsunaga, K., 1998. Size-fractionated iron concentrations and Fe(III) hydroxide solubilities in various coastal waters. Estuar. Coast. Shelf Sci. 47, 275–283. https://doi.org/10.1006/ecss.1998.0355

Kumar, V., Pandita, S., Preet, G., Sidhu, S., Sharma, A., Khanna, K., Kaur, P., Shreeya, A., Setia, R., 2021. Copper bioavailability , uptake , toxicity and tolerance in plants : A comprehensive review. Chemosphere 262, 127810. https://doi.org/10.1016/j.chemosphere.2020.127810

Laglera, L.M., Battaglia, G., van den Berg, C.M.G., 2007. Determination of humic substances in natural waters by cathodic stripping voltammetry of their complexes with iron. Anal. Chim. Acta 599, 58–66. https://doi.org/10.1016/j.aca.2007.07.059

Laglera, L.M., Sukekava, C., Slagter, H.A., Downes, J., Aparicio-Gonzalez, A., Gerringa, L.J.A., 2019. First Quantification of the Controlling Role of Humic Substances in the Transport of Iron across the Surface of the Arctic Ocean. Environ. Sci. Technol. https://doi.org/10.1021/acs.est.9b04240

Laglera, L.M., van den Berg, C.M.G., 2009. Evidence for geochemical control of iron by humic substances in seawater. Limnol. Oceanogr. 54, 610–619. https://doi.org/10.4319/lo.2009.54.2.0610

Langmuir, C., 2004. KM0417, R/V Kilo Moana [WWW Document]. URL https://www.marine-geo.org/tools/search/Files.php?data_set_uid=5911

Laporte, D., Rodríguez, F., González, A., Zúñiga, A., Castro-Nallar, E., Saéz, ~, Moenne, A., 2020. Copper-induced concomitant increases in photosynthesis, respiration, and C, N and S assimilation revealed by transcriptomic analyses in Ulva compressa (Chlorophyta). BMC Plant Biol. 20, 1–16. https://doi.org/10.1186/s12870-019-2229-5

Lawrence, N.S., Thompson, M., Prado, C., Jiang, L., Jones, T.G.J., Compton, R.G., 2002. Amperometric detection of sulfide at a boron doped diamond electrode: The electrocatalytic reaction of sulfide with ferricyanide in aqueous solution. Electroanalysis 14, 499–504. https://doi.org/10.1002/1521-4109(200204)14:7/8<499::AID-ELAN499>3.0.CO;2-P

Leal, M.F.C., van den Berg, C.M.G., 1998. Evidence for strong copper(I) complexation by organic ligands

in seawater. Aquat. Geochemistry 4, 49–75. https://doi.org/10.1023/A:1009653002399

Leal, M.F.C., Vasconcelos, M.T.S.D., van den Berg, C.M.G., 1999. Copper-induced release of complexing ligands similar to thiols by Emiliania huxleyi in seawater cultures. Limnol. Oceanogr. 44, 1750–1762. https://doi.org/10.4319/lo.1999.44.7.1750

Lewis, A.G., 1991. The biological importance of Copper. A Literature Review, International Copper Research Industry, 1–100.

Lin, J., Purdy, G.M., Schouten, H., Sempere, J.C., Zervas, C., 1990. Evidence from gravity data for focused magmatic accretion along the Mid-Atlantic Ridge. Nature 344, 627–632. https://doi.org/10.1038/344627a0

Liu, X., Millero, F.J., 2002. The solubility of iron in seawater. Mar. Chem. 77, 43–54. https://doi.org/10.1016/S0304-4203(01)00074-3

Lohan, M.C., Tagliabue, A., 2018. Oceanic micronutrients: Trace metals that are essential for marine life. Elements 14, 385–390. https://doi.org/10.2138/gselements.14.6.385

Lopachin, R.M., Gavin, T., 2017. Thiolate Sites : Relevance To Pathophysiological. Free Radic Res 50, 195–205. https://doi.org/10.3109/10715762.2015.1094184.REACTIONS

Lorenzo, J.I., Nieto-Cid, M., Álvarez-Salgado, X.A., Pérez, P., Beiras, R., 2007. Contrasting complexing capacity of dissolved organic matter produced during the onset, development and decay of a simulated bloom of the marine diatom Skeletonema costatum. Mar. Chem. 103, 61–75. https://doi.org/10.1016/j.marchem.2006.05.009

Luther, G.W., Tsamakis, E., 1989. Concentration and form of dissolved sulfide in the oxic water column of the ocean. Mar. Chem. 27, 165–177. https://doi.org/10.1016/0304-4203(89)90046-7

Luther W., G., Rozan F., T., Taillefert, M., Nuzzio B., D., Meo Di, C., Shank M., T., Lutz A., R., Cary Craig, S., 2001. Chemical speciation drives hydrothermal vent ecology. Nature 410, 813–816. https://doi.org/10.1038/35071069

Madkour, L.H., 2020a. Biological mechanisms of reactive oxygen species (ROS), in: Reactive Oxygen Species (ROS), Nanoparticles, and Endoplasmic Reticulum (ER) Stress-Induced Cell Death Mechanisms. pp. 19–35. https://doi.org/10.1016/B978-0-12-822481-6.00002-5

Madkour, L.H., 2020b. Oxidative stress and oxidative damage-induced cell death, in: Reactive Oxygen Species (ROS), Nanoparticles, and Endoplasmic Reticulum (ER) Stress-Induced Cell Death Mechanisms. pp. 175–197. https://doi.org/10.1016/B978-0-12-822481-6.00008-6

Manaban, S.E., Smith, M.J., 1973. Copper Micronutrient Requirement for Algae. Environ. Sci. Technol. 7, 829–833. https://doi.org/10.1021/es60081a013

Mantoura, R.F.C., Dickson, A., Riley, J.P., 1978. The complexation of metals with humic materials in natural waters. Estuar. Coast. Mar. Sci. 6, 387–408. https://doi.org/10.1016/0302-3524(78)90130-5

Marie, L., Pernet-Coudrier, B., Waeles, M., Gabon, M., Riso, R., 2015. Dynamics and sources of reduced sulfur, humic substances and dissolved organic carbon in a temperate river system affected by agricultural practices. Sci. Total Environ. 537, 23–32. https://doi.org/10.1016/j.scitotenv.2015.07.089

Marie, L., Pernet-Coudrier, B., Waeles, M., Riso, R., 2017. Seasonal variation and mixing behaviour of glutathione, thioacetamide and fulvic acids in a temperate macrotidal estuary (Aulne, NW France). Estuar. Coast. Shelf Sci. 184, 177–190. https://doi.org/10.1016/j.ecss.2016.11.018

McLeay, Y., Stannard, S., Houltham, S., Starck, C., 2017. Dietary thiols in exercise: Oxidative stress defence, exercise performance, and adaptation. J. Int. Soc. Sports Nutr. 14. https://doi.org/10.1186/s12970-017-0168-9

Millero, F.J., 1998. Solubility of Fe(III) in seawater. Earth Planet. Sci. Lett. 154, 323–329. https://doi.org/10.1016/s0012-821x(97)00179-9

Millero, F.J., 1986. The thermodynamics and kinetics of the hydrogen sulfide system in natural waters. Mar. Chem. 18, 121–147. https://doi.org/10.1016/0304-4203(86)90003-4

Mironov, I. V., & Tsvelodub, L. D. (1996). Complexation of copper(I) by thiourea in acidic aqueous solution. *Journal of Solution Chemistry*, *25*(3), 315–325. https://doi.org/10.1007/BF00972529

Moffett, J.W., Tuit, C.B., Ward, B.B., 2012. Chelator-induced inhibition of copper metalloenzymes in denitrifying bacteria. Limnol. Oceanogr. 57, 272–280. https://doi.org/10.4319/lo.2012.57.1.0272

Morelli, E., Scarano, G., 2004. Copper-induced changes of non-protein thiols and antioxidant enzymes in the marine microalga Phaeodactylum tricornutum. Plant Sci. 167, 289–296. https://doi.org/10.1016/j.plantsci.2004.04.001

Morris, J.J., Rose, A.L., Lu, Z., 2022. Redox Biology Reactive oxygen species in the world ocean and their impacts on marine ecosystems. Redox Biol. 52, 102285. https://doi.org/10.1016/j.redox.2022.102285

Moutin, T., 2015. OUTPACE, R/V L'Atalante [WWW Document]. URL https://outpace.mio.univ-amu.fr/?lang=fr

Muller, F.L.L., 2018. Exploring the potential role of terrestrially derived humic substances in the marine biogeochemistry of iron. Front. Earth Sci. 6. https://doi.org/10.3389/feart.2018.00159

Muller, F.L.L., Batchelli, S., 2013. Copper binding by terrestrial versus marine organic ligands in the coastal plume of River Thurso, North Scotland. Estuar. Coast. Shelf Sci. 133, 137–146. https://doi.org/10.1016/j.ecss.2013.08.024

Mullineaux, P.M., Exposito-Rodriguez, M., Laissue, P.P., Smirnoff, N., 2018. ROS-dependent signalling pathways in plants and algae exposed to high light: Comparisons with other eukaryotes. Free Radic. Biol. Med. 122, 52–64. https://doi.org/10.1016/j.freeradbiomed.2018.01.033

Nault, B.A., Campuzano-Jost, P., Day, D.A., Jo, D.S., Schroder, J.C., Allen, H.M., Bahreini, R., Bian, H., Blake, D.R., Chin, M., Clegg, S.L., Colarco, P.R., Crounse, J.D., Cubison, M.J., DeCarlo, P.F., Dibb, J.E., Diskin, G.S., Hodzic, A., Hu, W., Katich, J.M., Kim, M.J., Kodros, J.K., Kupc, A., Lopez-Hilfiker, F.D., Marais, E.A., Middlebrook, A.M., Andrew Neuman, J., Nowak, J.B., Palm, B.B., Paulot, F., Pierce, J.R., Schill, G.P., Scheuer, E., Thornton, J.A., Tsigaridis, K., Wennberg, P.O., Williamson, C.J., Jimenez, J.L., 2021. Chemical transport models often underestimate inorganic aerosol acidity in remote regions of the atmosphere. Commun. Earth Environ. 2, 1–13. https://doi.org/10.1038/s43247-021-00164-0

Navarrete, A., González, A., Gómez, M., Contreras, R.A., Díaz, P., Lobos, G., Brown, M.T., Sáez, ~, Moenne, A., 2019. Copper excess detoxification is mediated by a coordinated and complementary induction of glutathione, phytochelatins and metallothioneins in the green seaweed Ulva compressa. Plant Physiol. Biochem. 135, 423–431. https://doi.org/10.1016/J.PLAPHY.2018.11.019

NOAA, 2021. GEBCO undersea Feature Names Gazetteer [WWW Document]. URL https://www.ngdc.noaa.gov/gazetteer/

Oldham, V.E., Swenson, M.M., Buck, K.N., 2014. Spatial variability of total dissolved copper and copper speciation in the inshore waters of Bermuda. Mar. Pollut. Bull. 79, 314–320. https://doi.org/10.1016/J.MARPOLBUL.2013.12.016

Olson, K.R., 2019. Hydrogen sulfide, reactive sulfur species and coping with reactive oxygen species. Free Radic. Biol. Med. 140, 74–83. https://doi.org/10.1016/j.freeradbiomed.2019.01.020

Olson, K.R., Straub, K.D., 2015. The Role of Hydrogen Sulfide in Evolution and the Evolution of Hydrogen Sulfide in Metabolism and Signaling A Brief History of the Earth. Physiology 31, 2–72. https://doi.org/10.1152/physiol.00024.2015

Pál, M., Janda, T., Szalai, G., 2018. Interactions between plant hormones and thiol-related heavy metal chelators. Plant Growth Regul. 85, 173–185. https://doi.org/10.1007/s10725-018-0391-7

Pandey, M., Srivastava, A. K., D'Souza, S. F., & Penna, S. (2013). Thiourea, a ROS Scavenger, Regulates Source-to-Sink Relationship to Enhance Crop Yield and Oil Content in Brassica juncea (L.). PLoS ONE, 8(9). https://doi.org/10.1371/journal.pone.0073921

Parson, L.M., Wright, I.C., 1996. The Lau-Havre-Taupo back-arc basin : A southward-propagating, multi-stage evolution from rifting to spreading. Tectonophysics 263, 1–22.

Pelletier, B., Calmant, S., Pillet, R., 1998. Current tectonics of the Tonga-New Hebrides region. Earth Planet. Sci. Lett. 164, 263–276. https://doi.org/10.1016/S0012-821X(98)00212-X

Pernet-Coudrier, B., Waeles, M., Filella, M., Quentel, F., Riso, R.D., 2013. Simple and simultaneous determination of glutathione, thioacetamide and refractory organic matter in natural waters by DP-CSV. Sci. Total Environ. 463–464, 997–1005. https://doi.org/10.1016/j.scitotenv.2013.06.053

Plavšić, M., Ciglenečki, I., Strmečki, S., Bura-Nakić, E., 2011. Seasonal distribution of organic matter and copper under stratified conditions in a karstic, marine, sulfide rich environment (Rogoznica Lake, Croatia). Estuar. Coast. Shelf Sci. 92, 277–285. https://doi.org/10.1016/j.ecss.2011.01.004

Posacka, A.M., Semeniuk, D.M., Whitby, H., van den Berg, C.M.G., Cullen, J.T., Orians, K., Maldonado, M.T., 2017. Dissolved copper (dCu) biogeochemical cycling in the subarctic Northeast Pacific and a call for improving methodologies. Mar. Chem. 196, 47–61. https://doi.org/10.1016/J.MARCHEM.2017.05.007

Radford-Knęry, J., Cutter, G.A., 1994. Biogeochemistry of dissolved hydrogen sulfide species and carbonyl sulfide in the western North Atlantic Ocean. Geochim. Cosmochim. Acta 58, 5421–5431. https://doi.org/10.1016/0016-7037(94)90239-9

Rea, P.A., Vatamaniuk, O.K., Rigden, D.J., 2004. Weeds, worms, and more: papain's long-lost cousin. Plant Physiol. 136, 2463–2474. https://doi.org/10.1104/pp.104.048579.LONG-CHAIN

Resing, J., 2012. The Submarine Ring of Fire 2012, R/V Revelle [WWW Document]. URL https://oceanexplorer.noaa.gov/explorations/12fire/background/plan/plan.html

Resing, J., 2010. KM1024, R/V Kilo Moana [WWW Document]. URL http://laueruptions.blogspot.com/

Resing, J., 2009. R/V Thompson [WWW Document].

Resing, J., 2008. TN227, R/V Thompson [WWW Document]. URL http://ventslaubasin2008.blogspot.com/

Resing, J.A., Sedwick, P.N., German, C.R., Jenkins, W.J., Moffett, J.W., Sohst, B.M., Tagliabue, A., 2015. Basin-scale transport of hydrothermal dissolved metals across the South Pacific Ocean. Nature 523. https://doi.org/10.1038/nature14577

Reysenbach, A.-L., 2015. Lau Geomicrobiology [WWW Document]. URL http://laugeomicro2015.blogspot.com/2015_04_01_archive.html

Ritchie, J.D., Michael Perdue, E., 2003. Proton-binding study of standard and reference fulvic acids, humic acids, and natural organic matter. Geochim. Cosmochim. Acta 67, 85–96. https://doi.org/10.1016/S0016-7037(02)01044-X

Rubin, K., 2017. FK171110, R/V Falkor [WWW Document]. URL https://www.rvdata.us/search/cruise/FK171110

Sarma, N.S., Kiran, R., Reddy, M.R., Iyer, S.D., Peketi, A., Borole, D. V., Krishna, M.S., 2018. Hydrothermal Alteration Promotes Humic Acid Formation in Sediments: A Case Study of the Central Indian Ocean Basin. J. Geophys. Res. Ocean. 110–130. https://doi.org/10.1002/2017JC012940

Schellekens, J., Buurman, P., Kalbitz, K., Zomeren, A. Van, Vidal-torrado, P., Cerli, C., Comans, R.N.J., 2017. Molecular Features of Humic Acids and Fulvic Acids from Contrasting Environments. Environ. Sci. Technol. 51, 1330–1339. https://doi.org/10.1021/acs.est.6b03925

Schieber, M., Chandel, N.S., 2014. ROS function in redox signaling. Curr. Biol. 24, 453–462. https://doi.org/10.1016/j.cub.2014.03.034

Schmidt Ocean Institute, S., n.d. Hydrothermal vent schematic [WWW Document]. URL https://schmidtocean.org/wp-content/uploads/fk151121-guam-20151123-baker-plume.jpg

Shao, Y., Bao, M., Huo, W., Ye, R., Liu, Y., Lu, W., 2022. Production of artificial humic acid from biomass residues by a non-catalytic hydrothermal process. J. Clean. Prod. 335, 130302. https://doi.org/10.1016/j.jclepro.2021.130302

Sharma, A., Anthal, R., 2007. Humic Substances in Aquatic Ecosystems: A Review. Int. J. Innov. Res. Sci. Eng. Technol. (An ISO 3297. https://doi.org/10.15680/IJIRSET.2016.0510051

Shaw, T.J., Luther, G.W., Rosas, R., Oldham, V.E., Coffey, N.R., Ferry, J.L., Dias, D.M.C., Yücel, M., Thibault, A., Chanvalon, D., 2021. Fe-catalyzed sulfide oxidation in hydrothermal plumes is a source of reactive oxygen species to the ocean. Proc. Natl. Acad. Sci. U.S.A. 118, 1–7. https://doi.org/10.1073/pnas.2026654118

Shigemitsu, M., Yokokawa, T., Uchida, H., Kawagucci, S., Murata, A., 2021. Sedimentary supply of humic-like fluorescent dissolved organic matter and its implication for chemoautotrophic microbial activity in the Izu-Ogasawara Trench. Sci. Rep. 11, 1–10. https://doi.org/10.1038/s41598-021-97774-7

Slagter, H.A., Laglera, L.M., Sukekava, C., Gerringa, L.J.A., 2019. Fe-Binding Organic Ligands in the Humic-Rich TransPolar Drift in the Surface Arctic Ocean Using Multiple Voltammetric Methods. J. Geophys. Res. Ocean. 124, 1491–1508. https://doi.org/10.1029/2018JC014576

Smith, I.E.M., Price, R.C., 2006. The Tonga – Kermadec arc and Havre – Lau back-arc system : Their role in the development of tectonic and magmatic models for the western Pacific 156, 315–331. https://doi.org/10.1016/j.jvolgeores.2006.03.006

Steffens, J.C., 1990. The heavy metal-binding peptides of plants. Annu. Rev. Plant Physiol. Plant Mol. Biol. 41, 553–575. https://doi.org/10.1146/annurev.pp.41.060190.003005

Sukekava, C., Downes, J., Slagter, H.A., Gerringa, L.J.A., Laglera, L.M., 2018. Determination of the contribution of humic substances to iron complexation in seawater by catalytic cathodic stripping voltammetry. Talanta 189, 359–364. https://doi.org/10.1016/j.talanta.2018.07.021

Superville, P.J., Pižeta, I., Omanović, D., Billon, G., 2013. Identification and on-line monitoring of

reduced sulphur species (RSS) by voltammetry in oxic waters. Talanta 112, 55–62. https://doi.org/10.1016/j.talanta.2013.03.045

Sutak, R., Camadro, J.M., Lesuisse, E., 2020. Iron Uptake Mechanisms in Marine Phytoplankton. Front. Microbiol. 11, 1–14. https://doi.org/10.3389/fmicb.2020.566691

Swarr, G.J., Kading, T., Lamborg, C.H., Hammerschmidt, C.R., Bowman, K.L., 2016. Dissolved low-molecular weight thiol concentrations from the U.S. GEOTRACES North Atlantic Ocean zonal transect. Deep Sea Res. Part I Oceanogr. Res. Pap. 116, 77–87. https://doi.org/10.1016/J.DSR.2016.06.003

Tang, D., Hung, C.C., Warnken, K.W., Santschi, P.H., 2000. The distribution of biogenic thiols in surface waters of Galveston Bay. Limnol. Oceanogr. 45, 1289–1297. https://doi.org/10.4319/lo.2000.45.6.1289

Tang, D., Shafer, M.M., Karner, D.A., Armstrong, D.E., 2005. Response of nonprotein thiols to copper stress and extracellular release of glutathione in the diatom Thalassiosira weissflogii. Limnol. Oceanogr. https://doi.org/10.4319/lo.2005.50.2.0516

Tang, D., Warnken, K.W., Santschi, P.H., 2001. Organic complexation of copper in surface waters of Galveston Bay. Limnol. Oceanogr. 46, 321–330. https://doi.org/10.4319/lo.2001.46.2.0321

Theberge, S.M., Luther, G.W., Farrenkopf, A.M., 1997. On the existence of free and metal complexed sulfide in the Arabian Sea and its oxygen minimum zone. Deep Sea Res. Part II Top. Stud. Oceanogr. 44, 1381–1390. https://doi.org/10.1016/S0967-0645(97)00012-X

Tilliette, C., Taillandier, V., Bouruet-Aubertot, P., Grima, N., Maes, C., Montanes, M., Sarthou, G., Vorrath, M.-E., Arnone, V., Bressac, M., et al., 2022. DFe patterns impacted by shallow hydrothermal sources along a transect through the Tonga-Kermadec arc. Earth Sp. Sci. Open Arch. 43. https://doi.org/10.1029/2022GB007363

Truede, T., Smith, C., Wenzhöfer, F., Carney, E., Bernardino, A., Hannides, A., Krgüer, M., Boetius, A., 2009. Biogeochemistry of a deep-sea whale fall: Sulfate reduction, sulfide efflux and methanogenesis. Mar. Eco. Prog. Ser. 382. 1-21, https://doi.org/ 10.3354/meps07972

Ulricha, K., Jakoba, U., 2019. The role of thiols in antioxidant systems. Free Radic Biol Med 140, 14–27. https://doi.org/10.1016/j.physbeh.2017.03.040

van Laer, K., Hamilton, C.J., Messens, J., 2013. Low-Molecular-Weight Thiols in Thiol–Disulfide Exchange. Antioxid. Redox Signal. 18, 1642–1653. https://doi.org/10.1089/ars.2012.4964

Vraspir, J. M., & Butler, A. (2009). Chemistry of marine ligands and siderophores. In *Annual Review of Marine Science* (Vol. 1, pp. 43–63). https://doi.org/10.1146/annurev.marine.010908.163712

Walsh, M.J., Ahner, B.A., 2013. Determination of stability constants of Cu(I), Cd(II) & Zn(II) complexes with thiols using fluorescent probes. J. Inorg. Biochem. 128, 112–123. https://doi.org/10.1016/j.jinorgbio.2013.07.012

Wang, H., Liu, M., Wang, W., Zhou, H., Ellwood, M.J., Butterfield, D.A., Buck, N.J., Resing, J.A., 2022. Iron ligands and isotopes in hydrothermal plumes over backarc volcanoes in the Northeast Lau Basin, Southwest Pacific Ocean. Geochim. Cosmochim. Acta 336, 341–352. https://doi.org/10.1016/j.gca.2022.09.026

Wang, S., Sun, W., Huang, J., Zhai, S., 2023. S , Pb , and Fe isotope compositions of sulfides in middle and southern Okinawa Trough : Implying the complicated hydrothermal systems in back-arc spreading centers. Deep. Res. Part I 195, 104006. https://doi.org/10.1016/j.dsr.2023.104006

Whitby, H., Bressac, M., Sarthou, G., 2020a. Contribution of Electroactive Humic Substances to the

Iron - Binding Ligands Released During Microbial Remineralization of Sinking Particles Geophysical Research Letters 1–11. https://doi.org/10.1029/2019GL086685

Whitby, H., Bressac, M., Sarthou, G., Ellwood, M.J., Guieu, C., Boyd, P.W., 2020b. Contribution of Electroactive Humic Substances to the Iron-Binding Ligands Released During Microbial Remineralization of Sinking Particles. Geophys. Res. Lett. 47, 1–11. https://doi.org/10.1029/2019GL086685

Whitby, H., Hollibaugh, J.T., van den Berg, C.M.G., 2017. Chemical speciation of copper in a salt marsh estuary and bioavailability to thaumarchaeota. Front. Mar. Sci. 4, 1–15. https://doi.org/10.3389/fmars.2017.00178

Whitby, H., Posacka, A.M., Maldonado, M.T., van den Berg, C.M.G., 2018. Copper-binding ligands in the NE Pacific. Mar. Chem. 204, 36–48. https://doi.org/10.1016/J.MARCHEM.2018.05.008

Whitby, H., van den Berg, C.M.G., 2015. Evidence for copper-binding humic substances in seawater. Mar. Chem. https://doi.org/10.1016/j.marchem.2014.09.011

Williford, T., Amon, R.M.W., Benner, R., Kaiser, K., Bauch, D., Stedmon, C., Yan, G., Walker, S.A., van der Loeff, M.R., Klunder, M.B., 2021. Insights into the origins, molecular characteristics and distribution of iron-binding ligands in the Arctic Ocean. Mar. Chem. 231, 103936. https://doi.org/10.1016/j.marchem.2021.103936

Xu, K., Tang, Z., Liu, S., liao, Z., Xia, H., Liu, L., Wang, Z., Qi, P., 2018. Effects of low concentrations copper on antioxidant responses, DNA damage and genotoxicity in thick shell mussel Mytilus coruscus. Fish Shellfish Immunol. 82, 77–83. https://doi.org/10.1016/J.FSI.2018.08.016

Yang, L., Hong, H., Guo, W., Chen, C.T.A., Pan, P.I., Feng, C.C., 2012. Absorption and fluorescence of dissolved organic matter in submarine hydrothermal vents off NE Taiwan. Mar. Chem. 128–129, 64–71. https://doi.org/10.1016/j.marchem.2011.10.003

Yang, R., van den Berg, C.M.G., 2009. Metal complexation by humic substances in seawater. Environ. Sci. Technol. 43, 7192–7197. https://doi.org/10.1021/es900173w

Yücel, M., Gartman, A., Chan, C.S., Luther, G.W., 2011. Hydrothermal vents as a kinetically stable source of iron-sulphide-bearing nanoparticles to the ocean. Nat. Geosci. 4, 367–371. https://doi.org/10.1038/ngeo1148

Zellmer, K.E., Taylor, B., 2001. A three-plate kinematic model for Lau Basin opening. Geochemistry, Geophys. Geosystems 2. https://doi.org/10.1029/2000GC000106

Zhang, J.Z., Millero, F.J., 1994. Investigation of metal sulfide complexes in sea water using cathodic stripping square wave voltammetry. Anal. Chim. Acta 284, 497–504. https://doi.org/10.1016/0003-2670(94)85056-9

Zhang, X., Du, Z., Zheng, R., Luan, Z., Qi, F., Cheng, K., 2017. Development of a new deep-sea hybrid Raman insertion probe and its application to the geochemistry of hydrothermal vent and cold seep fluids. Deep. Res. Part I 123, 1–12. https://doi.org/10.1016/j.dsr.2017.02.005

Zhang, Z., Fan, W., Bao, W., Chen, C.T.A., Liu, S., Cai, Y., 2020. Recent developments of exploration and detection of shallow-water hydrothermal systems. Sustain. 12, 1–17. https://doi.org/10.3390/su12219109

Zigah, P.K., McNichol, A.P., Xu, L., Johnson, C., Santinelli, C., Karl, D.M., Repeta, D.J., 2017. Allochthonous sources and dynamic cycling of ocean dissolved organic carbon revealed by carbon isotopes. Geophys. Res. Lett. 44, 2407–2415. https://doi.org/10.1002/2016GL071348

Note for the reader

The following chapter is in preparation for submission to the journal Marine Chemistry.

To be submitted as: **Portlock, G**., Salaün, P., Dulaquais, G., Fourrier, P., Riso, R., Omanovic, D., Guieu, C., Bonnet, S., Whitby, H, Humic substances in the Western Tropical South Pacific: an intercomparison of electrochemical techniques

In this chapter, I analysed eHS using the eHS-Mo method (Pernet-Coudrier et al., 2013) and the eHS-Cu method (Whitby and van den Berg, 2015). I analysed these samples in Liverpool, UK. Analysis of eHS using the eHS-Fe method (Laglera et al., 2007; Sukekava et al., 2018) was carried out by G. Dulaquais in Brest, France. I ran pseudopolarography using the eHS-Mo method and the eHS-Cu method. G. Dulaquais ran pseudopolarography using the eHS-Fe method.

Chapter 2

Humic substances in the Western Tropical South Pacific: an intercomparison of electrochemical techniques.

Abstract

Electroactive humic substances (eHS) play a key role in the cycling of Fe and other trace metals in marine waters but understanding of their composition and biogeochemical cycling is severely lacking. eHS are thought to represent the metal-binding fraction of the humic substances pool, which itself is an operationally defined fraction of the wider dissolved organic matter (DOM) pool. Here, we compare results from three electroanalytical methods used for eHS quantification by cathodic stripping voltammetry (CSV) of their complexes with iron (eHS-Fe), with copper (eHS-Cu) or with molybdenum (eHS-Mo) at the mercury electrode in samples collected from the Western Tropical South Pacific (French GEOTRACES Tonga cruise). Two methods (eHS-Mo and eHS-Fe) were compared across the whole transect, encompassing waters experiencing hydrothermal activity and high nitrogen fixation, with the eHS-Cu method also compared at the most offshore, oligotrophic station. Analyses were

performed independently in separate laboratories, in Liverpool (UK; eHS-Mo, eHS-Cu) and Brest (France; eHS-Fe). Similar eHS concentrations were found by all methods in deep waters of the oligotrophic station, while significant variations were observed in the upper 1,000 meters. eHS concentrations determined by the Fe and Mo methods across the entire transect (N = 104) were strongly correlated (Pearson's correlation coefficient of 0.8) and not significantly different (two-tailed paired t-test, $p > 0.36$) although large differences were observed. Using scanned stripping voltammetry (pseudopolarography), we show that the pseudopolarograms of the river-derived SRFA standard is different than those obtained with the marine humics. Consequently, we find that the concentration determined by the method of standard addition is strongly dependent on the deposition potential, due to these inherent differences between the structure and composition of the analyte compared to the Suwannee River Fulvic Acid (SRFA) standard. We thus stress that agreement between voltametric methods should not be assumed and is likely dependent on the type of organic matter present. Interestingly, we observed that Fe-eHS (and to a lesser extent Cu-eHS) pseudopolarograms resembled the SRFA pseudopolarograms in deep waters compared to surface waters, possibly inferring that with depth marine eHS are become more terrestrial-like. Pseudopolarography might become a useful analytical tool to gain insights into the biogeochemical cycling of electroactive humic substances.

2.1. Introduction

Humic substances (HS) are ill-defined, refractory heterogeneous organic compounds of varying molecular weight, polarity and composition that are derived from the degradation of organic matter. They are present both in the dissolved and particulate fraction of the organic carbon pool and have a long residence time in the water column (Dulaquais et al., 2018b; Faganeli et al., 1995). Their sources to the marine system include land/rivers (Krachler et al., 2015; Muller, 2018), deep-sea sediments (Dulaquais et al., 2018b; Shigemitsu et al., 2021), atmospheric deposition (Krivácsy et al., 2008),

hydrothermal vents (Sarma et al., 2018; Yang et al., 2012), and biological activity through phytoplankton degradation, cell lysis, bacterially-mediated degradation of labile dissolved and particulate organic matter (Sarma et al., 2018; Tranvik, 1993; Whitby et al., 2020b). Photobleaching in sunlit surface waters has been suggested as one of the main sinks of HS (Omori et al., 2011). Bacterial degradation and removal by adsorption onto sinking particles might also be important removal processes (Longhini et al., 2021; Whitby et al., 2020a).

The definition of HS is operationally based: they are defined as those substances that can be extracted by elution through a hydrophobic sorbent resin (e.g. Amberlite XAD). After elution, HS can be refined into two components: humics acids (HA) and fulvic acids (FA) based on their solubility at pH 1, the former precipitating while the latter remains soluble. Here, we use the term HS to refer to both humic and fulvic acids (IHSS, 2022; Stevenson, 1994).

Interest in HS in the marine system has gained momentum in the last decade due to their likely role in the complexation of iron (Fe) (Laglera and van den Berg, 2009). Fe is a micronutrient limiting primary productivity in surface waters of an estimated 40% of the contemporary ocean (Hassler et al., 2020). Although one of the most abundant elements on earth, the poor solubility of its oxyhydroxide species is such that its concentration in seawater of pH 8 should not exceed 10 pM (Liu and Millero, 2002). With dissolved Fe levels being considerably higher at sub nM levels, the increased solubility is often attributed to complexation with dissolved organic ligands (Gledhill and Buck, 2012) and/or to the presence of colloidal species (e.g. FeS, pyrite, (Davison, 1991)). This stabilisation of Fe is essential because it decreases its scavenging (Fe is particle reactive and tend to adsorb on sinking particles), and thus increases its residence time in the water column (Gledhill and Buck, 2012). HS have been shown to be an important component of the Fe-complexing ligand pool in many locations (Dulaquais et al., 2018b; Gledhill and Buck, 2012; Kitayama et al., 2009; Laglera et al., 2019; Laglera and van den Berg, 2009; Muller, 2018; Su et al., 2018; Whitby et al., 2020c). Recent work suggests that HS are important for Fe complexation in the deep Atlantic (Whitby et al., 2020c), are the main ligands for the

transport of Fe in surface waters of the Arctic ocean (Laglera et al., 2019) and are responsible for the long range transport of Fe across the Northeast Pacific (Yamashita et al., 2020). The importance of HS is however not limited to Fe and they have been shown to be involved in the complexation of other metals such as copper (Cu) (Kogut and Voelker, 2001; Waeles et al., 2015; Whitby and van den Berg, 2015), manganese (Mn) (Oldham et al., 2017) and other metals (Yang and van den Berg, 2009). Reliable determination of HS, particularly the metal-binding fraction, is therefore fundamental.

Quantitative determination of HS is an analytical challenge. Natural water samples contain a wide range of different humic compounds having different polarity, aromaticity, composition, charge and thus different biogeochemical cycling due to e.g. different photoreactivity, complexing or adsorbing properties. Analytical techniques detect an average of a certain property making the quantification method both technique and standard dependent; direct comparison of quantitative results obtained with different techniques should thus be done carefully (Filella, 2014, 2010). Most quantitative methods are based on UV-visible light absorbance or fluorescence spectroscopy (Coble, 2007; Yamashita et al., 2020; Yamashita and Tanoue, 2009), size-exclusion chromatography coupled to various detectors (Dulaquais et al., 2018a) or electrochemistry (Laglera et al., 2007; Pernet-Coudrier et al., 2013; Sukekava et al., 2018; Whitby and van den Berg, 2015).

Electrochemical measurements are based on the adsorption properties of humic compounds on the mercury drop electrode. Several polarographic techniques can be used to detect and characterise humic compounds (Cominoli et al., 1980). They are based on the strong adsorbing properties of HS on the mercury drop surface by measuring a change in capacitive current, by measuring the decrease of the polarographic maximum of oxygen or by measuring the faradaic current of an oxido-reduction process of some functional groups of HS or metals form complexes with the humics. Capacitance based techniques suffer from interference of any other surface active substances (Cosović and Vojvodić, 1982). Although different adsorbing properties at different pH have recently been used to selectively measure HS over other surface active substances (Cuscov and Muller, 2015), the

quantification is indirect. Direct, selective and sensitive methods for HS determination are based on cathodic stripping voltammetry where a metal-humic complex is first adsorbed at the mercury drop surface before being reduced during the stripping step. HS determined through CSV methods are defined here as electroactive HS (eHS).

There are currently 3 CSV methods for eHS determination. The first published method is based on the formation of an electroactive molybdenum (VI)-HS complex (referred to here as eHS-Mo) in acidified (pH 1.9) seawater (Quentel et al., 1986). It was later refined to allow simultaneous determination of thiol-like compounds resembling thioacetamide and glutathione (Pernet-Coudrier et al., 2013). The second and third methods are based on the selective adsorption of electroactive Fe-HS (eHS-Fe) (Laglera et al., 2007; Sukekava et al., 2018) and electroactive Cu-HS (eHS-Cu) complexes (Whitby and van den Berg, 2015) respectively, both carried out in buffered pH 8 seawater. These 3 methods all follow a similar procedure: by saturating eHS naturally present in the sample with additions of sub µM levels of one of the 3 metals (Mo, Fe or Cu), their total concentration (i.e. [eHS-Mo], [eHS-Fe] or [eHS-Cu]) can be determined by standard addition, with Suwannee River Fulvic Acid (SRFA) being commonly used as a standard. The methods are sufficiently sensitive (LOD in the range of low $\mu g.L^{-1}$) to measure natural levels of eHS throughout the marine environment. Using the CSV techniques, eHS have been quantified in estuaries (Laglera et al., 2007; Riso et al., 2021; Waeles et al., 2013; Whitby et al., 2017; Whitby and van den Berg, 2015), coastal waters (Bundy et al., 2014; Laglera et al., 2007; Waeles et al., 2013; Whitby and van den Berg, 2015), and in surface and deep waters of the open ocean (Dulaquais et al., 2018b; Fourrier et al., 2022; Laglera et al., 2019; Laglera and van den Berg, 2009; Slagter et al., 2019, 2017; Whitby et al., 2018). eHS concentrations vary from thousands of $\mu g.L^{-1}$ in estuarine conditions down to tens of $\mu g.L^{-1}$ in the open ocean and have been estimated to represent 2-5% of the DOC (Dulaquais et al., 2018b; Laglera and van den Berg, 2009). While eHS is only a small fraction of the humic-like pool that represents 30-50% of the DOC (Fourrier et al., 2022; Zigah et al., 2017) its contribution to the complexation of Fe can be high (e.g. (Laglera et al., 2019; Whitby et al., 2020b)).

Few studies have compared HS concentrations determined by different methods. Comparison of eHS with HS concentrations determined by UV absorbance were in good agreement (within 15%) for both eHS-Fe (Laglera et al., 2007) and eHS-Cu (Whitby and van den Berg, 2015), suggesting that these 3 techniques are mainly sensitive to the same humic pool, however comparisons to fluorescence techniques showed very different humic profiles (Whitby et al., 2020b). The first direct comparison of electrochemical methods was reported between eHS-Fe and eHS-Mo in the river Mersey and coastal waters from Liverpool Bay (Laglera et al., 2007). This preliminary study found that both methods gave similarly high eHS concentrations in freshwater, but in coastal seawater, [eHS-Mo] were significantly higher than [eHS-Fe] (up to 10 times higher). On the other hand, excellent agreement between eHS-Fe and eHS-Mo was obtained in a variety of samples collected from open ocean (Atlantic and Pacific) and coastal waters (Dulaquais et al., 2018b). Similarly, levels detected by eHS-Cu agreed well with eHS-Fe in both coastal and open ocean locations (Abualhaija et al., 2015; Whitby et al., 2020a). This is in general agreement with the observation that Fe and Cu compete for at least some of the same binding sites of humic substances (Abualhaija et al., 2015; Yang and van den Berg, 2009).

All 3 methods are based on cathodic stripping voltammetric measurements where the analyte is first accumulated at the electrode surface at a specific potential (i.e. the deposition potential (E_{dep})) before being detected during the stripping scan. Each method also uses the method of standard addition where known concentrations of standard are added to the solution, allowing quantification of the original signal. This is a powerful technique when analytes and standard are identical but when this is not the case, the reported value is very much technique-dependent. In most work, the SRFA standard is used because it is the most characterised HS. It is extracted from a river and thus more representative of terrestrial environments where the composition, structure, adsorbing and complexing properties are likely different to marine-derived HS. A key difference between marine and terrestrial HS is the presence of lignins and tannins. Lignins are organic phenolic polymers that are abundant in plant cell walls. They are important in the growth and development of plants (Liu et al., 2018). Tannins are phenolic compounds, they are found in plant leaves, fruit, roots and wood. They

are used as a plant defence mechanism against grazers (Hassanpour et al., 2011). Both of these compounds are only present in terrestrial HS as they are derived from plants (Shevchenko and Bailey, 1996). There are also similarities between marine and terrestrial HS. Marine HS are comprised of complex paraffinic structures, which are major components in some terrestrial HS. The majority of HS produced in terrestrial environments are of microbial origin, which may account for similarities between marine and terrestrial HS (Hatcher et al., 1981).

Pseudopolarography, also called scanned stripping voltammetry, is a technique that uses the variation of the intensity of the signal of interest at varying E_{dep}. The technique has been used in anodic stripping voltammetry for metals such as Cu, Cd and Pb (Bi et al., 2013a, 2013b; Gibbon-Walsh et al., 2012; Tsang et al., 2006). It allows the estimation of the presence and potential origins of different classes of complexes, their stability constants and concentrations based on the number, potential and intensity of reduction waves. Cathodic pseudopolarography has only been used to differentiate between the presence of various thiols in marine waters by comparing the pseudopolarograms to those obtained with model compounds (Laglera and Tovar-Sánchez, 2014). The use of pseudopolarography for the characterisation of HS has to our knowledge so far not been reported. Similarly, the effect of the E_{dep} on the determination of eHS concentration by CSV has never been carefully assessed. Although concentrations are determined by the standard addition method, different concentrations will be obtained at different E_{dep} if the adsorbing and complexing characteristics of the standard are different from those of the natural eHS present in the water sample.

While two methods have been compared on a few samples (eHS-Fe with eHS-Cu along a salinity gradient (Whitby et al. 2015; Abualhaija et al. 2015) and in open ocean samples (Whitby et al. 2020), or eHS-Fe with eHS-Mo on coastal and open ocean samples (Laglera et al., 2007; Dulaquais et al., 2018b), such a detailed comparison of the 3 published CSV methods for the determination and voltammetric characterisation of HS concentrations has not been reported on the same samples to date. Here, we present such comparison in open ocean samples collected at various depths at one

oligotrophic station located in the western tropical South Pacific (WTSP). For each method, we also present the pseudopolarograms obtained in surface and bottom waters in comparison to that of the terrestrial standard SRFA. We determined the range of concentration (unit of µg. eq SRFA.L^{-1}) of each method, depending on the E_{dep} chosen for the standard addition procedure. In addition, we also present a comparison of HS concentrations determined by the Fe and Mo CSV methods along the entire Tonga transect (9 stations, 104 samples), i.e. water samples collected in the Melanesian, Lau basin and South Pacific Gyre. The experiments were carried out independently by two different laboratories but using the same SRFA standard for quantification. eHS-Mo and eHS-Cu were quantified at the University of Liverpool (UK) and eHS-Fe at "Laboratoire des sciences de l'Environnement Marin" (LEMAR, Fr).

2.2. Experimental

2.2.1. Sampling

The GPpr14 GEOTRACES TONGA cruise took place in the Western Tropical South Atlantic (WSTP) in January 2019 (Figure 2.1). Seawater samples were collected using a trace metal clean rosette (TMR, General Oceanics Inc. Model 1018 Intelligent Rosette), attached to a 6 mm diameter Kevlar line. After collection, Go-Flo bottles were transferred into a clean container for sampling. The seawater was filtered on-line through 0.45 µm using a polyethersulfone filter (Supor®), and collected in 60 mL Nalgene bottles, which were acid-cleaned according to GEOTRACES protocol (Cutter et al., 2017). Samples were immediately frozen at -20°C until analysis.

At station 8, 12 samples collected at various depth (Figure 2.1) were analysed by the 3 CSV methods, while at 6, only surface and deep waters samples were analysed. A total of 104 samples collected at various stations located in the adjacent Lau Basin and Melanesian waters and they were analysed for both eHS-Mo and eHS-Fe; eHS-Cu were not determined in those samples. The hydrography of the

Western Tropical South Pacific Ocean (WTSP) during November 2019 is described in detail in Chapter 3, section 3.3.1.

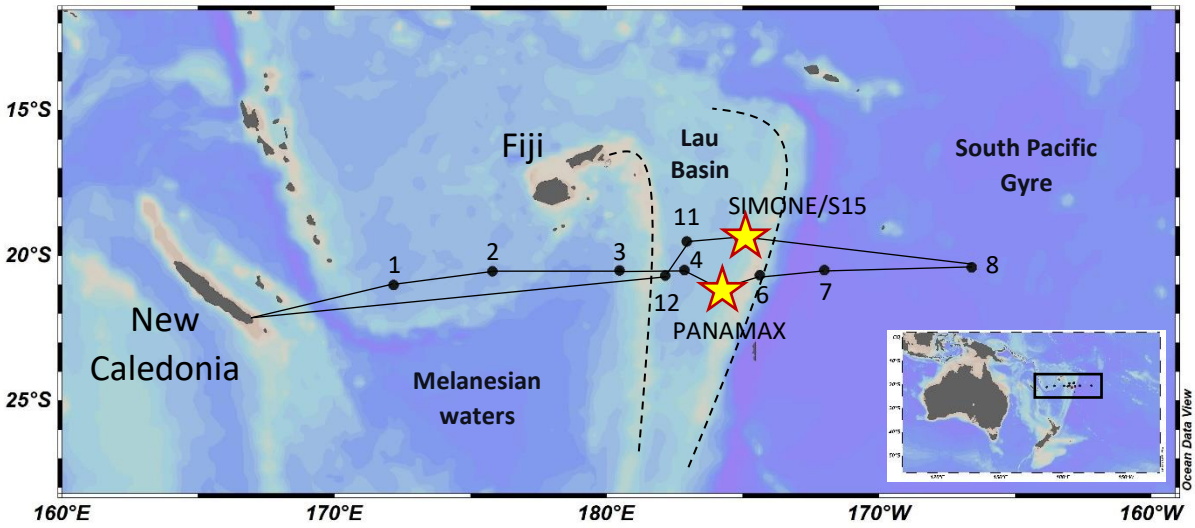

Figure 2.1. *Map of stations sampled during the TONGA 2019 (Grp14) cruise across the Western Tropical South Pacific Ocean (WTSP). Panamax and Simone were the two shallow hydrothermal vents. The cruise started and ended in New Caledonia. The black lines represent the cruise track. Black dashed lines separate the different oceanographic regions. Figures were generated using ODV software (Schlitzer, 2021).*

2.2.2. Voltammetric equipment

In both Liverpool and Brest, a potentiostat µAutolabIII was connected to a Metrohm 663 VA stand through the IME663 interface and was controlled by NOVA (version 2.1.4) or by GPES (Version 4.9) software. The working electrode was a hanging mercury drop electrode (HMDE), the reference electrode was Ag/AgCl with a glass salt bridge filled with 3 M KCl, and the counter electrode was a glassy carbon rod. Solutions were stirred (setting 4 on the VA stand) during the deposition step by a rotating polytetrafluoroethylene (PTFE) rod. In Liverpool, an automatic sampler was connected to the VA stand, allowing automatic loading, rinsing and emptying of the voltammetric cell. Standard additions were made automatically using Cavro syringe burettes. After each standard addition, the voltammetric cell was rinsed twice with MQ water for 30 s before loading of the next sample. In Brest, samples were loaded and standard additions performed manually.

2.2.3. Reagents

2.2.3.1. Liverpool

All solutions were prepared using ultrapure deionized water (>18 MΩ) from a Milli-Q system (Millipore, UK). Cu (BDH) and molybdenum (Fisher Scientific) standard solutions (10 µM) were prepared by appropriate dilution of 1g.L^{-1} atomic absorption spectroscopy standard solutions and acidified with 10 mM HCl (12M). A pH buffer of 1M boric acid (Analytical grade, Fisher Scientific) was prepared in 0.35M ammonia (trace metal grade, Fisher Scientific) and UV-digested for 45 minutes to remove organic contaminants. It was cleaned from trace metals by the addition of 100 µM MnO_2 (van den Berg, 1982) for several hours followed by filtration (0.2 µm cellulose nitrate membrane, Whatman) on the following day. This cleaning operation was repeated twice. Fulvic acid (FA) from the Suwannee River (International Humic Substances Society, 2S101F) was dissolved in MQ to a concentration of 10 mg.L^{-1}. Deep Sea Reference (DSR) seawater (Batch 20 – 2020 – Lot 08-20 and Batch 21 – 2021 – Lot 08-18) with certified DOC concentrations of 44-46 µM were obtained from Hansell laboratory in Miami. This water was collected at 700 m depth in the Florida Straits, acidified with HCl to pH 2. SRFA standard and DSR samples were kept in the dark at all times and in the fridge when not in use.

2.2.3.2. Brest

All solutions and cleaning procedures used ultrapure water (resistivity > 18.2 MΩ.cm^{-1}, MilliQ Element, Millipore®). An acidic solution (HCl, 0.01 M, Suprapur®, >99%) of 1.24 µmol L^{-1} Fe (III) was daily prepared from a stock solution (1 g L^{-1}, VWR, Prolabo, France). The borate buffer (H_3BO_3, 1M, Suprapur®, Merck, Germany, 99.8%) was prepared in 0.4 M ammonium solution (NH_4OH, Ultrapure normatom, VWR Chemical, USA, 20-22%). The potassium bromate solution ($KBrO_3$, 0.3 M, VWR Chemical, USA, ≥ 99.8%) was prepared in ultrapure water. Suwannee River Fulvic Acids (SRFA, 1S101F) were purchased at the International Humic Substances Society (IHSS). The SRFA standard stock

solution (22.86 mg SFRA L^{-1}) was prepared in ultrapure water and saturated with Fe according to its Fe binding capacity in seawater determined by Sukekava et al., 2018. Saturated SRFA solution equilibrated overnight before its use. Exact concentration of the SRFA stock solution was determined by size exclusion chromatography analysis (Dulaquais et al., 2018a).

2.2.4. Voltammetric determination of eHS

2.2.4.1. eHS-Mo Method

The voltammetric method was based on Pernet-Coudrier et al. (2013) but was adapted to include a background subtraction to increase sample throughput by decreasing detection limits while keeping the same deposition time as the original method (150 s) (Figure 2.2). Briefly, under a laminar flow hood, aliquots of seawater (8 mL) were pipetted into an acid-cleaned quartz voltammetric cell. The solution was spiked with 30 µL of 10 ppm Mo(VI), corresponding to [Mo(VI)] added of 375 nmol L^{-1}. The sample was then acidified to pH 2, and 300 s N_2 purge was applied. The analytical scan consisted of the application of a E_{dep} of 0 V applied for 150 s. The stirrer was on during the deposition and stopped during the 5 s equilibration step. Stripping was done in differential pulse mode, initiated at 0 V and terminated at -0.65 V with a modulation time of 60 ms, a modulation amplitude of 50 mV, a step potential of 2 mV and an interval time of 0.1 s. Because the eHS-Mo signal is present on a slightly curved baseline, background subtraction was applied by recording a background scan (using the same parameters as the analytical scan but with a 1 s deposition time) at the start of the standard addition procedure. This unique background scan was subtracted from all analytical scans (sample + standard additions) to give background-subtracted scans. The peak height of each background-subtracted voltammogram was quantified using ECDsoft. Smoothing was also applied (Savitsky-Golay, smoothing factor 10). The standard addition procedure consisted of a minimum of 4 repeat scans for the sample and each of the 2 standard additions of 40 µg eq SRFA.L^{-1}.

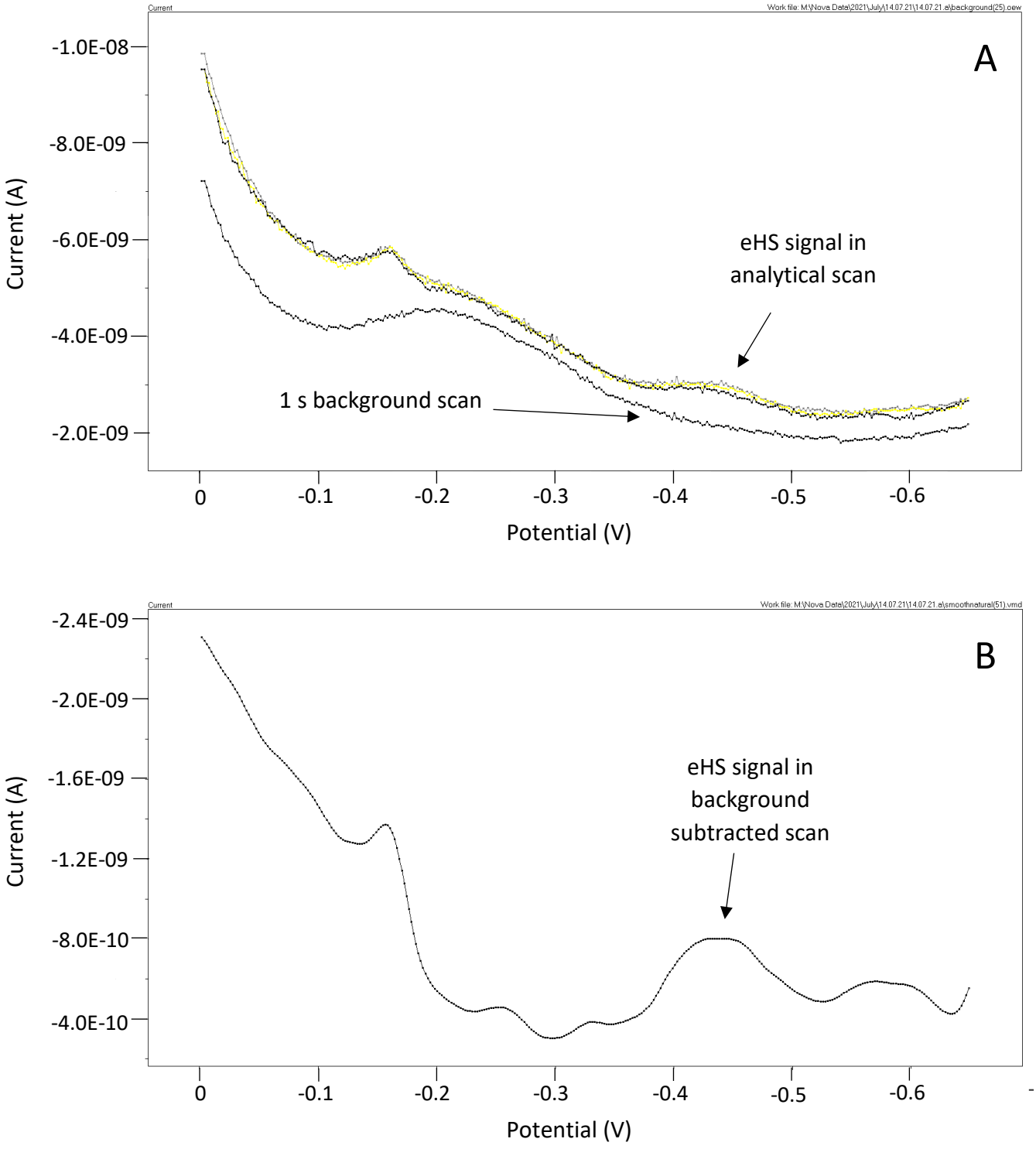

Figure 2.2. *(A) Cathodic stripping voltammogram of an analytical scan and a 1 s background scan using the Mo method (Pernet-Coudrier et al., 2013). Background scan used the same analytical parameters as the analytical scan but with a 1s deposition time. Analytical scan shows a small eHS-Mo signal. The 1 s background scan was used for background subtraction. Background subtraction was performed to flatten out the baseline, as the background is slightly curved. (B) is a background subtracted scan. background subtracted scan shows a larger eHS-Mo signal. This peak (between -0.35 V and -0.55 V) was used for the quantification of eHS.*

2.2.4.2. eHS-Cu Method

The method used here was originally published by Whitby et al. (2015). Under a laminar flow hood, aliquots of seawater (8 mL) were pipetted into an acid-cleaned quartz voltammetric cell. The concentration of eHS-Cu was determined using CSV in the presence of a 10 mM borate buffer (final pH 8.1) and excess Cu (30 nM). Briefly, following a 300 s purge with N_2 gas, a E_{dep} of +0.05 V was applied for up to 150 s, depending on the concentration of HS. After deposition, a 9 s quiescence time was imposed, followed by a 1 s potential jump to -0.2 V to remove any interference from iodide. The stripping scans were initiated at 0 V and terminated at -0.75 V using the differential pulse mode. Instrument settings were as follows: a modulation time of 40 ms, modulation amplitude of 50 mV, a step potential of 5 mV, and an interval time of 0.1 s. The eHS-Cu peak was present at a potential around -0.2 V. At the start of the sample analysis, a 1s background scan was carried out and subtracted from all subsequent analytical scans. This was carried out to remove the response for inorganic Cu and flatten the baseline. The concentration of eHS-Cu was quantified by the method of standard additions. For each sample, two additions of 40 µg eq SRFA.L^{-1} were made with 4 measurements per addition. The peak height of each background-subtracted voltammogram was quantified using ECDsoft. Smoothing was also applied (Savitsky-Golay, smoothing factor 10).

2.2.4.3. eHS-Fe Method

The method used here was initially developed by Laglera et al. (2007) and adapted by Sukekava et al. (2018). The concentration of eHS-Fe was determined using CSV in the presence of $KBrO_3$. $KBrO_3$ was added to the sample to act as an oxidant to boost the dissociation current of the Fe-eHS complex. In this study, the pH of samples was set to 8.00 ± 0.05 by adding a borate buffer (final concentration 10 mM) and adjusted with small additions of an ammonia solution. The concentration of Fe-HS was determined after the addition of 20nM Fe to saturate HS naturally present in the sample. After equilibration, aliquots (15 mL) of the sample were placed into three different teflon vials (Savillex ®); among them, two were spiked with a SRFA standard (2S101F; 50 and 100 µg L^{-1}). After overnight equilibration, samples were placed into a teflon voltammetric cell. Samples were purged (180 s of N_2; Alphagaz®, Air Liquide). An E_{dep} of -0.1 V was applied for up to 90 s. After the E_{dep} the stripping scans were initiated at 0 V and terminated at -0.8 V using the linear sweep mode, with a scan rate of 50mVs^{-1}. The eHS-Fe peak was present at a potential of around -0.5 V. For each aliquot, three voltammetric analyses were performed.

2.2.5. Pseudopolarography

The methods used for pseudopolarography of eHS were Pernet-Coudrier et al. (2013) (eHS-Mo), Laglera et al. (2007) (eHS-Fe), and Whitby et al. (2014) (eHS-Cu). Each pseudopolarogram was built up of a series of voltammetric scans where the eHS peak height was measured at various E_{dep}, creating a 'fingerprint' of the eHS in the seawater. Pseudopolarograms started at an E_{dep} of 0 V (eHS-Fe) or +0.1 V (eHS-Cu, eHS-Mo). The E_{dep} decreased by increments of -0.05 V or -0.1 V until the eHS peak was no longer visible. The deposition time was 150 s for the Cu and Mo procedures while 90 s was used for the Fe method. As pseudopolarography was used here only for qualitative purposes, only the eHS-Cu method required background subtraction to remove the inorganic Cu peak (as described in the published method). Pseudopolarograms of SRFA standards were carried out for each method to compare with the eHS found in seawater. Analysis of SRFA was carried out in UV-digested seawater

(UV-SW). UV-SW was prepared by 3 h irradiation in acid cleaned 30 mL quartz tubes with a 125 W high pressure mercury lamp (van den Berg, 2014).

2.2.6. Statistics

Concentrations of humics were measured using the standard addition procedure with the SRFA standard. Results are thus all provided in eq SRFA.L^{-1}. Error bars given show the standard deviation of the intercept, determined for each standard addition using Equation 1 (Harris, 2003).

$$s_x = \frac{s_y}{|\mathrm{m}|}\sqrt{\frac{1}{n} + \frac{\bar{y}^2}{m^2\ \sum(x_i - \bar{x})^2}} \qquad \text{Equation 1.}$$

Where s_x is the standard deviation of eHS, s_y is the standard deviation in peak intensity across all data points, m is the slope of the standard addition, n is the number of data points, $\bar{y}$ is the average peak height across all data points, x_i is the concentration of added humic for data point i, and $\bar{x}$ is the average concentration of humics across all data points of the standard addition procedure.

Statistics to compare the eHS concentrations obtained by the three CSV methods at station 8 were carried out using a non-parametric Wilcoxon signed rank two-tailed test for dependent sample due to the low sample size (N=12). A paired two-tailed t-test was used to assess any differences between eHS-Fe and eHS-Mo across the entire dataset (N=104).

2.3. Results

2.3.1. Analytical parameters

2.3.1.1. Importance of background subtraction

The eHS-Mo method presented by Pernet-Coudrier et al. (2013) suggested to use a E_{dep} of 0 V for 150 s without any background subtraction. In our case, we found that the background subtraction was necessary because for eHS-Mo, the eHS signal is present on a slightly curved baseline. The

concentration determined with background subtraction was consistently higher than without, but the increase was found to vary depending on the water sample being analysed (Table 2.1). For the DSR sample, the [eHS-Mo] increased by 8% with background subtraction, whereas Station 6 deep water increased by 23%. The most significant difference in [eHS-Mo] was in Station 6 surface water, which showed a 39% increase. Background subtraction was also applied for the eHS-Cu method to remove interference from inorganic Cu, as suggested in the original paper (Whitby and van den Berg, 2015).

Water	eHS-Mo ($\mu g.L^{-1}$) Background subtraction	eHS-Mo ($\mu g.L^{-1}$) No background subtraction
Deep Sea Reference (700m)	21.19 ± 3.20	19.35 ± 3.51
Station 6 deep (1,041m)	31.04 ± 2.53	23.86 ± 2.08
Station 6 surface (25m)	70.96 ± 8.4	43.03 ± 4.99

Table 2.1. *Comparison of the concentration of eHS-Mo obtained with and without background subtraction. The three water sources were used; Deep Seawater Reference sample (Hansell lab, Batch 21), Station 6 surface (25 m) and deep waters (1.041 m) (Latitude: 20.687S, Longitude: 174.379W). Error represent the average standard deviation of the standard additions.*

The [eHS-Mo] with and without background subtraction was also compared to the [eHS-Cu] using an internal reference (SCALE Underway fish, Southern Ocean, 49°20S 03°31'E) (Table 2S1). Without background subtraction, [eHS-Mo] was 16.55 ± 1.61 $\mu g.L^{-1}$ (N=5). When background subtraction was applied [eHS-Mo] increased to 38.84 ± 0.79 $\mu g.L^{-1}$ (N=5). This was similar to the [eHS-Cu] 41.92 ± 1.53 $\mu g.L^{-1}$ (N=5). These tests suggest that when measuring eHS-Mo, background subtraction is required for quantifying eHS, which is not commonly done.

2.3.1.2. Limit of detection

The limit of detection (LOD) was determined for the three electrochemical methods (Table 2.2) using E_{dep} of 0, +0.05 and -0.1 V for the Mo, Fe and Cu methods respectively. For eHS-Cu and eHS-Mo, seawater was UV digested to remove any organics in the solution, ensuring a contamination-free analytical procedure. Low levels of SRFA (eHS-Mo (8 $\mu g.L^{-1}$); eHS-Cu (20 $\mu g.L^{-1}$)), were then added to

the UV seawater and the detection limit was calculated as 3 times the standard deviation of repeated scans (minimum of 7). For eHS-Fe, the LOD was defined as three times the standard deviation of the lowest concentration measured (23.2 ± 3.0 µg eq-SRFA L^{-1}) and was estimated to be 9 µg eq-SRFA L^{-1} for a deposition time of 90s.

	eHS-Mo ($\mu g.L^{-1}$)	eHS-Fe ($\mu g.L^{-1}$)	eHS-Cu ($\mu g.L^{-1}$)
Limit of detection	3 (N=10)	9 (N=7)	9 (N=10)

Table 2.2. *The limit of detection (LOD) for the eHS-Cu, eHS-Mo and eHS-Fe methods. E_{dep} and deposition time are as follows: eHS-Mo, 0 V for 150 s. eHS-Fe, -0.1 V for 90 s. eHS-Cu, +0.05 V for 150 s. N represents the number of repeats.*

The reproducibility of the eHS-Mo method was estimated by performing 5 repeat measurements using standard additions of SRFA on Deep Seawater Reference (DSR) sample (Hansell lab, Batch 2019/20). The average concentration determined using E_{dep} = 0 V was 22.9 ± 1.4 $\mu g.L^{-1}$, giving a reproducibility of ~ 6.2%. The DSR was not measured with the eHS-Cu method due to a broad interference at the same position as the eHS-Cu peak (Figure 2.3). Because of this, SCALE water (SCALE Underway fish, Southern Ocean, 49°20S 03°31'E, mean eHS concentration 40.4 $\mu g.L^{-1}$) was used as an internal reference water. The SCALE in-house reference material was measured at the start of each day and showed good reproducibility during the course of the experiment (Table 2S2).

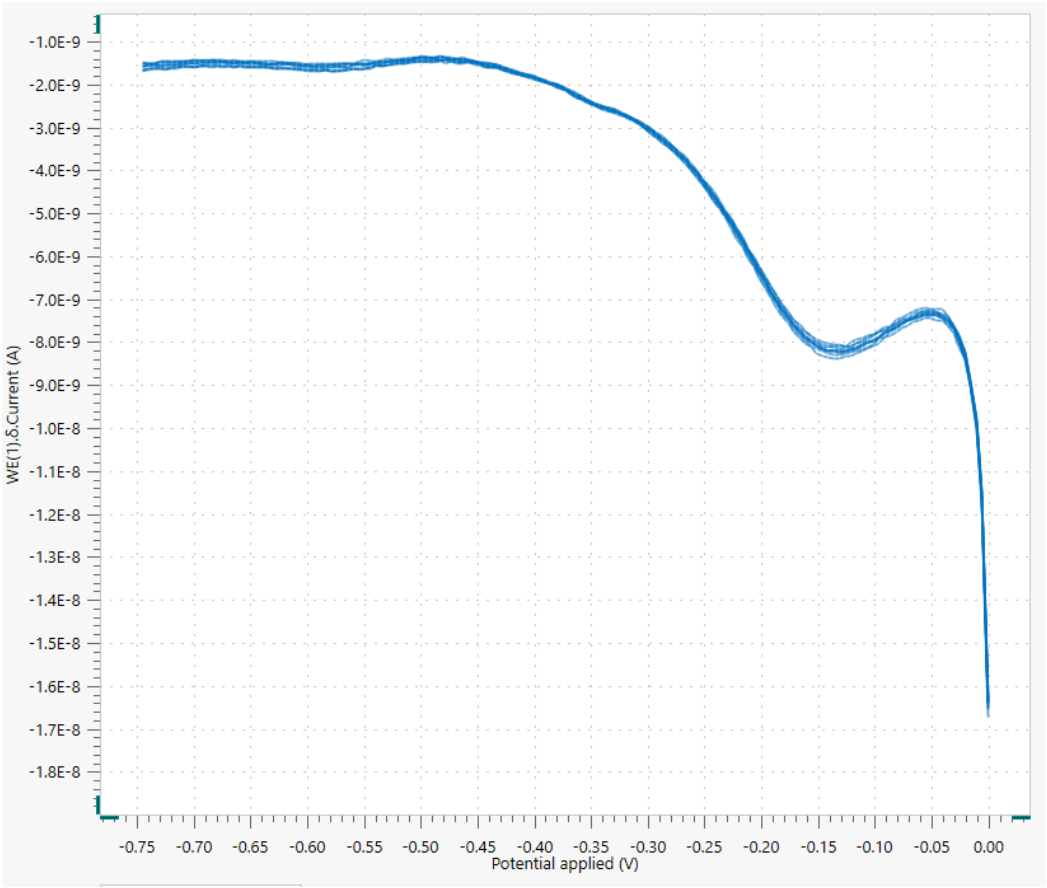

Figure 2.3. *Cathodic stripping voltammogram of the Deep Seawater Reference sample (Hansell lab, Batch 2019) after 30s deposition time using the eHS-Cu method. A large broad peak was in the same position as the eHS-Cu peak. Three additions were made, and there was no linear increase therefore, eHS-Cu could not be measured.*

2.3.2 Effect of deposition potentials

Preliminary experiments were first carried out in surface and bottom water samples from station 6 to visualise the effect of changing the deposition potential on the concentration of eHS being detected by the eHS-Mo procedure using the method of standard addition with SRFA. For both samples, when decreasing E_{dep} from 0 to -0.4 V, the concentrations obtained increased significantly (Figure 2.4A). In the surface water, the concentration increased from 71.0 ± 8.4 µg eq SRFA.L^{-1} (E_{dep}=0 V, N=1) to 122.4 ± 3.1 µg eq SRFA.L^{-1} (E_{dep}=-0.4 V, N=3), an increase of more than 60% of the original signal. In the bottom sample, the concentration increased even more, from 31.0 ± 2.5 µg eq SRFA.L-1 (E_{dep}=0 V, N=2) up to 107.9 ± 8.1 µg eq SRFA.L^{-1} (E_{dep}= -0.4 V, N=2), an increase of more than 350%. It is important to note that the sensitivities of the standard additions were very similar between surface and bottom

water samples (Figure 2.4B) at all the E_{dep} tested here showing that the matrix effect was the same for both samples. It also shows that a maximum sensitivity is obtained at E_{dep} between -0.4 and -0.2 V and that the sensitivity obtained at E_{dep} = 0 V is approximately twice lower.

The influence of the E_{dep} on eHS-Mo was also tested in the DSR (Hansell lab, batch 21). Here, [eHS-Mo] increased from 25.9 ± 2.2 µg eq SRFA.L^{-1} (N=10) to 55.4 ± 1.3 µg eq SRFA.L^{-1} (N=2) when using E_{dep} of 0 and -0.25 V respectively. It is, therefore, apparent that the choice of the E_{dep} affects the concentration of eHS being detected. In the samples tested here, higher eHS-Mo concentrations are obtained when decreasing E_{dep} from 0 down to -0.4 V. For comparison the [eHS-Fe] in the DSR was 54 ± 4 µg eq SRFA.L^{-1} (Dulaquais et al., 2018b).

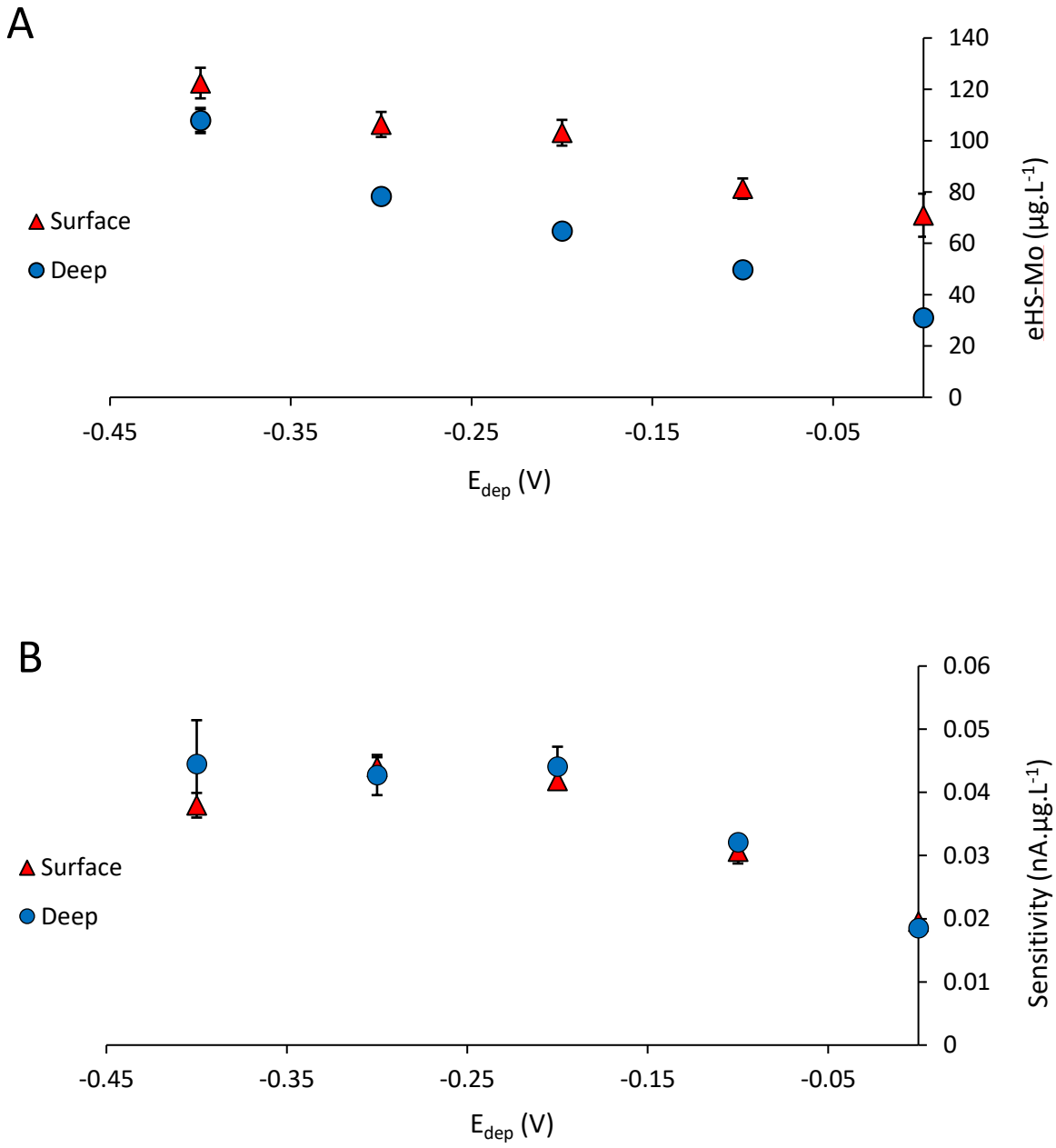

Figure 2.4. *(A) Influence of E_{dep} on (A) the concentration of eHS-Mo (equivalent of µg Suwannee River fulvic acid (SRFA).L^{-1}) determined by standard addition and on (B) the sensitivity of the standard additions (i.e. slope of SRFA signal). Each data point is the average of 3 (surface water) or 2 (deep water) standard additions apart for E_{dep} = 0 V, where only one standard addition was made. Error bars represent the standard deviation of the standard additions. Background subtraction scans (sample + standard additions) were used for the quantification of eHS-Mo. Samples were from station 6 of the TONGA 2019 cruise.*

Following these preliminary observations, pseudopolarograms of SRFA obtained in UV digested seawater were obtained and compared to pseudopolarograms of surface and bottom waters collected

at station 8 (Figure 2.5). Each pseudopolarogram was normalised to its highest peak current signal (i/i_{max}). Firstly, the shape of the pseudopolarograms were very different between methods. For eHS-Mo, a signal was obtained across a very wide range of deposition potentials, from 0 V down to at least -1.2 V for both the samples and SRFA standard. The range for eHS-Fe was from 0 V (most positive value tested) to -0.7 V for the SRFA standard and to -0.5 V for the natural samples. For eHS-Cu, the range was narrower, from 0.05 V down to -0.4 V for the SRFA and to -0.2 V for the natural samples. While the overall shape of the pseudopolarograms is similar for natural samples and SRFA using the molybdenum method, the shape of the respective pseudopolarograms for eHS-Cu and eHS-Fe were found to be very different between deep/surface and SRFA added to UV digested seawater. For the Cu method, maximum sensitivities (as seen by the peak height) of the surface, bottom and SRFA samples were obtained at deposition potentials of +0.05 V, +0.05 V and -0.05 V respectively, in general agreement with the E_{dep} of +0.05 V found as the optimum in the original method (Whitby and van den Berg, 2015). For the Fe method, maximum sensitivities of the surface, bottom and SRFA samples were -0.05 V, -0.1 V and -0.15 V respectively, in general agreement with the E_{dep} of -0.1 V found as optimum in the original method (Laglera et al., 2007). For the Mo method, all samples reached a maximum sensitivity at E_{dep} in the range of -0.3 to -0.45 V. This is also similar to the optimum E_{dep} (E_{dep}=-0.3 V) suggested in the original study (Quentel et al., 1986) but different to the E_{dep} (E_{dep}=0 V) suggested for the simultaneous determination of eHS, glutathione and thioacetamide like compounds (Pernet-Coudrier et al., 2013).

Figure 2.5 compares the normalised peak intensities between natural samples and SRFA standard varies with E_{dep} suggesting that the concentrations determined by the standard addition method will also vary according to this ratio, i.e. depending on the E_{dep}. Figure 2.6 presents the range of concentrations determined by standard addition at various E_{dep} for each voltammetric method. For eHS-Cu, E_{dep} of +0.05 and -0.05 V were chosen. For eHS-Fe methods, E_{dep} of 0, -0.1, -0.15, -0.25, -0.35 and -0.45 V were tested while for the eHS-Mo method, E_{dep} of 0, -0.25, -0.5 and -0.75 V were used.

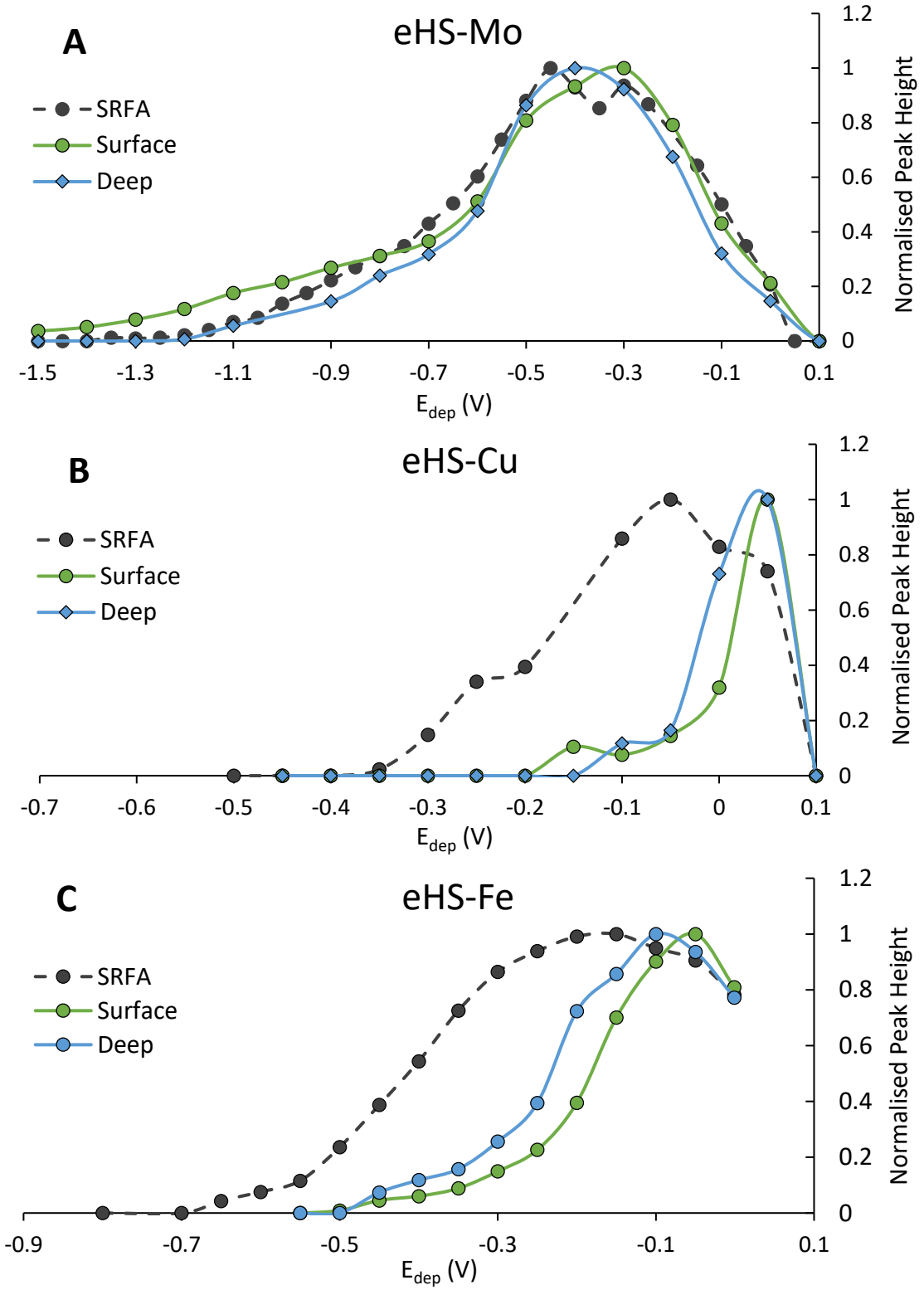

Figure 2.5. *Pseudopolarograms of the surface and deep water from station 8 using the different voltammetric methods with Suwannee River fulvic acid (SRFA) standard in UV digested seawater. (A) Pernet-Coudrier et al. (2013) (eHS-Mo method), (B) Whitby et al. (2014) (eHS-Cu method) and (C) Laglera et al. (2007) (eHS-Fe method). Concentration of SRFA standard are as followed; eHS-Mo (96 µg.L^{-1}), eHS-Cu (32 µg.L^{-1}) and eHS-Fe (84.4 µg.L^{-1}). Each point represents the peak height of the eHS signal. Peak height has been normalised to the highest peak value (=peak height/largest peak height).*

Large variations in concentrations were obtained for all methods when the E_{dep} was changed. For eHS-Mo, the highest and lowest concentrations were obtained at E_{dep} = -0.5 and 0 V respectively, in general agreement with results presented in Figure 2.4, where a decrease of deposition potentials in that range result in higher concentrations of humics being detected. Further decrease to E_{dep} = -0.75 V resulted in lower eHS concentrations. Large variations were also observed with the eHS-Fe method: the highest concentrations were obtained at -0.1 V and the lowest at -0.45 V. At this latter E_{dep}, a signal was detected in the shallower sample (25 m depth), no signal was detected at depth shallower than ~1,000 m before then increasing with depth. For eHS-Cu, an increase in [eHS] of almost 100% was observed when decreasing the E_{dep} by only 0.1 V, from +0.05 V down to -0.05 V. However, although eHS concentrations are clearly dependent on the E_{dep}, the overall shape of each profile is similar with higher concentrations being generally detected at the surface in the mixed layer (note that the Cu profile does not have an eHS value for the 25 m sample), a decrease in the AAIW, followed by a small increase in the middle of the PDW before another slight increase in the LCDW.

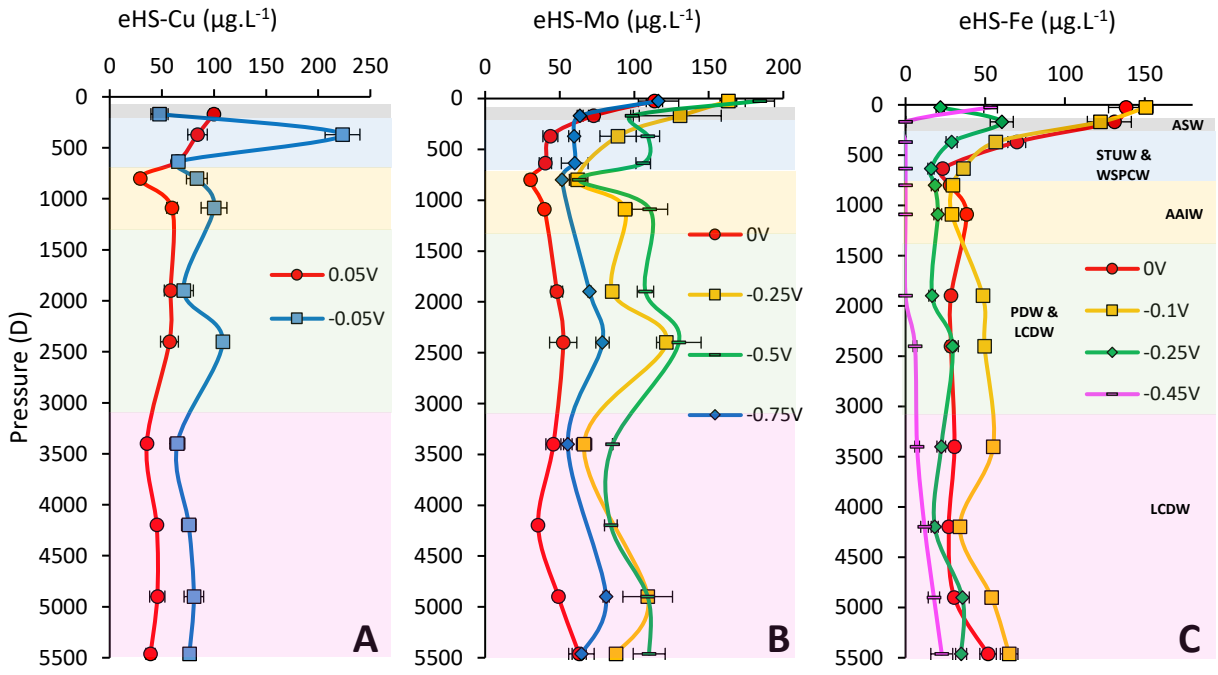

Figure 2.6. *eHS profiles using various E_{dep} using A) eHS-Cu, B) eHS-Mo and C) eHS-Fe method. Error bars represent the standard deviation of the intercept obtained for each individual standard addition. Colour blocks show the different water masses. Artifactual Surface Water (ASW), Subtropical Underwater (STUW), Western South Pacific Central Water (WSPCW), Antarctic Intermediate Water (AAIW), Pacific Deep Water (PDW) and Lower Circumpolar Deep Water (LCDW).*

2.3.3. Comparison of eHS-Mo, eHS-Fe and eHS-Cu at station 8

Figure 2.7 compares the eHS concentration profiles obtained by each method when using the published suggested deposition potential, i.e. +0.05 V for eHS-Cu (Whitby and van den Berg, 2015), -0.1 V for the eHS-Fe (Laglera and van den Berg, 2009; Sukekava et al., 2018) and 0 V for eHS-Mo (Pernet-Coudrier et al., 2013). The overall shape of the profile is the same: higher concentrations (up to 120-150 $\mu g.L^{-1}$) are detected at the surface, decreasing with depth down to 30 $\mu g.L^{-1}$ at approximately 1,000 m before remaining rather constant in the PDW and finally slightly increasing in the LCDW to levels of ~ 60-65 $\mu g.L^{-1}$. Over the entire profile, no statistical differences were detected between methods at the 95% significance level ($p > 0.05$). However, significant differences were observed in the upper water column. For instance, at the depth of 170 m, eHS-Mo and eHS-Fe were measured at 72 and 122 $\mu g.L^{-1}$ respectively, a 60% difference. Table 2.3 presents the average concentrations with standard deviation for each method along the entire profile, at the shallower depth (above 1100 m) and deeper depths (below 1100 m). The difference between methods is given by the average of the relative standard deviation (RSD) occurring between method at each specific depth (Table 2.3). In the top layer (depths between 0 and 1,100 m), the average RSD was $25.0 \pm 3.6\%$ (n=6) while in the depths below 1,100 m, the average dropped down to $8.0 \pm 4.5\%$ (n=6) showing a much better agreement between the 3 methods in the deeper waters of the PDW and LCDW waters than in the surface waters (STUW + AAIW) (Table 2.3). Although no significant differences were observed in terms of concentrations, it is apparent that the eHS-Cu method determined the highest eHS concentration at all 4 depths above 1,100 m (Figure 2.7, Table 2.3).

Depth range	eHS-Mo ($\mu g.L^{-1}$)	eHS-Fe ($\mu g.L^{-1}$)	eHS-Cu ($\mu g.L^{-1}$)	% difference
Entire profile (n = 10)	45.8 ± 11.6	51.4 ± 27.0	59.7 ± 19.7	16.5 ± 9.7
Above 1,100 m (n = 4)	45.4 ± 16.1	54.7 ± 39.3	67.9 ± 26.5	25.0 ± 3.6
Below 1,100 m (n = 6)	49.0 ± 9.0	51.0 ± 10.1	52.8 ± 9.4	8.0 ± 4.5

***Table 2.3**: Average concentrations over the profile (note that the data do not include the concentration measured in the mixed layer as there are no eHS-Cu data at that depth) and % difference (the average RSD calculated from the RSD obtained for [eHS-Mo], [eHS-Fe] and [eHS-Cu] obtained at each specific depth).*

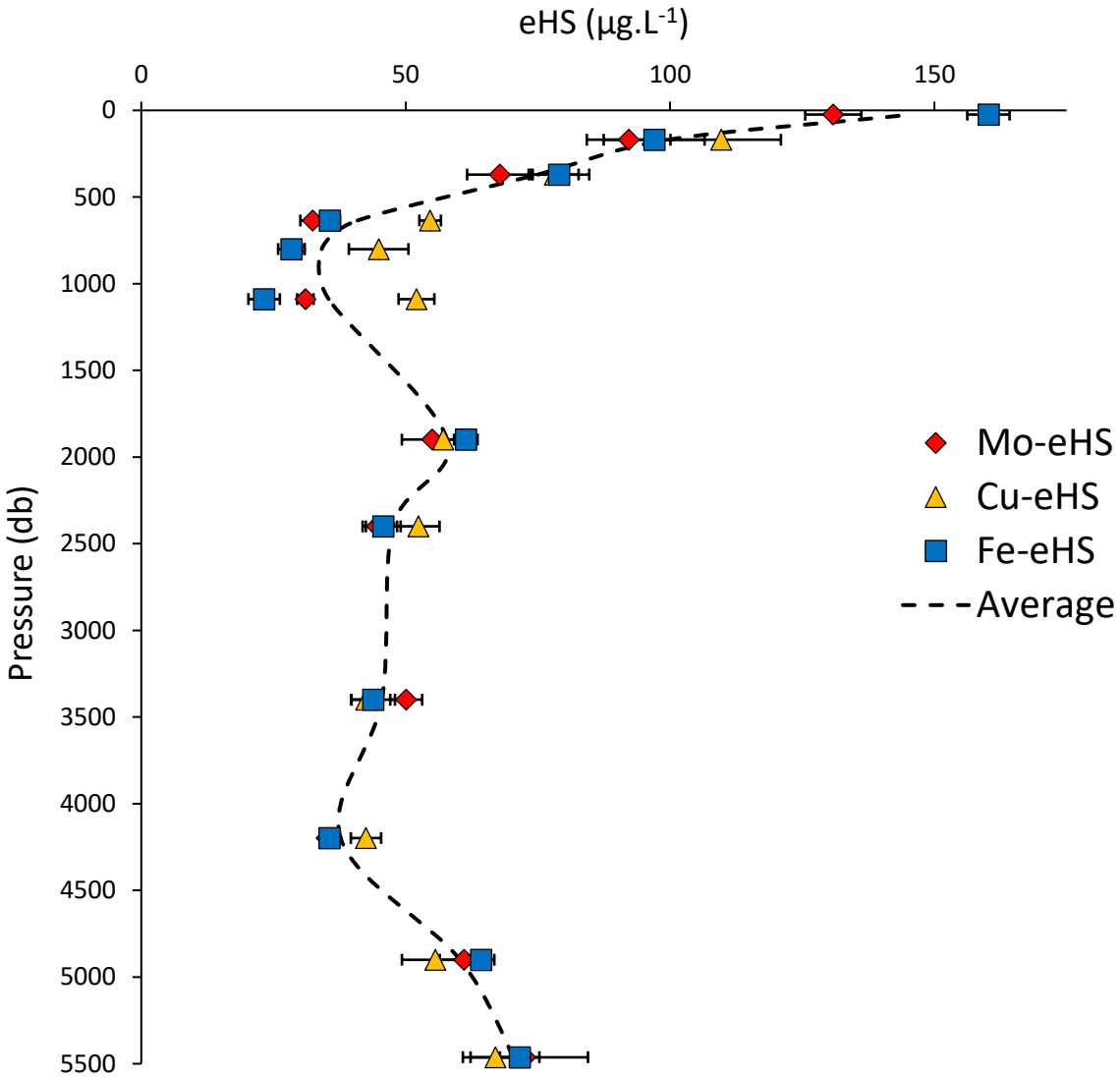

Figure 2.7. *eHS profiles at station 8 from the TONGA 2019 cruise. Concentrations determined by standard addition using published E_{dep} for each of the 3 voltammetric methods. E_{dep} are as followed; eHS-Mo (0 V), eHS-Cu (+0.05 V) and eHS-Fe (-0.1 V). Error bars represent the standard deviation of the intercept obtained for each individual standard addition. The dotted line indicates the average eHS concentration of those 3 methods.*

2.3.4. Comparison of eHS-Mo and eHS-Fe across the Tonga transect

A total of 104 samples collected during the Grp14 cruise were measured for eHS by both the Fe method (Brest) and the Mo method (Liverpool). The entire dataset gave an average concentration of 37.8 ± 19.8 and 39.2 ± 25.3 ug.eq SRFA.L^{-1} for eHS-Mo and eHS-Fe respectively; no statistical difference was apparent when running a two-tailed paired t-test between these two set of data ($P > 0.36$) and a

Pearson correlation coefficient was close to 0.8 indicating strong correlation. Nevertheless, differences as high as 250% were observed between methods (Figure 2.9). In Figure 2.9, for each station, the samples are ranked in order of decreasing depth (i.e. deep water on the left and shallow water on the right of each coloured section). The average percentage differences between [eHS-Fe] and [eHS-Mo] are given in Table 2.4. Station 6 had the largest difference between the two methods. At this station, the [eHS-Mo] almost always lower than [eHS-Fe]. At station 4, [eHS-Mo] were almost always higher than [eHS-Fe]. Station 8 had good agreement between both methods. No spatial patterns in these differences could be seen and differences were found both in surface and deeper waters (Figure 2.10).

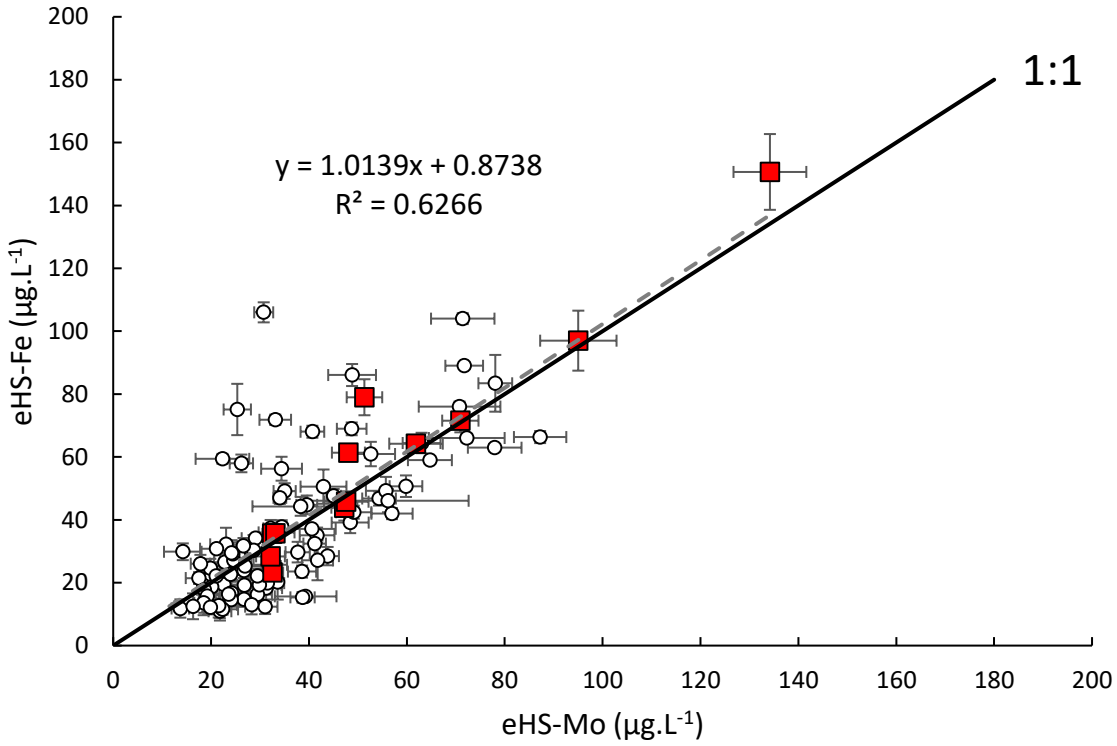

***Figure 2.8**. Comparison of the concentration of eHS-Fe vs eHS-Mo across the entire TONGA 2019 cruise transect. The deposition potentials used were recommended in the original method papers; eHS-Fe=-0.1 V (Laglera et al. (2007)), eHS-Mo=0 V (Pernet-Coudrier et al. (2013). The red squares represent the samples collected at station 8, an open ocean station. White circles represent the samples collected from the rest of the transect. These stations may have hydrothermal influence. Error bars represent the standard deviation of the intercept obtained for each individual standard addition. Grey dashed line represents the trend line from station 8. Black solid line represents the equivalence line.*

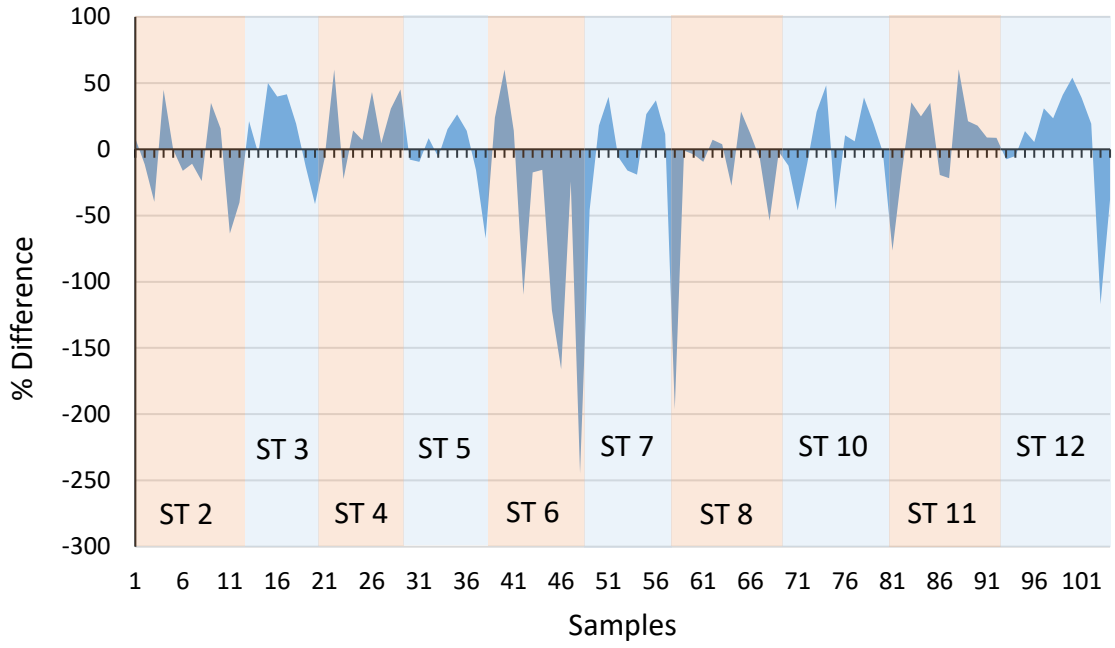

Figure 2.9. *Percentage of differences between eHS-Fe and eHS-Mo, relative to eHS-Mo for all stations. The deposition potentials used were recommended in the original method papers; eHS-Fe=-0.1 V (Laglera et al. (2007)), eHS-Mo=0 V (Pernet-Coudrier et al. (2013).*

ST2	ST3	ST4	ST5	ST6	ST7	ST8	ST10	ST11	ST12
25 ± 19 n=11	28 ± 17 n=10	26 ± 20 n=9	21 ± 18 n=9	82 ± 78 n=10	41 ± 56 n=9	14 ± 15 n=12	30 ± 22 n=11	23 ± 14 n=12	35 ± 30 n=11

Table 2.4: *Average of the percentage difference (absolute values) between eHS-Fe and eHS-Mo per stations. n represents the number of compared samples at each station.*

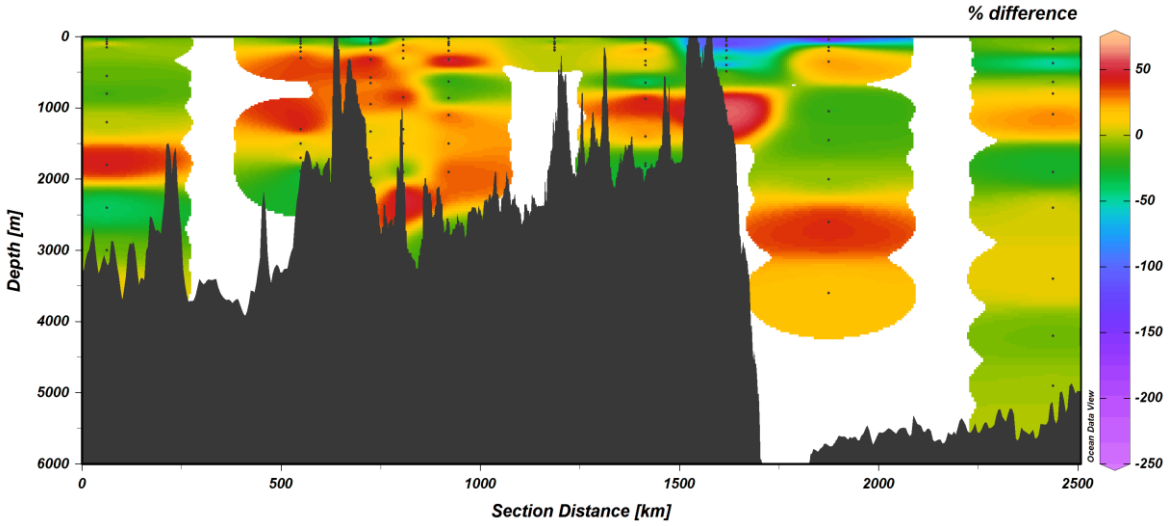

Figure 2.10. *Section plot of the percentage of differences between eHS-Fe and eHS-Mo across the TONGA 2019 cruise. Percentage of differences are relative to eHS-Mo for all stations. E_{dep} used were recommended in the original method papers; eHS-Fe=-0.1 V (Laglera et al. (2007)), eHS-Mo=0 V (Pernet-Coudrier et al. (2013). Figure generated using ODV software (Schlitzer, 2021).*

2.4. Discussion

2.4.1. Comparison of eHS concentrations

The shape of the profile of eHS concentrations through the water column at station 8 is similar between all methods, irrespective of the E_{dep} (Figure 2.7). The shape of the profile resembles those previously reported in the Mediterranean using the eHS-Mo method (Dulaquais et al., 2018b) the Arctic using eHS-Fe (Slagter et al., 2017), and in the Pacific using eHS-Cu (Whitby et al., 2018) with higher concentrations in the surface than at depth, suggesting biological production of eHS in surface waters and their microbial degradation in the water column.

The eHS concentrations detected by the standard addition method varies significantly with the deposition potential. In the samples tested here, decreasing of E_{dep} from 0 to -0.5 V increases significantly the concentration of eHS-Mo. A similar observation was also made in coastal waters of Liverpool Bay (Laglera et al., 2007). In this work, differences can also be seen in Figure 2.4 where SRFA sensitivity reaches a plateau value between -0.2 and -0.4 V while [eHS-Mo] continue to increase with

lowering E_{dep}. The reason for the different concentrations is likely due to differences in adsorbing and/or complexing behaviour between the natural eHS and the SRFA terrestrial standard resulting in the different shapes of the respective pseudopolarograms, as seen in Figure 2.5. If one considers the response of the SRFA as a proxy for sensitivity, it is clear that the concentration is dependent on the E_{dep} for both eHS-Fe and eHS-Cu methods. For eHS-Mo, the pseudopolarograms of the natural eHS and that of the SRFA obtained in UV digested seawater are fairly similar, suggesting that eHS concentrations should not vary significantly with E_{dep}. However, this is not what we observed when running standard additions at various E_{dep} which suggests that the sensitivity of the SRFA in UV digested and non-UV digested seawater is likely to be different, possibly due to the presence of natural surface-active substances that may impact its adsorption on the mercury electrode.

The pseudopolarograms generated using the eHS-Mo method, show a peak when using E_{dep} more negative than the halfwave potential, $E_{p/2}$. The $E_{p/2}$ is a significant point as it is the point at which half of the electrochemical reaction has occurred. In a typical voltammetric measurement using the eHS-Mo method, a E_{dep} is applied to accumulate the Mo-HS complex. The E_{dep} is required to be more positive than the $E_{p/2}$, as this allows for the accumulation of the target analyte (Mo-HS complex) on the electrode surface. After the deposition step, the E_{dep} is shifted in a negative direction, which causes the accumulated Mo-HS complex to undergo oxidation, leading to its removal from the electrode surface. At some point during this process, the oxidation potential of the complex will be reached, leading to the oxidation of the deposited species and the release of electrode, which causes a signal. For eHS-Mo method this signal is observed at -0.44 V (Equation 2)(Quentel and Elleouet, 2001).

$$Mo(V)\text{-}HS + e^- \rightarrow Mo(IV)\text{-}HS \qquad Ep = -0.44\ V \qquad \text{Equation 2.}$$

In other cathodic stripping voltammetry pseudopolarography measurements, after the quiescence period, the stripping step was initiated form the potential of the E_{dep} (Laglera et al., 2014; Laglera and Tovar-Sánchez, 2012). In this study, a fixed potential of 0 V was used at the start of the stripping step. As the potential become more negative while stripping, it is still allows for the accumulation the Mo-

HS complex onto the electrode surface, and therefore providing a signal after the halfwave potential, $E_{p/2}$.

For eHS-Fe and eHS-Cu methods, the analyses are performed at pH of ~ 8 and optimum E_{dep} are towards positive values for both natural humics and the SRFA standard (Figure 2.5). At this pH, the functional groups of the humics are mostly unprotonated, giving them an overall negative charge (Hunter, 1980). In seawater, the potential of zero charge at the Hg drop is around -0.5 V (Heyrovsky and Kuta, 1966), meaning that the electrode is increasingly positive when higher E_{dep} are used which results in higher attraction between the electrode surface and the humics. It is also apparent that both Fe-SRFA and Cu-SRFA complexes adsorb on the Hg drop surface at lower potentials (down to -0.65 and -0.3 V for Fe-SRFA and Cu-SRFA respectively) than the natural complexes (down to -0.45 and -0.15 V for eHS-Fe and eHS-Cu respectively). This different adsorption pattern highlights fundamental differences in composition/charge of the marine humics compare to terrestrial ones, the former having more aliphatic and less aromatic character than terrestrial humic (Ertel et al., 1986; Esteves et al., 2009; Harvey et al., 1983; Riso et al., 2021; Saito and Hayano, 1980). It is interesting to note that for eHS-Fe, the shape of the pseudopolarograms of the bottom water is in between those of the surface sample and the SRFA standard suggesting a gradual change in the nature of the eHS with depth, moving towards a more terrestrial-like behaviour. As move down the water column they are believed to become aromatic through processes such as bacterial remineralisation, which is characteristic of terrestrial-like eHS. Such observation of increased aromaticity through bacterial remineralisation was previously suggested (Whitby et al., 2020b) and has also been recently reported in the South Pacific gyre with low aromatic DOM being present in the photic layer (Osterholz et al., 2021). This change in the nature of the eHS as a function of depth is best exemplified by the appearance of an increasing eHS-Fe signal at depths lower than 1,100 m when using a deposition potential of -0.45 V (Figure. 2.6C).

In acidic conditions, the phenolic and carboxylic groups of eHS are protonated, and the overall HS charge is likely to be neutral, possibly positive if amino-N groups are important (Hunter, 1980). Increasing the deposition potential above the potential of zero-charge (-0.5 V) would effectively result in a weaker attraction (higher repulsion), in agreement with the pseudopolarograms obtained for the eHS-Mo and SRFA-Mo.

Finally, the comparison of published methods (Figure 2.7) provides remarkable similarities in the deeper waters but also significant variations in the upper waters suggesting that adsorption and/or complexing properties of freshly produced eHS and remineralised eHS are different. For eHS-Fe and eHS-Cu, both being measured at pH 8, this is consistent with previous results that have shown that both metals compete for eHS complexation in estuarine waters (Abualhaija et al., 2015), possibly through their carboxylate functional groups which are thought to be the main complexing moieties for Cu (Midorikawa and Tanoue, 1998). From an analytical viewpoint, this similarity suggests that the addition of the oxidant bromate used for catalytic enhancement of the eHS-Fe signal is not oxidising the eHS, at least within the time scale of the analysis.

2.4.2. Comparison of eHS-Fe and eHS-Mo across the Tonga transect

Previous studies have shown good agreement between eHS-Fe and eHS-Mo (Dulaquais et al., 2018b). In this study although there is good agreement between eHS-Fe and eHS-Mo across the dataset as a whole, large differences (up to almost 250%) were also detected when considering individual datapoints. The best agreement was obtained at station 8, while significant differences were obtained at stations 6 and 7. These differences might be due to different organic ligands being present at station 8 compared to the other stations. This study spread across 3 different oceanographic regions; Melanesian waters, the Lau Basin and the South Pacific Gyre. Station 6, 7 and 8 were all situated in the South Pacific Gyre, but station 6 and 7 were close to the Lau Basin and therefore could be influenced by hydrothermal activity and the abundance of diazatrophes.

The South Pacific gyre is quite different to the Lau Basin and the Melanesian waters and therefore the nature of the organic compounds in this region could be different, possibly explaining the results. The Lau Basin, is abundant with hydrothermal vent (Baker et al., 2019; Crawford et al., 2003; Zellmer and Taylor, 2001). These vents can be a source of eHS (Yang et al., 2012), as station 8 is situated quite far into the South Pacific Gyre it would not be influenced by the hydrothermal activity in the Lau Basin. This could explain the differences in agreement between station 8 and the rest of the transect.

In this study, stations 2, 7 and 8 are classed as oligotrophic waters, whereas stations 3, 4, PANAMAX, SIMONE, 11 and 12 were classed as mesotrophic (Bonnet et al., 2022). Stations 3, 4, PANAMAX, SIMONE, 11 and 12 are either situated or are close to the Lau Basin. The Lau Basin has high concentrations of diazotrophs (Bonnet et al., 2018, 2017), as a result of their phosphorus-rich, nitrogen-poor (Bonnet et al., 2018; Caffin et al., 2018) and dFe rich waters (Guieu et al., 2018; Tilliette et al., 2022; Wang et al., 2022). In addition, in the TONGA transect diazatrophs have found to be exported down to 1000m depth (Bonnet et al., 2022). Abundance of diazatrophs at station 8 was found to be two orders of magnitude lower compared to the rest of the transect (Bonnet et al., 2022). The elevated concentration of chlorophyll and diazotrophs in this region (except station 8) could explain why there are differences between eHS-Fe and eHS-Mo method. As station 8 was found to have low diazatrophs abundance this could explain why we see less variation at this station compared to the rest.

It is however puzzling that differences between the two procedures seems random, with positive and negative differences occurring at almost all stations (apart from station 6). Large differences between eHS-Fe and eHS-Mo have previously been reported in estuarine waters (Laglera et al., 2007).

2.4.3. Pseudopolarography as a tool for eHS quantification

Pseudopolarography is a quantitative technique that could be used to provide an understanding of the nature of the eHS present in the sample. This study showed differences in the pseudopolarograms

of surface and deep eHS and terrestrial eHS, suggesting a difference in structure. This will affect the concentration of eHS determined. It would be recommended to perform pseudopolarography on marine samples that can be compared to terrestrial standards to see which is the most similar shape, then use this standard for quantification. However, this can be time-consuming. Two commonly used terrestrial standards are fulvic acid (FA) and humic acid (HA) extracted from the Suwannee River (SR). Comparison of pseudopolarograms with the eHS-Mo method of SRHA and SFRA showed that SRHA was detectable to more negative potentials (-1.6 V), whereas SRFA was only detectable to -1.3 V (Figure 2S1). Therefore, applying an Edep between these values, e.g. -1.4 V, would let the user determine if the marine eHS was more SRHA-like or SFRA-like. Thus, applying an Edep of -1.4 V before quantification would be recommended to see if an eHS signal was obtained. If so, then the SRHA should be used; if no signal is visible, then SRFA. This should be a quick test to enable the user to determine the correct standard required for accurate quantification.

2.5. Conclusion

This work demonstrates that the concentration of eHS determined by each method (Mo, Cu or Fe) is dependent on the E_{dep} and that part of this variation is due to differences between the analyte and the terrestrial standard being used. We found that using the recommended deposition potentials given in the original methods, can show discrepancies in the eHS concentrations being detected, but it is important to note that this study was conducted in a highly dynamic region and is not representative of most oceanographic regions. Station 8, was the most representative open ocean sample. At this station, we found good agreement with all 3 methods, which shows that at this station it appears that all 3 methods are sensitive to the same type of compounds.

The shape of pseudopolarograms using the eHS-Mo method were similar for natural samples and for SRFA, while the pseudopolarograms using the eHS-Fe and eHS-Cu methods showed differences

between natural samples and SRFA, with the adsorption of the SRFA standard occurring over a much lower E_{dep} than the natural eHS. Pseudopolarograms using all methods show slight differences between the surface and deep sample. The most noticeable differences were observed using the eHS-Fe method and the least noticeable was using eHS-Mo method. In all methods the deeper samples were more similar to the SRFA standard than those of surface waters, which would agree with the structure and composition of eHS changing through remineralisation to become more terrestrial-like as a function of depth.

To our knowledge, the use of pseudopolarography for the characterisation of eHS has not been attempted. We suggest a move towards pseudopolarography before quantification of eHS to compare pseudopolarograms of marine eHS to a commonly used terrestrial standard (SRFA). This was to see if it was representative of the eHS in the sample to achieve accurate quantification.

2.6. References

Abualhaija, M.M., Whitby, H., van den Berg, C.M.G., 2015. Competition between copper and iron for humic ligands in estuarine waters. Mar. Chem. 172, 46–56. https://doi.org/10.1016/J.MARCHEM.2015.03.010

Averett, R.C., Leenheer, J.A., McKnight, D.M., Thorn, K.A., 1994. Humic substances in the Suwannee River, Georgia: interactions, properties, and proposed structures. US Geol. Surv. Water-Supply Pap. 2373. https://doi.org/10.3133/wsp2373

Baker, E.T., Walker, S.L., Massoth, G.J., Resing, J.A., 2019. The NE Lau Basin: Widespread and abundant hydrothermal venting in the back-arc region behind a superfast subduction zone. Front. Mar. Sci. 6, 1–15. https://doi.org/10.3389/fmars.2019.00382

Bi, Z., Salaün, P., van den Berg, C.M.G., 2013a. The speciation of lead in seawater by pseudopolarography using a vibrating silver amalgam microwire electrode. Mar. Chem. 151, 1–12. https://doi.org/10.1016/J.MARCHEM.2013.02.003

Bi, Z., Salaün, P., van den Berg, C.M.G., 2013b. Determination of lead and cadmium in seawater using a vibrating silver amalgam microwire electrode. Anal. Chim. Acta 769, 56–64. https://doi.org/10.1016/J.ACA.2013.01.049

Bonnet, S., Benavides, M., Moigne, F.A.C. Le, Camps, M., Torremocha, A., Grosso, O., Dimier, C., Spungin, D., Berman-frank, I., Garczarek, L., Cornejo-castillo, F.M., 2022. Diazotrophs are overlooked contributors to carbon and nitrogen export to the deep ocean. ISME J. Vol. 17, 47–58. https://doi.org/10.1038/s41396-022-01319-3

Bonnet, S., Caffin, M., Berthelot, H., Grosso, O., Benavides, M., Helias-Nunige, S., Guieu, C., Stenegren, M., Foster, R.A., 2018. In-depth characterization of diazotroph activity across the western tropical South Pacific hotspot of N2 fixation (OUTPACE cruise). Biogeosciences 15, 4215–4232. https://doi.org/10.5194/bg-15-4215-2018

Bonnet, S., Caffin, M., Berthelot, H., Moutin, T., 2017. Hot spot of N2 fixation in the western tropical South Pacific pleads for a spatial decoupling between N2 fixation and denitrification. Proc. Natl. Acad. Sci. U. S. A. 114, E2800–E2801. https://doi.org/10.1073/pnas.1619514114

Bundy, R.M., Biller, D. V., Buck, K.N., Bruland, K.W., Barbeau, K.A., 2014. Distinct pools of dissolved iron-binding ligands in the surface and benthic boundary layer of the California current. Limnol. Oceanogr. 59, 769–787. https://doi.org/10.4319/lo.2014.59.3.0769

Caffin, M., Moutin, T., Ann Foster, R., Bouruet-Aubertot, P., Michelangelo Doglioli, A., Berthelot, H., Guieu, C., Grosso, O., Helias-Nunige, S., Leblond, N., Gimenez, A., Alexandra Petrenko, A., De Verneil, A., Bonnet, S., 2018. N2 fixation as a dominant new N source in the western tropical South Pacific Ocean (OUTPACE cruise). Biogeosciences 15, 2565–2585. https://doi.org/10.5194/bg-15-2565-2018

Carr, N., Davis, C.E., Blackbird, S., Daniels, L.R., Preece, C., Woodward, M., Mahaffey, C., 2019. Seasonal and spatial variability in the optical characteristics of DOM in a temperate shelf sea. Prog. Oceanogr. 177, 101929. https://doi.org/10.1016/j.pocean.2018.02.025

Coble, P.G., 2007. Marine optical biogeochemistry: The chemistry of ocean color. Chem. Rev. 107, 402–418. https://doi.org/10.1021/cr050350+

Cominoli, A., Buffle, J., Haerdi, W., 1980. Voltammetric study of humic and fulvic substances. Part III. Comparison of the capabilities of the various polarographic techniques for the analysis of humic and fulvic substances. J. Electroanal. Chem. 110, 259–275. https://doi.org/10.1016/S0022-0728(80)80378-0

Cosović, B., Vojvodić, V., 1982. The application of ac polarography to the determination of surface-active substances in seawater. Limnol. Oceanogr. 27, 361–369. https://doi.org/10.4319/lo.1982.27.2.0361

Crawford, W.C., Hildebrand, J.A., Dorman, L.M., Webb, S.C., 2003. Tonga Ridge and Lau Basin crustal structure from seismic refraction data Tonga Ridge and Lau Basin crustal structure from seismic refraction data. J. Geophys. Res. Atmos. 108. https://doi.org/10.1029/2001JB001435

Cuscov, M., Muller, F.L.L., 2015. Differentiating humic and algal surface active substances in coastal waters by their pH-dependent adsorption behaviour. Mar. Chem. 174, 35–45. https://doi.org/10.1016/j.marchem.2015.05.002

Cutter, G., Casciotti, K., Croot, P., Geibert, W., Heimbürger, L.-E., Lohan, M., Planquette, H., Flierdt, T. van de, 2017. Sampling and Sample-handling Protocols for GEOTRACES Cruises. http://dx.doi.org/10.25607/OBP-2

Davison, W., 1991. The solubility of iron sulphides in synthetic and natural waters at ambient temperature. Aquat. Sci. 53. 309-329. https://doi.org/10.1007/BF00877139

Dulaquais, G., Breitenstein, J., Waeles, M., Marsac, R., Riso, R., 2018a. Measuring dissolved organic matter in estuarine and marine waters: Size-exclusion chromatography with various detection methods. Environ. Chem. 15, 436–449. https://doi.org/10.1071/EN18108

Dulaquais, G., Waeles, M., Gerringa, L.J.A., Middag, R., Rijkenberg, M.J.A., Riso, R., 2018b. The Biogeochemistry of Electroactive Humic Substances and Its Connection to Iron Chemistry in the North East Atlantic and the Western Mediterranean Sea. J. Geophys. Res. Ocean. 123, 5481–

5499. https://doi.org/10.1029/2018JC014211

Ertel, J.R., Hedges, J.I., Devol, A.H., Richey, J.E., Nazarg, M. De, Ribeiro, G., 1986. Dissolved humic substances of the Amazon River system 31, 139–154. https://doi.org/10.4319/lo.1986.31.4.0739

Esteves, V.I., Otero, M., Duarte, A.C., 2009. Comparative characterization of humic substances from the open ocean, estuarine water and fresh water. Org. Geochem. 40, 942–950. https://doi.org/10.1016/j.orggeochem.2009.06.006

Faganeli, J., Kovač, N., Leskovšek, H., Pezdič, J., 1995. Sources and fluxes of particulate organic matter in shallow coastal waters characterized by summer macroaggregate formation. Biogeochemistry 29, 71–88. https://doi.org/10.1007/BF00002595

Filella, M., 2014. Understanding what we are measuring: Standards and quantification of natural organic matter. Water Res. 50, 287–293. https://doi.org/10.1016/j.watres.2013.12.015

Filella, M., 2010. Quantifying "humics" in freshwaters: Purpose and methods. Chem. Ecol. 26, 177–186. https://doi.org/10.1080/02757540.2010.494159

Fourrier, P., Dulaquais, G., Guigue, C., Giamarchi, P., Sarthou, G., Whitby, H., Riso, R., 2022. Characterization of the vertical size distribution, composition and chemical properties of dissolved organic matter in the (ultra)oligotrophic Pacific Ocean through a multi-detection approach. Mar. Chem. 240, 104068. https://doi.org/10.1016/j.marchem.2021.104068

Gibbon-Walsh, K., Salaün, P., Van Den Berg, C.M.G., 2012. Pseudopolarography of copper complexes in seawater using a vibrating gold microwire electrode. J. Phys. Chem. A 116, 6609–6620. https://doi.org/10.1021/jp3019155

Gledhill, M., Buck, K.N., 2012. The organic complexation of iron in the marine environment: A review. Front. Microbiol. 3, 1–17. https://doi.org/10.3389/fmicb.2012.00069

Guieu, C., Bonnet, S., Petrenko, A., Menkes, C., Chavagnac, V., Desboeufs, K., Maes, C., Moutin, T., 2018. Iron from a submarine source impacts the productive layer of the Western Tropical South Pacific (WTSP). Nat. Sci. Reports 1–9. https://doi.org/10.1038/s41598-018-27407-z

Harris, D.C., 2003. Quantitative Chemical Analysis, W. H. Freeman. New York. https://doi.org/10.1016/B978-0-444-40826-6.50009-1

Harvey, G. r., Tokar, J. m., Boran, D., Chesal, L.A., 1983. The structure of marine fulvic and humic acids. Mar. Biol. 12, 119–132. https://doi.org/10.1016/0304-4203(83)90075-0

Hassanpour, S., Maheri-Sis, N., Eshratkhah, B., Mehmandar, F.B., 2011. Plants and secondary metabolites (Tannins): A Review. Int. J. For. Soil Eros. 1, 47–53.

Hassler, C., Cabanes, D., Blanco-Ameijeiras, S., Sander, S.G., Benner, R., 2020. Importance of refractory ligands and their photodegradation for iron oceanic inventories and cycling. Mar. Freshw. Res. 71, 311–320. https://doi.org/10.1071/MF19213

Hatcher, P.G., Maciel, G.E., Dennis, L.W., 1981. Aliphatic structure of humic acids; a clue to their origin. Org. Geochem. 3, 43–48. https://doi.org/10.1016/0146-6380(81)90012-7

Heyrovsky, J., Kuta, J., 1966. Principles of Polarography. Academic Press, London.

Hunter, K.A., 1980. Microelectrophoretic properties of natural surface-active organic matter in coastal seawater. Limnol. Oceanogr. 25, 807–822. https://doi.org/10.4319/lo.1980.25.5.0807

IHSS, 2022. Isolation of IHSS Samples [WWW Document].

Kitayama, S., Kuma, K., Manabe, E., Sugie, K., Takata, H., Isoda, Y., Toya, K., Saitoh, S., Takagi, S., Kamei,

Y., 2009. Controls on iron distributions in the deep water column of the North Pacific Ocean : Iron (III) hydroxide solubility and marine humic-type dissolved organic matter. J. Geophys. Res. 114, 1–13. https://doi.org/10.1029/2008JC004754

Kogut, M.B., Voelker, B.M., 2001. Strong copper-binding behavior of terrestrial humic substances in seawater. Environ. Sci. Technol. 35, 1149–1156. https://doi.org/10.1021/es0014584

Krachler, R., Krachler, R.F., Wallner, G., Hann, S., Laux, M., Cervantes Recalde, M.F., Jirsa, F., Neubauer, E., von der Kammer, F., Hofmann, T., Kepplera, B.K., 2015. River-derived humic substances as iron chelators in seawater. Mar. Chem. 174, 85–93.

Krivácsy, Z., Kiss, G., Ceburnis, D., Jennings, G., Maenhaut, W., Salma, I., Shooter, D., 2008. Study of water-soluble atmospheric humic matter in urban and marine environments. Atmos. Res. 87, 1–12. https://doi.org/10.1016/j.atmosres.2007.04.005

Laglera, L.M., Battaglia, G., van den Berg, C.M.G., 2007. Determination of humic substances in natural waters by cathodic stripping voltammetry of their complexes with iron. Anal. Chim. Acta. 599, 58–66. https://doi.org/10.1016/j.aca.2007.07.059

Laglera, L.M., Sukekava, C., Slagter, H.A., Downes, J., Aparicio-Gonzalez, A., Gerringa, L.J.A., 2019. First Quantification of the Controlling Role of Humic Substances in the Transport of Iron across the Surface of the Arctic Ocean. Environ. Sci. Technol. https://doi.org/10.1021/acs.est.9b04240

Laglera, L.M., Downes, J., Tovar-Sánchez, A., Monticelli, D., 2014. Cathodic pseudopolarography: A new tool for the identification and quantification of cysteine, cystine and other low molecular weight thiols in seawater. Anal. Chim. Acta. 839, 24-33. https://doi.org/ 10.1016/j.aca.2014.05.026

Laglera, L.M., Tovar-Sánchez, A., 2012. Direct recognition and quantification by voltammetry of thiol/thioamide mixes in seawater. Talanta 89, 496–504. https://doi.org/10.1016/j.talanta.2011.12.075

Laglera, L.M., van den Berg, C.M.G., 2009. Evidence for geochemical control of iron by humic substances in seawater. Limnol. Oceanogr. 54, 610–619. https://doi.org/10.4319/lo.2009.54.2.0610

Liu, Q., Luo, L., Zheng, L., 2018. Lignins: Biosynthesis and biological functions in plants. Int. J. Mol. Sci. 19. https://doi.org/10.3390/ijms19020335

Liu, X., Millero, F.J., 2002. The solubility of iron in seawater. Mar. Chem. 77, 43–54. https://doi.org/10.1016/S0304-4203(01)00074-3

Longhini, C.M., Mahieu, L., Fabian, S., van den Berg, C.M.G., Salaün, P., Neto, R.R., 2021. Coastal waters contamination by mining tailings: What triggers the stability of iron in the dissolved and soluble fractions? Limnol. Oceanogr. 66, 171–187. https://doi.org/10.1002/lno.11595

Midorikawa, T., Tanoue, E., 1998. Molecular masses and chromophoric properties of dissolved organic ligands for copper(II) in oceanic water. Mar. Chem. 62, 219–239. https://doi.org/10.1016/S0304-4203(98)00040-1

Muller, F.L.L., 2018. Exploring the potential role of terrestrially derived humic substances in the marine biogeochemistry of iron. Front. Earth Sci. 6. https://doi.org/10.3389/feart.2018.00159

Oldham, E., Mucci, A., Tebo, B.M., Luther, G.W., 2017. Soluble Mn (III)– L complexes are abundant in oxygenated waters and stabilized by humic ligands. Geochim. Cosmochim. Acta 199, 238–246. https://doi.org/10.1016/j.gca.2016.11.043

Omori, Y., Hama, T., Ishii, M., Saito, S., 2011. Vertical change in the composition of marine humic-like

fluorescent dissolved organic matter in the subtropical western North Pacific and its relation to photoreactivity. Mar. Chem. 124, 38–47. https://doi.org/10.1016/j.marchem.2010.11.005

Osterholz, H., Kilgour, D.P.A., Storey, D.S., Lavik, G., Ferdelman, T.G., Niggemann, J., Dittmar, T., 2021. Accumulation of DOC in the South Pacific Subtropical Gyre from a molecular perspective. Mar. Chem. 231, 103955. https://doi.org/10.1016/j.marchem.2021.103955

Pernet-Coudrier, B., Waeles, M., Filella, M., Quentel, F., Riso, R.D., 2013. Simple and simultaneous determination of glutathione, thioacetamide and refractory organic matter in natural waters by DP-CSV. Sci. Total Environ. 463–464, 997–1005. https://doi.org/10.1016/j.scitotenv.2013.06.053

Quentel, F., Elleouet, C., 2001. Square-Wave Voltammetry of Molybdenum-Fulvic Acid Complex. Electroanalysis 13, 1030–1035. https://doi.org/https://doi.org/10.1002/1521-4109(200108)13:12<1030::AID-ELAN1030>3.0.CO;2-6

Quentel, F., Madec, C., Bihan, A. Le, Courtot-coupez, J., 1986. Determination des Substances Humiques en Milieu Marin Par Redissolution Cathodique a L'Electrode a Coutte Pendante de Mercure. Enviromental Anal. 19, 325–344.

Riso, R., Mastin, M., Aschehoug, A., Davy, R., Devesa, J., Laës-Huon, A., Waeles, M., Dulaquais, G., 2021. Distribution, speciation and composition of humic substances in a macro-tidal temperate estuary. Estuar. Coast. Shelf Sci. 255. https://doi.org/10.1016/j.ecss.2021.107360

Saito, Y., Hayano, S., 1980. Distribution of oxygen-containing functional groups and elements in humic acids from marine sediments. J. Oceanogr. Soc. Japan 36, 59–67. https://doi.org/10.1007/BF02209356

Sarma, N.S., Kiran, R., Reddy, M.R., Iyer, S.D., Peketi, A., Borole, D. V., Krishna, M.S., 2018. Hydrothermal Alteration Promotes Humic Acid Formation in Sediments: A Case Study of the Central Indian Ocean Basin. J. Geophys. Res. Ocean. 110–130. https://doi.org/10.1002/2017JC012940

Schlitzer, R., 2021. Ocean Data View.

Shevchenko, S., Bailey, G.W., 1996. Life after death: Lignin-humic relationships reexamined. Crit. Rev. Environ. Sci. Technol. 26, 95–153. https://doi.org/10.1080/10643389609388488

Shigemitsu, M., Yokokawa, T., Uchida, H., Kawagucci, S., Murata, A., 2021. Sedimentary supply of humic-like fluorescent dissolved organic matter and its implication for chemoautotrophic microbial activity in the Izu-Ogasawara Trench. Sci. Rep. 11, 1–10. https://doi.org/10.1038/s41598-021-97774-7

Slagter, H.A., Laglera, L.M., Sukekava, C., Gerringa, L.J.A., 2019. Fe-Binding Organic Ligands in the Humic-Rich TransPolar Drift in the Surface Arctic Ocean Using Multiple Voltammetric Methods. J. Geophys. Res. Ocean. 124, 1491–1508. https://doi.org/10.1029/2018JC014576

Slagter, H.A., Reader, H.E., Rijkenberg, M.J.A., Rutgers van der Loeff, M., de Baar, H.J.W., Gerringa, L.J.A., 2017. Organic Fe speciation in the Eurasian Basins of the Arctic Ocean and its relation to terrestrial DOM. Mar. Chem. 197, 11–25. https://doi.org/10.1016/j.marchem.2017.10.005

Stevenson, F.J., 1994. Humus Chemistry: Genesis, Composition, Reactions, 2nd ed. Wiley.

Su, H., Yang, R., Li, Y., Wang, X., 2018. Chemosphere In fl uence of humic substances on iron distribution in the East China Sea. Chemosphere 204, 450–462. https://doi.org/10.1016/j.chemosphere.2018.04.018

Sukekava, C., Downes, J., Slagter, H.A., Gerringa, L.J.A., Laglera, L.M., 2018. Determination of the contribution of humic substances to iron complexation in seawater by catalytic cathodic stripping

voltammetry. Talanta 189, 359–364. https://doi.org/10.1016/j.talanta.2018.07.021

Tilliette, C., Taillandier, V., Bouruet-Aubertot, P., Grima, N., Maes, C., Montanes, M., Sarthou, G., Vorrath, M.-E., Arnone, V., Bressac, M., et al., 2022. DFe patterns impacted by shallow hydrothermal sources along a transect through the Tonga-Kermadec arc. Earth Sp. Sci. Open Arch. 43. https://doi.org/10.1029/2022GB007363

Tranvik, L.J., 1993. Microbial transformation of labile dissolved organic matter into humic-like matter in seawater. FEMS Microbiol. Ecol. 12, 177–183. https://doi.org/10.1111/j.1574-6941.1993.tb00030.x

Tsang, J.J., Rozan, T.F., Hsu-Kim, H., Mullaugh, K.M., Luther, G.W., 2006. Pseudopolarographic determination of Cd2+ complexation in freshwater. Environ. Sci. Technol. 40, 5388–5394. https://doi.org/10.1021/es0525509

van den Berg, C., 2014. UV digestion apparatus. [WWW Document]. URL http://pcwww.liv.ac.uk/~sn35/Site/ UV_digestion_apparatus.html

van den Berg, C.M.G., 1982. Determination of copper complexation with natural organic ligands in seawater by equilibration with MnO2 II. Experimental procedures and application to surface seawater. Mar. Chem. 11, 323–342. https://doi.org/10.1016/0304-4203(82)90029-9

Waeles, M., Riso, R., Pernet-Coudrier, B., Quentel, F., Durrieu, G., Tissot, C., 2013. Annual cycle of humic substances in a temperate estuarine system affected by agricultural practices. Geochim. Cosmochim. Acta 106, 231–246. https://doi.org/10.1016/j.gca.2012.12.040

Waeles, M., Tanguy, V., Riso, R.D., 2015. Chemosphere On the control of copper colloidal distribution by humic substances in the Penzé estuary. Chemosphere 119, 1176–1184. https://doi.org/10.1016/j.chemosphere.2014.09.107

Wang, H., Liu, M., Wang, W., Zhou, H., Ellwood, M.J., Butterfield, D.A., Buck, N.J., Resing, J.A., 2022. Iron ligands and isotopes in hydrothermal plumes over backarc volcanoes in the Northeast Lau Basin, Southwest Pacific Ocean. Geochim. Cosmochim. Acta 336, 341–352. https://doi.org/10.1016/j.gca.2022.09.026

Whitby, H., Bressac, M., Sarthou, G., Ellwood, M.J., Guieu, C., Boyd, P.W., 2020a. Contribution of Electroactive Humic Substances to the Iron-Binding Ligands Released During Microbial Remineralization of Sinking Particles. Geophys. Res. Lett. 47, 1–11. https://doi.org/10.1029/2019GL086685

Whitby, H., Hollibaugh, J.T., van den Berg, C.M.G., 2017. Chemical Speciation of Copper in a Salt Marsh Estuary and Bioavailability to Thaumarchaeota. Front. Mar. Sci. https://doi.org/10.3389/fmars.2017.00178

Whitby, H., Planquette, H., Cassar, N., Bucciarelli, E., Osburn, C.L., Janssen, D.J., Cullen, J.T., González, A.G., Völker, C., Sarthou, G., 2020b. A call for refining the role of humic-like substances in the oceanic iron cycle. Sci. Rep. 10, 1–12. https://doi.org/10.1038/s41598-020-62266-7

Whitby, H., Posacka, A.M., Maldonado, M.T., van den Berg, C.M.G., 2018. Copper-binding ligands in the NE Pacific. Mar. Chem. 204, 36–48. https://doi.org/10.1016/J.MARCHEM.2018.05.008

Whitby, H., van den Berg, C.M.G., 2015. Evidence for copper-binding humic substances in seawater. Mar. Chem. 173, 282-290. https://doi.org/10.1016/j.marchem.2014.09.011

Yamashita, Y., Nishioka, J., Obata, H., Ogawa, H., 2020. Shelf humic substances as carriers for basin-scale iron transport in the North Pacific. Sci. Rep. 10, 1–10. https://doi.org/10.1038/s41598-020-61375-7

Yamashita, Y., Tanoue, E., 2009. Basin scale distribution of chromophoric dissolved organic matter in the Pacific Ocean. Limnol. Oceanogr. 54, 2, 598–609. https://doi.org/10.4319/lo.2009.54.2.0598

Yang, L., Hong, H., Guo, W., Chen, C.T.A., Pan, P.I., Feng, C.C., 2012. Absorption and fluorescence of dissolved organic matter in submarine hydrothermal vents off NE Taiwan. Mar. Chem. 128–129, 64–71. https://doi.org/10.1016/j.marchem.2011.10.003

Yang, R., van den Berg, C.M.G., 2009. Metal complexation by humic substances in seawater. Environ. Sci. Technol. 43, 7192–7197. https://doi.org/10.1021/es900173w

Zellmer, K.E., Taylor, B., 2001. A three-plate kinematic model for Lau Basin opening. Geochemistry, Geophys. Geosystems 2, 5, https://doi.org/10.1029/2000GC000106

Zigah, P.K., McNichol, A.P., Xu, L., Johnson, C., Santinelli, C., Karl, D.M., Repeta, D.J., 2017. Allochthonous sources and dynamic cycling of ocean dissolved organic carbon revealed by carbon isotopes. Geophys. Res. Lett. 44, 2407–2415. https://doi.org/10.1002/2016GL071348

2.7. Supplementary

Method	E_{dep} (V)	t_{dep} (s)	Concentration $\mu g.L^{-1}$
Mo-eHS No background subtraction (N=5)	0	150	16.55 ± 1.61
Mo-eHS Background subtraction (N=5)	0	150	38.84 ± 0.79
eHS-Cu (N=5)	0.05	150	41.92 ± 1.53

Table 2S1*. Comparison of the concentration of eHS obtained from the SCALE internal reference water (SCALE Underway fish, Southern Ocean, 49°20S 03°31'E) using the eHS-Cu and eHS-Mo methods. The concentration of eHS-Mo shown with and without background subtraction. n represents the number of repeats. Error represent the average standard deviation of the standard additions.*

Date	Method	Water	Concentration ($\mu g.L^{-1}$)
14.04.21	eHS-Cu	SCALE	38.27 ± 2.53
15.04.21	eHS-Cu	SCALE	41.61 ± 3.89
16.04.21	eHS-Cu	SCALE	40.56 ± 2.57
19.04.21	eHS-Cu	SCALE	42.39 ± 2.05
23.04.21	eHS-Cu	SCALE	40.02 ± 1.18
26.04.21	eHS-Cu	SCALE	40.3 ± 9.66
27.04.21	eHS-Cu	SCALE	32.88 ± 3.94
28.04.21	eHS-Cu	SCALE	48.15 ± 1.67
29.04.21	eHS-Cu	SCALE	34.76 ± 2.3
05.05.21	eHS-Mo	SCALE	36.87 ± 2.07
07.05.21	eHS-Mo	SCALE	44.87 ± 5.46
10.05.21	eHS-Mo	SCALE	35.01 ± 4.97
11.05.21	eHS-Mo	SCALE	42.36 ± 2.1
13.05.21	eHS-Mo	SCALE	35.95 ± 4.26
17.05.21	eHS-Mo	SCALE	34.72 ± 1.51

***Table 2S2**. Reproducibility of measurements of SCALE internal reference. Internal reference was measured each day before analysis of sample. This would help to identify any problems with the measurement or reagents. The average concentration of eHS in the SCALE water was determined at 41.91 ± 3.01 and 37.08 ± 1.67 $\mu g.L^{-1}$ by the eHS-Cu and the eHS-Mo methods, respectively. For each method, acceptable concentrations obtained were within 20% of the average. Error represent the standard deviation of the standard additions*.

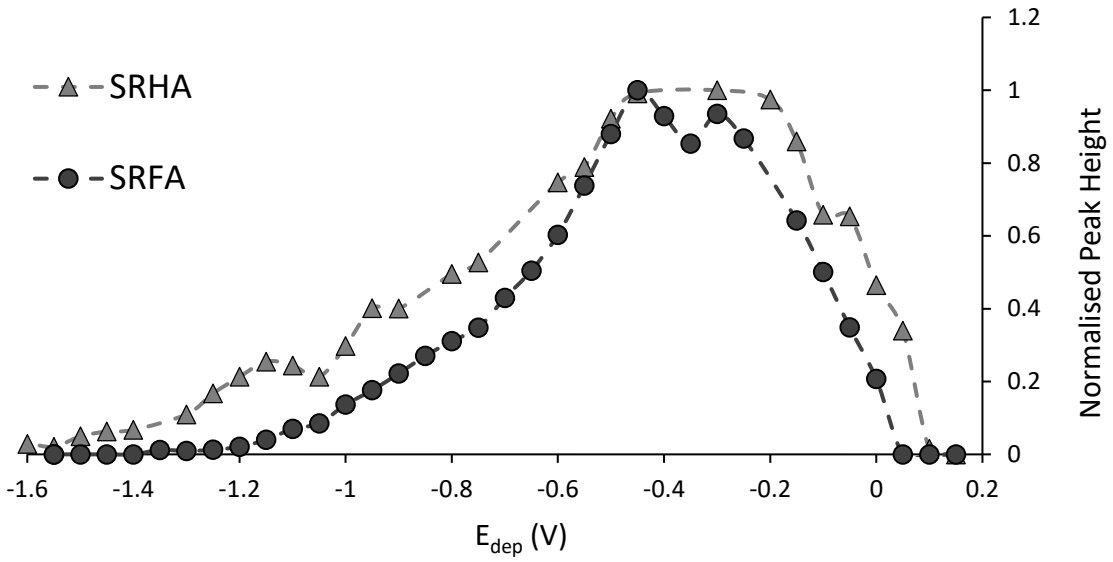

Figure 2S1. *Comparison of pseudopolarogram of Suwannee River fulvic acid (SRFA) standard and Suwannee River humic acid (SRHA) standard. SRHA and SRFA standards were added to UV digested seawater. Concentration of SRFA and SRHA was 96 µg.L^{-1}. The method used was from Pernet-Coudrier et al. (2013) (eHS-Mo method). Each point represents the peak height of the eHS signal. Peak height has been normalised to the highest peak value (=peak height/largest peak height). Voltammetric analysis was carried out at pH was 2.*

Note for the reader

The following chapter is in preparation for submission to the journal Frontiers Research Topic 'Hydrothermal and submarine volcanic activity: Impacts on ocean chemistry and plankton dynamics'.

To be submitted as: **Portlock, G**., Whitby, H., Tilliette, C., Bonnet, S., Guieu, G., Salaün, P: Distribution and behaviour of thiols and humic-like substances in the oligotrophic and hydrothermal waters of the Western South Tropical Pacific

In this chapter, I provided the voltammetric determination of eHS, RSS. Dissolved Fe data was provided by C. Tilliette. Dissolved trace metal data was provided by D. Gonzalez-Santana.

Chapter 3

Distribution and behaviour of reduced sulphur substances and humic-like substances in the oligotrophic and hydrothermal waters of the Western South Tropical Pacific

Abstract

Organic ligands are important as they can control trace metal bioavailability and solubility. Amongst the various groups of ligands involved in metal complexation are reduced sulphur subtances (RSS) and humic substances. Due to the variety of compounds within these two groups, their analytical detection is not trivial nor standardised, and there is still much to learn about their biogeochemistry.

Here, we present a quantitative and semi-qualitative data set of species-specific RSS (thioacetamide-like (TA-like) and glutathione-like (GSH-like compounds) and electroactive humic substances (eHS) in the Western Tropical South Pacific (WTSP) Ocean. Concentrations of thioacetamide-like compounds (48 to 984 nM), glutathione-like compounds (0.61 to 6.23 nM), and electroactive humic substances (11.47 to 134 $\mu g.L^{-1}$ eq SRFA) were measured by cathodic stripping voltammetry (CSV). Elevated

concentrations of TA-like compounds were found in the Melanesian waters. At the hydrothermal impacted station of PANAMAX, elevated concentrations of TA-like compounds, GSH-like compounds and eHS were detected suggesting that hydrothermal vents are either a direct or an indirect source of these compounds. Elevated concentrations of eHS were also found in the South Pacific Gyre, in general agreement with high DOC levels.

Cathodic pseudopolarography profiles of marine samples were used for the qualitative analysis of RRS and eHS. We show slight differences between surface and deep water eHS, which indicates a change in the nature of eHS with depth.

3.1. Introduction

In natural waters, trace metals, such as copper (Cu) and iron (Fe), are essential micronutrients. Both are involved in many metabolic processes, such as respiration (Falkowski et al., 1998; Ridge et al., 2008), photosynthesis (Barón et al., 1995; Peers and Price, 2006; Raven et al., 1999) and also are important for multiple steps in the nitrogen cycle (Francis et al., 2005; Jacquot et al., 2014; Merchant et al., 2006; Pauleta et al., 2013; Philippot, 2002; Ward, 2011). However, Cu can also induce toxic effects on marine organisms (Brand et al., 1986; Debelius et al., 2011; Moffett et al., 1997), and Fe is highly insoluble in seawater, therefore limiting primary production in up to 40% of the ocean (Moore et al., 2001). Organic ligands are essential to trace metals as they influence the metals geochemistry and bioavailability (Coale and Bruland, 1988; Gledhill and van den Berg, 1994; Nimmo et al., 1989; Rue and Bruland, 1995; Wu and Luther, 1995). There is a wide variety of organic ligands in seawater, and although the identities of some ligands remain unknown, reduced sulphur subtances (RSS) and humic substances (HS) have been identified as part of the organic ligand pool (Laglera and van den Berg, 2003; Leal and van den Berg, 1998; Tang et al., 2001; Yang and van den Berg, 2009).

RSS are a group of compounds that possess a reduced sulphur function group. Various RSS include glutathione (GSH), cysteine (CYS) and thioacetamide (TA). RSS can form strong complexes with a wide array of trace metals, including Cu, lead (Pb) and cadmium (Cd) (Vasconcelos and Leal, 2001). RSS can also bind with Fe in anaerobic conditions (Bulletin et al., 1998; Pavelko, 2015). They can be produced by microbes in response to various environmental stressors, to act as a reactive oxygen species (ROS) scavenger (Baba and Bhatnagar, 2016; Dupont et al., 2004; Navarrete et al., 2019) or in response to metals or light (Ahner et al., 2002; Dupont and Ahner, 2005). ROS are highly reactive chemicals formed from oxygen, which include the superoxide anion (O_2^-), hydrogen peroxide (H_2O_2), and hydroxyl radicals (OH·) (Morris et al., 2022; Schieber and Chandel, 2014). Due to their high reactivity, ROS can disrupt normal cell function and can lead to oxidative stress. RSS are able to combat ROS stress as they are able to remove these reactive species by accepting their unpaired electron (McLeay et al., 2017; Morelli and Scarano, 2004). Aerobic organisms produce ROS as a byproduct in processes such as photosynthesis, photorespiration and oxidative phosphorylation (Apel and Hirt, 2004; Diaz and Plummer, 2018; Mullineaux et al., 2018).

HS are an operationally defined fraction of dissolved organic matter (DOM) and vary in molecular weight, polarity and composition. They can be subdivided into two fractions: humic acids (HA), which precipitate below pH 2 and fulvic acids (FA), which are soluble even at low pH. They are produced in both marine and terrestrial environments from microbial activities and degradation (Ferrari et al., 1996; Lorenzo et al., 2007). Hydrothermal vents can also be a source of marine HS (Yang et al., 2012). HS contain metal-binding functional groups, forming complexes with a variety of different trace metals, including Fe and Cu (Laglera and van den Berg, 2009; Whitby and van den Berg, 2015). However, only a small fraction of HS (~ 5% of dissolved organic carbon (DOC)) can bind with metals (Dulaquais et al., 2018; Laglera and van den Berg, 2009). This fraction is called electroactive HS (eHS). eHS have been shown to be an important part of the ligand pool for both metals in coastal and open ocean regions (Batchelli et al., 2010; Dulaquais et al., 2019, 2018; Whitby et al., 2020b, 2018), with Fe and Cu competing for humic complexation in coastal waters (Abualhaija et al., 2015).

The Western Tropical South Pacific (WTSP) is a vast oceanic region that extends from Australia to the western boundary of the South Pacific Gyre. Within the WTSP is the Tonga-Kermadec Arc where the Pacific plate is subducted under the Australian plate, causing a region of extensive hydrothermal activity (Baker et al., 2019; German et al., 2006). Situated within the WTSP is the Lau Basin, that has both deep and shallow hydrothermal vents, which are able to release high concentrations of metals, including Fe (Guieu et al., 2018; Tilliette et al., 2022; Wang et al., 2022). This, coupled with the Lau Basin phosphorus-rich and nitrogen-poor waters (Bonnet et al., 2018; Caffin et al., 2018), has led to an extensive bloom of diazotrophs, causing the area to be a hotspot for N_2 fixation (Bonnet et al., 2018, 2017).

Recently more attention has been focused on the importance of shallow hydrothermal vents in ocean chemistry (Guieu et al., 2018; Tilliette et al., 2023). Due to their shallow depth (<200 m), the buoyant hydrothermal plumes reach the surface waters (Zhang et al., 2020), which can be either beneficial or detrimental to surface communities. As a response to the hydrothermal fluids, surface communities may release increased concentrations of RSS and eHS. This study aims to understand the distribution of RSS and eHS within the WTSP, which can help us to understand the cycling of trace metals in this region.

Here we present the distribution of RRS and humic-like substances in the Western Tropical South Pacific (WSPT) during the French GEOTRACES TONGA (shallow hydroThermal sOurces of trace elemeNts: potential impacts on biological productivity and the bioloGicAl carbon pump) cruise that took place from the 31st October to 5th December 2019. Cathodic stripping voltammetry (CSV) was used to determine the concentrations of RSS and electroactive humic substances in this region to try to identify sources and sinks of these compounds. Cathodic pseudopolarography profiles of marine samples were used for the qualitative analysis of RSS and eHS.

3.2. Experimental

3.2.1. Sampling

Samples were collected during the GEOTRACES TONGA (GPpr14) (Guieu and Bonnet, 2019) research cruise, which took place onboard the R/V L'Atalante from 31 October to 5 December 2019, a transect extending from New Caledonia to the western end of the South Pacific gyre (Figure 3.1A). During the cruise, samples were collected using a trace metal clean polyurethane powder-coated aluminium frame rosette (TMR, General Oceanics Inc. Model 1018 Intelligent Rosette), which was attached to a 6 mm diameter Kevlar line. After the samples were collected, the Go-Flo bottles were transferred into a clean container for sampling. Seawater was filtered through a 0.45 µm polyethersulfone filter (Supor®) and collected in 125 mL Nalgene LDPE bottles. The bottles were acid-cleaned according to the GEOTRACES protocol (Cutter et al., 2017). Immediately after collection, samples were double bagged and stored at −20 ◦C until analysis.

3.2.2. Voltammetric equipment

A µAutolabIII potentiostat was connected to a Metrohm 663 VA stand through the IME663 interface. The three-electrode cell consisted of a hanging mercury drop electrode (HMDE) as the working electrode, a glassy carbon rod as the counter electrode and an Ag/AgCl with a glass salt bridge filled with 3 M KCl as the reference electrode. The solution was purged with nitrogen gas (N_2) before measurement and stirred during deposition using a rotating polytetrafluoroethylene (PTFE) rod (setting 4 on the VA stand). Connected to the VA stand was an automatic sampler (https://sites.google.com/site/daromasoft/home/autosampler) allowing the automatic loading and emptying of the voltammetric cell. Standard additions were made automatically using syringe burettes. The voltammetric cell was rinsed twice with MQ for 30 s between samples. Voltammetric analyses were controlled by NOVA (version 2.1.4).

For eHS and RSS pseudopolarography, the set-up remained the same; however, the equipment differed for the sulphide pseudopolarography. For sulphide pseudopolarography, a µAutolab (Eco Chemie, Netherlands) was connected to a Metrohm 663 VA stand through the IME663 interface and was controlled by GPES (Version 4.9) software. The working electrode was a 25 µm silver amalgam microwire (Goodfellow, UK) fitted in a polypropylene pipette tip and a vibrator as described by (Bi et al., 2013a). The counter electrode was an iridium wire (2 cm in length, 150 µm diameter), and the reference electrode was an Ag/AgCl with a glass salt bridge filled with 3 M KCl. The vibrator ran at 1.5 V, which gave a frequency of approximately 170 Hz. It was controlled by the stirrer control of the software. For sulphide pseudopolarography, the solution was not purged.

3.2.3. Reagents

Water used for rinsing and dilution of reagents was ultrapure deionized water (>18 MΩ) from a Milli-Q system (Millipore, UK). Molybdenum (Fisher Scientific) standard solution (10 µM) were prepared by diluting atomic absorption spectroscopy standard solutions of 1 $g.L^{-1}$ in 10 mM HCl (12 M). Fulvic acid from the Suwannee River (SRFA) (International Humic Substances Society, 2S101F) was dissolved in MQ to a concentration of 10 $mg.L^{-1}$. Thioacetamide (TA) (Fisher Scientific) and glutathione (GSH) (reduced, Sigma-Aldrich, UK) were used as standards for RSS groups (Pernet-Coudrier et al., 2013). Standards were acidified with HCl (12 M) to pH 2 and were kept in the fridge when not in use. Hg plating solution was prepared from $Hg(NO_3)_2$ (Fluka, UK) in a 0.1 M Sodium Nitrate (Sigma-Aldrich, UK) and 10 mM HCl (Fisher UK) solution. A stock solution of 0.1 M NaS was prepared from $Na_2S.xH_2O$ (Aldrich). Sulphide stock solutions and dilutions were prepared daily. Both standards were kept in the dark to avoid photodegradation. For sulphide analysis a 1 M boric acid (Analytical grade, Fisher Scientific) pH buffer was used. The buffer was prepared in 0.35 M ammonia (trace metal grade, Fisher Scientific). To remove organic and trace metal contaminants the solution was UV-digested and 100

µM MnO_2 (van den Berg, 1982) was added. The buffer was left overnight and was then filtered using a 0.2 µm cellulose nitrate membrane (Whatman).

3.2.4. Concentrations of RSS and electroactive humic substances

The CSV analytical settings were based on Pernet-Coudrier et al. (2013), but for measurement of the eHS concentration, the method was adapted to include a background subtraction (see section 2.3.1.1). The Pernet-Coudrier et al. (2013) (eHS-Mo) method was selected for the quantification of eHS as it experienced fewer interference issues compared to the eHS-Fe (Laglera et al., 2007) and the eHS-Cu (Whitby and van den Berg, 2015) methods. For the eHS-Fe method, in samples of excess inorganic Fe the eHS-Fe peak is unstable due to Fe precipitation (Abualhaija et al., 2015). The samples used in this study were collected waters with intense hydrothermal activity resulting in high concentrations of Fe (Guieu et al., 2018; Tilliette et al., 2022; Wang et al., 2022), therefore the eHS-Fe method was not selected for the quantification of eHS in this study. When using the eHS-Cu method, some samples showed a large, broad interference peak in the same position as the eHS-Cu peak (Figure 2.3), which inhibited the quantification of eHS. For this reason, the eHS-Cu method was not selected for the quantification of eHS in this study.

Briefly, under a laminar flow hood, 10 mL of seawater sample was loaded into an acid-cleaned voltammetric quartz cell. The solution was acidified to pH 2 and spiked with 30 µL of 10 ppm Mo(VI), corresponding to 375 nmol L^{-1}. A 300 s N_2 purging period was applied followed by a 150 s deposition time with deposition potential (E_{dep}) at 0 V with stirring. After deposition, a 5 s rest time was applied. A stripping scan using differential pulse mode started from 0 V to −0.6 V with a modulation time of 60 ms, a modulation amplitude of 50 mV, a step potential of 2 mV and an interval time of 0.1 s. Quantification of RSS and eHS was done by standard addition. A minimum of 4 repeat scans were performed for the sample and for each of the 2 standard additions. The peak height was measured using ECDSOFT (Omanović and Branica, 1998). Smoothing was also applied (Savitsky-Golay, smoothing

factor 10). For the eHS, a background scan was performed and subtracted from all subsequent scans, due to the curved baseline in the region of humic measurement. The background scan was performed using a 1 s deposition step with otherwise identical parameters to the analytical scan; subtraction of this resulted in an improved baseline and improved reproducibility between scans. Deep Sea Reference (DSR) seawater (Hansell lab, Batch 21 – 2021 – Lot 08-18) was used daily to check the validity of the procedure. DSR seawater was collected from 700 m depth in the Florida Straits and acidified with HCl to pH 2. The concentration of eHS obtained was 26.36 $\mu g.L^{-1}$ eq SRFA, for TA it was 56.12 nM eq TA (n=10), and there was no GSH present. The reproducibility was calculated by carrying 10 identical standard addition procedures of a DSR seawater (eHS, RSD=11.7%; TA, RSD=13.9%; n=10) (Hansell lab, batch 2021).

3.2.5. Pseudopolarography

Cathodic pseudopolarography for RSS, eHS and sulphide measurements were carried out. The method was initially published by Laglera et al., (Laglera and Tovar-Sánchez, 2014) to identify reduced sulphur substances. Multiple E_{dep} were applied to the electrode to obtain characteristic ip vs E_{dep} profiles (pseudopolarograms). For RSS, pseudopolarograms started at 0 V and decreased by increments of -0.03 V until -0.72 V. Pseudopolarograms for eHS were based on the Mo-eHS method (Pernet-Coudrier et al., 2013), started at +0.1 V, and the E_{dep} decreased by increments of -0.05 V until no peak was visible. For RSS and eHS pseudos, the working electrode was a HMDE.

For sulphide pseudopolarography, the working electrode was a 25 µM silver amalgam wire electrode instead of the HMDE. The silver amalgam wire electrodes was prepared using the method from (Bi et al., 2013b). A Cu wire was inserted through a 100 µL pipette tip. The wire was connected to a 25 µm silver wire using a conductive, adhesive silver solution (Leitsilber L100, Maplin, UK). The Cu wire was pulled back leaving the silver microwire exposed then the pipette tip. The tip was melted to secure the microwire by holding in the mouth of a tubular oven set to 450 °C. The silver microwire was

amalgamated with Hg prior to use by plating at −0.4 V (600 s) from an unstirred solution of 2 mM Hg(II) solution (pH 2). The amalgam electrode was then transferred to Milli-Q water and left overnight.

Sulphide is a highly unstable compound and is lost from the sample quickly, including through complexation with mercury (Al-farawati and van den Berg, 1997). The benefit of using the silver amalgam wire electrode is that there is a low concentration of Hg, which limits the loss of sulphide through complexation with Hg. In addition, there is no purging of the sample (with N_2 or argon (Ar)). Purging cannot be used when measuring sulphides to avoid its volatilisation. The pH was increased to 9.2 with addition of NaOH which enabled the sulphide peak to be stable for a longer period of time (Aumond et al., 2012). Sulphide pseudopolarograms were initiated from -1 V. The E_{dep} increased by increments of +0.05 V. The deposition time was 10 s at each E_{dep}.

Pseudopolarograms of standards (TA, GSH and SRFA) were carried out for each method to compare with the RSS and eHS found in seawater. Analysis of standards were carried out in UV-digested seawater (UV-SW). UV-SW was prepared by 3 h irradiation in acid cleaned 30 mL quartz tubes with a 125 W high pressure mercury lamp (van den Berg, 2014). Sulphide standard pseudopolarograms were carried out in 0.6 M NaCl (Fisher Scientific, UK) at pH 9.2. The concentration of standards used were as follows: eHS = 96 µg.L^{-1}, TA = 100 nM, GSH = 150 nM and sulphide = 1 µM.

3.2.6. Error calculations

Concentrations of compounds were measured using standard addition. Error bars given show the standard deviation of the intercept, determined for each standard addition using Equation 1 (Harris, 2003).

$$S_x = \frac{s_y}{|\mathrm{m}|}\sqrt{\frac{1}{n} + \frac{\bar{y}^2}{m^2\ \sum(x_i - \bar{x})^2}} \qquad \text{Equation 1.}$$

Where s_x is the standard deviation of the compound being measured, s_y is the standard deviation in peak intensity across all data points, m is the slope of the standard addition, n is the number of data points, $\bar{y}$ is the average peak height across all data points, x_i is the concentration of added standard for data points i, and $\bar{x}$ is the average concentration across all data points of the standard addition procedure.

3.3. Results

3.3.1 Hydrography

A detailed account of the hydrography during November 2019 is described by Tilliette et al. 2022 (Tilliette et al., 2022). The surface water temperature varied from 23.04 to 27.32 ˚C in the upper 100 m, and the salinities ranged from 35.06 to 35.47 (Figure 3.1B and 3.1C). Subtropical Underwater (STUW) and the Western South Pacific Central Water (WSPCW) dominated the main thermocline (200 - 700 m). The intermediate layer (700 – 1,300 m) is comprised of Antarctic Intermediate Waters (AAIW), while the deep layer (> 1,300 m) contained two water masses: Pacific Deep Water (PDW) and the Lower Circumpolar Deep Water (LCDW). Across the cruise transect, the different water masses were distributed uniformly, except for PDW and LCDW. These water masses were displayed differently across the eastern and western parts of the transect. PDW was dominant in the Melanesian waters and Lau basin, whereas in the Melanesian waters, LCDW was only present between 2,500 m and the seafloor. The Lau Basin has low contribution of LCDW. However, in the deepest waters of the South Pacific gyre, LCDW is the sole contributor.

Stations 2 and 3 were in the Melanesian basin in the western part of the transect while stations 4, 11 and 12 were in the Lau Basin in the central part of the transect. Stations 6, 7 and 8 were in the South Pacific Gyre, in the eastern part of the transect. In this study, there were two hydrothermal stations “PANAMAX” and “SIMONE”. The hydrothermal sources were detected from the acoustic anomalies (Tilliette et al., 2022). At the time of this study, the SIMONE site displayed multiple acoustic anomalies

observed suggesting the presence of multiple weak sources (C. Tilliette et al., 2022). Four substations were sampled in the vicinity of SIMONE (T1, T2, T3 and T5) but only the furthest away (T1, 15 km away from hydrothermal vent) was analysed here. This station is referred as “S15”.

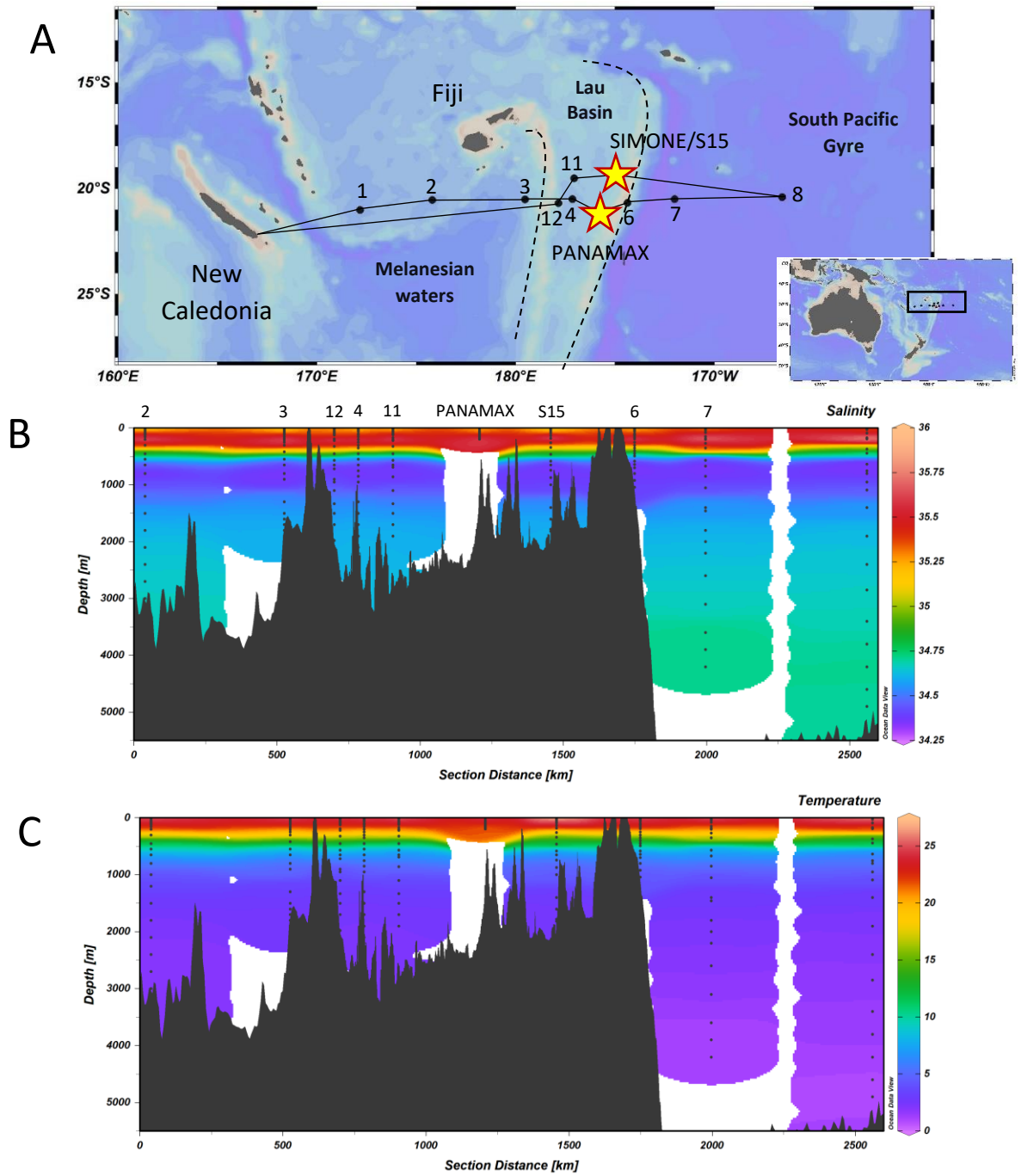

Figure 3.1. *(A) Map of stations sampled during the TONGA 2019 (Grp14) cruise across the Western Tropical South Pacific Ocean (WTSP). In the WTSP there are three distinct regions (separated by dashed lines): Melanesian waters, Lau Basin and South Pacific Gyre. The cruise started and ended in New Caledonia. The black lines represent the cruise track, and the numbers are the stations. The stars are the two shallow hydrothermal vents, PANAMAX and SIMONE. S15 was 15 km away from the SIMONE hydrothermal source but S15 still had high acoustic anomalies (Tilliette et al., 2022). (B) Salinity and (C) temperature section plots in the WTSP between 1st Nov and 5th December 2019. Figures were generated using ODV software (Schlitzer, 2021).*

3.3.2 RSS and eHS distribution in the WTSP Ocean

Two distinct types of RSS-like compounds were identified (Figure 3.2). These compounds behaved electrochemically in a similar way to thioacetamide and glutathione (Figure 3.3) and will therefore be referred to as thioacetamide-like (TA-like) and glutathione-like (GSH-like) compounds throughout the text. The distribution of TA-like, GSH-like and eHS compounds along the cruise transect are presented in Figure 3.4.

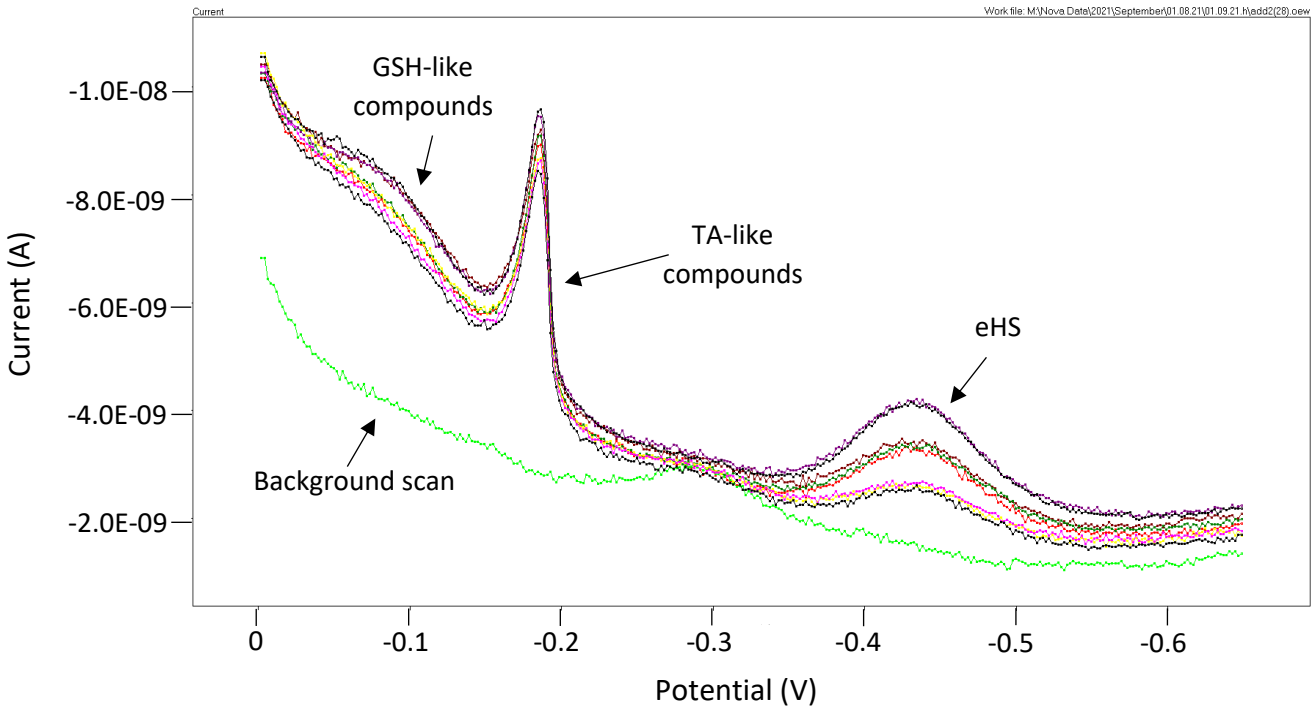

Figure 3.2. *Cathodic stripping voltammogram using the Mo method (Pernet-Coudrier et al., 2013). This method allows for the simultaneous quantification of thioacetamide-like (TA-like), glutathione-like (GSH-like) compounds and electroactive humic substances (eHS). Background scan used the same analytical parameters as the analytical scan but with a 1s deposition time. This scan is used for the background subtraction for eHS quantification.*

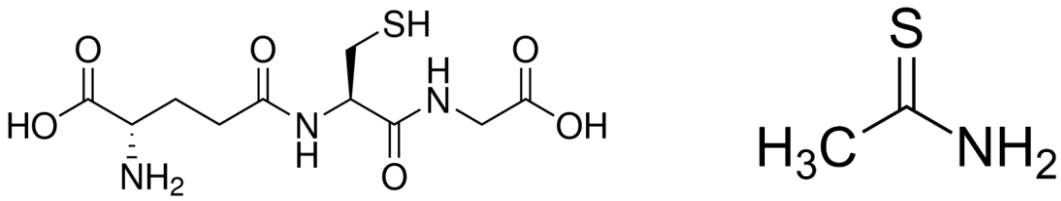

Figure 3.3. *Chemical structures of thioacetamide (A) and glutathione (B).*

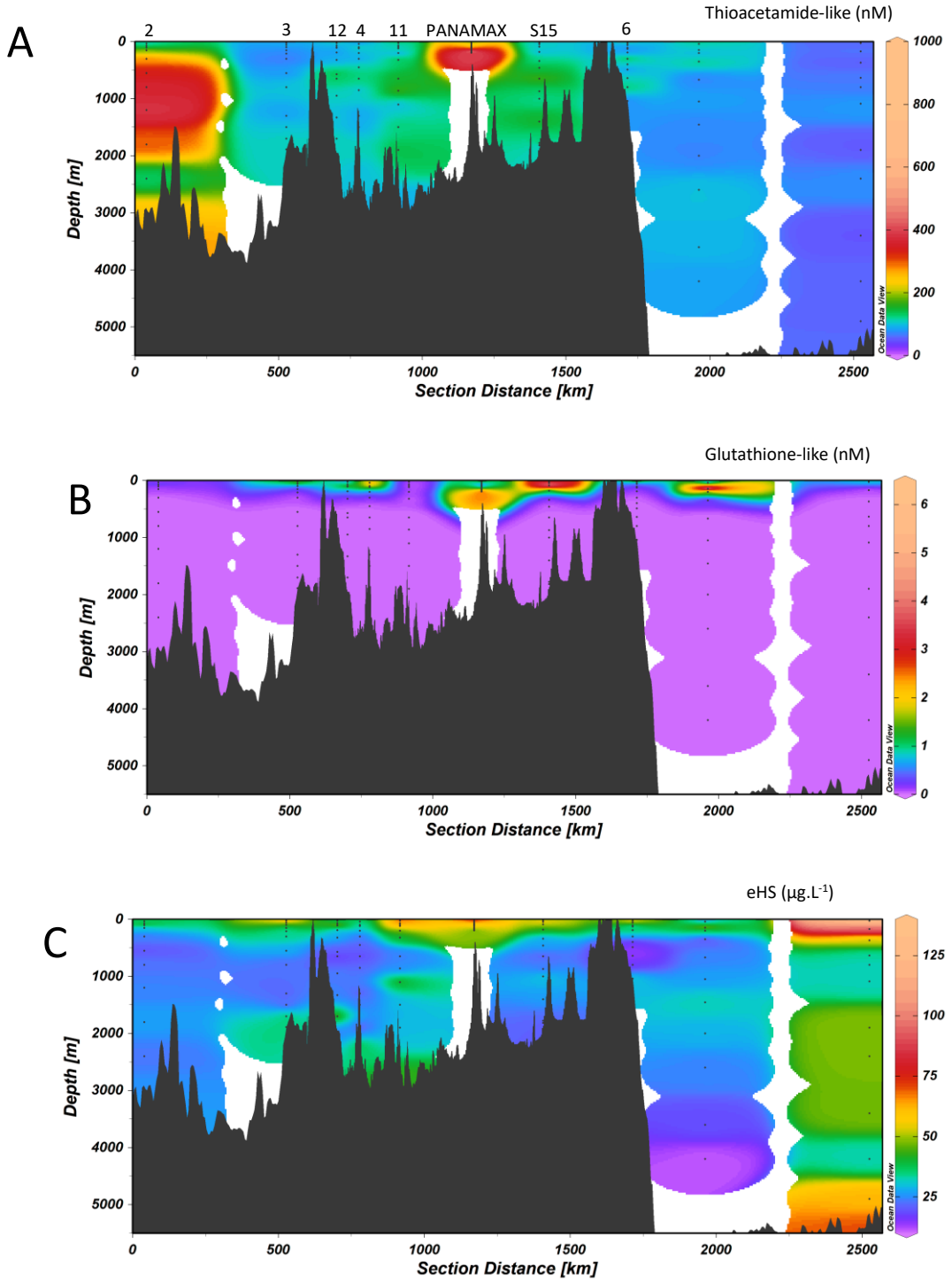

Figure 3.4. *(A). The distribution of thioacetamide-like (TA-like) compounds (B), glutathione-like (GSH-like) compounds (C) and electroactive humic substances (eHS). Numbers refer to stations and PANAMAX and S15 refer to the two hydrothermal sites. S15 was 15 km away from the SIMONE hydrothermal source but S15 still had high acoustic anomalies. Figures were generated using ODV software (Schlitzer, 2021).*

The data was grouped in oceanographically similar regions to compare vertical profiles of TA-like, GSH-like compounds and eHS in the WTSP (Figure 3.4).

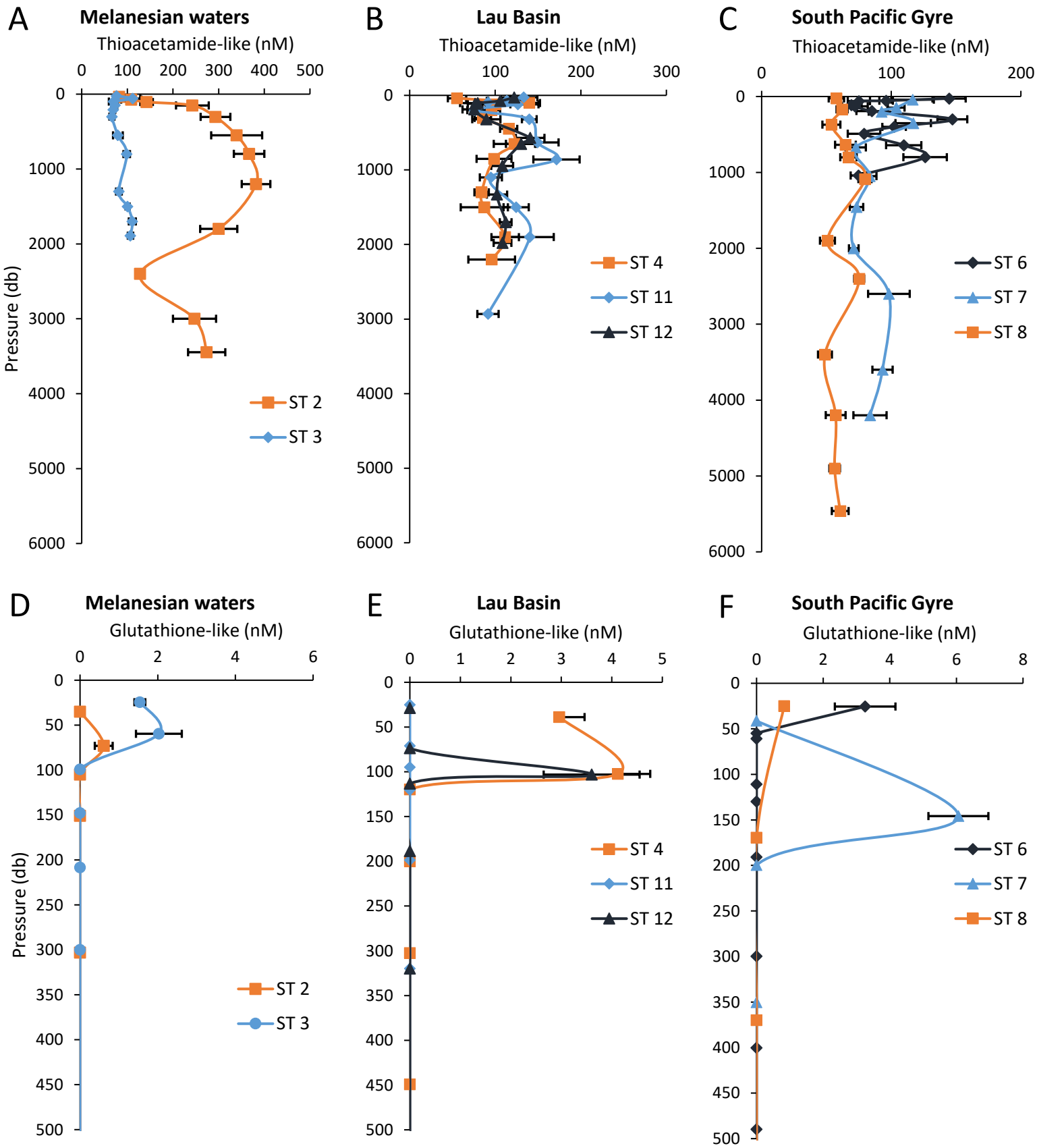
A
Melanesian waters
Thioacetamide-like (nM)
0 100 200 300 400 500
Pressure (db)
0 1000 2000 3000 4000 5000 6000
ST 2
ST 3
B
Lau Basin
Thioacetamide-like (nM)
0 100 200 300
ST 4
ST 11
ST 12
C
South Pacific Gyre
Thioacetamide-like (nM)
0 100 200
ST 6
ST 7
ST 8
D
Melanesian waters
Glutathione-like (nM)
0 2 4 6
Pressure (db)
0 50 100 150 200 250 300 350 400 450 500
ST 2
ST 3
E
Lau Basin
Glutathione-like (nM)
0 1 2 3 4 5
ST 4
ST 11
ST 12
F
South Pacific Gyre
Glutathione-like (nM)
0 2 4 6 8
ST 6
ST 7
ST 8

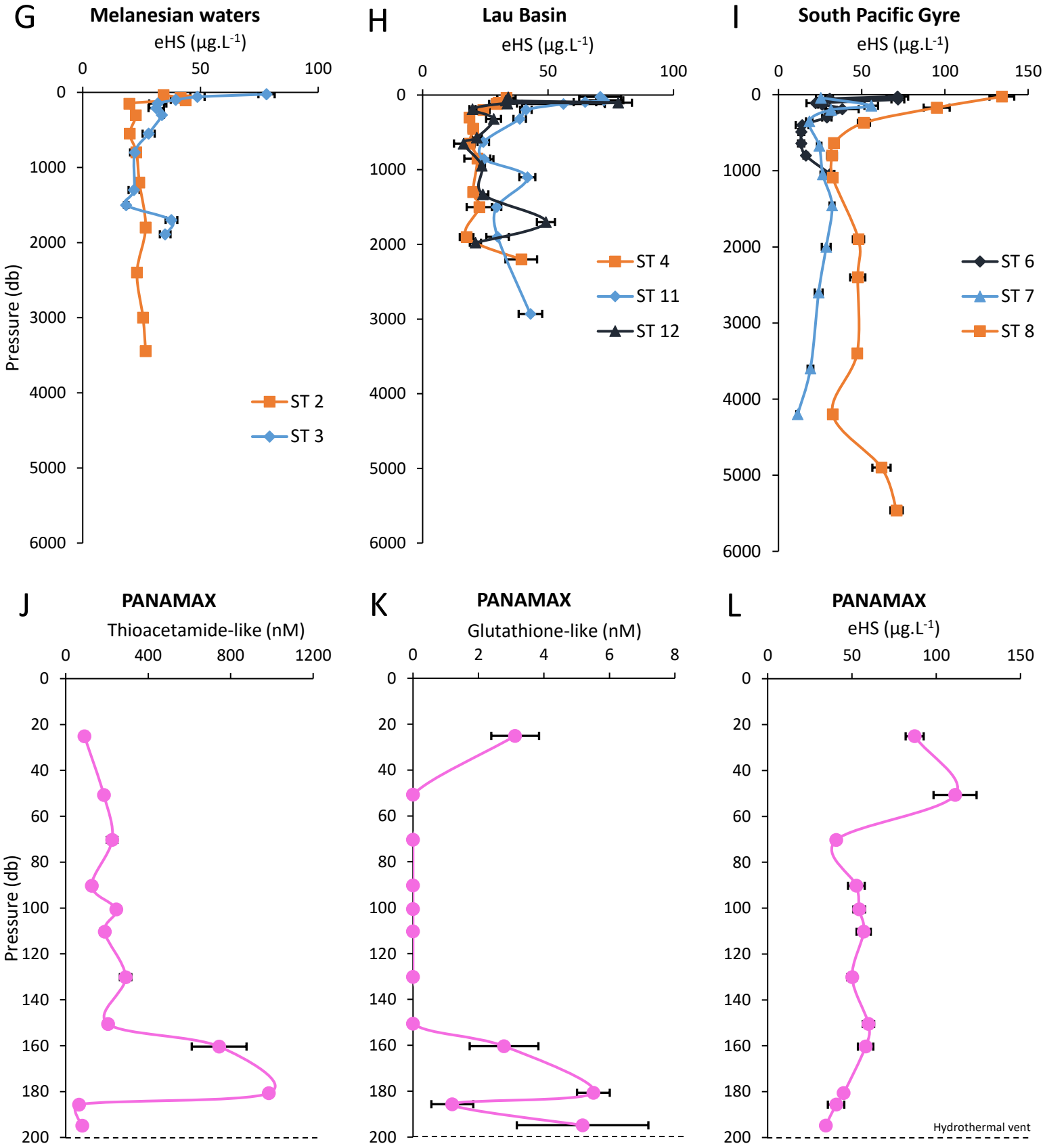
G
Melanesian waters
eHS (µg.L-1)
0
50
100
Pressure (db)
1000
2000
3000
4000
5000
6000
ST 2
ST 3
H
Lau Basin
eHS (µg.L-1)
0
50
100
ST 4
ST 11
ST 12
I
South Pacific Gyre
eHS (µg.L-1)
0
50
100
150
ST 6
ST 7
ST 8
J
PANAMAX
Thioacetamide-like (nM)
0
400
800
1200
Pressure (db)
20
40
60
80
100
120
140
160
180
200
K
PANAMAX
Glutathione-like (nM)
0
2
4
6
8
L
PANAMAX
eHS (µg.L-1)
0
50
100
150
Hydrothermal vent

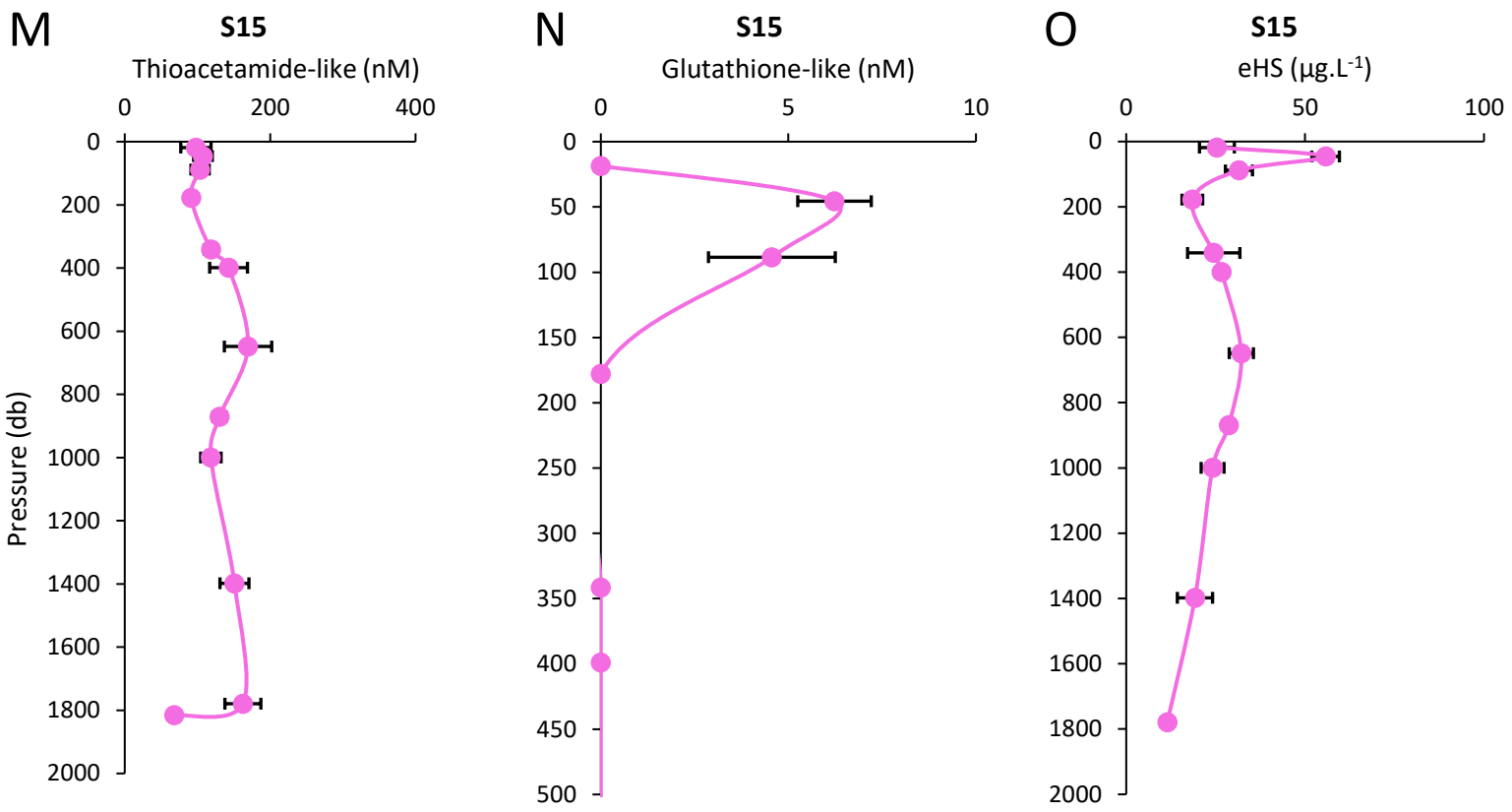

Figure 3.5. *Profiles of thioacetamide-like (TA-like) compounds (A-C), glutathione-like (GSH-like) compounds (D-F) and electroactive humic substances (eHS) (G-I) in the Melanesian Basin, Lau Basin and South Pacific gyre. Profiles for the stations at the PANAMAX and S15 volcanic sites for TA-like, GSH-like, and eHS have been plotted separately (J-O). S15 was 15 km away from the SIMONE hydrothermal source but S15 still had high acoustic anomalies. Dashed line represents the depth of the hydrothermal vent. TA-like and eHS profiles from each region were plotted over the entire water column, while GSH-like compounds are shown to 500 m. Concentrations were obtained using standard addition calibration. Error bars represent the standard deviation from the calibration.*

3.3.2.1. Thioacetamide-like compounds

TA-like compounds were present throughout the whole water column at all stations. The concentration of TA-like compounds ranged from 48 to 984 nM (Figure 3.3B) with an average of 131 ± 16 nmol L^{-1} (TA equivalent, n=119). The highest concentration of TA-like compounds was at a depth of 181 m at PANAMAX (vent depth 200 m). TA-like concentrations were higher in the Melanesian waters (mean 165 ± 19 nM) than in the Lau Basin and in the South Pacific Gyre (mean 108 ± 16 nM and 84 ± 9 nM respectively). At station 2 (Figure 4A), concentrations of TA-like compounds were high

compared to the rest of the transect (mean 242 ± 31 nM at station 2 compared to 119 ± 14 nM mean across the cruise), with a maximum concentration of 381 ± 31 nM at 1200 m. Station 8 had the lowest concentration of TA-like compounds overall (mean 61 ± 6 nM).

3.3.2.2. Glutathione-like compounds

At most stations, GSH-like compounds were only detected in the surface waters (upper 200 m). The concentration ranged from 0.61 ± 0.23 nM to 6.23 ± 0.98 nM, with the maximum concentration observed at 46 m at station 7 in the South Pacific Gyre (Figure 3.4F). At PANAMAX, concentrations of GSH-like compounds were elevated above the hydrothermal vent (Figure 3.4K).

3.3.2.3. eHS

The concentrations of eHS ranged from 11.5 ± 0.8 to 134 ± 7 $\mu g.L^{-1}$ eq SRFA, mean 37 ± 3 $\mu g.L^{-1}$ (Figure 3.4D, n = 119). At most stations eHS concentrations were higher in the upper 200 m, remained fairly constant at depths deeper than 300 m, with a slight increase in concentration in the bottom waters at stations 3, 4, 6 and 8. Station 8 had an increased concentration of eHS (mean 57 ± 4 $\mu g.L^{-1}$) compared to the rest of the transect (mean 35 ± 3 $\mu g.L^{-1}$). Station 8 and PANAMAX had an elevated average concentration of eHS compared to the rest of the transect (Station 8; mean 57 ± 4 $\mu g.L^{-1}$, PANAMAX; mean 58 ± 4 $\mu g.L^{-1}$). Samples from S15 showed similar concentration and trends to other non-hydrothermally influenced eHS profiles.

3.3.3 Pseudopolarography

3.3.3.1. RSS Pseudopolarography

At neutral pH, multiple RSS peaks coalesce, making it hard to distinguish between them. Pseudopolarography is a technique where varying E_{dep} are applied to the electrode. The signal of

interest is measured at the different E_{dep} and plotted to create a unique ip vs E_{dep} profile (pseudopolarogram). Comparing pseudopolarograms of RSS found in seawater to model compounds can help with the identification of the RSS found in seawater. All pseudopolarograms were normalised to the largest peak intensity (i/i_{max}) for comparative purposes. Pseudopolarograms of model compounds (TA and GSH) were obtained in UV digested seawater (Figure 3.5A). The shape of the TA and GSH pseudopolarograms differ. A voltammetric signal for GSH was detectable until -0.5 V, and TA peak was only detectable until -0.075 V.

Pseudopolarograms of surface and bottom waters at PANAMAX (surface = 25 m; deep = 180 m), S15 (surface = 20 m; deep = 1780 m) and station 8 (surface = 25 m; deep = 5462 m) are present in Figure 3.5B-D. A RSS peak was detectable until -0.5 V in bottom waters at both PANAMAX and station 8. In the surface waters a RSS peak was detectable until -0.1 V (PANAMAX), and -0.18 V (Station 8). S15 is different compared to the other stations. The RSS peak in the bottom waters was detectable until -0.15 V, which is more positive than PANAMAX and station 8. It is also the same for the surface waters.

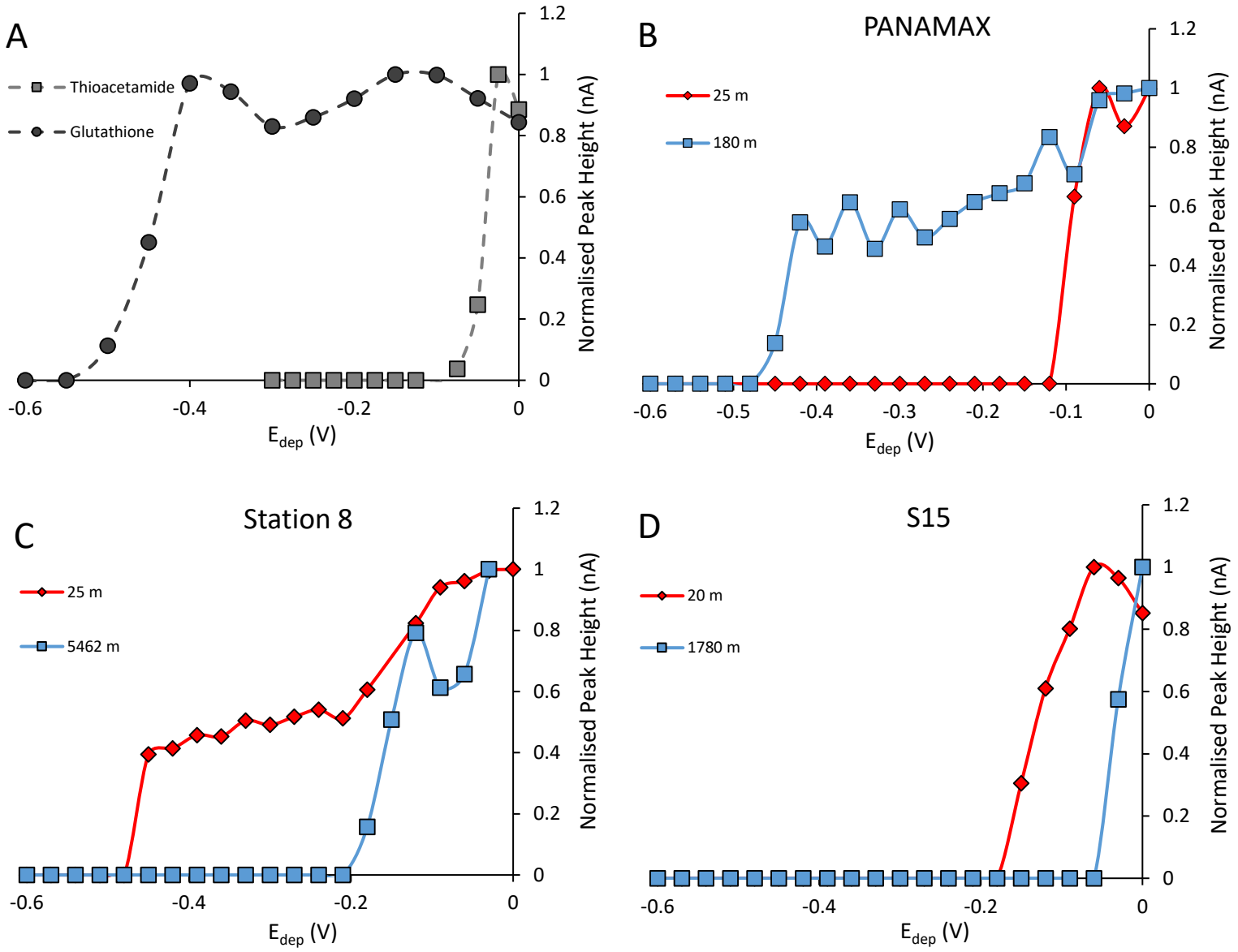

Figure 3.6. *(A) Pseudopolarograms of thioacetamide (TA) and glutathione (GSH), in UV digested seawater. Pseudopolarograms reduced sulphur substances found in the surface and bottom waters from PANAMAX (B), station 8 (C) and S15 (D) using the method developed by Laglera et al., (2014). were initiated at 0 V and decreased by increments of -0.05 V. Each point represents the peak height of the RSS signal. Peak height has been normalised to the highest peak value (=peak height/largest peak height). Solutions were at natural pH.*

3.3.3.2. Sulphide Pseudopolarography

During analysis of the PANAMAX plume (180 m), a large peak was observed in the 1 s background scan (which is subtracted from each scan to flatten the baseline and improve measurement of eHS, see section 3.3.1.1.) (Figure 3.S3). This peak was observed in the same peak position as TA-like

compounds. Free sulphide produces the same voltammetric peak as thioacetamide (Pernet-Coudrier et al., 2013). During the analytical scan, the peak height decreased with time (Figure 3.S1), which is characteristic of sulphide, due to the volatilisation of H_2S, which is more critical in acidic pH. Sulphide peaks decrease rapidly in voltammetric analysis as it is removed from seawater (Aumond et al., 2012; Cline and Richards, 1969; Deleon et al., 2012). Because of this, it was suspected that sulphide could be present in the sample. Therefore, pseudopolarography of the PANAMAX plume (180 m) was carried out. Pseudopolarography at station 2 (797 m, [TA] = 367 ± 33 nM) was also carried out as this sample had a high concentration of TA-like compounds.

The sulphide standard peak increased between the potentials -0.7 to -0.6 V, after which the peak is also stable. For station 2, a peak is visible at Edep > -0.65 V and increases until -0.5 V. For the plume at PANAMAX, the pseudopolarogram mimics the sulphide standard.

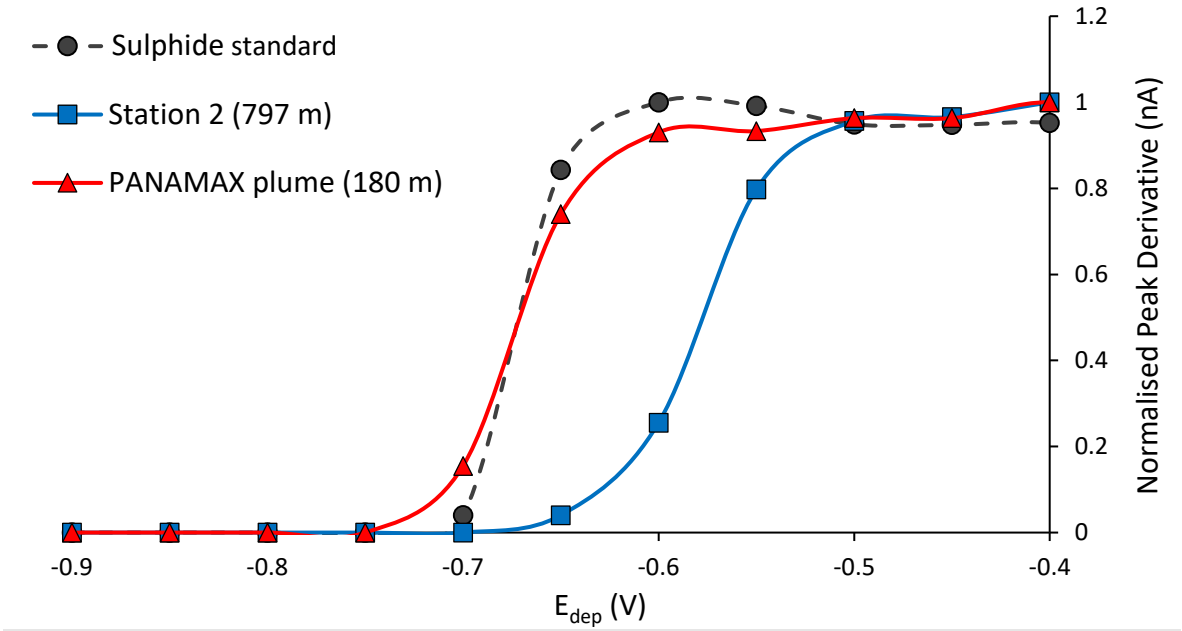

Figure 3.7. *Pseudopolarograms of station 2 (797 m) and above the plume at PANAMAX (180 m, station 5). A fresh sample from the PANAMAX plume was defrosted for sulphide pseudopolarogram. Sulphide standard (1 µM) in 0.6 M NaCl. Solutions were buffered to pH 9.2. Pseudopolarograms were initiated at -1 V and increased by increments of -0.05 V. Each point represents the peak height of the RSS signal. Peak height has been normalised to the highest peak value (=peak height/largest peak height).*

3.3.3.3. eHS Pseudopolarography

Figure 3.7A shows profiles of SRFA (2S101F) and SRHA (2S101H), two common standards used to quantify humic substances (Figure 3.7A). Standards were added to UV digested seawater at pH 2 in the presence of Mo(VI). The overall shape of the pseudopolarograms in the surface and deep waters from stations 2, 8 and S15 resemble the SRFA standard (Figure 3.7B and 4.7C). All samples reached a maximum sensitivity at E_{dep} in the range of -0.3 to -0.45 V. eHS in the surface water were detected at more negative potentials than those in deep water.

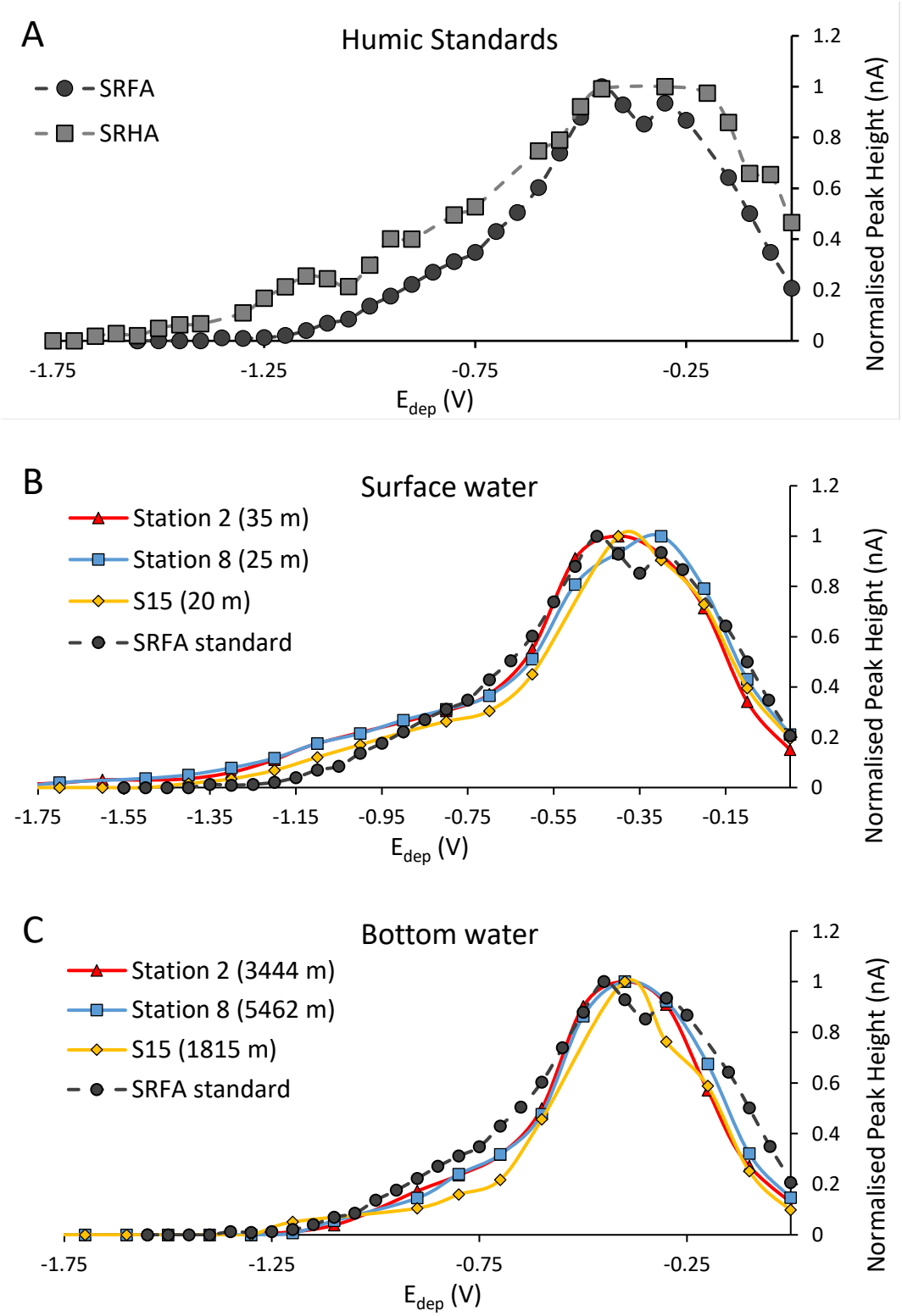

Figure 3.8. *(A) Pseudopolarograms of 96 µg.L^{-1} of Suwannee River fulvic acid (SRFA) standard and Suwannee River humic acid (SRHA) standard, two common humic standards. Standards were added to UV digested seawater. (SRFA) standard was compared to eHS in the surface (B) and bottom water (C) from stations 2, 8 and S15. The method using the Mo-eHS method (Pernet-Coudrier et al., 2013). Each point represents the peak height of the eHS signal. Peak height has been normalised to the highest peak value (=peak height/largest peak height). Voltammetric analysis was carried out at pH 2.*

3.4. Discussion

3.4.1. RSS in the WTSP Ocean

TA-like compounds were detected in all samples at all depths, whereas GSH-like compounds were only detected in the upper 200 m. Comparison of the vertical profiles of TA-like and GSH-like compounds suggest a combination of distinct and common processes drive their biogeochemical cycling. For example, near the surface (upper 100 m) at stations 2, 3 and 4, concentrations of both TA-like and GSH-like compounds were lower than in underlying waters. The decrease in RSS concentrations in surface waters is likely due to photochemical destruction, which has been demonstrated to occur on the order of hours (Gomez-Saez et al., 2017; Laglera and van den Berg, 2006; Moingt et al., 2010). However, in water away from direct sunlight, TA is stable for long periods of time (Howard, 2017; Mallory, 1968) while GSH is only stable for a few hours (Petzold and Sadler, 2008).

There are not many published ocean profiles of TA-like compounds. In the Northeast Pacific, a TA-like compound was observed and the concentration ranged from 22 to 480 pM in thiourea-equivalents (Whitby et al., 2018). This is an order of magnitude lower than those observed (in TA-equivalents) in this study. In the Northeast Pacific study, analyses were carried out at natural pH, at which thiourea and TA-like compounds produce the same voltammetric signal. In CSV, thiourea is more sensitive and therefore produces a larger voltammetric signal than TA for the same concentration (Al-Farawati and van den Berg, 1997; Al-Farawati and Van Den Berg, 2001) leading to lower estimated concentrations when using a thiourea standard. However, Laglera et al. 2003 compared the concentration of RSS obtained in the Scheldt estuary with both thiourea and thioacetamide standards. It was found that using the thioacetamide standard gave a concentration of 70 nM and 35 nM for thiourea (Laglera and van den Berg, 2003), a difference of 100%.

The profiles of GSH-like compounds are similar to those previously reported in the North Atlantic Ocean (Kading, 2013; Swarr et al., 2016) and Subarctic Pacific (Dupont et al., 2006) only being detected in upper waters. The average concentration of GSH-like compounds in this study was slightly higher

than the previous studies, with a mean concentration of 3.4 ± 0.8 nM compared to maximum concentrations of 0.8, 1.7 and 2.2 nM GSH in studies by Dupont et al. (2006), Kading (2013) and Swarr et al. (2016) respectively.

Marine microbes have been shown to produce RSS when exposed to light order to reduce oxidative stress (Mangal et al., 2020). In November 2019 in the WTSP marine microbes were exposed to sunlight for ~13 h per day, therefore we would expect to see a correlation between RSS and Chl *a*. However, in this study, we found no correlation between the distribution of TA-like compounds or GSH-like compounds with Chl *a* (data not shown).

High RSS concentrations (>500 nM) have been measured in the Black Sea (Mopper and Kieber, 1991) and sediment pore waters (Chapman et al., 2009) where conditions are sulphidic. While such high concentrations were not observed in our study, the nearby volcanic and hydrothermal activity could contribute to higher RSS concentrations.

3.4.2. Hydrothermal influence of RSS production

Above the hydrothermal plume at PANAMAX (181 m), we saw an increase in both TA-like (984 ± 19 nM; Figure 3.4J) and GSH-like compounds (5.2 ± 0.5 nM; Figure 3.4K), suggesting that the production of these compounds is related to hydrothermal activity.

Some hydrothermal vents are suspected to be a source of RSS. Cu-binding ligands with log K similar to RSS have been detected in hydrothermal vents (Jacquot and Moffett, 2015; Sylvia G Sander and Koschinsky, 2011). One study in particular found that hydrothermal vents in the Tonga-Kermadec Arc produced high concentrations of Cu-binding ligands (up to 4000 nM). Upon further investigation they concluded that RSS contributed to this pool (Sander et al., 2006). However, RSS were not found to be released from hydrothermal vents in the East Pacific Rise (Ruacho et al., 2020).

It has been suggested that the formation of thiols in hydrothermal fluids is due to the reaction of CO/CO_2 with sulfide. PANAMAX is an active hydrothermal site that produced high concentrations of CO_2 (up to 645 µM) (Tilliette et al., 2022) and H_2S has been shown to be produced from this vent (this study). For the formation of thiols from sulfide and CO/CO_2 the solution needs to be at temperatures of 325℃ (Schulte and Rogers, 2001). The exact temperature of the plume was not measured in this study, however previous studies have shown that hydrothermal fluids can exceed 400℃ (Foustoukos and Seyfried, 2007; Koschinsky et al., 2008), suggesting this mechanism could contribute to the production of thiols from hydrothermal vents near sampling locations in this study.

The increased concentration of RSS could be of biological origin. RSS are known to complex with trace metals to help with either trace metal uptake or detoxification (Dupont and Ahner, 2005; Huang et al., 2018; Navarrete et al., 2019; Rea et al., 2004; Steffens, 1990). RSS are soft Lewis bases and can form strong complexes with soft acids, which include metals such as Cu^+, Hg^+ and Cd^{2+} (Jensen, 1978). PANAMAX is a shallow hydrothermal vent, with vent fluids reaching the photic layer. Hydrothermal fluids are enriched with metals (Chen et al., 2018). However, the effect that trace metals have on biology is not just based on the concentration but its chemical speciation. For example, Cu is both a nutrient and a toxicant for marine microbes but Cu toxicity is largely dependent on the abundance of Cu(II) (Brand et al., 1986; Debelius et al., 2011; Moffett et al., 1997). Elevated concentrations of Cu(II) can be toxic and induce oxidative stress (Kennedy et al., 2020). In this study, concentrations of dCu at PANAMAX was measured at 0.38 nM nmol kg^{-1}, but hydrothermal vents can release high concentrations of Cu(II) (Sylvia G. Sander and Koschinsky, 2011). This can trigger the production of RSS by surface communities to detoxify Cu stress.

Hydrothermal vents also emit high levels of ROS (Shaw et al., 2021), which can also induce production of RSS.

3.4.3. RSS identification

During voltammetric RSS analysis, it is the sulphur group in the RSS compound that reacts with the Hg on the HMDE, forming a RSS-Hg complex. During the voltammetric stripping scan, the Hg in the complex is reduced which creates a voltammetric signal equating to the change in current (Laglera and van den Berg, 2003; Turner et al., 1975). The peak height of this signal is measured for RSS quantification. Therefore, compounds that also contain a sulphur group can produce a similar voltammetric signal, which coalesce at natural pH. The Mo method (Pernet-Coudrier et al., 2013) is carried out at pH 1.95 and can distinguish between the following RSS: thiourea, thioacetamide, glutathione, cysteine and N-acetyl-L-cysteine. Despite this, some RSS can still appear in the same position. For example, free sulphide and thioacetic acid produce a peak in the same region as thioacetamide. Pseudopolarography is a qualitative analytical technique that can provide information on the nature/structure of the compound of interest. During pseudopolarography, each RSS shows a distinct behaviour (Laglera and Tovar-Sánchez, 2012, 2014). Comparing pseudopolarograms of RSS in natural waters to model standards can help to identify the RSS in the sample. This technique can also be beneficial to see if the standard is representative of the compound of interest in the sample.

Pseudopolarograms of the surface and bottom waters at station 8, PANAMAX and S15 were performed to compare to those obtained in UV digested seawater amended with model thiol compounds. GSH and TA were the model compounds used for the comparison because suspected thiol peaks in the samples appeared in the same position as TA and GSH using CSV in acidic conditions. Thiol pseudopolarography was carried out at natural pH, which causes multiple thiol peaks to appear in the same position and coalesce. This could allow for simultaneous identification of the thiol compounds present, as it is possible to tell if both GSH and TA were present in the sample. Thiols such as TA are more sensitive to Hg than GSH and produces a larger signal (Laglera and Tovar-Sánchez, 2012) for the same concentration. TA is only detectable at more positive potentials (Figure 3A). In pseudopolarography, if a sample has a mixture of TA and GSH at more negative potentials (<-0.075 V), only GSH will be detected. At more positive potentials, both GSH and TA will be detected. The

combination of the absorption of both thiols on the Hg drop and TA being more sensitive GSH will cause an increase in peak height when depositing at more positive potentials.

TA-like compounds were present in all samples that were selected for pseudopolarography. GSH-like compounds were only found at station 8 surface (25 m) and PANAMAX bottom (180 m) waters out of the 6 samples selected. The shape of the pseudopolarograms from station 8 bottom (5462 m), PANAMAX surface (25 m), S15 surface (20 m) and S15 bottom (1780 m) do not match the shape of the pseudopolarogram of the TA standard (Figure 3.S1). This suggests that TA is similar to, but is not the exact compound responsible for, the peak of the TA-like compounds found in this study. TA is not known to be present in marine environments, but it has been observed in estuarine and river waters (Marie et al., 2017, 2015; Superville et al., 2013). Phytoplankton have been shown to exude a RSS electrochemically similar to TA (Leal et al., 1999). TA is also potentially toxic to marine life. It has been found that 50nM of TA can cause inhibition of growth in phytoplankton (Vasconcelos et al., 2002). Concentrations of TA-like compounds found in this study were higher than 50nM. In addition, the shape of pseudopolarograms from each station differ suggesting the composition or chemical structures of the RSS detected differ between samples, although this difference could also be attributed to multiple types of RSS present within the same sample.

The shape of the pseudopolarograms from station 8 surface (25 m) and PANAMAX bottom (180 m) were similar (Figure 3.5B and C). Both pseudopolarograms presented a response over a wide range of depositon potential (> ~ -0.45 V). Comparing these pseudopolarograms to the GSH standard, they were similar (Figure 3.S2). GSH is common in marine waters (Dupont et al., 2006; Gao and Guéguen, 2018; Tang et al., 2000; Whitby et al., 2018), this coupled with the matching pseudopolarograms suggest that GSH was present in the samples. In addition, both pseudoplarograms presented an increase signal at higher deposition potentials (> ~ -0.1 V) indicating the presence of another RSS that is responding similarly to TA (Figure 3.5A) or thiourea (data not shown).

3.4.4. Sulphide at PANAMAX

Hydrothermal vents are known to be a source of sulphides which have been reported to be present at high concentrations in such environments (µM to mM) (Cotte et al., 2018; Damm et al., 1995; Dias et al., 2010) and the Lau Basin has been shown to release high amounts of sulphide (Hsu-kim et al., 2008; Yücel et al., 2011). Quantification of sulphides can be complicated as they are unstable. However, cathodic pseudopolarography can be used to detect their presence. Sulphides can be detected at more negative potentials than RSS (Al-Farawati and van den Berg, 1997) with a peak apparent for Edep > -0.7 V (Figure 3.6), i.e. much lower than for RSS such TA, TU or GSH. The shape of the pseudopolarogram above the plume at PANAMAX matched the pseudopolarograms of the sulphide standard, strongly suggesting that sulphide was being released from PANAMAX. The presence of sulphide could have interfered with TA measurements. However, this is unlikely as the TA-like compounds are stable, and purging in acidic conditions should rapidly removes the sulphide from the sample. We did not quantify sulphides in this sample.

3.4.5. RSS at station 2

At station 2, high concentrations of TA-like compounds were present compared to the rest of the transect. Due to the high sensitivity of sulphide with Hg, a sample from station 2 (797 m) was selected for pseudopolarography to check for the presence of sulphide. In pseudopolarography of sulphide, a voltammetric signal is detected until -0.7 V, at more negative potentials the there is no longer a signal. The shape of a pseudopolarogram of the sulphide standard differed to that of a sample from station 2 (797 m) suggesting that sulphide was not present in this sample (Figure 3.6). If sulphide was present in the sample, even at low concentrations we would still see a voltammetric signal until -0.7 V. From the quantification of RSS using the Pernet-Coudrier method (Section 3.3.1.2.), we know that only a TA-like compound was detected (Figure 3.4.A and D), but when comparing the shape of the pseudopolarograms from station 2 and the TA standard, they also do not match (Figure 3.S4). The

pseudopolarogram from station 2 is wider (peak detectable until -0.65 V) than the TA standard (peak detectable until -0.075 V) (Figure 3.5A). This pseudopolarogram is also different to the RSS pseudopolarograms in section 4.3. The high concentration of RSS and the wide pseudopolarogram indicates differences in RSS type(s) or structure of a RSS-containing compound at this station.

One possibility previously presented for the identity of these TA-like compounds is a thiocarbonyl tail attached to a larger compound such as methanobactin (Whitby et al., 2018). Methanobactins are low molecular mass (<1,200 Da) multidentate ligands that have thioamide moieties (DiSpirito et al., 2016; Kim et al., 2004) and very high copper-binding strengths (Choi et al., 2006). Methane-oxidizing bacteria produce methanobactins to acquire Cu (DiSpirito et al., 2016; El Ghazouani et al., 2012; Hakemian et al., 2005). Concentrations of dCu at station 2 (mean 0.05 nM kg^{-1}) were very low compared to the rest of the transect (mean 1.25 nM kg^{-1}) (Gonzalez-santana et al., 2023). Concentrations of the TA-like compound have been shown to correlate well with strong Cu-binding ligands in salt marshes (Whitby et al., 2017) and methanobactins were hypothesized to contribute to the strong Cu-binding ligand pool in intermediate waters of the Northeast Pacific (Wong et al., 2021). We therefore hypothesise that the voltammetric signal we ascribe to TA could be the thioamide moieties on a larger thiocarbonyl compound, such as methanobactin (Figure 3.9). Voltammetric measurements of methanobactins observed a peak at -0.6 V, which at natural pH, is around the same position as RSS (El Ghazouani et al., 2012, 2011). This shows that methanobactins could produce a signal similar to RSS. It could then be assumed that the voltammetric peak could move to more positive potentials in acidic conditions, as is observed with RSS. However, to our knowledge, this has yet to be investigated.

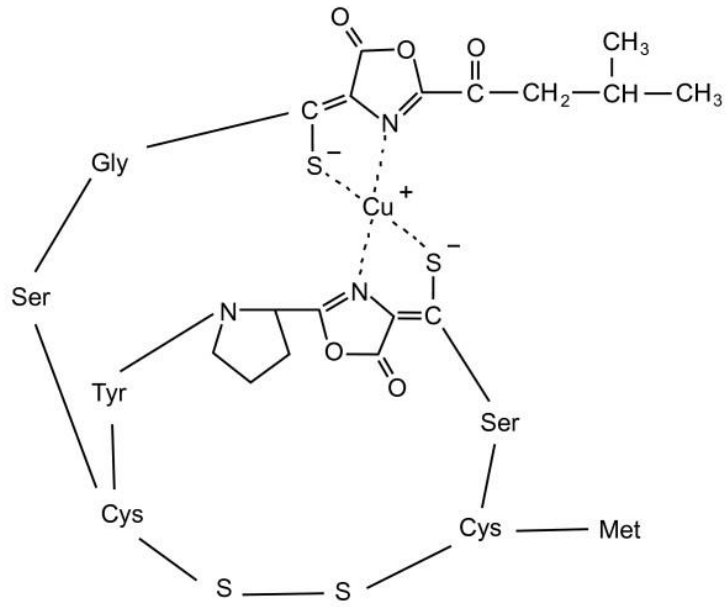

Figure 3.9. *Proposed chemical structure of the methanobactin bound with Cu. Figure obtained from Pesch et al., 2011.*

3.4.6. Electroactive humic substances in the WTSP Ocean

The vertical profiles of eHS are similar to those previously reported elsewhere, with enrichment in upper waters and lower concentrations in the deep sea (Dulaquais et al., 2018; Fourrier et al., 2022; Gao and Guéguen, 2018; Whitby et al., 2018). The high concentrations of eHS in upper waters is likely due to the active production of eHS. Phytoplankton can produce eHS as either a by-product of microbial respiration, algal exudation or decay (Ferrari et al., 1996; Lorenzo et al., 2007; Nelson et al., 2007). In this study, there was a weak but significant correlation between eHS and Chl *a* in the upper 500 m (r^2 = 0.08, n = 56, p-value < 0.05) (Figure 3.S5). The weak correlation could be due to active production of eHS through other processes, such as bacterial remineralisation or photo oxidation of triglycerides and fatty acids (Kieber et al., 1997). The concentration of eHS was lower in surface waters, which corresponds to humic degradation due to photo-oxidation (Brinkmann et al., 2003; Dainard et al., 2015; Liu et al., 2010; Yamashita et al., 2010). At stations 3, 4, 6 and 8, there were elevated eHS concentrations close to the sediment (Figure 3.4G-H). Sediments are considered a source of humics

(Dulaquais et al., 2018; Shigemitsu et al., 2021) due to biota in the sediments, which can supply fresh humics into the water column (Aiken et al., 2017; Zhang et al., 2016).

The concentration of eHS detected during the TONGA cruise was higher than in other areas in the Pacific Ocean. Typically, eHS concentrations in other parts of the Pacific have been reported to range from 0.6 to 63 $\mu g.L^{-1}$ (Cabanes et al., 2020; Whitby et al., 2018) compared to 11.5 to 134 $\mu g.L^{-1}$ found here. The WTSP experiences high biological production due to the phosphorus and Fe-rich waters (Guieu et al., 2018; Tilliette et al., 2022; Wang et al., 2022). The WTSP also experiences intense hydrothermal activity (Baker et al., 2019; German et al., 2006; Pelletier et al., 1998). Hydrothermal vents could be a source of eHS (see section 4.8), which could also contribute to the elevated concentration of eHS detected in this region.

3.4.7. Electroactive humic substances at Station 8

At station 8, eHS concentrations were higher (average 57 ± 4 $\mu g.L^{-1}$) than the rest of the transect (average 35 ± 3 $\mu g.L^{-1}$) although it is located in the South Pacific Gyre which is classed as an oligotrophic region (Dandonneau et al., 2006), due to low chlorophyll a concentrations (< 0.03 $\mu g\ L^{-1}$) (Claustre and Maritorena, 2003; Morel et al., 2007). Station 7 (~600 km from station 8) was also situated in the South Pacific Gyre but did not have elevated eHS (average 27 ± 2 $\mu g.L^{-1}$).

eHS only represent a small fraction of the HS pool (Dulaquais et al., 2018; Fourrier et al., 2022). The HS pool is a fraction of the DOC, typically around 50% (Fourrier et al., 2022; Zigah et al., 2017). Humic-like fluorescent DOM ($FDOM_{HS}$) was detected using excitation-emission matrix (EEM) fluorescence (Coble, 2007, 1996; Mladenov et al., 2011; Yamashita and Tanoue, 2003) at both stations 7 and 8 and showed similar behaviour to eHS, where the average concentration of FDOMHS was higher at station 8 (2.42 quinine sulfate unit (QSU)), than station 7 (1.87 QSU).

eHS and $FDOM_{HS}$ both contribute to the DOC pool. DOC concentrations at station 8 did not show the same elevated concentrations (average 51 µmol DOC kg^{-1}), compared to station 7 or the rest of the transect (average 56 µmol DOC kg^{-1}). The vertical distribution of the DOC was similar to the eHS, with elevated concentrations in the surface and quasi-constant with depth. At station 7 and 8 the concentrations of DOC at in the surface waters were higher (~78 µmol DOC kg^{-1}) and similar to other DOC measurements in the Pacific gyres (Buck et al., 2018; Ge et al., 2022; Osterholz et al., 2021; Zigah et al., 2017). Even though the DOC concentrations at both stations 7 and 8 were similar the concentrations of both eHS and $FDOM_{HS}$ were not, suggesting compositional differences of DOC between the sites. These stations are both situated on the edge of the South Pacific Gyre, with station 8 is closer to the centre.

The South Pacific Gyre is known to accumulate DOC in the surface waters (Osterholz et al., 2021), because in oligotrophic regions phytoplankton and other marine organisms tend to produce more organic matter than is consumed, due to limited nutrient concentrations (Biersmith and Benner, 1998). The organic matter is then transformed into DOC (Asmala et al., 2018). The depth of South Pacific Gyres depth varies. This study is located on the western boundary of the South Pacific Gyres, and the Eastern Australia current can circulate at depths greater than 1000 m (Britannica, 2019). The Gyres circulation limits exchange with surrounding regions, contributing to the accumulation of DOC over time. DOC can be consumed by microorganisms, including bacteria, and transformed into HS (Romera-Castillo et al., 2011). Even though the South Pacific Gyre is oligotrophic, there is still a significant amount of bacterial activity (Halm et al., 2011; Reintjes et al., 2019; Van Wambeke et al., 2008b; Walsh et al., 2015). As station 8 is closer to the centre of the gyre, it likely has limited exchange with the surrounding areas. The combination of accumulated DOC and high bacterial abundance and limited exchange with surrounding regions could lead to the elevated concentrations of eHS at station 8.

3.4.8. Electroactive humic substances in hydrothermal waters

The concentration of eHS at PANAMAX was high (mean 58 ± 4 $\mu g.L^{-1}$) compared to the rest of the transect (mean 35 ± 3 $\mu g.L^{-1}$). Hydrothermal vents can be a source of HS. This can be through the alteration of DOM or active production from autochthonous microbial communities (Hawkes et al., 2016; Sarma et al., 2018; Yang et al., 2012).

HS are a component of DOM. In normal seawater conditions, DOM is very resistant to degradation (Flerus et al., 2012; Hansell et al., 2012), but high temperatures can thermally alter DOM. At 100 °C DOM becomes unstable and the composition begins to alter, and at temperature >325 °C DOM is completely destroyed (Hawkes et al., 2016). It requires temperatures of 180 °C to transform DOM into HS (Shao et al., 2023), but the acidity of the vent also plays an important part in HS production. Acidic hydrothermal conditions favour the production of HS precursors, and alkaline hydrothermal conditions are suitable for the formation of HS (Shao et al., 2022). The importance of pH could explain why some hydrothermal vents have been found to be a source of HS, and some have not. A study focusing on submarine hydrothermal vents near Northeast Taiwan, found that white smoker hydrothermal vents were a source of humic-like compounds, whereas yellow vents appeared to not be (Yang et al., 2012). White smoker hydrothermal vents emit alkaline fluids (pH around 9-9.8) (Arndt, 2011; Kelley et al., 2001), while yellow vents are acidic (pH 1.5). In our study, hydrothermal fluids from PANAMAX were at pH 6.5.

Autochthonous microbial communities around hydrothermal systems have also been found to be a source of HS (Sarma et al., 2018). Due to the harsh environment environments, these communities can be carbon-limited (Bradley et al., 2009), but microbial communities in these regions can produce DOC from inorganic carbon (McCarthy et al., 2011). Around these vents live thermogenic bacteria, which can withstand temperatures >60 °C (Zeng et al., 2021). These thermogenic bacteria can transform the fresh DOC into HS.

Unlike deep sea vents, the PANAMAX vent is situated at 200m. The elevated concentration of eHS around PANAMAX could therefore also be linked to higher production of HS from surface communities stimulated by Fe-rich vent fluids reaching the photic layer (Tilliette et al., 2022). At this station, the maximum concentration of eHS was observed at 51 m (Figure 3.4L). This station also had the highest Chl *a* concentration compared to the rest of the transect. It is therefore likely HS in our samples originate from biological activity and not hydrothermal alteration of DOM, as we do not see an increase in the hydrothermal plume as with TA-like and GSH-like compounds.

3.4.9. Humic substances in metal complexation

HS are ligands for a wide range of trace metals (Mantoura et al., 1978) but have been of particular interest for their complexation with Fe. In marine waters, Fe is primarily present in the form Fe(III), which is insoluble (Liu and Millero, 2002), but its binding with ligands increases its solubility (Buck et al., 2016; Gledhill and van den Berg, 1994; Hassler and Schoemann, 2009; Rue and Bruland, 1995) and, therefore, its bioavailability. HS are one of the most important ligands for Fe (Hassler et al., 2017; Laglera and van den Berg, 2009) and are believed to account for 7% of Fe-binding ligands in surface waters and 41% in deep waters (Hassler et al., 2020), and potentially much more in some regions (Laglera et al., 2019; Slagter et al., 2019; Whitby et al., 2020a).

For the quantification of eHS, standards from the Suwannee River (SRFA and SRHA) are typically used, which are well characterised. Terrestrially-derived HS have been extensively studied compared to marine-derived HS. Comparisons of terrestrial and marine HS have shown differences in their chemical composition, which could affect Fe binding (Harvey et al., 1983; Hertkorn et al., 2006; L. Malcolm, 1990; Muller, 2018). Terrestrial HS tend to be large molecules with many aromatic rings, whereas marine HS are aliphatic and carboxyl-rich (Fourrier et al., 2022; Harvey et al., 1983; Hedges et al., 1992; Williford et al., 2021), although both pools contain HS of microbial origin. Comparing the pseudopolarograms of HS in the TONGA samples (Figure 3.7B and 4.7C) to the pseudopolarograms of

SRHA and SRFA (Figure 3.7A) indicates that HS in this region are more electrochemically similar to SRFA. SRFA is relatively small compared to SRHA (SRHA ~1000 - 10,000 Da; SRFA 500 - 2000 Da) (Averett et al., 1994) and contains a large number of carboxylic acid groups (Ritchie and Michael Perdue, 2003).

Even though pseudopolarography shows that marine HS in the TONGA samples are similar to SRFA, the Fe-binding sites could differ. HS have a variety of different moieties that Fe could bind with, but the site at which Fe will bind to HS depends on the Fe speciation. Fe(III) is a hard Lewis acid. Hard Lewis acid's tend to form strong complexes with hard ligands, for example, OH^- or COO^- (Jensen, 1978). This is consistent with Fourrier, et al., (2022), who found that carboxylates were the main functional group that bound Fe to marine HS (Fourrier et al., 2022; Heerah and Reader, 2022).

There are slight differences between the surface and deep HS pseudopolarograms (Figure 3.8B and 3.8C). Surface HS were detectable at more negative potentials than deep HS. The differences between the surface and deep HS indicate that with depth there is a change in the nature of the HS. This is consistent with DOM transformation with depth through bacterial processing, which has been shown to increase HS aromaticity and the density of binding sites (Williford et al., 2021), which can affect the Fe binding capacity. Figure 3.10 shows the relationship between the concentrations of eHS and dissolved Fe from the TONGA cruise. With increasing depth, the ratio of dFe to eHS increases. Since eHS are thought to be the dominant ligand for Fe in deeper waters, the agreement between dFe and the SRHA binding capacity would agree with the hypothesis that HS binding capacities increase with depth due to increased HS aromaticity (Whitby et al., 2020b), however the actual Fe-binding capacity was not measured in these samples.

For terrestrial HS, the aromaticity and Fe-binding capacity appear positively related (Kikuchi et al., 2017). In contrast, Fourrier et al., (2022) found that in marine HS, Fe-binding moieties are aliphatic (Fourrier et al., 2022). Furthermore, analysis using SRFA should give concentrations of eHS that are higher than with SRHA, accounting for differences in binding capacity (Laglera and van den Berg,

2009). However, few studies have considered what happens when the composition (and binding capacity) of HS changes between samples when a single standard is used across a study. Yang et al. found the binding capacity of natural FA and HA-like material changed along a salinity gradient, and differences in concentration and Fe-binding were obtained depending on whether the FA or HA standard was used (Yang et al., 2017).

The discrepancy between terrestrial and marine HS binding sites and relationship to aromaticity could be explained by recent work demonstrating that the formation of geopolymerised substances can occur on the order of days to weeks (Curti et al., 2021). Iron nanoparticles behave as a catalyst, driving the formation of aromatic HS-like material through the transformation of carboxyl-rich moieties on the iron surface, which can then remain attached and 'grow' at the Fe interface, decreasing in carboxylic nature in the process (Curti et al., 2021). These could potentially appear as a metal-humic complexes detected by CSV; investigation into this hypothesis is ongoing.

The ratio of dFe to HS in samples from the Northeast Pacific suggested an apparent Fe-binding capacity similar to SRFA (Whitby et al., 2020), which was also seen in our study (assuming HS are the dominant ligand for Fe). HS in the deep waters of the North Atlantic had a higher apparent Fe-binding capacity, closer to that of SRHA; similar results were observed in our study for eHS in the deep waters of the Lau Basin. HS from the North Atlantic are more terrestrial in nature due to the subduction of humic-rich Arctic waters with a strong terrestrial component (Laglera et al., 2019). The Lau Basin has abundant hydrothermal vents (Baker et al., 2019; Beaulieu et al., 2013). HS produced in hydrothermal environments likely originate from thermogenic bacteria (Sarma et al., 2018). This could suggest that hydrothermally-derived HS is more similar to terrestrial and deep-sea HS than fresh marine HS found in upper waters, but further investigation is required.

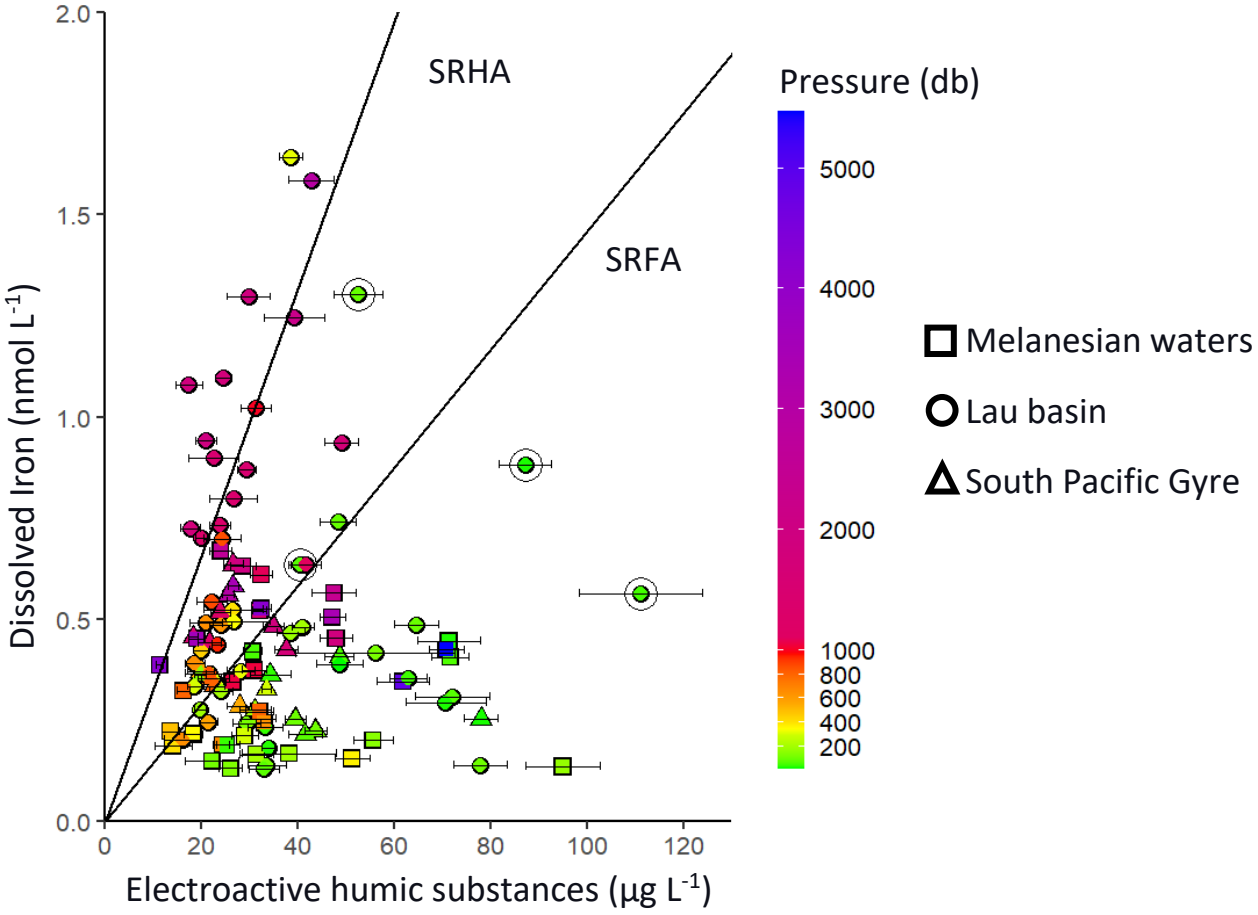

Figure 3.10. *The relationship between the concentrations of electroactive humic substances and dissolved iron from the TONGA cruise. Points are coloured by pressure. The different shapes represent the different oceanographic regions across the TONGA. The lines represent the iron binding capacities for terrestrial humic standards (Suwannee River fulvic acid (SRFA) and humic acid (SRHA)). The upper line is representative of SRHA (32 ± 2.2 nM Fe.mg^{-1} SRHA), and the lower line is representative of SRFA, the standard used in this study (14.6 ± 0.7 nM Fe.mg^{-1} SRFA) (Laglera and van den Berg, 2009; Sukekava et al., 2018). Highlighted circles were from the hydrothermal station PANAMAX. Figure generated using R studio software.*

3.5. Conclusion

This study provides the quantitative and semi-qualitative data set of species-specific RSS (TA and GSH-like compounds) and eHS in the WTSP Ocean. GSH-like compounds were only present in the surface waters (<200 m), whereas TA-like compounds were present across the whole transect. In the hydrothermal plume at PANAMAX, there were elevated concentrations of both GSH-like and TA-like compounds. The increased concentrations are likely due to either the formation of RSS from the reaction of CO/CO_2 with sulphide or the production of these RSS from biology to either help with the

uptake or detoxification of metals. Sulphide was also present at PANAMAX, which is consistent with reports that the Lau Basin produces high concentrations of sulphide (Hsu-kim et al., 2008; Yücel et al., 2011).

Station 2 also saw elevated concentrations of TA-like compounds. Pseudopolarography was used at station 2 to try and identify the TA-like compounds. A comparison of the station 2 pseudopolarogram and TA standard pseudopolarogram showed that they did not match. The high concentration of RSS and the wide pseudopolarogram indicates differences in RSS type(s) or structure of a RSS-containing compound at this station. A possibility presented for the identity of these TA-like compounds is a thiocarbonyl tail attached to a larger compound such as methanobactin. There have been some studies carried out on methanobactins with cyclic voltammetry, but to our knowledge, methanobactins have yet to be measured at pH 2 or using pseudopolarography.

The vertical profiles of eHS are similar to those previously reported elsewhere, with enrichment in upper waters and lower concentrations in the deep sea. Station 8 (average 57 ± 4 µg.L-1) and PANAMAX (mean 58 ± 4 µg.L-1) had elevated concentrations of eHS compared to the rest of the transect (average 35 ± 3 µg.L-1). Station 8 was located in the South Pacific Gyre, which is an oligotrophic region. The South Pacific Gyre has been shown to accumulate DOC and has high bacterial abundance, which could explain elevated concentrations of eHS at station 8.

Pseudopolarography found that eHS in the WTSP are similar to SRFA, therefore, showing that SRFA was the best standard for the quantification of eHS in the WTSP. There were slight differences between the pseudopolarogram of the surface and bottom water, indicating a change in the nature of eHS with depth. In the water column, HS evolve and change through processes like remineralization. This can affect HS ability to bind with trace metals. From this study, we found that the HS Fe-binding capacity increased with depth, and the Lau Basin had a higher Fe-binding capacity than the South Pacific Grye and Melanesian waters. This shows that with depth, more Fe can bind with HS and that in hydrothermal water, HS have a higher ability to bind with Fe.

3.6. References

Abualhaija, M.M., Whitby, H., van den Berg, C.M.G., 2015. Competition between copper and iron for humic ligands in estuarine waters. Mar. Chem. 172, 46–56. https://doi.org/10.1016/J.MARCHEM.2015.03.010

Ahner, B.A., Wei, L., Oleson, J.R., Ogura, N., 2002. Glutathione and other low molecular weight thiols in marine phytoplankton under metal stress. Mar. Ecol. Prog. Ser. 232, 93–103. https://doi.org/10.3354/meps232093

Aiken, G., McKnight, D., Harnish, R., Wershaw, R., 2017. Geochemistry of Aquatic Humic Substances in the Lake Fryxell Basin, Antarctica. Springer 34, 157–188.

Al-Farawati, R., van den Berg, C.M.G., 1997. The determination of sulfide in seawater by flow-analysis with voltammetric detection. Mar. Chem. 57, 277–286. https://doi.org/10.1016/S0304-4203(97)00014-5

Al-Farawati, R., Van Den Berg, C.M.G., 2001. Thiols in coastal waters of the western North Sea and English Channel. Environ. Sci. Technol. 35, 1902–1911. https://doi.org/10.1021/es000073i

Apel, K., Hirt, H., 2004. REACTIVE OXYGEN SPECIES: Metabolism, Oxidative Stress, and Signal Transduction. Annu. Rev. Plant Biol. 55, 373–399. https://doi.org/10.1146/annurev.arplant.55.031903.141701

Arndt, N., 2011. White Smoker, in: Encyclopedia of Astrobiology. p. 1779. https://doi.org/https://doi.org/10.1007/978-3-642-11274-4_1691

Aumond, V., Waeles, M., Salaün, P., Gibbon-Walsh, K., van den Berg, C.M.G., Sarradin, P.M., Riso, R.D., 2012. Sulfide determination in hydrothermal seawater samples using a vibrating gold micro-wire electrode in conjunction with stripping chronopotentiometry. Anal. Chim. Acta 753, 42–47. https://doi.org/10.1016/j.aca.2012.09.044

Averett, R.C., Leenheer, J.A., McKnight, D.M., Thorn, K.A., 1994. Humic substances in the Suwannee River, Georgia: interactions, properties, and proposed structures. US Geol. Surv. Water-Supply Pap. 2373.

Baba, S.P., Bhatnagar, A., 2016. Role of thiols in oxidative stress. Physiol. Behav. 176, 139–148. https://doi.org/10.1016/j.physbeh.2017.03.040

Baker, E.T., Walker, S.L., Massoth, G.J., Resing, J.A., 2019. The NE Lau Basin: Widespread and abundant hydrothermal venting in the back-arc region behind a superfast subduction zone. Front. Mar. Sci. 6, 1–15. https://doi.org/10.3389/fmars.2019.00382

Barón, M., Arellano, J.B., Gorgé, J.L., 1995. Copper and photosystem II: A controversial relationship. Physiol. Plant. 94, 174–180. https://doi.org/10.1111/j.1399-3054.1995.tb00799.x

Batchelli, S., Muller, F.L.L., Chang, K.C., Lee, C.L., 2010. Evidence for strong but dynamic iron-humic colloidal associations in humic-rich coastal waters. Environ. Sci. Technol. 44, 8485–8490. https://doi.org/10.1021/es101081c

Beaulieu, S.E., Baker, E.T., German, C.R., Maffei, A., 2013. An authoritative global database for active submarine hydrothermal vent fields. Geochemistry, Geophys. Geosystems 14, 4892–4905. https://doi.org/10.1002/2013GC004998

Bi, Z., Salaün, P., van den Berg, C.M.G., 2013a. Determination of lead and cadmium in seawater using a vibrating silver amalgam microwire electrode. Anal. Chim. Acta 769, 56–64.

https://doi.org/10.1016/J.ACA.2013.01.049

Bi, Z., Salaün, P., VandenBerg, C.M.G., 2013b. Study of Bare and Mercury-Coated Vibrated Carbon, Gold and Silver Microwire Electrodes for the Determination of Lead and Cadmium in Seawater by Anodic Stripping Voltammetry. Electroanalysis 25, 357–366. https://doi.org/10.1002/elan.201200446

Biersmith, A., Benner, R., 1998. Carbohydrates in phytoplankton and freshly produced dissolved organic matter. Mar. Chem. 63, 131–144. https://doi.org/10.1016/S0304-4203(98)00057-7

Bonnet, S., Caffin, M., Berthelot, H., Grosso, O., Benavides, M., Helias-Nunige, S., Guieu, C., Stenegren, M., Foster, R.A., 2018. In-depth characterization of diazotroph activity across the western tropical South Pacific hotspot of N2 fixation (OUTPACE cruise). Biogeosciences 15, 4215–4232. https://doi.org/10.5194/bg-15-4215-2018

Bonnet, S., Caffin, M., Berthelot, H., Moutin, T., 2017. Hot spot of N2 fixation in the western tropical South Pacific pleads for a spatial decoupling between N2 fixation and denitrification. Proc. Natl. Acad. Sci. U. S. A. 114, E2800–E2801. https://doi.org/10.1073/pnas.1619514114

Bradley, A.S., Hayes, J.M., Summons, R.E., 2009. Extraordinary 13C enrichment of diether lipids at the Lost City Hydrothermal Field indicates a carbon-limited ecosystem. Geochim. Cosmochim. Acta 73, 102–118. https://doi.org/10.1016/j.gca.2008.10.005

Brand, L.E., Sunda, W.G., Guillard, R.R.L., 1986. Reduction of marine phytoplankton reproduction rates by copper and cadmium. J. Exp. Mar. Bio. Ecol. 96, 225–250. https://doi.org/10.1016/0022-0981(86)90205-4

Brinkmann, T., Sartorius, D., Frimmel, F.H., 2003. Photobleaching of humic rich dissolved organic matter. Aquat. Sci. 65, 415–424. https://doi.org/10.1007/s00027-003-0670-9

Buck, K.N., Gerringa, L.J.A., Rijkenberg, M.J.A., 2016. An Intercomparison of Dissolved Iron Speciation at the Bermuda Atlantic Time-series Study (BATS) Site: Results from GEOTRACES Crossover Station A. Front. Mar. Sci. 3, 1–14. https://doi.org/10.3389/fmars.2016.00262

Bulletin, R.C., Synthesis, P., Academy, R., Federation, R., 1998. Letters to the Editor. A new mechanochemical reaction of thiols with iron metal. Russ. Chem. Bull. 47, 2316–2317.

Cabanes, D.J.E., Norman, L., Bowie, A.R., Strmečki, S., Hassler, C.S., 2020. Electrochemical evaluation of iron-binding ligands along the Australian GEOTRACES southwestern Pacific section (GP13). Mar. Chem. 219, 103736. https://doi.org/10.1016/j.marchem.2019.103736

Caffin, M., Moutin, T., Ann Foster, R., Bouruet-Aubertot, P., Michelangelo Doglioli, A., Berthelot, H., Guieu, C., Grosso, O., Helias-Nunige, S., Leblond, N., Gimenez, A., Alexandra Petrenko, A., De Verneil, A., Bonnet, S., 2018. N2 fixation as a dominant new N source in the western tropical South Pacific Ocean (OUTPACE cruise). Biogeosciences 15, 2565–2585. https://doi.org/10.5194/bg-15-2565-2018

Chapman, C.S., Capodaglio, G., Turetta, C., Berg, C.M.G. van den, 2009. Benthic fluxes of copper, complexing ligands and thiol compounds in shallow lagoon waters. Mar. Environ. Res. 67, 17–24. https://doi.org/10.1016/j.marenvres.2008.07.010

Chen, X.G., Lyu, S.S., Garbe-Schönberg, D., Lebrato, M., Li, X., Zhang, H.Y., Zhang, P.P., Chen, C.T.A., Ye, Y., 2018. Heavy metals from Kueishantao shallow-sea hydrothermal vents, offshore northeast Taiwan. J. Mar. Syst. 180, 211–219. https://doi.org/10.1016/j.jmarsys.2016.11.018

Choi, D.W., Zea, C.J., Do, Y.S., Semrau, J.D., Antholine, W.E., Hargrove, M.S., Pohl, N.L., Boyd, E.S., Geesey, G.G., Hartsel, S.C., Shafe, P.H., McEllistrem, M.T., Kisting, C.J., Campbell, D., Rao, V., De

La Mora, A.M., DiSpirito, A.A., 2006. Spectral, kinetic, and thermodynamic properties of Cu(I) and Cu(II) binding by methanobactin from methylosinus trichosporium OB3b. Biochemistry 45, 1442–1453. https://doi.org/10.1021/bi051815t

Claustre, H., Maritorena, S., 2003. The Many Shades of Ocean Blue. Science (80-.). 302, 27–28.

Cline, J.D., Richards, F.A., 1969. Oxygenation of hydrogen sulfide in seawater at constant salinity, temperature, and pH. Environ. Sci. Technol. 3, 838–843. https://doi.org/10.1021/es60032a004

Coale, K.H., Bruland, K.W., 1988. Copper complexation in the Northeast Pacific. Limnol. Oceanogr. 33, 1084–1101. https://doi.org/10.4319/lo.1988.33.5.1084

Cotte, L., Omanović, D., Waeles, M., Laës, A., Cathalot, C., Sarradin, P.M., Riso, R.D., 2018. On the nature of dissolved copper ligands in the early buoyant plume of hydrothermal vents. Environ. Chem. 15, 58–73. https://doi.org/10.1071/EN17150

Curti, L., Moore, O.W., Babakhani, P., Xiao, K.Q., Woulds, C., Bray, A.W., Fisher, B.J., Kazemian, M., Kaulich, B., Peacock, C.L., 2021. Carboxyl-richness controls organic carbon preservation during coprecipitation with iron (oxyhydr)oxides in the natural environment. Commun. Earth Environ. 2. https://doi.org/10.1038/s43247-021-00301-9

Cutter, G., Casciotti, K., Croot, P., Geibert, W., Heimbürger, L.-E., Lohan, M., Planquette, H., Flierdt, T. van de, 2017. Sampling and Sample-handling Protocols for GEOTRACES Cruises.

Dainard, P.G., Guéguen, C., McDonald, N., Williams, W.J., 2015. Photobleaching of fluorescent dissolved organic matter in Beaufort Sea and North Atlantic Subtropical Gyre. Mar. Chem. 177, 630–637. https://doi.org/10.1016/j.marchem.2015.10.004

Damm, K.L.V., Oosting, S.E., Kozlowski, R., Buttermore, L.G., Colodner, D.C., Edmonds, H.N., Edmond, J.M., Grebmeier, J.M., 1995. Evolution of East Pacific Rise hydrothermal vent fluids following a volcanic eruption. Nature 375, 47–50. https://doi.org/10.1038/375047a0

Dandonneau, Y., Montel, Y., Blanchot, J., Giraudeau, J., Neveux, J., 2006. Temporal variability in phytoplankton pigments, picoplankton and coccolithophores along a transect through the North Atlantic and tropical southwestern Pacific. Deep. Res. Part I Oceanogr. Res. Pap. 53, 689–712. https://doi.org/10.1016/j.dsr.2006.01.002

Debelius, B., Forja, J.M., Lubián, L.M., 2011. Toxicity of copper, nickel and zinc to Synechococcus populations from the Strait of Gibraltar. J. Mar. Syst. 88, 113–119. https://doi.org/10.1016/j.jmarsys.2011.02.009

Deleon, E.R., Stoy, G.F., Olson, K.R., 2012. Passive loss of hydrogen sulfide in biological experiments. Anal. Biochem. 421, 203–207. https://doi.org/10.1016/j.ab.2011.10.016

Dias, D., do Nascimento, P.C., Jost, C.L., Bohrer, D., de Carvalho, L.M., Koschinsky, A., 2010. Voltammetric determination of low-molecular-weight sulfur compounds in hydrothermal vent fluids-studies with hydrogen sulfide, methanethiol, ethanethiol and propanethiol. Electroanalysis 22, 1066–1071. https://doi.org/10.1002/elan.200900472

Diaz, J.M., Plummer, S., 2018. Production of extracellular reactive oxygen species by phytoplankton: past and future directions. J. Plankton Res. 40, 655–666. https://doi.org/10.1093/plankt/fby039

DiSpirito, A.A., Semrau, J.D., Murrell, J.C., Gallagher, W.H., Dennison, C., Vuilleumier, S., 2016. Methanobactin and the Link between Copper and Bacterial Methane Oxidation. Microbiol. Mol. Biol. Rev. 80, 387–409. https://doi.org/10.1128/mmbr.00058-15

Dulaquais, G., Waeles, M., Breitenstein, J., Knoery, J., Riso, R., 2019. Links between size fractionation, chemical speciation of dissolved copper and chemical speciation of dissolved organic matter in

the Loire estuary. Environ. Chem. https://doi.org/10.1071/EN19137

Dulaquais, G., Waeles, M., Gerringa, L.J.A., Middag, R., Rijkenberg, M.J.A., Riso, R., 2018. The Biogeochemistry of Electroactive Humic Substances and Its Connection to Iron Chemistry in the North East Atlantic and the Western Mediterranean Sea. J. Geophys. Res. Ocean. 123, 5481–5499. https://doi.org/10.1029/2018JC014211

Dupont, C.L., Ahner, B.A., 2005. Effects of copper, cadmium, and zinc on the production and exudation of thiols by Emiliania huxleyi. Limnol. Oceanogr. 50, 508–515. https://doi.org/10.4319/lo.2005.50.2.0508

Dupont, C.L., Goepfert, T.J., Lo, P., Wei, L., Ahner, B.A., 2004. Diurnal cycling of glutathione in marine phytoplankton: Field and culture studies. Limnol. Oceanogr. 49, 991–996. https://doi.org/10.4319/lo.2004.49.4.0991

Dupont, C.L., Moffett, J.W., Bidigare, R.R., Ahner, B.A., 2006. Distributions of dissolved and particulate biogenic thiols in the subartic Pacific Ocean. Deep. Res. Part I Oceanogr. Res. Pap. 53, 1961–1974. https://doi.org/10.1016/j.dsr.2006.09.003

El Ghazouani, A., Baslé, A., Firbank, S.J., Knapp, C.W., Gray, J., Graham, D.W., Dennison, C., 2011. Copper-binding properties and structures of methanobactins from methylosinus trichosporium OB3b. Inorg. Chem. 50, 1378–1391. https://doi.org/10.1021/ic101965j

El Ghazouani, A., Baslé, A., Gray, J., Graham, D.W., Firbank, S.J., Dennison, C., 2012. Variations in methanobactin structure influences copper utilization by methane-oxidizing bacteria. Proc. Natl. Acad. Sci. U. S. A. 109, 8400–8404. https://doi.org/10.1073/pnas.1112921109

Falkowski, P.G., Barber, R.T., Smetacek, V., 1998. Biogeochemical Controls and Feedbacks on Ocean Primary Production 281, 200–206.

Ferdelman, T.G., Klockgether, G., Downes, P., Lavik, G., 2019. Nutrient Data from CTD Nisken Bottles from Sonne Expedition SO-245 "UltraPac". PANGAEA. https://doi.org/https://doi.org/10.1594/PANGAEA.899228

Ferrari, G.M., Dowell, M.D., Grossi, S., Targa, C., 1996. Relationship between the optical properties of chromophoric dissolved organic matter and total concentration of dissolved organic carbon in the southern Baltic Sea region. Mar. Chem. 55, 299–316. https://doi.org/10.1016/S0304-4203(96)00061-8

Flerus, R., Lechtenfeld, O.J., Koch, B.P., McCallister, S.L., Schmitt-Kopplin, P., Benner, R., Kaiser, K., Kattner, G., 2012. A molecular perspective on the ageing of marine dissolved organic matter. Biogeosciences 9, 1935–1955. https://doi.org/10.5194/bg-9-1935-2012

Fourrier, P., Dulaquais, G., Guigue, C., Giamarchi, P., Sarthou, G., Whitby, H., Riso, R., 2022. Characterization of the vertical size distribution, composition and chemical properties of dissolved organic matter in the (ultra)oligotrophic Pacific Ocean through a multi-detection approach. Mar. Chem. 240, 104068. https://doi.org/10.1016/j.marchem.2021.104068

Foustoukos, D.I., Seyfried, W.E., 2007. Fluid Phase Separation Processes in Submarine Hydrothermal Systems. Rev. Mineral. Geochemistry 65, 213–239. https://doi.org/10.2138/rmg.2007.65.7

Francis, ~, Roberts, K.J., Beman, J.M., Santoro, A.E., Oakley, B.B., 2005. Ubiquity and diversity of ammonia-oxidizing archaea in water columns and sediments of the ocean. Proc. Natl. Acad. Sci. U. S. A. 102, 14683–14688. https://doi.org/10.1073/pnas.0506625102

Gao, Z., Guéguen, C., 2018. Distribution of thiol, humic substances and colored dissolved organic matter during the 2015 Canadian Arctic GEOTRACES cruises. Mar. Chem. 203, 1–9.

https://doi.org/10.1016/j.marchem.2018.04.001

German, C.R., Baker, E.T., Connelly, D.P., Lupton, J.E., Resing, J., Prien, R.D., Walker, S.L., Edmonds, H.N., Langmuir, C.H., 2006. Hydrothermal exploration of the Fonualei Rift and Spreading Center and the Northeast Lau Spreading Center. Geochemistry, Geophys. Geosystems 7, 1–15. https://doi.org/10.1029/2006GC001324

Gledhill, M., van den Berg, C.M.G., 1994. Determination of complexation of iron(III) with natural organic complexing ligands in seawater using cathodic stripping voltammetry. Mar. Chem. 47, 41–54. https://doi.org/10.1016/0304-4203(94)90012-4

Gomez-Saez, G. V., Pohlabeln, A.M., Stubbins, A., Marsay, C.M., Dittmar, T., 2017. Photochemical Alteration of Dissolved Organic Sulfur from Sulfidic Porewater. Environ. Sci. Technol. 51, 14144–14154. https://doi.org/10.1021/acs.est.7b03713

Gonzalez-santana, D., Sarthou, G., Planquette, H., 2023. Dissolved Trace metal distribution in the Western Tropical South Pacific. Front. Mar. Sci. (in prep).

Guieu, C., Bonnet, S., 2019. TONGA 2019 cruise, R/V L'Atalante [WWW Document]. https://doi.org/https://doi.org/10.17600/18000884

Guieu, C., Bonnet, S., Petrenko, A., Menkes, C., Chavagnac, V., Desboeufs, K., Maes, C., Moutin, T., 2018. Iron from a submarine source impacts the productive layer of the Western Tropical South Pacific (WTSP). Nat. Sci. Reports 1–9. https://doi.org/10.1038/s41598-018-27407-z

Hakemian, A.S., Tinberg, C.E., Kondapalli, K.C., Telser, J., Hoffman, B.M., Stemmler, T.L., Rosenzweig, A.C., 2005. The copper chelator methanobactin from Methylosinus trichosporium OB3b binds copper(I). J. Am. Chem. Soc. 127, 17142–17143. https://doi.org/10.1021/ja0558140

Halm, H., Lam, P., Ferdelman, T.G., Lavik, G., Dittmar, T., Laroche, J., D'Hondt, S., Kuypers, M.M.M., 2011. Heterotrophic organisms dominate nitrogen fixation in the south pacific gyre. ISME J. 6, 1238–1249. https://doi.org/10.1038/ismej.2011.182

Hansell, D.A., Carlson, ~, Schlitzer, R., 2012. Net removal of major marine dissolved organic carbon fractions in the subsurface ocean. Global Biogeochem. Cycles 26, 1–9. https://doi.org/10.1029/2011GB004069

Harris, D.C., 2003. Quantitative Chemical Analysis, W. H. Freeman. New York. https://doi.org/10.1016/B978-0-444-40826-6.50009-1

Harvey, G. r., Tokar, J. m., Boran, D., Chesal, L.A., 1983. The structure of marine fulvic and humic acids. Mar. Biol. 12, 119–132. https://doi.org/10.1016/0304-4203(83)90075-0

Hassler, C., Cabanes, D., Blanco-Ameijeiras, S., Sander, S.G., Benner, R., 2020. Importance of refractory ligands and their photodegradation for iron oceanic inventories and cycling. Mar. Freshw. Res. 71, 311–320. https://doi.org/10.1071/MF19213

Hassler, C.S., Schoemann, V., 2009. Bioavailability of organically bound Fe to model phytoplankton of the Southern Ocean. Biogeosciences 6, 2281–2296. https://doi.org/10.5194/bg-6-2281-2009

Hassler, C.S., van den Berg, C.M.G., Boyd, P.W., 2017. Toward a regional classification to provide a more inclusive examination of the ocean biogeochemistry of iron-binding ligands. Front. Mar. Sci. 4. https://doi.org/10.3389/fmars.2017.00019

Hawkes, J.A., Hansen, C.T., Goldhammer, T., Bach, W., Dittmar, T., 2016. Molecular alteration of marine dissolved organic matter under experimental hydrothermal conditions. Geochim. Cosmochim. Acta 175, 68–85. https://doi.org/10.1016/j.gca.2015.11.025

Hedges, J.I., Hatcher, P.G., Ertel, J.R., Meyers-schulte, K.J., 1992. A comparison of dissolved humic humic substances from seawater with Amazon River counterparts by 13C-NMR spectrometry. Geochim. Cosmochim. Acta 56, 1753–1757.

Heerah, K.M., Reader, H.E., 2022. Towards the identification of humic ligands associated with iron transport through a salinity gradient. Sci. Rep. 12, 1–11. https://doi.org/10.1038/s41598-022-19618-2

Hertkorn, N., Benner, R., Frommberger, M., Schmitt-Kopplin, P., Witt, M., Kaiser, K., Kettrup, A., Hedges, J.I., 2006. Characterization of a major refractory component of marine dissolved organic matter. Geochim. Cosmochim. Acta 70, 2990–3010. https://doi.org/10.1016/j.gca.2006.03.021

Howard, P.H., 2017. Handbook of Environmental Degradation Rates. Lewis Publishers, Boca Raton.

Hsu-kim, H., Mullaugh, K.M., Tsang, J.J., Yucel, M., Iii, G.W.L., 2008. Formation of Zn- and Fe-sulfides near hydrothermal vents at the Eastern Lau Spreading Center : implications for sulfide bioavailability to chemoautotrophs. Geochem. Trans. 14, 1–14. https://doi.org/10.1186/1467-4866-9-6

Huang, X.G., Li, S. xing, Liu, F.J., Lan, W.R., 2018. Regulated effects of Prorocentrum donghaiense Lu exudate on nickel bioavailability when cultured with different nitrogen sources. Chemosphere 197, 57–64. https://doi.org/10.1016/j.chemosphere.2018.01.014

Jacquot, J.E., Horak, R.E.A., Amin, S.A., Devol, A.H., Ingalls, A.E., Armbrust, E.V., Stahl, D.A., Moffett, J.W., 2014. Assessment of the potential for copper limitation of ammonia oxidation by Archaea in a dynamic estuary. Mar. Chem. 162, 37–49. https://doi.org/10.1016/j.marchem.2014.02.002

Jacquot, J.E., Moffett, J.W., 2015. Copper distribution and speciation across the International GEOTRACES Section GA03. Deep Sea Res. Part II Top. Stud. Oceanogr. 116, 187–207. https://doi.org/10.1016/J.DSR2.2014.11.013

Jensen, W.B., 1978. The Lewis Acid-Base Definitions: A Status Report. Chem. Rev. 78.

Kading, T., 2013. Distribution of thiols in the northwest Atlantic Ocean.

Kelley, D.S., Karson, J.A., Blackman, D.K., Früh-Green, G.L., Butterfield, D.A., Lilley, M.D., Olson, E.J., Schrenk, M.O., Roe, K.K., Lebon, G.T., Rivizzigno, P., 2001. An off-axis hydrothermal vent field near the mid-atlantic ridge at 30° n. Nature 412, 145–149. https://doi.org/10.1038/35084000

Kennedy, L., Sandhu, J.K., Harper, M.E., Cuperlovic-culf, M., 2020. Role of glutathione in cancer: From mechanisms to therapies. Biomolecules 10, 1–27. https://doi.org/10.3390/biom10101429

Kieber, R.J., Hydro, L.H., Seaton, P.J., 1997. Photooxidation of triglycerides and fatty acids in seawater: Implication toward the formation of marine humic substances. Limnol. Oceanogr. 42, 1454–1462. https://doi.org/10.4319/lo.1997.42.6.1454

Kikuchi, T., Fujii, M., Terao, K., Jiwei, R., Lee, Y.P., Yoshimura, C., 2017. Correlations between aromaticity of dissolved organic matter and trace metal concentrations in natural and effluent waters: A case study in the Sagami River Basin, Japan. Sci. Total Environ. 576, 36–45. https://doi.org/10.1016/j.scitotenv.2016.10.068

Kim, H.J., Graham, D.W., DiSpirito, A.A., Alterman, M.A., Galeva, N., Larive, C.K., Asunskis, D., Sherwood, P.M.A., 2004. Methanobactin, a Copper-Acquisition Compound from Methane-Oxidizing Bacteria. Science (80-.). 305, 1612 LP – 1615.

Koschinsky, A., Garbe-Schönberg, D., Sander, S., Schmidt, K., Gennerich, H.H., Strauss, H., 2008. Hydrothermal venting at pressure-temperature conditions above the critical point of seawater, 5°S on the Mid-Atlantic Ridge. Geology 36, 615–618. https://doi.org/10.1130/G24726A.1

L. Malcolm, R., 1990. The uniqueness of humic substances in each of soil, stream and marine environments. Anal. Chim. Acta 232, 19–30. https://doi.org/10.1016/S0003-2670(00)81222-2

Laglera, L.M., Battaglia, G., van den Berg, C.M.G., 2007. Determination of humic substances in natural waters by cathodic stripping voltammetry of their complexes with iron. Anal. Chim. Acta. 599, 58–66. https://doi.org/10.1016/j.aca.2007.07.059

Laglera, L.M., Downes, J., Tovar-Sánchez, A., Monticelli, D., 2014. Cathodic pseudopolarography: A new tool for the identification and quantification of cysteine, cystine and other low molecular weight thiols in seawater. Anal. Chim. Acta. 839, 24-33. https://doi.org/ 10.1016/j.aca.2014.05.026

Laglera, L.M., Sukekava, C., Slagter, H.A., Downes, J., Aparicio-Gonzalez, A., Gerringa, L.J.A., 2019. First Quantification of the Controlling Role of Humic Substances in the Transport of Iron across the Surface of the Arctic Ocean. Environ. Sci. Technol. https://doi.org/10.1021/acs.est.9b04240

Laglera, L.M., Tovar-Sánchez, A., 2012. Direct recognition and quantification by voltammetry of thiol/thioamide mixes in seawater. Talanta 89, 496–504. https://doi.org/10.1016/j.talanta.2011.12.075

Laglera, L.M., van den Berg, C.M.G., 2009. Evidence for geochemical control of iron by humic substances in seawater. Limnol. Oceanogr. 54, 610–619. https://doi.org/10.4319/lo.2009.54.2.0610

Laglera, L.M., van den Berg, C.M.G., 2006. Photochemical oxidation of thiols and copper complexing ligands in estuarine waters. Mar. Chem. 101, 130–140. https://doi.org/10.1016/j.marchem.2006.01.006

Laglera, L.M., van den Berg, C.M.G., 2003. Copper complexation by thiol compounds in estuarine waters. Mar. Chem. 82, 71–89. https://doi.org/10.1016/S0304-4203(03)00053-7

Leal, M.F.C., van den Berg, C.M.G., 1998. Evidence for strong copper(I) complexation by organic ligands in seawater. Aquat. Geochemistry 4, 49–75. https://doi.org/10.1023/A:1009653002399

Leal, M.F.C., Vasconcelos, M.T.S.D., van den Berg, C.M.G., 1999. Copper-induced release of complexing ligands similar to thiols by Emiliania huxleyi in seawater cultures. Limnol. Oceanogr. 44, 1750–1762. https://doi.org/10.4319/lo.1999.44.7.1750

Liu, S., Lim, M., Fabris, R., Chow, C.W.K., Drikas, M., Korshin, G., Amal, R., 2010. Multi-wavelength spectroscopic and chromatography study on the photocatalytic oxidation of natural organic matter. Water Res. 44, 2525–2532. https://doi.org/10.1016/j.watres.2010.01.036

Liu, X., Millero, F.J., 2002. The solubility of iron in seawater. Mar. Chem. 77, 43–54. https://doi.org/10.1016/S0304-4203(01)00074-3

Lorenzo, J.I., Nieto-Cid, M., Álvarez-Salgado, X.A., Pérez, P., Beiras, R., 2007. Contrasting complexing capacity of dissolved organic matter produced during the onset, development and decay of a simulated bloom of the marine diatom Skeletonema costatum. Mar. Chem. 103, 61–75. https://doi.org/10.1016/j.marchem.2006.05.009

Mallory, E.C., 1968. A Thioacetamide-Precipitation Procedure for Determining Trace Elements in Water 281–295. https://doi.org/10.1021/ba-1968-0073.ch017

Mangal, V., Phung, T., Guéguen, C., 2020. An estimation of sulfur concentrations released by three algae (Chlorella vulgaris, Chlamydomonas reinhardtii, Scenedesmus obliquus) in response to variable growth photoperiods. Environ. Sci. Pollut. Res. 27, 12491–12498. https://doi.org/10.1007/s11356-020-07812-6

Mantoura, R.F.C., Dickson, A., Riley, J.P., 1978. The complexation of metals with humic materials in natural waters. Estuar. Coast. Mar. Sci. 6, 387–408. https://doi.org/10.1016/0302-3524(78)90130-5

Marie, L., Pernet-Coudrier, B., Waeles, M., Gabon, M., Riso, R., 2015. Dynamics and sources of reduced sulfur, humic substances and dissolved organic carbon in a temperate river system affected by agricultural practices. Sci. Total Environ. 537, 23–32. https://doi.org/10.1016/j.scitotenv.2015.07.089

Marie, L., Pernet-Coudrier, B., Waeles, M., Riso, R., 2017. Seasonal variation and mixing behaviour of glutathione, thioacetamide and fulvic acids in a temperate macrotidal estuary (Aulne, NW France). Estuar. Coast. Shelf Sci. 184, 177–190. https://doi.org/10.1016/j.ecss.2016.11.018

McCarthy, M.D., Beaupré, S.R., Walker, B.D., Voparil, I., Guilderson, T.P., Druffel, E.R.M., 2011. Chemosynthetic origin of 14C-depleted dissolved organic matter in a ridge-flank hydrothermal system. Nat. Geosci. 4, 32–36. https://doi.org/10.1038/ngeo1015

McLeay, Y., Stannard, S., Houltham, S., Starck, C., 2017. Dietary thiols in exercise: Oxidative stress defence, exercise performance, and adaptation. J. Int. Soc. Sports Nutr. 14. https://doi.org/10.1186/s12970-017-0168-9

Merchant, S.S., Allen, M.D., Kropat, J., Moseley, J.L., Long, J.C., Tottey, S., Terauchi, A.M., 2006. Between a rock and a hard place: Trace element nutrition in Chlamydomonas. Biochim. Biophys. Acta - Mol. Cell Res. 1763, 578–594. https://doi.org/10.1016/j.bbamcr.2006.04.007

Moffett, J., Brand, L.E., Croot, P.L., Barbeau, K.A., 1997. Cu speciation and cyanobacterial distribution in harbors subject to anthropogenic Cu inputs. Limnol. Oceanogr. https://doi.org/10.4319/lo.1997.42.5.0789

Moingt, M., Bressac, M., Bélanger, D., Amyot, M., 2010. Role of ultra-violet radiation, mercury and copper on the stability of dissolved glutathione in natural and artificial freshwater and saltwater. Chemosphere 80, 1314–1320. https://doi.org/10.1016/j.chemosphere.2010.06.041

Moore, J.K., Doney, S.C., Glover, D.M., Fung, I.Y., 2001. Iron cycling and nutrient-limitation patterns in surface waters of the World Ocean. https://doi.org/10.1016/S0967-0645(01)00109-6

Mopper, K., Kieber, D.J., 1991. Distribution and biological turnover of dissolved organic compounds in the water column of the Black Sea. Deep. Res. Part A 38, S1021–S1047. https://doi.org/10.1016/s0198-0149(10)80022-6

Morel, A., Gentili, B., Claustre, H., Babin, M., Bricaud, A., Ras, J., Tièche, F., 2007. Optical properties of the “clearest” natural waters. Limnol. Oceanogr. 52, 217–229. https://doi.org/10.4319/lo.2007.52.1.0217

Morelli, E., Scarano, G., 2004. Copper-induced changes of non-protein thiols and antioxidant enzymes in the marine microalga Phaeodactylum tricornutum. Plant Sci. 167, 289–296. https://doi.org/10.1016/j.plantsci.2004.04.001

Morris, J.J., Rose, A.L., Lu, Z., 2022. Redox Biology Reactive oxygen species in the world ocean and their impacts on marine ecosystems. Redox Biol. 52, 102285. https://doi.org/10.1016/j.redox.2022.102285

Muller, F.L.L., 2018. Exploring the potential role of terrestrially derived humic substances in the marine biogeochemistry of iron. Front. Earth Sci. 6. https://doi.org/10.3389/feart.2018.00159

Mullineaux, P.M., Exposito-Rodriguez, M., Laissue, P.P., Smirnoff, N., 2018. ROS-dependent signalling pathways in plants and algae exposed to high light: Comparisons with other eukaryotes. Free

Radic. Biol. Med. 122, 52–64. https://doi.org/10.1016/j.freeradbiomed.2018.01.033

Navarrete, A., González, A., Gómez, M., Contreras, R.A., Díaz, P., Lobos, G., Brown, M.T., Sáez, ~, Moenne, A., 2019. Copper excess detoxification is mediated by a coordinated and complementary induction of glutathione, phytochelatins and metallothioneins in the green seaweed Ulva compressa. Plant Physiol. Biochem. 135, 423–431. https://doi.org/10.1016/J.PLAPHY.2018.11.019

Nelson, N.B., Siegel, D.A., Carlson, ~, Swan, C., Smethie, W.M., Khatiwala, S., 2007. Hydrography of chromophoric dissolved organic matter in the North Atlantic. Deep. Res. Part I Oceanogr. Res. Pap. 54, 710–731. https://doi.org/10.1016/j.dsr.2007.02.006

Nimmo, M., van den Berg, C.M.G., Brown, J., 1989. The chemical speciation of dissolved nickel, copper, vanadium and iron in Liverpool Bay, Irish Sea. Estuar. Coast. Shelf Sci. 29, 57–74. https://doi.org/10.1016/0272-7714(89)90073-5

Omanović, D., Branica, M., 1998. Automation of Voltammetric Measurements by Polarographic Analyser PAR 384B. Croat. Chem. Acta 71, 421–433.

Osterholz, H., Kilgour, D.P.A., Storey, D.S., Lavik, G., Ferdelman, T.G., Niggemann, J., Dittmar, T., 2021. Accumulation of DOC in the South Pacific Subtropical Gyre from a molecular perspective. Mar. Chem. 231, 103955. https://doi.org/10.1016/j.marchem.2021.103955

Pauleta, S.R., Dell'Acqua, S., Moura, I., 2013. Nitrous oxide reductase. Coord. Chem. Rev. 257, 332–349. https://doi.org/10.1016/j.ccr.2012.05.026

Pavelko, G.F., 2015. Reaction of thiols and organic disulfides with iron group metals and their oxides. Russ. J. Inorg. Chem. 60, 1394–1398. https://doi.org/10.1134/S0036023615110121

Peers, G., Price, N.M., 2006. Copper-containing plastocyanin used for electron transport by an oceanic diatom. Nature 441, 341–344. https://doi.org/10.1038/nature04630

Pelletier, B., Calmant, S., Pillet, R., 1998. Current tectonics of the Tonga-New Hebrides region. Earth Planet. Sci. Lett. 164, 263–276. https://doi.org/10.1016/S0012-821X(98)00212-X

Pernet-Coudrier, B., Waeles, M., Filella, M., Quentel, F., Riso, R.D., 2013. Simple and simultaneous determination of glutathione, thioacetamide and refractory organic matter in natural waters by DP-CSV. Sci. Total Environ. 463–464, 997–1005. https://doi.org/10.1016/j.scitotenv.2013.06.053

Pesch, M. L., Christl, I., Barmettler, K., Kraemer, S. M., & Kretzschmar, R. (2011). Isolation and purification of Cu-free methanobactin from Methylosinus trichosporium OB3b. *Geochemical Transactions*, *12*(1), 2. https://doi.org/10.1186/1467-4866-12-2

Petzold, H., Sadler, P.J., 2008. Oxidation induced by the antioxidant glutathione (GSH). Chem. Commun. 4413–4415. https://doi.org/10.1039/b805358h

Philippot, L., 2002. Denitrifying genes in bacterial and Archaeal genomes. Biochim. Biophys. Acta - Gene Struct. Expr. 1577, 355–376. https://doi.org/10.1016/S0167-4781(02)00420-7

Raven, J.A., Evans, M.C.W., Korb, R.E., 1999. The role of trace metals in photosynthetic electron transport in O2-evolving organisms. Photosynth. Res. 60, 111–150. https://doi.org/10.1023/A:1006282714942

Rea, P.A., Vatamaniuk, O.K., Rigden, D.J., 2004. Weeds, worms, and more: papain's long-lost cousin. Plant Physiol. 136, 2463–2474. https://doi.org/10.1104/pp.104.048579.LONG-CHAIN

Reintjes, G., Tegetmeyer, H.E., Bürgisser, M., Orlic, S., Tews, I., Zubkov, M., Voß, D., Zielinski, O., Quast, C., Glöckner, F.O., Amann, R., Ferdelman, T.G., Fuchsa, B.M., 2019. On-Site Analysis of Bacterial

Communities of the Ultraoligotrophic South Pacific Gyre. Appl. Environ. Biol. 85, 1–14.

Ridge, P.G., Zhang, Y., Gladyshev, V.N., 2008. Comparative genomic analyses of copper transporters and cuproproteomes reveal evolutionary dynamics of copper utilization and its link to oxygen. PLoS One 3. https://doi.org/10.1371/journal.pone.0001378

Ritchie, J.D., Michael Perdue, E., 2003. Proton-binding study of standard and reference fulvic acids, humic acids, and natural organic matter. Geochim. Cosmochim. Acta 67, 85–96. https://doi.org/10.1016/S0016-7037(02)01044-X

Romera-Castillo, C., Sarmento, H., Alvarez-Salgado, X.A.Á., Gasol, J.M., Marrasé, C., 2011. Net production and consumption of fluorescent colored dissolved organic matter by natural bacterial assemblages growing on marine phytoplankton exudates. Appl. Environ. Microbiol. 77, 7490–7498. https://doi.org/10.1128/AEM.00200-11

Ruacho, A., Bundy, R.M., Till, C.P., Roshan, S., Wu, J., Barbeau, K.A., 2020. Organic dissolved copper speciation across the U.S. GEOTRACES equatorial Pacific zonal transect GP16. Mar. Chem. 225. https://doi.org/10.1016/j.marchem.2020.103841

Rue, E.L., Bruland, K.W., 1995. Complexation of iron(III) by natural organic ligands in the Central North Pacific as determined by a new competitive ligand equilibration/adsorptive cathodic stripping voltammetric method. Mar. Chem. 50, 117–138. https://doi.org/10.1016/0304-4203(95)00031-L

Sander, Sylvia G., Koschinsky, A., 2011. Metal flux from hydrothermal vents increased by organic complexation. Nat. Geosci. 4, 145–150. https://doi.org/10.1038/ngeo1088

Sander, S.G., Koschinsky, A., Massoth, G., Stott, M., Hunter, K.A., 2006. Organic complexation of copper in deep-sea hydrothermal vent systems. Environ. Chem. 4, 81–89. https://doi.org/https://doi.org/10.1071/EN06086

Sarma, N.S., Kiran, R., Reddy, M.R., Iyer, S.D., Peketi, A., Borole, D. V., Krishna, M.S., 2018. Hydrothermal Alteration Promotes Humic Acid Formation in Sediments: A Case Study of the Central Indian Ocean Basin. J. Geophys. Res. Ocean. 110–130. https://doi.org/10.1002/2017JC012940

Schieber, M., Chandel, N.S., 2014. ROS function in redox signaling. Curr. Biol. 24, 453–462. https://doi.org/10.1016/j.cub.2014.03.034

Schlitzer, R., 2021. Ocean Data View.

Schulte, M.D., Rogers, K.L., 2001. Thiols in hydrothermal solution: Standard partial molal properties and their role in the organic geochemisty of hydrothermal enviroments.

Shao, Y., Bao, M., Huo, W., Ye, R., Ajmal, M., Lu, W., 2023. From biomass to humic acid : Is there an accelerated way to go ? Chem. Eng. J. 452, 139172. https://doi.org/10.1016/j.cej.2022.139172

Shao, Y., Bao, M., Huo, W., Ye, R., Liu, Y., Lu, W., 2022. Production of artificial humic acid from biomass residues by a non-catalytic hydrothermal process. J. Clean. Prod. 335, 130302. https://doi.org/10.1016/j.jclepro.2021.130302

Shaw, T.J., Luther, G.W., Rosas, R., Oldham, V.E., Coffey, N.R., Ferry, J.L., Dias, D.M.C., Yücel, M., Thibault, A., Chanvalon, D., 2021. Fe-catalyzed sulfide oxidation in hydrothermal plumes is a source of reactive oxygen species to the ocean. Proc. Natl. Acad. Sci. U.S.A. 118, 1–7. https://doi.org/10.1073/pnas.2026654118

Shigemitsu, M., Yokokawa, T., Uchida, H., Kawagucci, S., Murata, A., 2021. Sedimentary supply of humic-like fluorescent dissolved organic matter and its implication for chemoautotrophic

microbial activity in the Izu-Ogasawara Trench. Sci. Rep. 11, 1–10. https://doi.org/10.1038/s41598-021-97774-7

Slagter, H.A., Laglera, L.M., Sukekava, C., Gerringa, L.J.A., 2019. Fe-Binding Organic Ligands in the Humic-Rich TransPolar Drift in the Surface Arctic Ocean Using Multiple Voltammetric Methods. J. Geophys. Res. Ocean. 124, 1491–1508. https://doi.org/10.1029/2018JC014576

Steffens, J.C., 1990. The heavy metal-binding peptides of plants. Annu. Rev. Plant Physiol. Plant Mol. Biol. 41, 553–575. https://doi.org/10.1146/annurev.pp.41.060190.003005

Sukekava, C., Downes, J., Slagter, H.A., Gerringa, L.J.A., Laglera, L.M., 2018. Determination of the contribution of humic substances to iron complexation in seawater by catalytic cathodic stripping voltammetry. Talanta 189, 359–364. https://doi.org/10.1016/j.talanta.2018.07.021

Superville, P.J., Pižeta, I., Omanović, D., Billon, G., 2013. Identification and on-line monitoring of reduced sulphur species (RSS) by voltammetry in oxic waters. Talanta 112, 55–62. https://doi.org/10.1016/j.talanta.2013.03.045

Swarr, G.J., Kading, T., Lamborg, C.H., Hammerschmidt, C.R., Bowman, K.L., 2016. Dissolved low-molecular weight thiol concentrations from the U.S. GEOTRACES North Atlantic Ocean zonal transect. Deep Sea Res. Part I Oceanogr. Res. Pap. 116, 77–87. https://doi.org/10.1016/J.DSR.2016.06.003

Tang, D., Hung, C.C., Warnken, K.W., Santschi, P.H., 2000. The distribution of biogenic thiols in surface waters of Galveston Bay. Limnol. Oceanogr. 45, 1289–1297. https://doi.org/10.4319/lo.2000.45.6.1289

Tang, D., Warnken, K.W., Santschi, P.H., 2001. Organic complexation of copper in surface waters of Galveston Bay. Limnol. Oceanogr. 46, 321–330. https://doi.org/10.4319/lo.2001.46.2.0321

Tilliette, C., Gazeau, F., Portlock, G., Bonnet, S., Guigue, C., Leblond, N., Lory, C., Marie, D., Montanes, M., Pulido-, E., Sarthou, G., Tedetti, M., Vorrath, M., Whitby, H., Guieu, C., 2023. Influence of shallow hydrothermal fluids release on the functioning of phytoplankton communities. Front. Mar. Sci.

Tilliette, C., Taillandier, V., Bouruet-Aubertot, P., Grima, N., Maes, C., Montanes, M., Sarthou, G., Vorrath, M.-E., Arnone, V., Bressac, M., et al., 2022. DFe patterns impacted by shallow hydrothermal sources along a transect through the Tonga-Kermadec arc. Earth Sp. Sci. Open Arch. 43. https://doi.org/10.1029/2022GB007363

Turner, J.A., Abel, R.H., Osteryoung, R.A., 1975. Normal Pulse Polarographic Analysis Based on Mercury Anodization: Sulfide and Iodide. Anal. Chem. 47, 1343–1347.

van den Berg, C., 2014. UV digestion apparatus. [WWW Document]. URL http://pcwww.liv.ac.uk/~sn35/Site/ UV_digestion_apparatus.html

van den Berg, C.M.G., 1982. Determination of copper complexation with natural organic ligands in seawater by equilibration with MnO2 II. Experimental procedures and application to surface seawater. Mar. Chem. 11, 323–342. https://doi.org/10.1016/0304-4203(82)90029-9

Van Wambeke, F., Bonnet, S., Moutin, T., Raimbault, P., Alarcón, G., Guieu, C., 2008a. Factors limiting heterotrophic bacterial production in the southern Pacific Ocean. Biogeosciences 5, 833–845. https://doi.org/10.5194/bg-5-833-2008

Van Wambeke, F., Obernosterer, I., Moutin, T., Duhamel, S., Ulloa, O., Claustre, H., 2008b. Heterotrophic bacterial production in the eastern South Pacific: Longitudinal trends and coupling with primary production. Biogeosciences 5, 157–169. https://doi.org/10.5194/bg-5-157-2008

Vasconcelos, M.T.S.D., Leal, M.F.C., 2001. Antagonistic interactions of Pb and Cd on Cu uptake, growth inhibition and chelator release in the marine algae Emiliania huxleyi. Mar. Chem. 75, 123–139. https://doi.org/10.1016/S0304-4203(01)00029-9

Vasconcelos, M.T.S.D., Leal, M.F.C., van den Berg, C.M.G., 2002. Influence of the nature of the exudates released by different marine algae on the growth, trace metal uptake and exudation of Emiliania huxleyi in natural seawater. Mar. Chem. 77, 187–210.

Walsh, E.A., Smith, D.C., Sogin, M.L., D'Hondt, S., 2015. Bacterial and archaeal biogeography of the deep chlorophyll maximum in the South Pacific Gyre. Aquat. Microb. Ecol. 75, 1–13. https://doi.org/10.3354/ame01746

Wang, H., Liu, M., Wang, W., Zhou, H., Ellwood, M.J., Butterfield, D.A., Buck, N.J., Resing, J.A., 2022. Iron ligands and isotopes in hydrothermal plumes over backarc volcanoes in the Northeast Lau Basin, Southwest Pacific Ocean. Geochim. Cosmochim. Acta 336, 341–352. https://doi.org/10.1016/j.gca.2022.09.026

Ward, B.B., 2011. Measurement and distribution of nitrification rates in the oceans, 1st ed, Methods in Enzymology. Elsevier Inc. https://doi.org/10.1016/B978-0-12-381294-0.00013-4

Whitby, H., Bressac, M., Sarthou, G., 2020a. Contribution of Electroactive Humic Substances to the Iron - Binding Ligands Released During Microbial Remineralization of Sinking Particles. Geophys. Res. Lett. 1–11. https://doi.org/10.1029/2019GL086685

Whitby, H., Hollibaugh, J.T., van den Berg, C.M.G., 2017. Chemical Speciation of Copper in a Salt Marsh Estuary and Bioavailability to Thaumarchaeota. Front. Mar. Sci. https://doi.org/10.3389/fmars.2017.00178

Whitby, H., Planquette, H., Cassar, N., Bucciarelli, E., Osburn, C.L., Janssen, D.J., Cullen, J.T., González, A.G., Völker, C., Sarthou, G., 2020b. A call for refining the role of humic-like substances in the oceanic iron cycle. Sci. Rep. 10, 1–12. https://doi.org/10.1038/s41598-020-62266-7

Whitby, H., Posacka, A.M., Maldonado, M.T., van den Berg, C.M.G., 2018. Copper-binding ligands in the NE Pacific. Mar. Chem. 204, 36–48. https://doi.org/10.1016/J.MARCHEM.2018.05.008

Whitby, H., van den Berg, C.M.G., 2015. Evidence for copper-binding humic substances in seawater. Mar. Chem. https://doi.org/10.1016/j.marchem.2014.09.011

Williford, T., Amon, R.M.W., Benner, R., Kaiser, K., Bauch, D., Stedmon, C., Yan, G., Walker, S.A., van der Loeff, M.R., Klunder, M.B., 2021. Insights into the origins, molecular characteristics and distribution of iron-binding ligands in the Arctic Ocean. Mar. Chem. 231, 103936. https://doi.org/10.1016/j.marchem.2021.103936

Wong, K.H., Obata, H., Kim, T., Kondo, Y., Nishioka, J., 2021. New insights into the biogeochemical cycling of copper in the subarctic Pacific: Distributions, size fractionation, and organic complexation. Limnol. Oceanogr. 66, 1424–1439. https://doi.org/10.1002/lno.11695

Wu, J., Luther, G.W., 1995. Complexation of Fe(III) by natural organic ligands in the Northwest Atlantic Ocean by a competitive ligand equilibration method and a kinetic approach. Mar. Chem. 50, 159–177. https://doi.org/10.1016/0304-4203(95)00033-N

Yamashita, Y., Cory, R.M., Nishioka, J., Kuma, K., Tanoue, E., Jaffé, R., 2010. Fluorescence characteristics of dissolved organic matter in the deep waters of the Okhotsk Sea and the northwestern North Pacific Ocean. Deep. Res. Part II Top. Stud. Oceanogr. 57, 1478–1485. https://doi.org/10.1016/j.dsr2.2010.02.016

Yang, L., Hong, H., Guo, W., Chen, C.T.A., Pan, P.I., Feng, C.C., 2012. Absorption and fluorescence of

dissolved organic matter in submarine hydrothermal vents off NE Taiwan. Mar. Chem. 128–129, 64–71. https://doi.org/10.1016/j.marchem.2011.10.003

Yang, R., Su, H., Qu, S., Wang, X., 2017. Capacity of humic substances to complex with iron at different salinities in the Yangtze River estuary and East China Sea. Sci. Rep. 7, 1–9. https://doi.org/10.1038/s41598-017-01533-6

Yang, R., van den Berg, C.M.G., 2009. Metal complexation by humic substances in seawater. Environ. Sci. Technol. 43, 7192–7197. https://doi.org/10.1021/es900173w

Yücel, M., Gartman, A., Chan, C.S., Luther, G.W., 2011. Hydrothermal vents as a kinetically stable source of iron-sulphide-bearing nanoparticles to the ocean. Nat. Geosci. 4, 367–371. https://doi.org/10.1038/ngeo1148

Zeng, X., Alain, K., Shao, Z., 2021. Microorganisms from deep-sea hydrothermal vents. Mar. Life Sci. Technol. 3, 204–230. https://doi.org/10.1007/s42995-020-00086-4

Zhang, Y., Du, J., Ding, X., Zhang, F., 2016. Comparison study of sedimentary humic substances isolated from contrasting coastal marine environments by chemical and spectroscopic analysis. Environ. Earth Sci. 75, 1–14. https://doi.org/10.1007/s12665-016-5263-8

Zhang, Z., Fan, W., Bao, W., Chen, C.T.A., Liu, S., Cai, Y., 2020. Recent developments of exploration and detection of shallow-water hydrothermal systems. Sustain. 12, 1–17. https://doi.org/10.3390/su12219109

Zigah, P.K., McNichol, A.P., Xu, L., Johnson, C., Santinelli, C., Karl, D.M., Repeta, D.J., 2017. Allochthonous sources and dynamic cycling of ocean dissolved organic carbon revealed by carbon isotopes. Geophys. Res. Lett. 44, 2407–2415. https://doi.org/10.1002/2016GL071348

3.7. Supplementary

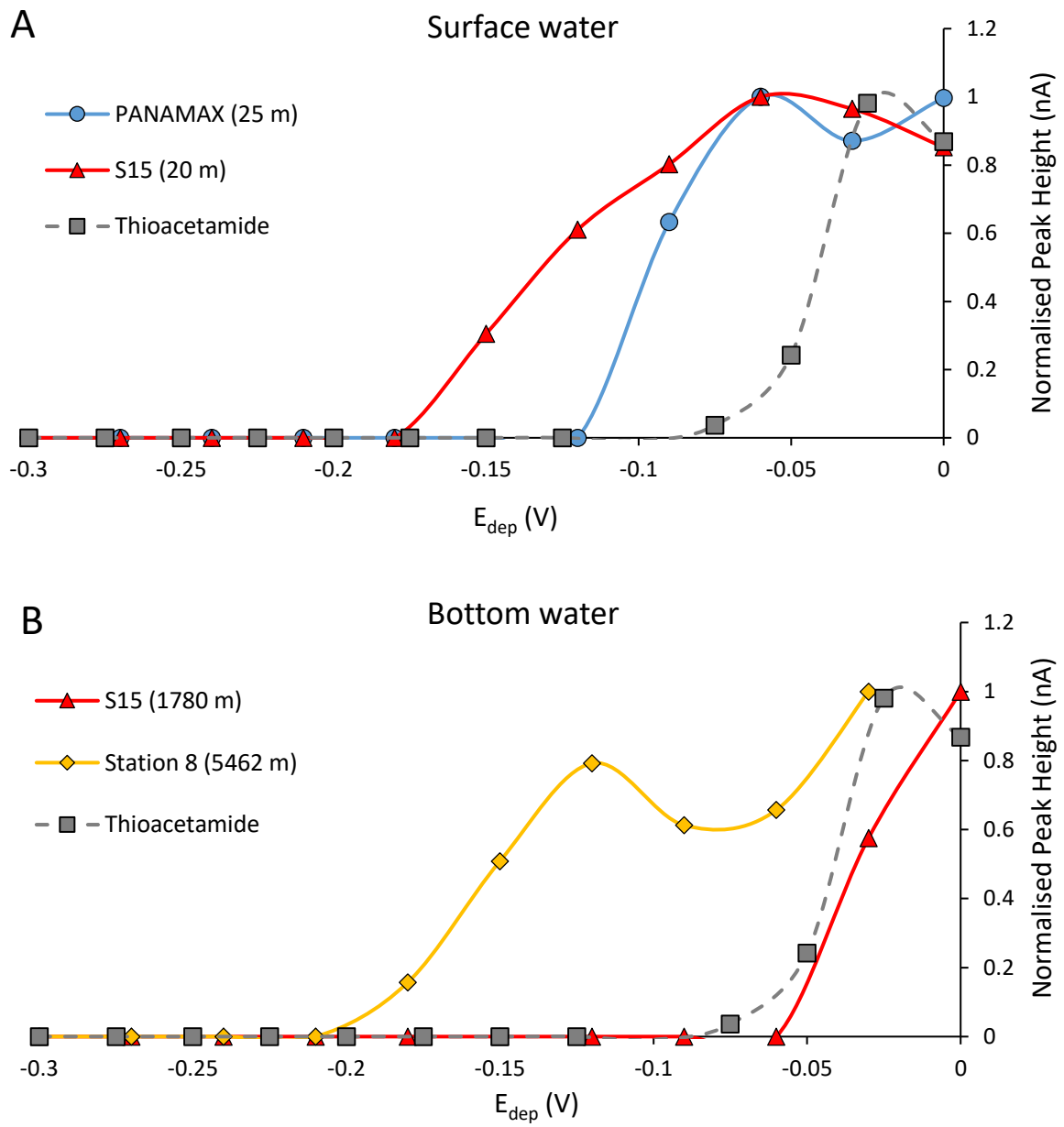

Figure 3.S1. *(A) Comparison of pseudopolarograms of PANAMAX and S15 surface waters with thioacetamide (TA) standard. (B) Comparison of pseudopolarograms of station 8 and S15 bottom waters with thioacetamide (TA) standard. Pseudopolarograms of TA standard were in UV digested seawater. Method used was developed by Laglera et al., (2014). Solutions were at natural pH. Each point represents the peak height of the RSS signal. Peak height has been normalised to the highest peak value (=peak height/largest peak height).*

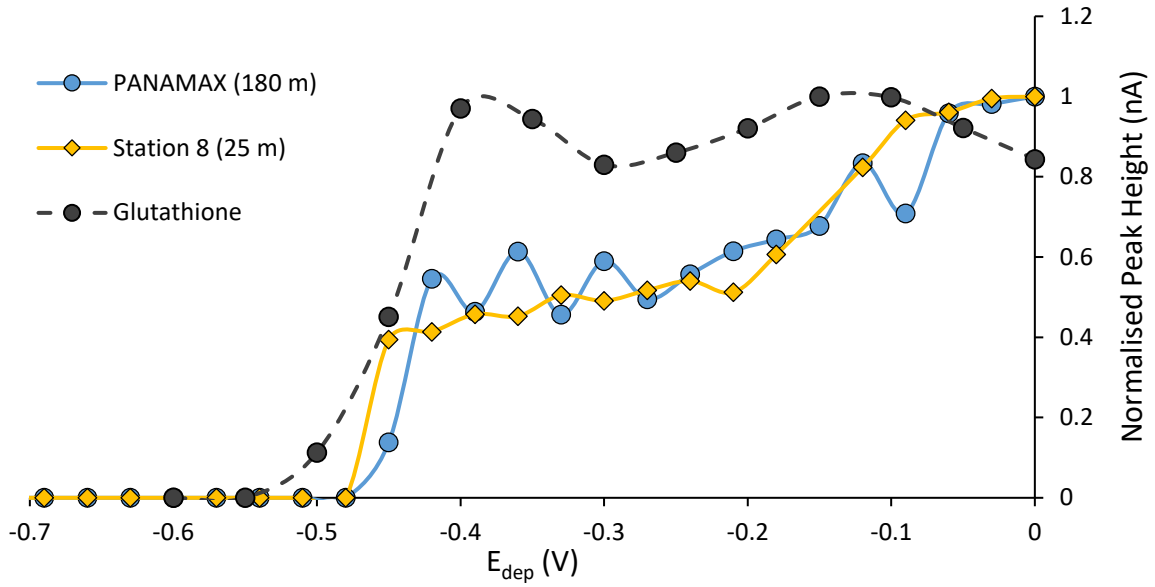

Figure 3.S2. *Comparison of pseudopolarograms of station 8 surface and PANAMAX bottom waters with glutathione (GSH) standard. Pseudopolarograms of GSH standard were in UV digested seawater. Method used was developed by Laglera et al., (2014). Solutions were at natural pH. Each point represents the peak height of the RSS signal. Peak height has been normalised to the highest peak value (=peak height/largest peak height).*

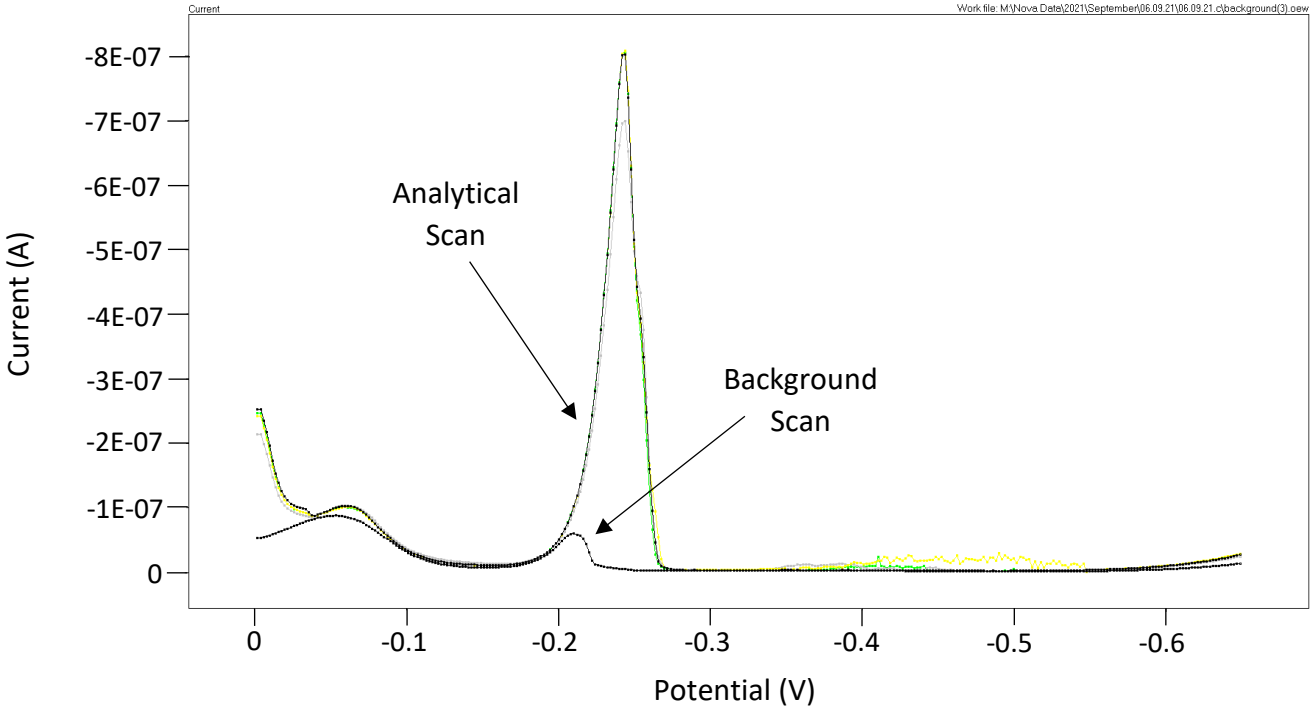

Figure 3.S3*. Cathodic stripping voltammogram above the plume at PANAMAX (797 m) using the Mo method (Pernet-Coudrier et al., 2013). This sample was suspected to contain sulphide as a relatively large peak was observed in the background scan. The peak in the analytical scan was unstable and decreased with time. The background scan is the same as the analytical scan but with a 1s deposition time. Analytical scan used Edep of 0 V for 150 s.*

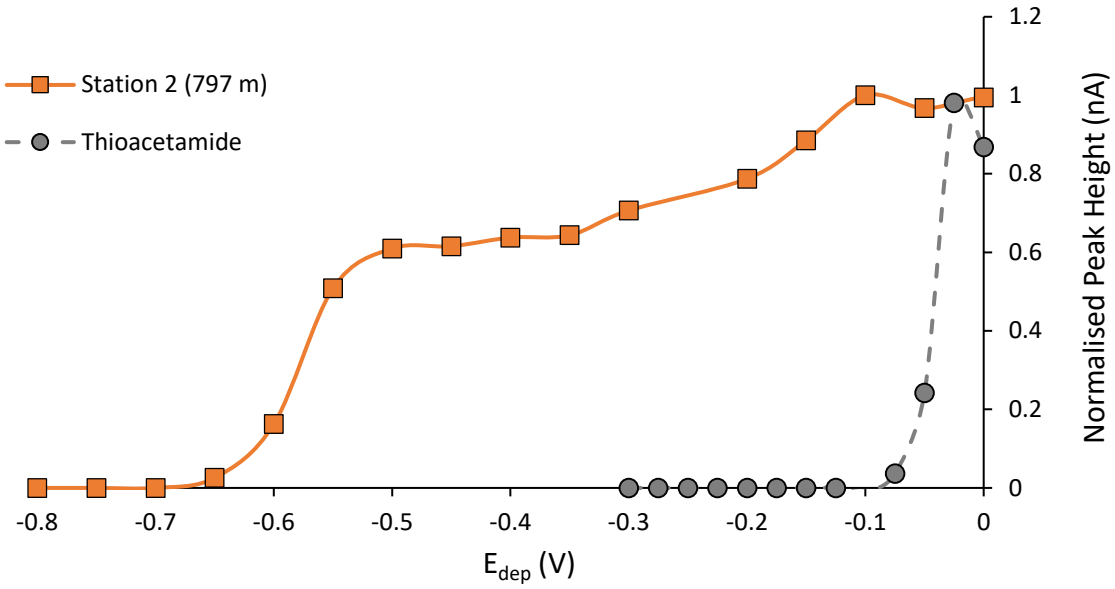

Figure 3.S4. *Comparison of pseudopolarograms of station 2 (797 m) with thioacetamide (TA) standard. Pseudopolarograms of TA standard was in UV digested seawater. Method used was developed by Laglera et al., (2014). Solutions were at natural pH. Each point represents the peak height of the RSS signal. Peak height has been normalised to the highest peak value (=peak height/largest peak height).*

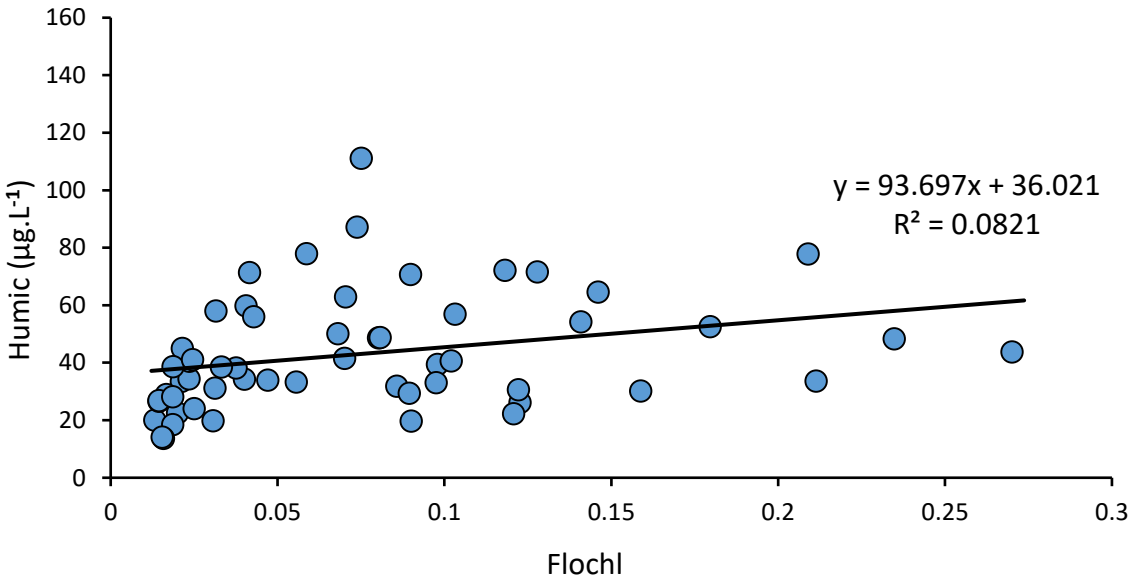

Figure 3.S5. *Correlation between electroactive humic substances (eHS) and FloChl in the upper 500m Stations 7 and 8 are not included, as the fluorimeter was unmounted at these stations.*

Note for the reader

The following chapter is in preparation for submission to the journal Frontiers Research Topic 'Hydrothermal and submarine volcanic activity: Impacts on ocean chemistry and plankton dynamics'.

To be submitted as: **Portlock, G**., Tilliette, C., Bonnet, S., Guieu, G., Gonzalez-Santana, D, : Whitby, H., Salaün, P.: The impact of shallow hydrothermal fluids on the production of RSS-like compounds and humic substances. An incubation study.

In this chapter, I ran the voltammetric determination of eHS, RSS. Copper determination and speciation was co-jointly done with PS. Dissolved Fe data was provided by C. Tilliette. Dissolved trace metal data was provided by D. Gonzalez-Santana. Experiment and sample collection were ran by F. Gazeau and onboard participants of GEOTRACES TONGA (GPpr14).

At the time of submission dissolved trace metal data measured by ICP –MS had not been validated and thus remains preliminary.

Chapter 4

The impact of shallow hydrothermal fluids on the production of RSS-like compounds and humic substances. An incubation study.

Abstract

The Western Tropical South Pacific (WTSP) Ocean has some of the most active zones for submarine volcanic activity in the world ocean. In particular, the Tonga-Kermadec arc hosts many shallow hydrothermal vents (<200 m), which can be a source of large amounts of trace metals. The fluids from these vents are directly released into the photic layer. This can be beneficial to the phytoplankton as it is a source of nutrients, but can also be toxic. Minicom experiments were designed to understand the impact of hydrothermal fluids on phytoplankton communities in the WTSP. In these experiments, different volumes of hydrothermal fluids were mixed with surface water and the communities' response was monitored.

Here we compare the concentration and speciation of eHS, RSS and copper at the start (<24h) and end (> 8 days) of the experiment. The aim of this study is to assess if eHS and RSS are directly or

indirectly produced by mixing hydrothermal fluids with surface waters. We show that concentrations of eHS, thioacetamide-like and glutathione-like compounds all increased in comparison to the control (no hydrothermal fluids). A clear increase in copper concentration was observed for all minicosm experiments, suggesting the dissolution and/or remineralisation of copper-containing particles present in the surface waters occurred or contamination from the water tanks. Using pseudopolarography, we show that most samples present a labile Cu wave (i.e. potentially bioavailable/toxic) at levels up to 1 nM, possibly due to copper-humic complexes. Our results also suggest the presence of a large voltammetrically inert fraction. The benefits and limitations of Cu pseudopolarography are discussed.

4.1. Introduction

Minicom experiments were designed to understand the impact of shallow hydrothermal fluids on surface communities. The experiment consisted of two separate incubation studies that took place onboard during the GEOTRACES TONGA (GPpr14) (Guieu and Bonnet, 2019) research cruise. Different volumes of hydrothermal fluids were mixed with surface water to understand the biological response for different mixing scenarios. Two shallow hydrothermal vents were selected for the experiment (PANAMAX and SIMONE). The two vents have different characteristics, with PANAMAX being more active than SIMONE. The first experiment (V1) used hydrothermal fluids from the shallow vent 'PANAMAX'. This experiment took place from 11/11/2019 - 20/11/2019 (9 days). The second experiment occurred from 24/11/2019 - 02/12/2019 (8 days), and the hydrothermal fluids were from 'SIMONE'.

In this chapter, we use voltammetry to present the species-specific RSS (thioacetamide-like and glutathione-like compounds), electroactive humic substances (eHS) concentrations and copper speciation (dissolved Cu and pseudopolarography) obtained in this experiment. We relate our results

to the biological and chemical observations to assess the driving factors that could determine the production and release of these compounds.

4.2. Experimental

4.2.1. Experimental design

A detailed account of the minicosms experiment is described by Tillette et al., 2022 (Tilliette et al., 2023). Briefly, there were two minicosm experiments (V1 and V2) that were conducted as part of the GEOTRACES TONGA (GPpr14) (Guieu and Bonnet, 2019) research cruise. Experiments took place in nine 300 L high-density polyethylene (HDPE) tanks. The tanks were installed inside a light-isolated, air-conditioned, clean-room container. Temperature, light and irradiance spectrum and intensity were controlled.

Before the experiment, the tanks were washed with a high-pressure cleaner (Kärcher®). They were then filled with a mixture of fresh water and surfactant (Decon™) and left for 24 h before being rinsed and filled with Milli-Q water acidified to pH 2 with hydrochloric acid (Suprapure HCl, Supelco®). This cleaning solution was left for 24 h. Finally, the tanks were emptied and rinsed with deionized water.

4.2.2. Sampling locations

There were two sequential experiments, V1 and V2. Surface water was sampled in both cases east of the TONGA arc, at the western boundary of the South Pacific Gyre (Figure 4.1). This was because the water would not be influenced by volcanic activity, and the chlorophyll concentrations were low (< 0.1 mg m^{-3}). The hydrothermal fluids were collected from two shallow hydrothermal vents (PANAMAX for V1 and SIMONE for V2). The hydrothermal fluids were collected from depths that had high acoustic and chemical anomalies. For the V1 experiment, surface water was collected from 5 m depth at 21.69 °S, 174.71 °W. The hydrothermal fluids were collected from 200 m depth at the PANAMAX shallow

hydrothermal vent, at 21.15 °S, 175.735 °W. For the V2 experiment, surface water was collected from 5 m depth at 19.5 °S, 173.61 °W. The hydrothermal fluids were taken from 200 m depth at the SIMONE shallow hydrothermal vent, at 19.4 °S, 175.13 °W. At the time of this experiment, PANAMAX seemed to be more active than SIMONE (Tilliette et al., 2022). For V1, surface seawater and hydrothermal fluids were pumped into the tanks with a clean, high-speed peristaltic pump. The hydrothermal fluids were filtered through a 10 µm filter. For the V2 experiment, it was decided to add lower volumes of hydrothermal fluids to the surface water to follow the gradient: 0, 1, 2, 5, 10, 20, 30 and 40 liters. Due to the lower volumes of fluids required, hydrothermal fluids for V2 were collected using the CTD. In this study, surface water and hydrothermal fluids are referred to as 'end members'.

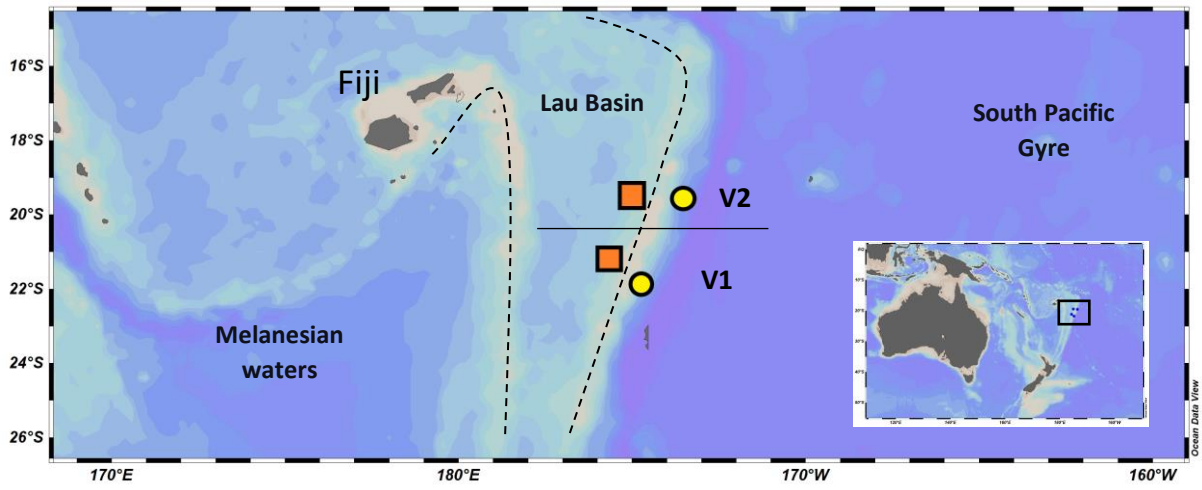

***Figure 4.1**. Map showing the location of the end members in the minicosms experiments. Surface water sites are the yellow circle and hydrothermal fluid sites are the orange square. Black dashed lines separate the different oceanographic regions. Figures were generated using ODV software (Schlitzer, 2021).*

4.2.3. Mixing protocol

There were nine minicosm tanks. One tank (M9) was used to sample the end members. Seven tanks were enriched with hydrothermal fluids and the final tank was the control experiment. The enriched minicosms followed a gradient approach (table 4.1). The total volume in each tank was 275 L.

Minicosms were mixed by a rotating propeller, set to nine rotations per minute, allowing the particles to remain suspended.

In preparation, all nine minicosm tanks were filled with 275 L of surface water and left overnight. The next day the M9 was sampled. After the sampling of M9, the tank was emptied and rinsed with Milli-Q.

The hydrothermal fluids were then collected directly into M9. Surface water was then removed from seven minicosm tanks and replaced with hydrothermal fluids. Hydrothermal fluids were not added to the surface waters straight away. For V1, hydrothermal fluids were added to surface water 3 h 30 after hydrothermal fluid collection. For V2, hydrothermal fluids were added 4 h 45 after hydrothermal fluid collection.

V1	Enrichment	Control	1.8%	3.6%	5.5%	7.3%	9.1%	10.9%	14.5%
	Volume of fluid (L)	0	5	10	15	20	25	30	40
	Volume of surface water (L)	275	270	265	260	255	250	245	235
V2	Enrichment	Control	0.4%	0.7%	1.8%	3.6%	7.3%	10.9%	14.5%
	Volume of fluid (L)	0	1	2	5	10	20	30	40
	Volume of surface (L)	275	274	273	270	265	255	245	235

Table 4.1. *The volume of surface water and hydrothermal fluid used in both minicosm experiments. Enrichment (%) is the proportion of hydrothermal fluid added to surface waters. V1 used hydrothermal fluids from PANAMAX. V2 used hydrothermal fluids from SIMONE.*

4.2.4. Sample collection

After the initial mixing of the end members, sampling of water from the minicosms was conducted at different intervals throughout the experiments. For both experiments, samples were collected after

12 h, 24 h, 48 h, 96 h and 144 h (table 4.2). The only difference in terms of sampling was the final day; for V1 the final sampling was 216 h after the mixing of the end members whereas it was 192 h for V2. Samples were collected from a sampling tube that was connected to each minicosm.

Experiment	Time (days)					
V1	12 h (day 0.5)	24 h (day 1)	48 h (day 2)	96 h (day 4)	144 h (day 6)	216 h (day 9)
V2	12 h (day 0.5)	24 h (day 1)	48 h (day 2)	96 h (day 4)	144 h (day 6)	192 h (day 8)

Table 4.2. *Time when the minicosm samples were collected. The experiment started when the end members were mixed.*

Samples were collected in acid-cleaned bottles according to the GEOTRACES protocol (Cutter et al., 2017). Samples were collected by gravity and filtered on sterile Sartobran® 300 cartridges (0.45 µm pre-filtration and 0.2 µm final filtration). Immediately after collection, samples were double bagged and stored at −20 ◦C until analysis.

Samples analysed for eHS and RSS for V1 were the 12 h (day 0.5), 48h (day 2), 96 h (day 4) and 216 h (day 9). For V2, samples analysed were the 24 h (day 1), 96 h (day 4) and 192 h (day 8). Samples analysed for Cu were the initial samples (12h and 24h for V1 and V2 respectively) and final (216 and 192 h for V1 and V2 respectively) of the control (no fluid) and highest mixing ratio of the hydrothermal fluids (14.5%).

4.2.5. Experimental monitoring

The temperature, irradiance and pH during both experiments are shown in Figure 4S1/4S2. The temperature of the minicosms was regulated using 500 W immersed heating resistors. Temperature data loggers were placed in the centre of each minicosm and recorded the temperature continuously. Natural light was reproduced using LED lights that were fitted inside the tanks. The light was programmed with a 12 h light and dark cycle. The irradiance was continuously recorded using sensors from *PAR Biospherical Instruments* (i.e. photosynthetically active radiation sensor - between 400 and

700 nm). A maximum PAR was reached (≈ 735 µE m^{-2} s^{-1}) between 9.30 a.m. and 5 p.m. The pH was recorded after sampling; measurements were carried out using a spectrophotometer *Agilent Cary60 UV-Vis.*

4.2.5. Analytical methods

4.2.5.1. Voltammetric equipment

Voltammetric measurements of humics and RSS were carried out using a Metrohm 663 VA stand which was connected to a µAutolabIII potentiostat through the IME663 interface. The software NOVA (version 2.1.4) controlled the measurements. The working electrode was a static mercury drop electrode (SMDE) with a drop size of 0.40 mm^2. The reference electrode was a commercial Ag/AgCl//3 M KCl electrode, and the counter electrode was a glassy carbon rod. Solutions (10 mL) were placed in a quartz voltammetric cell and stirred using a rotating polytetrafluoroethylene (PTFE) rod (setting 4 on the VA stand). An automatic sampler was connected to the VA stand to enable automatic loading and emptying of the voltammetric cell. Standard additions were made automatically using syringe burettes. The entire procedure was controlled through the Nova software allowing fully automated measurements. The voltammetric cell was rinsed twice with MQ for 30 s between each samples.

For eHS pseudopolarography, the set up remained the same as that described in Chapter 4 of this thesis.

For Cu analysis (total concentrations and pseudopolarograograms), the potentiostat was a µAutolab connected to a IME663 interface and controlled by the GPES software (version 4.9). Measurements were made in a polypropylene cup (maximum capacity: 30 mL) using a gold microwire electrode (10 µm diameter, 2-3 mm long), an iridium wire electrode (150 µm diameter, 4-5 mm long) and an Ag/AgCl//KCl(3 M) reference electrode. No autosampler was used and measurements were done in the presence of oxygen. Pseudopolarograms were carried out at natural pH while total concentrations were measured in acidified (pH 1.9, HCl) and UV digested (45 min in acid-cleaned quartz tube)

seawater. The working electrode was vibrated (140 Hz) during the conditioning and deposition time of stripping measurements while stagnant during the stripping stage. For total Cu analysis, the polypropylene cup was rinsed with Milli-Q water between samples. For pseudopolarograms, a different polypropylene cup was used and was not rinsed between samples to maintain conditioning and minimise adsorption processes during the course of the analysis.

4.2.5.2. Reagents

Ultrapure deionized water (>18 MΩ) from a Milli-Q system (Millipore, UK) was used for rinsing and dilutions of reagents. A 10 ppm molybdenum (VI) (Fisher Scientific) solution was prepared by diluting atomic absorption spectroscopy standard solutions of 1 $g.L^{-1}$ in 10 mM HCl (12 M). Thioacetamide (TA) (Fisher Scientific) and glutathione (GSH) (reduced, Sigma-Aldrich) were used as standards for RSS groups (Pernet-Coudrier et al., 2013). Suwannee River fulvic acid (SRFA) (International Humic Substances Society, 2S101F) was dissolved in Milli-Q to a concentration of 10 $mg.L^{-1}$. All ligand standards were acidified to pH 2 with HCl (12 M) and were kept in the fridge when not being used.

4.2.5.3. Voltammetric analysis

4.2.5.4.1. RSS and humic concentrations

The analytical settings used for RSS and eHS analysis were based on Pernet-Coudrier et al. (2013), however, the method was adapted to include a background subtraction. The Pernet-Coudrier et al. (2013) (eHS-Mo) method was selected for the quantification of eHS as it experienced fewer interference issues compared to the eHS-Fe (Laglera et al., 2007) and the eHS-Cu (Whitby and van den Berg, 2015) methods. For the eHS-Fe method, in samples of excess inorganic Fe the eHS-Fe peak is unstable due to Fe precipitation (Abualhaija et al., 2015). The samples used in this study were collected waters with intense hydrothermal activity resulting in high concentrations of Fe (Guieu et al., 2018; Tilliette et al., 2022; Wang et al., 2022), therefore the eHS-Fe method was not selected for the

quantification of eHS in this study. When using the eHS-Cu method, some samples showed a large, broad interference peak in the same position as the eHS-Cu peak (Figure 2.3), which inhibited the quantification of eHS. For this reason, the eHS-Cu method was not selected for the quantification of eHS in this study.

Briefly, under a laminar flow hood, 10 mL aliquots of seawater were placed into an acid-cleaned quartz voltammetric cell. The seawater was spiked with 30 µl of 10 ppm Mo(VI) and acidified to pH 2. A 300 s N_2 purging period was applied to remove oxygen from the seawater. A deposition potential of 0 V was applied for 150 s. The stirrer was on during the deposition and stopped during the 5 s equilibration step. A stripping scan using differential pulse mode started from 0 V to −0.6 V with a modulation time of 60 ms, a modulation amplitude of 50 mV, a step potential of 2 mV and an interval time of 0.1 s. For humic quantification a 1 s background scan was performed. A background scan had identical parameters to the analytical scan however, the deposition time was reduced from 150 s to 1 s. Concentrations compounds were determined by standard addition. Peak heights were measured using ECDSOFT (Omanović and Branica, 1998). A minimum of 4 repeat scans for the sample and each of the 2 standard additions. To check the validity of the procedure a Deep Sea Reference (DSR) seawater (Hansell lab, Batch 21 – 2021 – Lot 04-21) was used daily. The concentration of eHS obtained was 25.9 $\mu g.L^{-1}$ eq SRFA, for TA it was 60.1 nM eq TA, and there was no GSH present. The reproducibility was calculated by carrying 10 identical standard addition procedures of a DSR seawater (eHS RSD=11.7%; TA RSD=13.9%; n=10) (Hansell lab, batch 2021).

4.2.5.4.2. Pseudopolarography of humics

Cathodic pseudopolarography of eHS were carried out. Cathodic pseudopolarography was initially published to identify reduced sulphur substances (Laglera and Tovar-Sánchez, 2014). Multiple deposition potentials were applied to the electrode to obtain characteristic ip vs Edep profiles (pseudopolarograms). The method used for pseudopolarography of eHS was from Pernet-Coudrier et

al., (2013). Pseudopolarograms were initiated from +0.1 V, and the deposition potential decreased by increments of -0.05 V until no peak was visible.

4.2.5.4.3. Copper total concentration

Cu analysis was done using anodic stripping voltammetry using differential pulse anodic stripping voltammetry. The stripping parameters were 100 ms interval, 10 ms pulse time, 50 mV amplitude with a 6 mV step. The potential sequence consisted of an analytical scan and a background scan. The analytical scan included a conditioning step (0.55 V for 10 s) followed by a deposition step (-1.3 V for 120-300 s) and an equilibrium step (2 s) before the stripping stage which was done from 0 to 0.55 V. The background scan was the same as the analytical scan but with a 5 s deposition time at -1.3 V. Quantification of the Cu peak was done on the background-subtracted scan (background scan subtracted from the analytical scan) using the peak derivative given by the GPES software. The Cu peak was typically present at a potential of ~ 280 mV with a half-peak with of typically 54-60 mV. Cu concentration was determined by the method of standard addition with typically 5 repeat measurements of the Cu signal in the sample followed by triplicate measurements of a minimum of 2 standard additions. The detection limit was estimated as 3 times the standard deviation of 7 repeat measurements obtained in 12 mM HCl containing low Cu levels (0.5 nM) giving a LoD of approximately 35 pM (deposition time of 300 s).

4.2.5.4.4. Copper pseudopolarography

Cu pseudopolarograms were obtained by running successive differential pulse ASV scans at various deposition potentials. The stripping parameters were the same as those used for total Cu determination, i.e. 100 ms interval, 10 ms pulse time, 50 mV amplitude and a 6 mV step. Background subtraction was also used. The analytical scan consisted of a deposition potential (varied from -1.3 V to 0.3 V, every 50 mV) for typically 300 s, followed by a desorption potential (-1.3 V for 2 s), an equilibrium time (1s) and stripping from 0 to 0.55 V. The background scan consisted of a conditioning potential (10 s at +0.55 V), a desorption step (-1.3 V for 2 s), equilibrium time (1 s) and stripping from

0 to 0.55 V. The Cu peak was again quantified with the peak derivative given by the GPES software. The peak was typically present at a potential of ~220 mV, similar to that obtained in acidic conditions. Between each DPASV scans, an additional conditioning scan consisting of 30 s at +0.55 V followed by 30 s at -1.3 V was done to avoid potential build-up of adsorbed organic material at the surface of the gold electrode when positive deposition potential are used. No significant differences in pseudopolarograms were seen with/without this additional scan but it was kept as a precautionary measure, similar to what was used in the original study (Gibbon-Walsh et al., 2012). In addition, 5 or 10 measurements at -1.3 V were carried out before and after each pseudopolarogram experiment. This was done to stabilise the signal before starting the pseudopolarography and the check the stability of the signal before/after analysis.

To relate the intensity of the peak to concentrations, the sensitivity of the electrode was measured by titrating the natural oxygenated sample (or composite samples) with Cu. In a specific polypropylene cell (to avoid any carry over of Cu), successive additions of Cu were made in the cell and triplicate ASV measurements were made at a deposition potential of -1.3 V. The peak intensity was plotted as a function of added Cu, resulting in a typical complexing titration curve with a linear increase at high copper additions. This linear increase is indicative of the saturation of the ligand and indicates the sensitivity of the measurement in this sample (or composite sample). Typically, such linear relationship was obtained for Cu concentrations above 10 nM. This sensitivity was then normalised to the deposition time (units in $nA.V^{-1}.nM^{-1}.s^{-1}$) and used to estimate Cu concentrations from the peak intensity obtained at all deposition potentials. It is therefore assumed that this sensitivity is: 1- valid for all deposition potentials and 2- is directly proportional to the deposition time. The first assumption was tested in UV digested acidified (pH 2) seawater for which Cu intensity signal was found constant at deposition potentials below 0.1 V. The second assumption had been tested previously (Gibbon-Walsh et al., 2012) and was also found to be valid here.

The concentrations reported in the pseudopolarograms below are still termed as “estimated” concentrations for the following reasons:

1- the sensitivity was not always measured in each individual sample; instead, it was measured in a composite sample, made of the various seawater collected at the start and end of the minicosm experiment. This is not ideal because different sensitivities can be obtained in samples that have different levels surface active substances. In addition, the electrode history (so- called ‘memory effects’) may also impact the sensitivity of the gold solid electrode;

2- the Cu signal measured before/after pseudopolarograms was not always stable and tended to decrease, by up to 50%. The decrease was higher in samples containing low Cu concentrations, which required a high deposition time (up to 720s). Typical time in the voltammetric cell for 720 s deposition was more than 6h. The appearance of a small Hg peak was often observed that may affect Cu deposition and/or stripping from the gold surface.

3- The sensitivity used to relate peak intensity to concentrations were obtained at a deposition potential of -1.3 V. Although this sensitivity is constant at different deposition potentials in UV digested pH 2 seawater, it does not ascertain that this is also true in natural samples where adsorption of organic matter and/or other metals is potential dependent.

4- The sensitivity is obtained after saturation of the ligands, i.e. it is only due to inorganic copper which has a diffusion coefficient that may be widely different from the complexes being detected when varying the deposition potential.

4.2.5.3. Dissolved trace metal measurements

After collection, minicosm samples were acidified with hydrochloric acid (HCl, Ultrapure® Merck) (pH ~1.7). Samples were double bagged and stored in the dark at room temperature.

Concentrations of dissolved trace metal measurements were carried out at Ifremer, France, using an Element XR™ HR-SF-ICP-MS instrument (Thermo Fisher, Bremen, Germany), coupled with an ESI

seaFAST-pico™ introduction system. The measurements were carried out at Pôle Spectrométrie Océan (IFREMER, France). This method used was analytically similar to that of Lagerström et al. (2013).

4.2.6. Error calculations for standard additions:

Concentrations of RSS, eHS and Cu were calculated using the standard addition method. Error bars given in all the graphs correspond to the standard deviation of the intercept, determined for each standard addition using Equation 1 (Harris, 2003).

$$S_x = \frac{s_y}{|\mathrm{m}|}\sqrt{\frac{1}{n} + \frac{\bar{y}^2}{m^2\ \sum(x_i - \bar{x})^2}} \qquad \text{Equation 1.}$$

Where s_x is the standard deviation of the compound being measured, s_y is the standard deviation in peak intensity across all data points, m is the slope of the standard addition, n is the number of data points, $\bar{y}$ is the average peak height across all data points, x_i is the concentration of added standard for data points i, and $\bar{x}$ is the average concentration across all data points of the standard addition procedure.

4.3. Results

In these experiments, two different RSS were detected. These RSS were electrochemically similar to thioacetamide and glutathione. Therefore, these compounds are referred to as thioacetamide-like (TA-like) and glutathione-like (GSH-like) compounds (Figure 3.2 (see chapter 3)).

4.3.1. V1 (PANAMAX hydrothermal fluid enrichments)

For V1, the temperature ranged from 25.3 °C to 26.1 °C with an average of 25.8 °C (Figure 4S1). Minicosms 1.8% and 9.1% fluid mixing both had the lowest average temperature (25.3 °C), however this temperature was within the range of surface seawater temperatures. Therefore, it is unlikely that

the results from this experiment were impacted. The surface water pH was 8.07 and the hydrothermal fluid was 6.46 (Figure 4S2). When the hydrothermal fluid was mixed with the surface water, the pH of the minicosms decreased relative to the mixing ratio. On day 0.5 the pH of fluid-enriched experiments varied from 8.06 (control) to 7.85 (14.5%); over the course of the experiment, the pH converged together; 8.01 (control) to 7.94 (14.5%).

4.3.1.1. Thioacetamide-like compounds: V1

TA-like compounds were detected in all samples over the course of the whole experiment. In the control sample, the concentration of TA-like compounds ([TA-like]) fluctuated, increasing slightly over the course of the experiment (70 ± 10 nM to 98 ± 9 nM) (Figure 4.2A). A maximum concentration was obtained on day 4 of the experiment (107 ± 7 nM). In contrast, all the hydrothermal fluid-enriched experiments, except 10.9% fluid mixing, saw an increase of TA-like compounds day 0.5 after the initial mixing, with the 14.5% fluid mixing having the most significant increase (88%). However, there was no correlation between the percentage of fluid mixing and the increase of TA-like compounds (R^2=0.41, p=0.31). After day 2 [TA-like] decreased in all fluid-enriched experiments. By the end of the experiment, all the fluid-enriched tanks except 9.1% showed higher [TA-like] compared to the control. In the surface end member, [TA-like] was 73 ± 9 nM and for the hydrothermal fluid end member, [TA-like] was 92 ± 5 nM.

4.3.1.2. Glutathione-like compounds: V1

GSH-like compounds were not detected in the end members. In the control sample, no GSH-like compounds were detected until day 4 (0.67 ± 0.02 nM), from when [GSH-like] increased until the final day (8 ± 2 nM (Figure 4.2B). All the fluid-enriched experiments expect 9.1% mixing, had GSH-like compounds present within day 2 after initial mixing. The [GSH-like] increased for most experiments over the 8 days. Experiment 3.6%, 5.5% and 7.3% fluid mixing had maximum [GSH-like] on day 4 after

which the concentration decreased. There was no correlation between the percentage of fluid enrichment and [GSH-like]. By the end of the experiment, all the fluid mixed experiments except 1.8% showed higher [GSH-like] compared to the control. In both the surface and hydrothermal fluid end members, [GSH-like] was below detection limit.

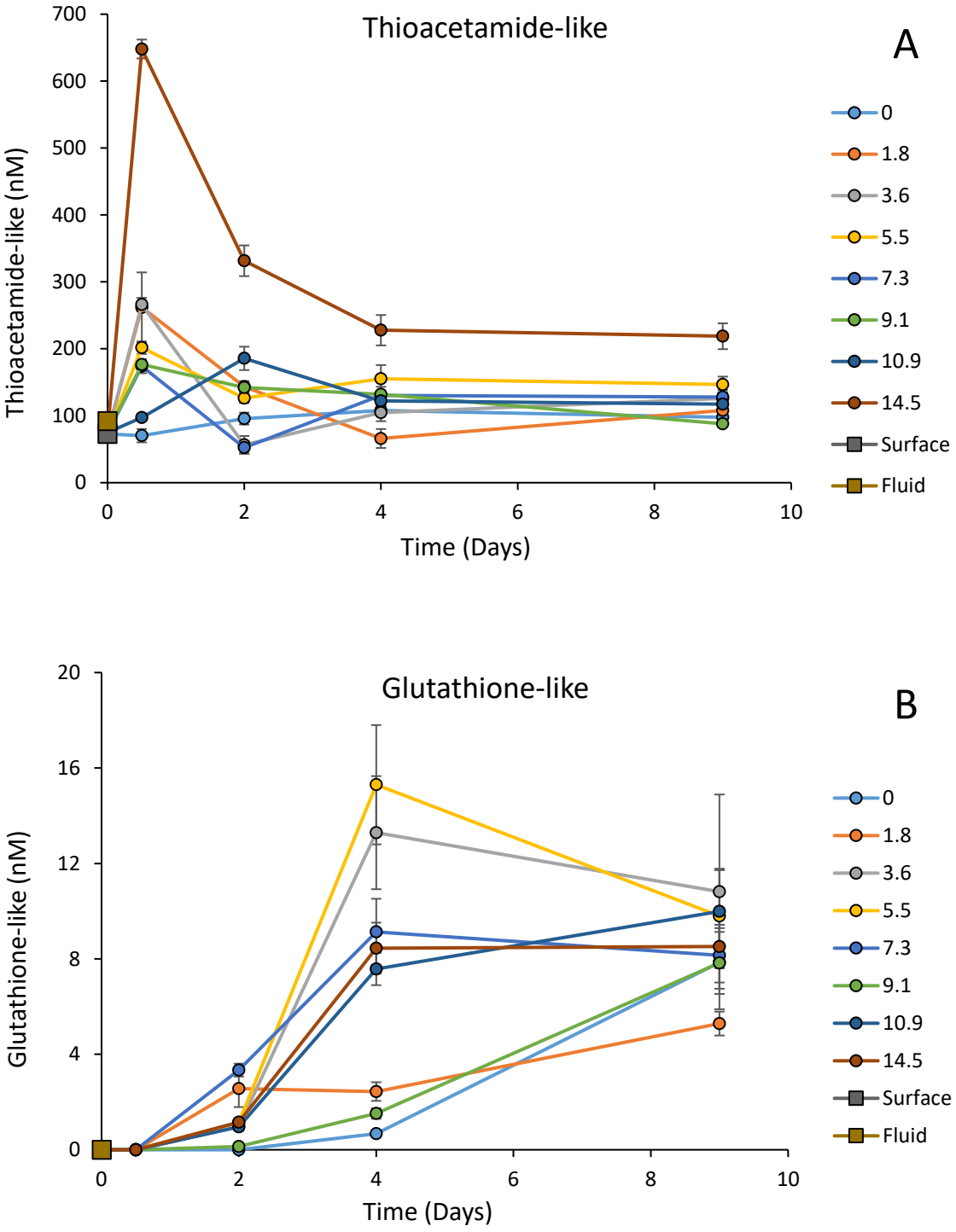

Figure 4.2. *Temporal dynamics of reduced sulphur substances (RSS) during the V1 minicosm experiment (duration 9 days). RSS were electrochemically similar to thioacetamide and glutathione. Therefore, concentrations are presented as equivalent of nM thioacetamide-like (TA).L^{-1} (A) and equivalent of nM glutathione-like (GSH).L^{-1} (B). Numbers in legend represent the % of hydrothermal fluid enrichment. Hydrothermal fluids were collected from PANAMAX. RSS concentrations were measured in the surface (grey square) and fluid (orange square) end members. Error bars represent the standard deviation of the intercept obtained for each individual standard addition.*

4.3.1.3. Electroactive humic substances: V1

In the V1 control sample, the concentration of electroactive humic substances ([eHS]) decreased from 70 ± 5 µg.L^{-1} eq SRFA to 48 ± 3 µg.L^{-1} within the first 48 h (Figure 4.3). After 48 h, the [eHS] increased continuously until the final day, when it reached a concentration of 113 ± 7 µg.L^{-1}. All fluid mixed experiments followed a similar pattern to the control, except for 3.6% and 14.5% mixing. In these experiments, the [eHS] increased day 0.5 after the initial mixing instead of decreasing like the rest of the mixes. On day 9 of the experiment, all the fluid mixes except 14.5% showed lower [eHS] compared to the control. In the surface end member, [eHS] was 70 ± 5 µg.L^{-1} and for the hydrothermal fluid end member, [eHS] was 22 ± 4 µg.L^{-1}.

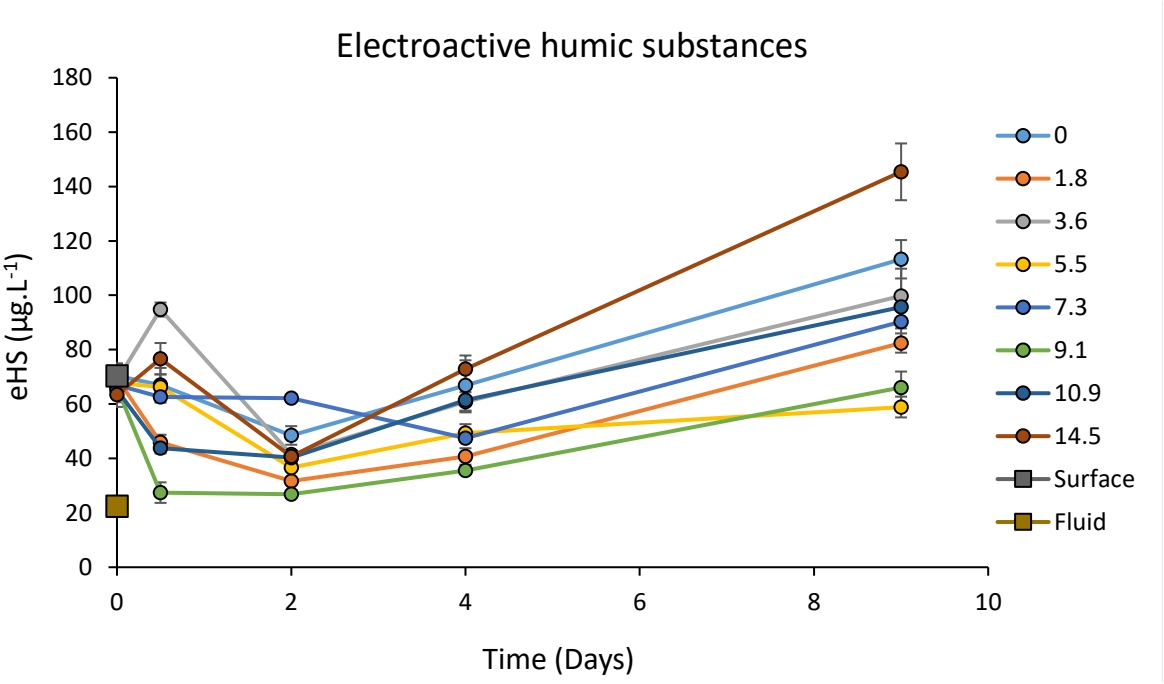

Figure 4.3. *Temporal dynamics of electroactive humic substances (eHS) during the V1 minicosm experiment (duration 9 days). Concentrations are presented as eHS in µg SRFA eq.L^{-1}. Numbers in legend represent the % of hydrothermal fluid enrichment. Hydrothermal fluids were collected from PANAMAX. eHS concentrations were measured in the surface (grey square) and fluid (orange square) end members. Error bars represent the standard deviation of the intercept obtained for each individual standard addition.*

4.3.1.4 Dissolved Copper: V1

Total dissolved copper concentrations were determined both by voltammetry and by ICP-MS. In the V1 control treatment (surface water, no hydrothermal fluids), the total Cu concentration in the minicosm tank obtained by voltammetry increased from 2.4 nM at t=12h to 7.1 nM at the end of the experiment (t=9 days). In the presence of hydrothermal fluids (14.5%), the total concentrations also increased, from 2.7 nM (t =12h) to 9.2 nM after 9 days.

The pseudopolarograms obtained in those samples are shown in Figure 4.4 with the estimated fraction of the total concentration being detected by voltammetry at each E_{dep}. For both type of samples (without (Control) and with 14.5% hydrothermal fluid), a Cu signal is detected for E_{dep} below -0.2 V. When decreasing E_{dep}, the intensity of the signal increases until ~ -0.8 to -1 V before decreasing at lower E_{dep} (-1 to -1.3 V). In the control sample at 24 h, an estimated maximum of 0.8 nM of Cu is detected, representing 40% of the total. At the end of the experiment (after 9 days), up to 1.8 nM Cu is measured, representing an estimated 30% of the total concentration. In the hydrothermal sample, up to 2 nM are detected after 24h and up to 3.3 nM after day 9, representing approximately 70% and 36% of the total Cu. Interestingly, all four pseudopolarograms present an early wave at ~ -0.1 V indicative of the presence of fast-dissociating weak Cu complexes. The presence of other stronger complexes can be inferred by the increasing signal at lower deposition potential, with sometimes, the presence of well-defined “waves” such as -0.7 V in the 14.5% hydrothermal sample, t = 9 days. Comparison of the pseudopolarograms at the start and end of the minicosms experiment show that the absolute concentration of Cu being detected is higher at the end, although it represents a lower proportion of the total concentration. Our estimation suggests that a large proportion of the Cu is electrochemically inert within the range of deposition potential used here.

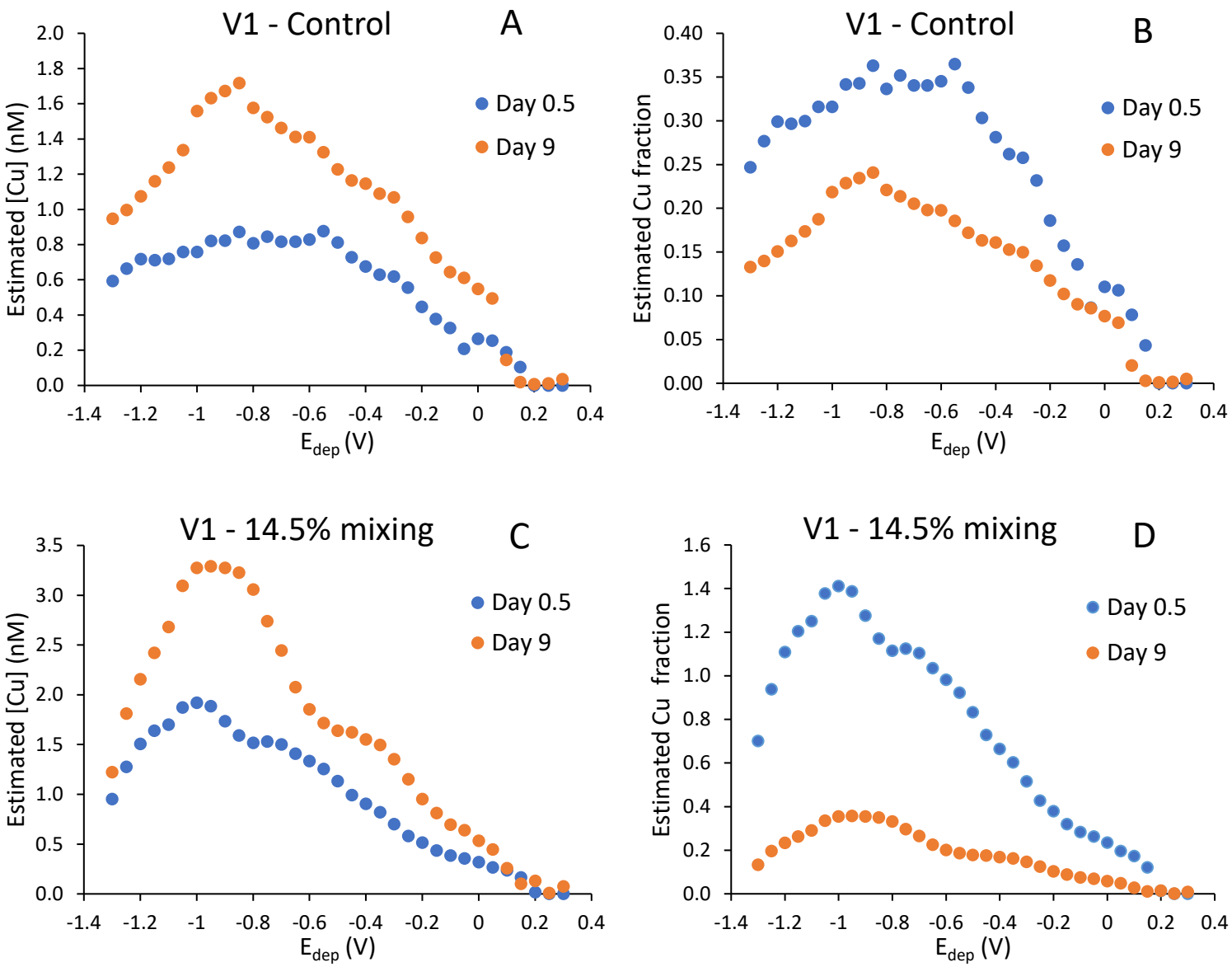

Figure 4.4. *Estimated dCu concentrations in the V1 minicosm experiments in control (A) and in 14.5% mixing (C) experiments. At -1 V, Cu-complexes are reduced providing an estimation of the dCu concentrations. dCu concentrations are presented in nM. Estimated dCu fraction in the V1 minicosm experiments in control (B) and in 14.5% mixing (D) experiments. Estimated Cu fraction is the difference between the total dCu and the maximum reduced dCu during pseudopolarography. dCu that could not be reduced during pseudopolarography, is classed as inert.*

4.3.2. V2 (SIMONE hydrothermal fluid enrichments)

For V2 the temperature ranged from 26.6 °C to 26.9 °C with an average of 26.8 °C (Figure 4S1). The pH of the surface water was 8.09 and 7.68 for the hydrothermal fluid (Figure 4S2). On day 0.5, the pH varied slightly between the different fluid enriched experiments. 14.5% fluid enriched had the lowest

pH (8.05) and 0.7% fluid enriched had the highest pH (8.10). On the final day (day 8) the pH of all experiments ranged from 8.6 to 8.5.

4.3.2.1. Thioacetamide-like compounds: V2

In the control sample, the [TA-like] decreased by 30% 24 h after the start of the experiment. After this [TA-like] increased over time until it reached a maximum concentration of 127 ± 6 nM (Figure 4.5A). All fluid-enriched tanks followed a similar pattern to the control, with the maximum [TA-like] on the final day (day 8). The exception was 0.7% fluid mixing where the maximum [TA-like] was on the 4th day (2 ± 1.2 nM). On the final day all fluid mixes except 0.7% and 10.9% showed higher [TA-like] compared to the control. In the surface end member, [TA-like] was 129 ± 7 nM and for the hydrothermal fluid end member, [TA-like] was 131 ± 8 nM.

4.3.2.2. Glutathione-like compounds: V2

In the control sample, GSH-like compounds were only present on the final day of the experiment (2 ± 0.6 nM). For all the hydrothermal fluid mixes except 1.8%, GSH was present 4 days after initial mixing. All experiments had the highest [GSH-like] on the final day, except for 3.6% mixing, which had the maximum concentration on day 4 (5 ± 2 nM). On the final day, all the fluid mixes except 0.4% and 14.5% had lower [GSH-like] than the control (Figure 4.5B). In the both the surface and hydrothermal fluid end members, [GSH-like] was undetectable.

4.3.2.3. Electroactive humic substances: V2

In the control sample, the concentration of eHS increased from 62 ± 8 $\mu g.L^{-1}$ (day 1) to 97 ± 6 $\mu g.L^{-1}$ (day 8) during the experiment. In all the fluid-enriched tanks the [eHS] decreased 1 day after the initial mixing. After day 1 the [eHS] increased until the end of the experiment. In all fluid mixes, the maximum

eHS concentration was obtained on the final day (day 9) of the experiment. All the fluid mixes except 7.3% had higher [eHS] than the control (Figure 4.6). In the surface end member, [eHS] was 62 ± 8 $\mu g.L^{-1}$ and for the hydrothermal fluid end member, [eHS] was 43 ± 6 $\mu g.L^{-1}$.

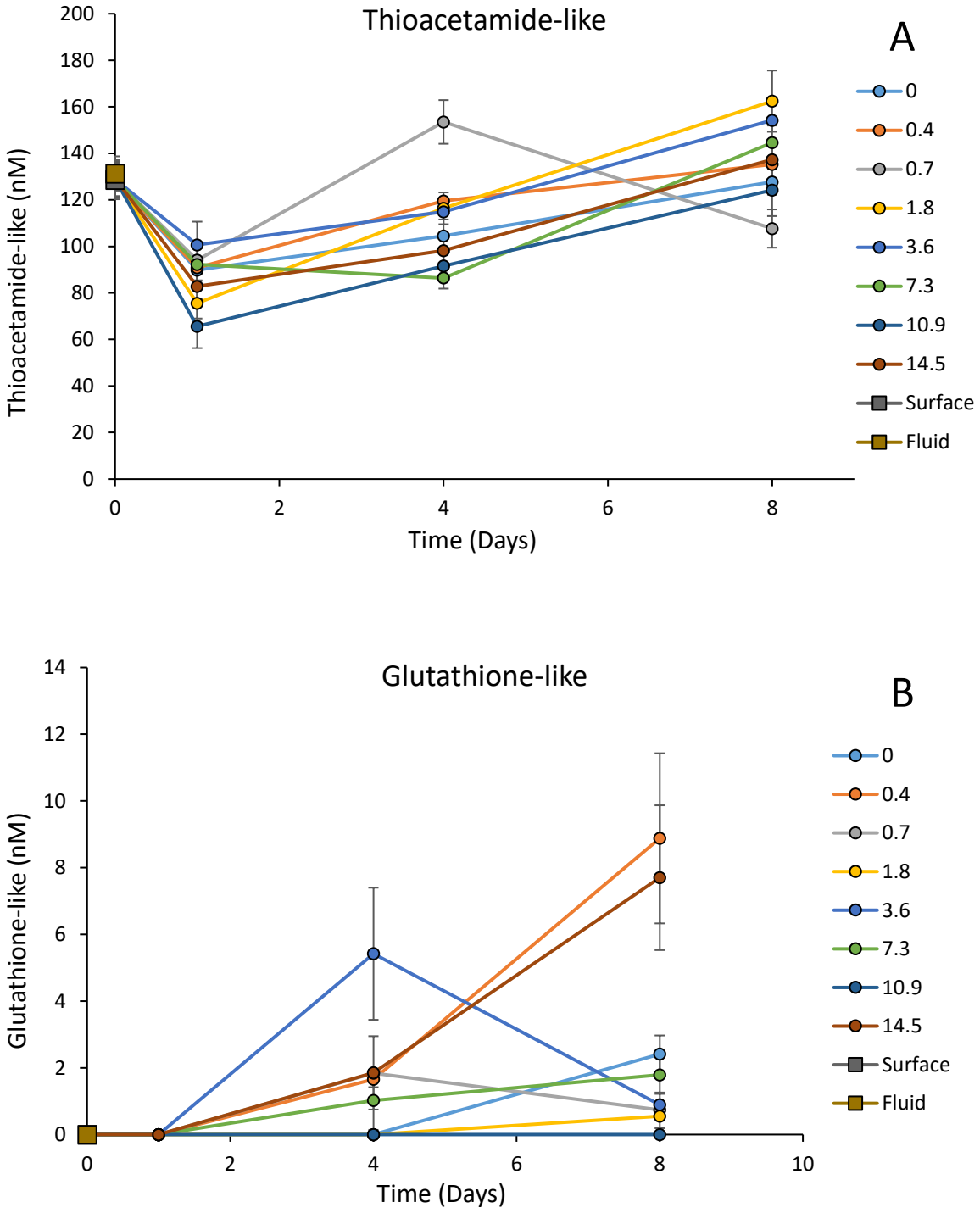

Figure 4.5. *Temporal dynamics of reduced sulphur substances (RSS) during the V2 minicosm experiment (duration 8 days). RSS were electrochemically similar to thioacetamide and glutathione. Therefore, concentrations are presented as equivalent of nM thioacetamide-like (TA).L^{-1} (A) and equivalent of nM glutathione-like (GSH).L^{-1} (B). Numbers in legend represent the % of hydrothermal fluid enrichment. Hydrothermal fluids were collected from SIMONE. RSS concentrations were measured in the surface (grey square) and fluid (orange square) end members. Error bars represent the standard deviation of the intercept obtained for each individual standard addition.*

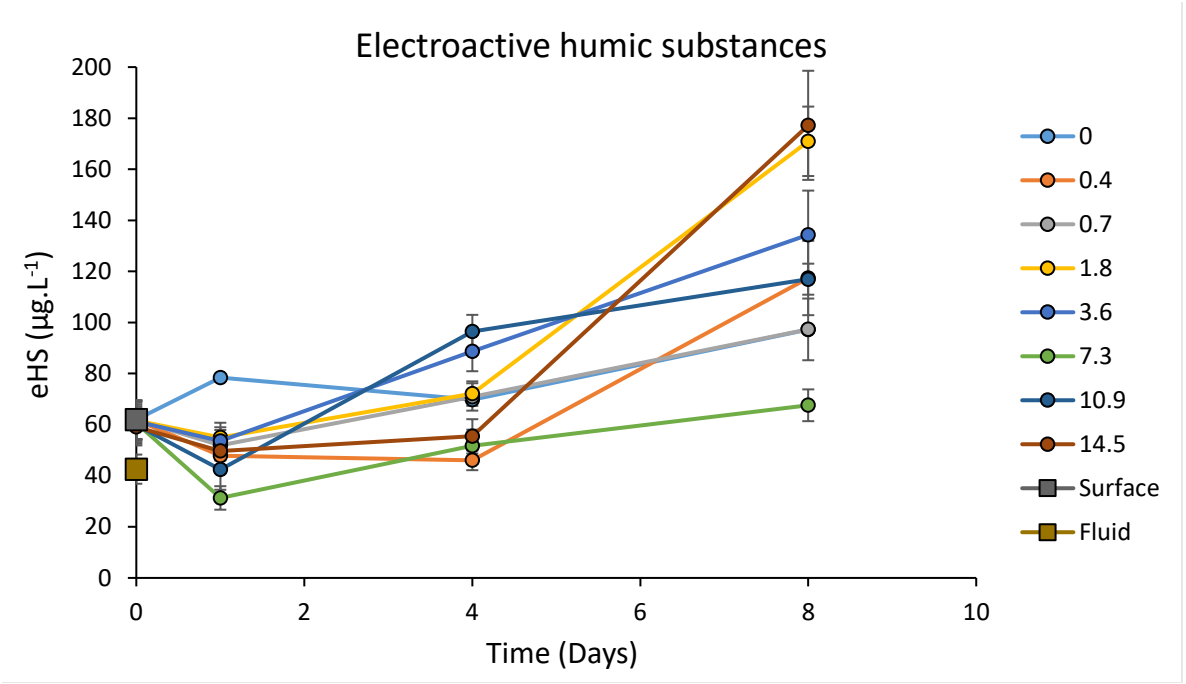

Figure 4.6. *Temporal dynamics of electroactive humic substances (eHS) during the V2 minicosm experiment (duration 8 days). Concentrations are presented as eHS in µg SRFA eq.L^{-1}. Numbers in legend represent the % of hydrothermal fluid enrichment. Hydrothermal fluids were collected from SIMONE. eHS concentrations were measured in the surface (grey square) and fluid (orange square) end members. Error bars represent the standard deviation of the intercept obtained for each individual standard addition.*

4.3.2.4 Dissolved Copper: V2

In the control treatment (surface water, no hydrothermal fluids), the total Cu concentration in the minicosms measured by voltammetry increased from 1.8 nM at t = 24h and 6.2 nM at the end of the experiment (t = 8 days). In the presence of hydrothermal fluids (14.5%), the total concentrations also increased, from 2.0 nM after the initial mixing (t =24h) up to 6.3 nM after 8 days.

The pseudopolarograms obtained in those samples are shown in Figure 4.7 with the estimated fraction of the total concentration being detected by voltammetry at each E_{dep}. Similar to the Panamax minicosms experiments, the Cu signal was much higher after 8 days than after 24 h. In the control sample, Cu concentrations increased from an estimated 0.4 to 2.5 nM while in presence of 14.5% hydrothermal fluid, the estimated Cu concentration increased from ~ 1 nM to more than 5 nM at the

end of the experiment. In contrast to the V1 experiment, a Cu signal was only obtained E_{de} below 0 V in the early stage of the experiment (both in the absence and presence of the hydrothermal fluid); no signals were obtained in the range 0.2 – 0 V suggesting the absence of fast-dissociating complexes. However, by the end of the experiment and in both the absence and presence of the hydrothermal fluids, a wave at ~ +0.15 V is clearly detected. Such a wave is close to the inorganic wave obtained in UV digested sample and is indicative of the presence of labile Cu complexes, i.e. weak complexes that dissociate within the time required to travel through the diffusion layer.

The Cu fraction detected by voltammetry was variable with minicosm experimental time, both in the control (V1: from ~40% (12 h) to ~25% (day 9) (Figure 4.4B); V2: from ~20% (24 h) to ~40% (day 8) (Figure 4.7B)). In the sample with 14.5% hydrothermal fluid (V1: from ~40% (12 h) to ~140% (day 9) (Figure 4.4D); V2: from ~50% (24 h) to ~80% (day 8) (Figure 4.7D)).

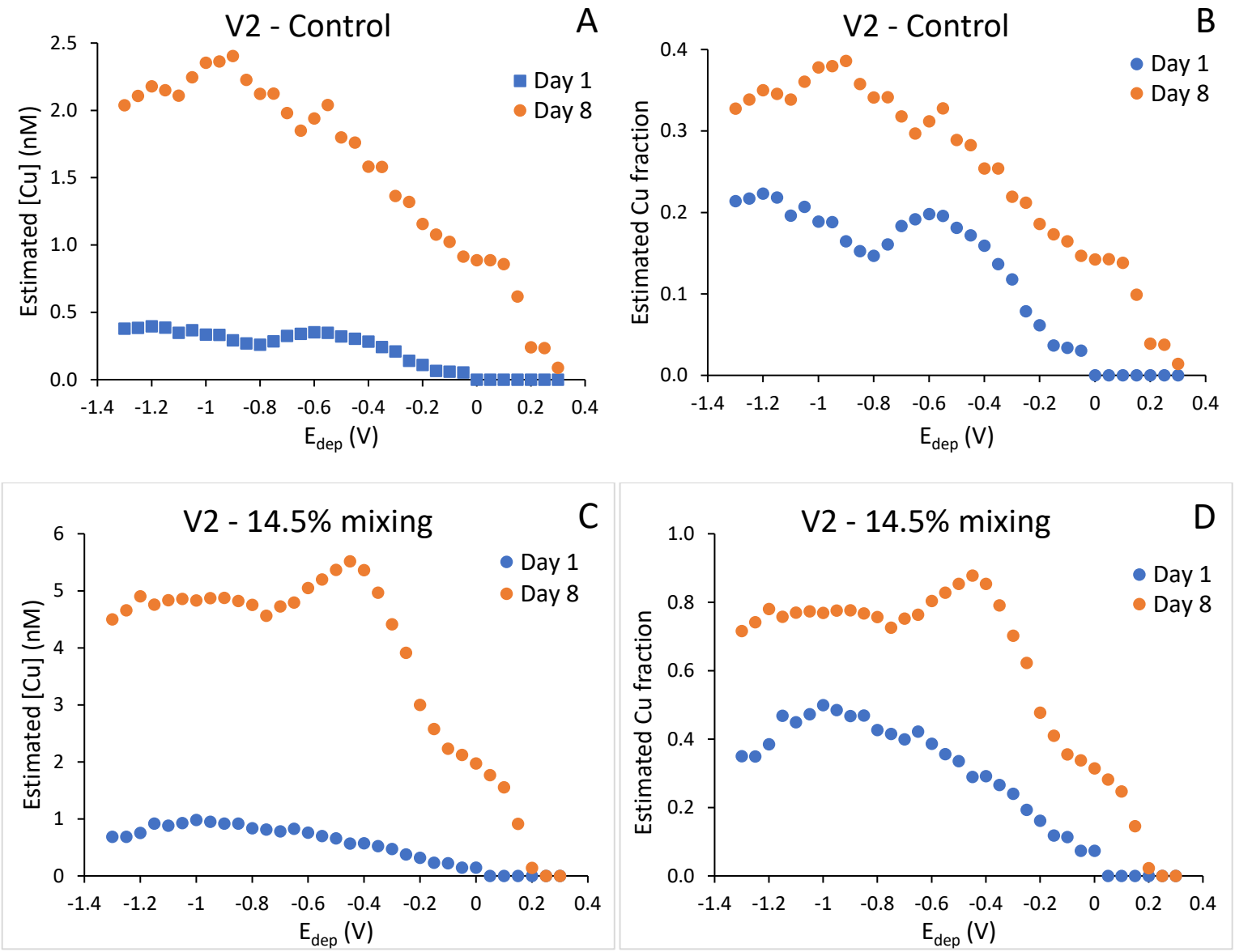

Figure 4.7. *Estimated dCu concentrations in the V2 minicosm experiments in control (A) and in 14.5% mixing (C) experiments. At -1 V, Cu-complexes are reduced providing an estimation of the dCu concentrations. dCu concentrations are presented in nM. Estimated dCu fraction in V2 minicosm experiments in control (B) and in 14.5% mixing (D) experiments. Estimated Cu fraction is the difference between the total dCu and the maximum reduced dCu during pseudopolarography. dCu that could not be reduced during pseudopolarography, is classed as inert.*

4.3.3. eHS pseudopolarograms

For eHS pseudopolarograms, the peak height has been normalised to the highest peak value for comparative purposes. In both experiments, pseudopolarography was carried out on the control and highest fluid-enriched sample (14.5%). For V1, samples were used from day 0.5 and the final day (day

9) (Figure 4.8A and 4.9B). For V2, samples were used from day 1 and the final day (day 8) (Figure 4.8C and 4.9D). In all samples the maximum sensitivity was at E_{dep} -0.45 V.

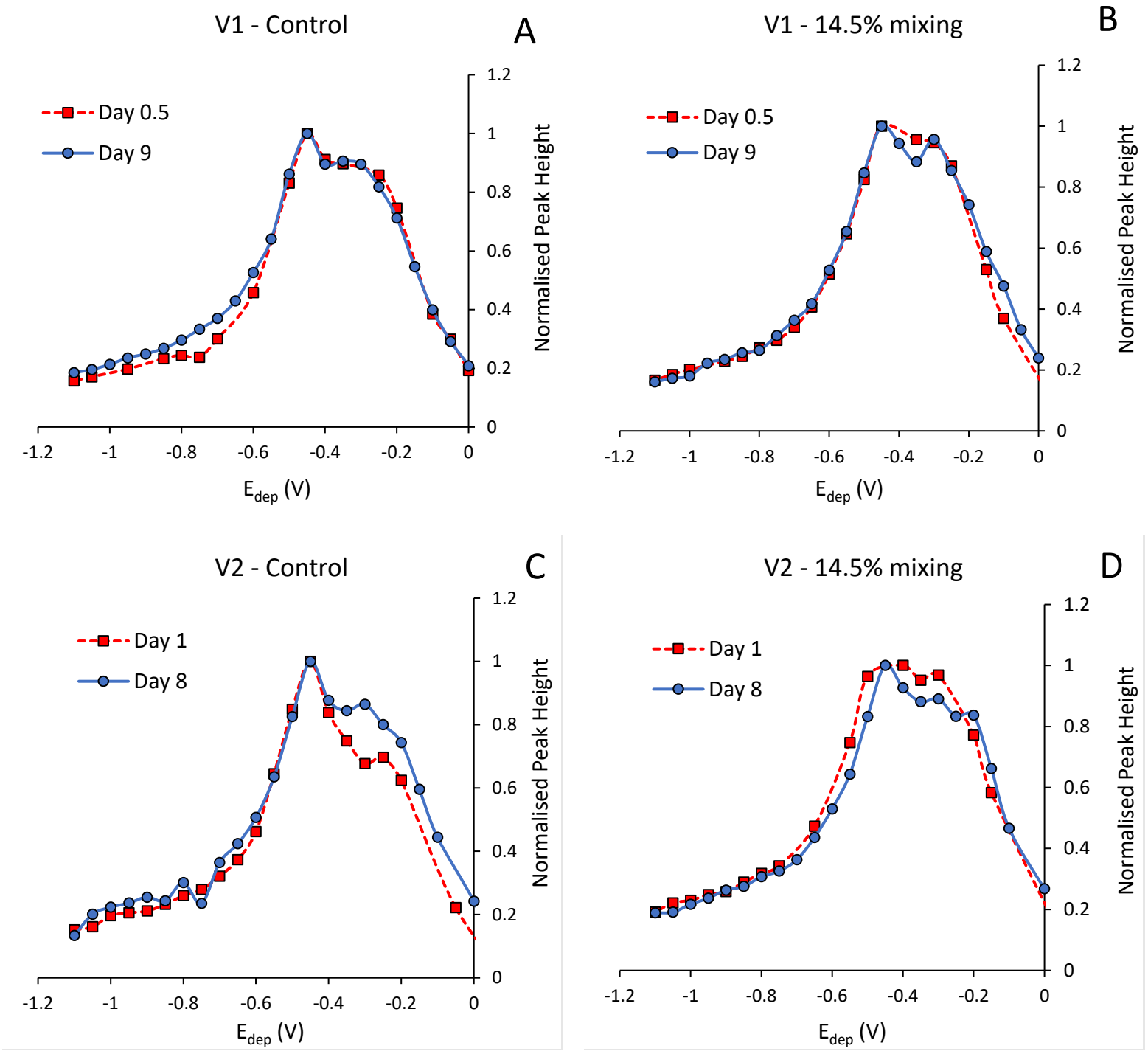

Figure 4.8. *Pseudopolarograms of electroactive humic substances (eHS) in the control sample (A and C) and the highest fluid enriched sample (14.5%) (B and D) from both minicosm experiments. Measurements were carried out using the method developed by Pernet-Coudrier et al. (2013) with an adsorption time of 150 s. Each point represents the peak height of the eHS signal. Peak height has been normalised to the highest peak value (=peak height/largest peak height). Voltammetric analysis was carried out at pH 2.*

4.4. Discussion

The objective of the minicosms experiments was to understand the impact of shallow hydrothermal fluids on surface communities. Figure 4S3 to 4S4 shows the dynamics of surface communities with the addition of hydrothermal fluid from V1 and V2. Hydrothermal fluids were rich in trace metals and nitrate. The combination of these factors meant that in most samples, the addition of hydrothermal fluids increased the growth of surface communities compared to the control.

4.4.1. Release of Thioacetamide-like compounds.

In the V1 fluid-enriched samples, an increase of TA-like compounds was observed 12 h after the initial mixing. This increase was not seen in the V1 control, indicating that the mixing of the hydrothermal fluids is the driver for the production of these compounds, and it is likely of biological origin. Tillette et al., 2022 suggested that RSS, including TA-like compounds were produced by *Synechococcus* ecotypes in order to detoxify the environment. Phytoplankton have been shown to produce RSS to complex with trace metals when in high metal environments (Courbot et al., 2004; Dupont and Ahner, 2005; Navarrete et al., 2019; Steffens, 1990; Vasconcelos and Leal, 2001). Here, the addition of hydrothermal fluids might have increased the concentrations of some metals (Tilliette et al., 2023), potentially triggering the production and release of TA-like compounds. The hydrothermal fluids in V1 had higher concentrations of dFe and dMn than V2, but had lower concentrations of dNi, dCu, dZn and dPb (Table 4S1). Even though there are lower concentrations of potentially toxic trace metals such as dCu in V1 compared to V2, toxicity depends on trace metal speciation. Low concentrations of Cu(II) have been shown to be toxic to some marine microbes (Brand et al., 1986). At the time of the experiment, hydrothermal fluids from PANAMAX (V1) had a lower pH than SIMONE (V2) (Figure 4S2). Lower pH is associated with higher concentrations of Cu(II) (Lewis et al., 2016; Richards et al., 2011), this could explain why we see an increase in TA-like compounds within the first 12 h, for V1 but not V2.

In the V2 experiment, all samples follow a similar trend. The TA-like compounds decrease within the first day and then steadily increase with time. Phytoplankton have been found to actively exude a TA-like compound (Leal et al., 1999). TA is toxic to microorganisms causing inhibition of growth (Vasconcelos et al., 2002). Understanding the identity of these RSS are discussed in Chapter 3, section 3.4.3.

4.4.2. Similarities between the behaviour of TA-like compounds and DFe

For V1, the [TA-like] and the [dFe] follow a similar pattern (Figure 4.9). RSS are not known to be a Fe ligand; however, the identification of the TA-like compounds remains unknown. When measuring RSS with voltammetry, the sulphur group in the RSS compound adsorbs on the HMDE (Laglera and van den Berg, 2003; Turner et al., 1975). Therefore, other compounds that contain a sulphur group can produce a similar signal. With the Pernet-Coudrier method, sulphide and thioacetic acid were shown to produce a signal in the same position as TA (Pernet-Coudrier et al., 2013). Sulphides are known to be a ligand for dFe (Dyrssen, 1988; Luther et al., 2001; Theberge et al., 1997; Yücel et al., 2011), but due to the purging and the acidic conditions, the sulphide can be removed from the sample. If sulphide is present in a sample it can produce a large peak in the 1s background (Figure 3.S3. (Chapter 3)), and in the analytical scan the peak is not stable. In this study, the peak for TA-like compounds was stable, indicating that sulphide was not a major contributor to the TA peak when this sample was analysed.

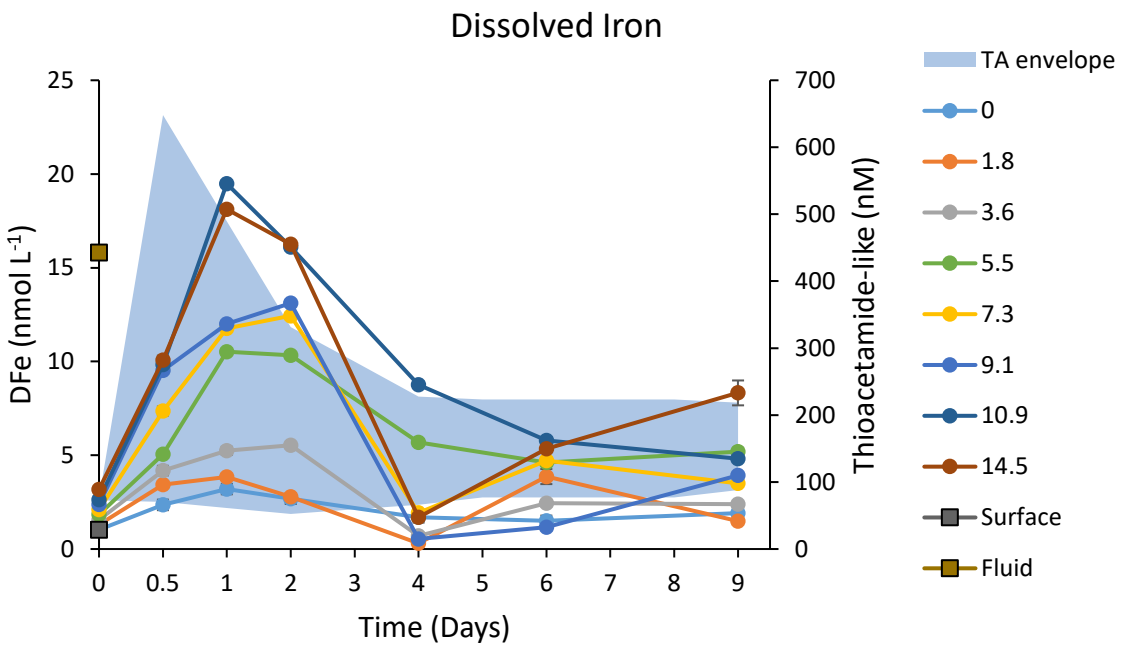

Figure 4.9. *Temporal dynamics of dissolved iron (dFe) during the V1 minicosm experiment (duration 9 days). Numbers in legend represent the % of hydrothermal fluid enrichment. Hydrothermal fluids were collected from PANAMAX. dFe concentrations were measured in the surface (grey square) and fluid (orange square) end members. An envelope (blue) for TA-like compounds, encompassing the maximum and minimum concentration obtained in this study. Error bars represent the standard deviation of the intercept obtained for each individual standard addition.*

The concentrations of dissolved iron (blue line) and iron-binding ligands (green circles, where available), with an envelope (red) for electroactive humic substances (eHS), encompassing the maximum and minimum iron-binding capacities reported for terrestrial IHSS standards13,27. (a) Station P26 in the Northeast Pacific (Line P); (b) Surface samples (~5 m) Northwest Atlantic (Bermuda AE1714), with salinity included below; (c–g) Stations G1-G77 depth profiles from the North Atlantic (GEOVIDE GA01). Error bars show standard deviation, which for eHS is included within the envelope. Spaces in the eHS boundaries show eHS sampling points. Figure generated using Matlab software.

4.4.3. Glutathione-like compounds

In both experiments, GSH-like compounds were not present for a few days after the initial mixing, but [GSH-like] increased with time. Comparing the [GSH-like] on the final day of both experiments, V1

showed a higher production of GSH-like compounds compared to V2 (Figure 4.10), although both V1 and V2 present relatively high concentrations on the final day, at around 7-8 nM.

GSH is one of the most abundant RSS both intracellularly and in marine waters (Ahner et al., 2002; Dupont et al., 2004; Giovanelli, 1987). It has multiple key roles in the marine cycle, therefore there are several variables that control the production of GSH. Within phytoplankton, GSH protects chloroplasts against reactive oxygen species (ROS) by acting as an antioxidant (Fahey et al., 1987; Matrai and Vetter, 1988). GSH can also be produced to either act as a detoxifying agent against potentially toxic trace metals (Dupont and Ahner, 2005; Kawakami et al., 2006; Navarrete et al., 2019) or to help with trace metal uptake. *Prorocentrum donghaiense* Lu release GSH in low Ni environments to help with uptake (Huang et al., 2018). Strongly bound dCu is not bioavailable (Moriyasu and Moffett, 2022), therefore phytoplankton can produce GSH to act as a 'weak ligand shuttle'. GSH is able to form weaker complexes with Cu which can then be bioavailable (Semeniuk et al., 2015).

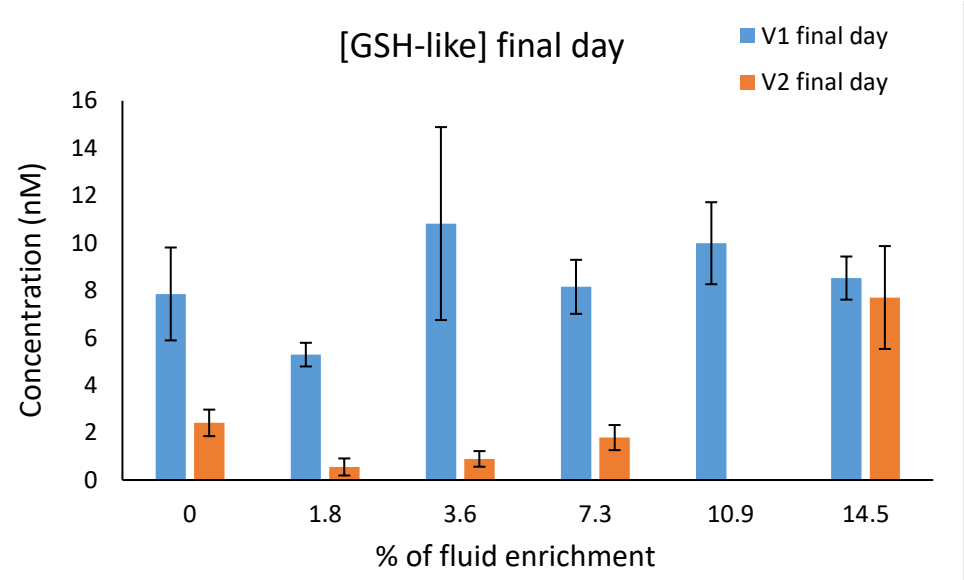

Figure 4.10. *Comparison of the production of GSH-like compounds in the V1 and V2 experiments. The production of GSH-like compounds was calculated by the increase of GSH-like compounds from the first to the final day. Error bars represent the standard deviation of the intercept obtained for each individual standard addition.*

4.4.4. GSH-like compounds response to trace metals

Previous incubation studies have found that the liberation of GSH is likely as a detoxifying agent against metal toxicity as it can help microbes control trace metal uptake, in particular exposure to Cu and Cd (Ahner et al., 2002; Vasconcelos and Leal, 2001). In both experiments, dCu was low in surface waters (ICP-MS: V1 = 2.02 nmol L^{-1}; V2 = 2.85 nmol L^{-1}), and hydrothermal fluid (ICP-MS: V1 = 0.84 nmol L^{-1}; V2 = 2.04 nmol L^{-1}), but the concentration increased with time in all experiments (Table 4.3). On the final day, the concentration of dCu was significantly higher than at the start, both for V1 and V2. In the hydrothermal fluids, there were high concentrations of particulate Cu (pCu; V1 = 494 pmol L^{-1}, V2 = 20.4 pmol L^{-1}) (Planquette et al., 2023). The increase of dCu over time could partially be due the remineralisation from particulate Cu (Richon and Tagliabue, 2019), but the increase of dCu was higher than the total pCu. This suggests contamination from the minicosm tanks and increase concentration of dCu overtime could be due to leaching.

There was no dCd data, however in the hydrothermal fluid, there were elevated concentrations of pCd (V1 = 4.84 pmol L^{-1}, V2 = 0.23 pmol L^{-1}), compared to the surface waters (V1 = 0.42 pmol L^{-1}, V2 = n.a pmol L^{-1}) (Planquette et al., 2023). Remineralisation from particulate Cd could cause an increase in dCd which could led to an increase in GSH over time. As GSH, production is dependent on the exposure of marine microbes to dCu and dCd (Dupont and Ahner, 2005; Leal et al., 1999) this could be a potential reason for why the production of GSH-like is higher in V1 than in V2.

4.4.5. Release of GSH-like compounds from biological breakdown

The increase in [GSH-like] could also be due to the degradation of Cyanobacteria. In the V1 experiment, *Prochlorococcus* and *Synechococcus*, increase in abundance at the beginning of the experiment and then decrease (Figure 4S3). In the V2 experiment, *Prochlorococcus* slowly decreases over time and *Synechococcus* either increases slightly or remains fairly constant. Over the experiment, [dCu] increases, which can increase the amount of bioavailable and toxic Cu(II). Cu is able to accept or

donate electrons as it changes oxidation state which can promote the formation of ROS in cells (Gaetke et al., 2014; Halliwell and Gutteridget, 1984). Large amounts of ROS are able to induce oxidative stress in cells, which can damage lipids, proteins and nucleic acids leading to membrane destruction, protein dysfunction, and DNA destruction (Ercal et al., 2002; Mann et al., 2002). These processes can lead to impaired cell growth and or cell death (T.M.Florence and J.L.Stauber, 1986; Zhivotovsky, 2012). Cyanobacteria in particular are extremely sensitive to [dCu] (Brand et al., 1986). The breakdown of these microbes could release the intracellular GSH-like compounds into the marine environment. As V1 had the largest decrease in cyanobacteria it could also contribute the higher [GSH-like] in V1. It is likely that a combination of these processes caused the increase of GSH-like compounds.

4.4.6. Production of electroactive humic substances

The degradation and production of eHS are similar in both experiments. Within the first 24 – 48 h, there was a decrease in [eHS], after which the concentration continuously increased until the end of the experiment. This decrease cannot be explained solely on the grounds of dilution with hydrothermal fluids that contain lower eHS levels than surface waters. The decrease in the first few days could be due to the consumption of eHS by heterotrophic bacteria, archaea, and photoautotroph species (Donderski and Burkowska, 2000; Dulaquais et al., 2018). The decrease could also be due to the removal of eHS through sorption onto particles (Kell et al., 1994; Longhini et al., 2021). Hydrothermal vents in the TONGA arc are a major source of particulates compared to other areas in the southwest tropical Pacific (Kim et al., 2016), which is likely why we see a decrease of [eHS] upon the mixing of hydrothermal fluids (Figure 4.3 and 4.7).

eHS are produced through a number of different processes. In surface waters, microbial production is a source of eHS. This can be through microbial remineralisation, decay and photooxidation of triglycerides and fatty acids (Ferrari et al., 1996; Kieber et al., 1997; Lorenzo et al., 2007; Whitby et al.,

2020). In both of the control samples, the concentration of eHS increased at similar rates, during the experiment (V1 = 60% (9 days); V2 = 57% (8days)) (Figure 4.11). This indicates that in the surface water, the overall production of eHS was similar in both samples, even though the water was taken from different locations. The addition of hydrothermal fluids to the surface water affected the production of eHS. In all the V1 fluid enriched samples (except for 14.5%), less eHS were produced compared to the control, suggesting the addition of the fluid slowed down eHS production. In contrast, for V2, the addition of the hydrothermal fluids increased the amount of eHS, compared to the control.

There were higher concentrations of particulate trace metals found in V1 compared to V2, which likely had an effect on biological production. The rate of growth proxied by Chl *a*, viruses, bacteria and picoeukarytoes was lower in V1 compared to V2 (Figure 4S4), suggesting that in V1 the addition of hydrothermal fluid inhibited the growth of these microorganisms, consequently limiting the production of eHS.

In all the V2 hydrothermal fluid enriched minicosms, except 7.3%, the [eHS] was higher than the control, indicating that the addition of the hydrothermal fluid promoted the production of eHS. In V2, the concentration of trace metals was lower than in V1. Some trace metals can be both a nutrient and a toxicant, depending on their concentration. There was an increase in growth from the surface communities with the addition of hydrothermal fluids. This could suggest that the trace metals in the hydrothermal fluids could have been a nutrient for these communities, promoting growth. The hydrothermal fluid in V2 was also high in nitrate.

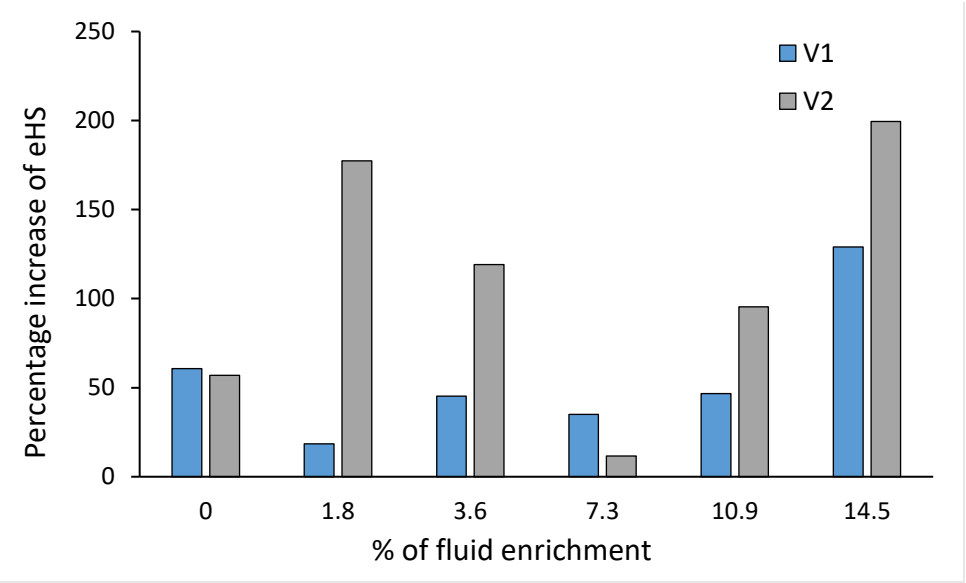

Figure 4.11. *Comparison of the percentage increase of eHS in the V1 and V2 experiments. The percentage increase of eHS was calculated by the increase of eHS from the first to the final day.*

4.4.7. Effect of hydrothermal fluids on eHS structure

Pseudopolarography is an empirical technique that can be used to provide an understanding of the nature/structure of the compound of interest supposing there were suitable standards to compare with. At this stage, the technique provides a fingerprint that is representative of the eHS present in the sample. For the quantification of eHS, terrestrial standards from the International Humic Substances Society are commonly used (Dulaquais et al., 2018; Laglera et al., 2019; Whitby et al., 2018). Comparing pseudopolarograms of eHS found in samples to the terrestrial standards is beneficial as it can show if the standard is representative of the compound of interest in the sample, therefore allowing for accurate quantification. For example, Figure 4S5 shows the pseudopolarograms of the eHS found in the Celtic sea. Comparing this to the pseudopolarograms of SRFA (2S101F) and SRHA (2S101H) (two commonly used standard for the quantification of eHS) shows that SRHA has a similar shape to the pseudopolarograms in the Celtic sea. Therefore, SRHA is the best standard to use for the analysis of this sample. In this experiment, eHS pseudopolarograms of the first and the final

day were conducted on the control sample and on the 14.5% hydrothermal enrichment sample in both V1 and V2 minicosms. This was done to assess if: 1- the nature of the eHS changed during the experiment and 2- if hydrothermal fluids had a direct or indirect impact on the nature of eHS.

Pseudopolarograms of eHS found in the samples appear to be more similar to SRFA than SRHA (Figure 4.12). Marine eHS have been reported to be more similar to SRFA as they are aliphatic, carboxylic acid rich and have few or no aromatic protons (Fourrier et al., 2022; Harvey et al., 1983; Williford et al., 2021). There are differences in the pseudopolarograms on the controls and the 14.5% hydrothermal enriched samples. The shape of the pseudopolarograms in the V1 control remains the same in day 0.5 and day 9, indicating that the same type of eHS is produced. For V2, the shape of the pseudopolarograms in the control changes slightly at Edep > -0.4 V between day 1 and day 8, possibly showing a change in the nature of eHS. This experiment was more biologically active than V1, with a higher growth rate shown by increases in Chl *a*, viruses, bacteria and picoeukarytoes, the higher abundance of microbes could affect the nature of eHS (figure 4S4).

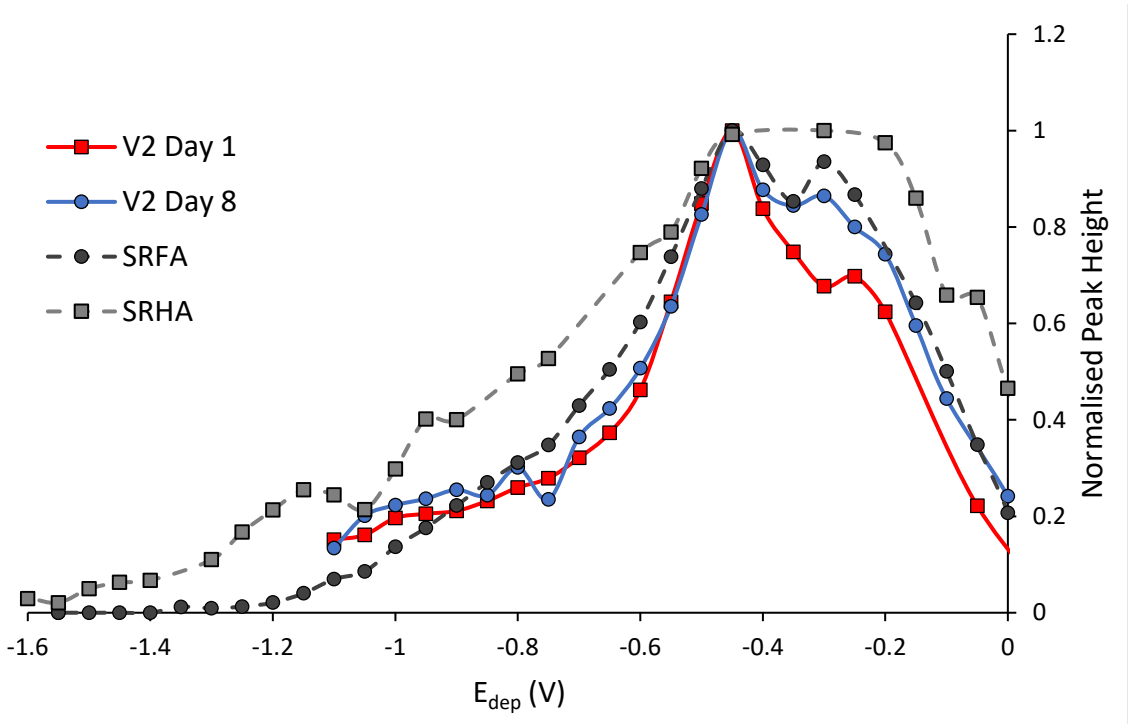

***Figure 4.12**. Comparison of pseudopolarograms of electroactive humic substances (eHS) found in the samples from V2 control samples (day 1 and 8) with Suwannee River fulvic acid (SRFA) and*

Suwannee River humic acid (SRHA) standards. Pseudopolarograms of 96 µg/L of SRFA and SRHA. Standards were added to UV digested seawater. Measurements were carried out using the method developed by Pernet-Coudrier et al. (2013) with an adsorption time of 150 s. Each point represents the peak height of the eHS signal. Peak height has been normalised to the highest peak value (=peak height/largest peak height). Voltammetric analysis was carried out at pH 2.

The addition of hydrothermal fluids in the minicosms changed the pseudopolarogram of the eHS (Figure 4.13). Autochthonous microbial communities around hydrothermal systems have been found to be a source of eHS (Sarma et al., 2018; Yang et al., 2012). Hydrothermal fluids were directly pumped into the minicosm tanks therefore meaning that these autochthonous microbial communities were probably added to the mix. The autochthonous microbial communities could be producing a different type of humic compared to the surface communities, leading to the change in the shape of the pseudopolarogram.

Hydrothermal fluids can exceed 400˚C (Foustoukos and Seyfried, 2007; Koschinsky et al., 2008), which can cause thermogenic modifications to the eHS. Hydrothermal vents also emit high levels of ROS. In high temperature conditions ROS can alter the composition of eHS (Shaw et al., 2021). Both of these process have been found to increase aromaticity and altering the amount of carboxylic groups (Dittmar and Paeng, 2009; Hawkes et al., 2016; Rossel et al., 2017, 2015). The shape of the pseudopolarograms in both the fluid enriched samples were similar between the start and the end of the experiment. The temperature was monitored throughout the experiment and they did not show significant changes compared to the control suggesting that in this experiment thermogenic modifications to eHS with the addition of hydrothermal fluid is unlikely.

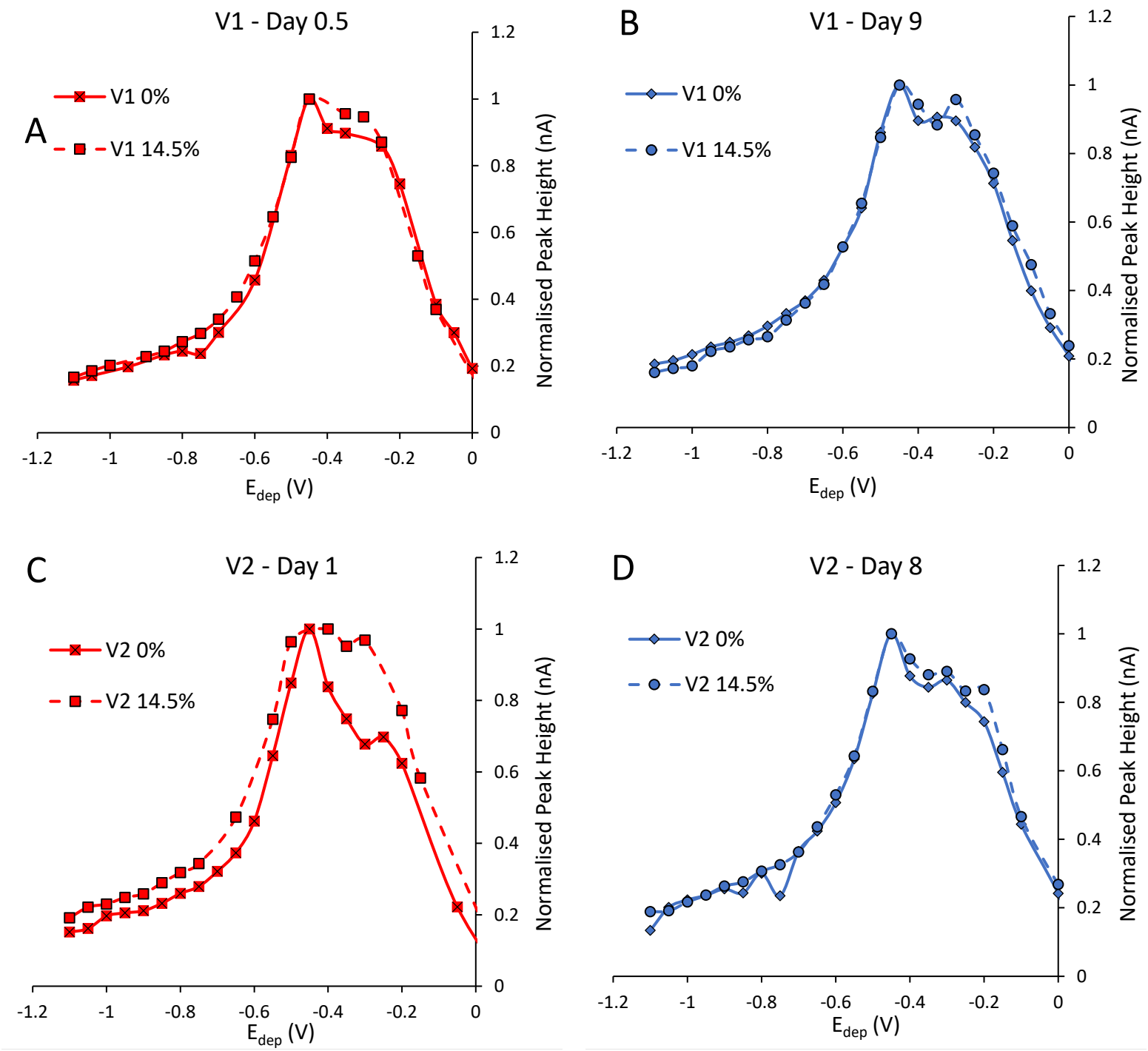

Figure 4.13. *Comparison of electroactive humic substances (eHS) pseudopolarograms from 0% and 14.5% mixing of the first (A and C) and final day (B and D) from both experiments. Pseudopolarograms obtained using the Mo-eHS method (Pernet-Coudrier et al., 2013) with an adsorption time of 150 s. Each point represents the peak height of the eHS signal. Peak height has been normalised to the highest peak value (= peak height/largest peak height).*

4.4.8. Change of Cu speciation

Both ICP-MS and voltammetry measurements show that total dCu concentrations significantly increase as a function of time in V1 and V2 minicosms experiments (Table 4.3). The increase is similar in both the control experiments and in the 14.5% mixing hydrothermal fluids which would suggest that most of the Cu was initially present in the surface water, in a particulate form. However, the Cu concentrations detected in particulate matter in surface waters are well below the nanomolar level (Planquette et al., 2023) which is far too low to explain the relatively high Cu concentrations measured at the end of the experiment (up to 10-12 nM). It is therefore likely that the origin of this Cu is from contamination from the tanks with a progressive leaching out explaining the continuous increase of Cu concentrations as a function of time. Nevertheless, the release of this copper can only be favored by the increase of Cu ligands detected here by voltammetry (eHS, GSH-like and TA-like compounds). A previous study has shown that Cu-SRFA and Cu-SRHA complexes are labile (Gibbon-Walsh et al., 2012) with a wave located at around 0.1 V, close to the inorganic wave. Interestingly, for V2, both in the presence and absence of hydrothermal fluids, there is no such labile wave at the start of the experiment when the Cu concentration is relatively low (~ 1.8 – 2.0 nM, Table 4.3) but it is clearly present at the end of the experiment (Figure 4.7) when dCu has increased significantly (~ 6.3 nM). The magnitude of this labile wave is estimated at 0.9 and 2.0 nM for the control and the 14.5% mixing respectively which is in broad agreement with eHS concentrations that were determined as ~ 92 μg SRFA eq. L^{-1} and 149 μg SRFA eq. L^{-1} respectively. For V1, a labile wave is always observed, slightly more noticeable at the end of the experiment but not as well defined as for V2, representing a maximum of 0.6 nM Cu.

The Cu-GSH complex is stronger than Cu-humics and displays a pseudopolarographic wave at approximately -0.92 V on the gold electrode (Gibbon-Walsh, 2012). GSH-like compounds were detected here both in V1 and V2 but at significantly higher levels in V1 experiment. Here, Cu

pseudopolarograms do not display a wave at -0.92 V. In the V1 experiment, the peak intensity decreases at E_{dep} below ~-0.9 V, highlighting the presence of interfering compounds, possibly another metal that would deposit on the gold electrode at these low deposition potentials. In the V2 experiment, the signal remains fairly constant in this range of deposition potentials but there is no Cu wave at the position expected for Cu-GSH complex, suggesting that such a complex is not present.

All but one pseudopolarogram suggests the presence of a voltammetrically inert fraction that ranges from ~ 10% to 80% with an average of almost 60% of dCu. This fraction cannot be reduced at the lowest deposition potential used here (-1.3 V). However, the uncertainties related to the determination of the sensitivity (detailed above in section 4.2.5.3.4.) might also be quite large but are currently unknown. For instance, a labile fraction of almost 140% of the total was determined in V1 14.5% mixing at day 0.5 suggesting that the sensitivity determined in the composite sample might not be suited. The values given in Table 4.3 are thus best estimate.

	Voltammetry (ICP-MS) nM	Labile wave nM	Inert fraction nM (%)
V1 – Control – Day 0.5	2.40 ± 0.05 (2.9)	0.25	1.56 (65%)
V1 – Control – Day 9	7.13 ± 0.11 (10.0)	0.6	5.34 (75%)
V1 – 14.5% mixing – Day 0.5	1.36 ± 0.05 (0.6)	?	?
V1 – 14.5% mixing – Day 9	9.22 ± 0.31 (12.0)	0.5	7.2 (60%)
V2 – Control – Day 1	1.77 ± 0.13 (2.7)	< 0.05	1.4 (~80%)
V2 – Control – Day 8	6.23 ± 0.14 (4.9)	0.9	3.7 (~60%)
V2 – 14.5% mixing – Day 1	1.96 ± 0.08 (2.9)	< 0.05	0.9 (~55%)
V2 – 14.5% mixing – Day 8	6.28 ± 0.28 (6.1)	2	0.7 (12%)
V1 surface water	n.d. (2.0)	n.a.	n.a.
V1 hydrothermal fluid	n.d. (0.8)	n.a.	n.a.
V2 surface water	n.d.	n.a.	n.a.
V2 hydrothermal fluid	n.d.	n.a.	n.a.

Table 4.3. *Dissolved Cu concentrations obtained by voltammetry and ICP-MS. Cu concentrations are presented in nM. The labile wave is the estimated concentration of dCu that was reducible before the Cu -0.2V (inorganic Cu peak). The inert fraction was estimated by the difference between the total dCu and the maximum reduced dCu during pseudopolarography. The inert fraction was the faction of dCu that could not be reduced —concentration presented in nM and % of the total Cu.*

4.5. Conclusion

The WTSP is a highly complex environment with high nitrogen fixation rates and shallow hydrothermal vents directly pumping hydrothermally-influenced water into the phototrophic layer. These factors can affect the biology in this environment, affecting the production of organic ligands. This study highlights the complexity of understanding the biological production of organic ligands. Here, we present evidence for the biological production of TA-like, GSH-like compounds and eHS in response to hydrothermal fluids. Experiment consisted of two minicosm experiments using mixes of hydrothermal fluid from two hydrothermal vents systems, PANAMAX (V1) and SIMONE (V2). V1 had high concentrations of trace metals in the hydrothermal fluids, whereas V2 was less concentrated. In V1, the addition of these fluids to the surface waters prompted high production of TA-like compounds 12 hours after the initial mixing, indicating a biological response to high levels of toxic trace metals to detoxify the environment. V2 also showed active production of TA-like compounds. GSH-like compounds were not present immediately but were produced over time in both experiments, with more were created in V1 than in V2. GSH-like compounds were likely produced as a response to trace metal detoxification, trace metal uptake or biological breakdown. eHS in both studies follow a similar pattern with an initial decrease in concentration and then increase with time.

This study also employed pseudopolarography to see how the addition of hydrothermal fluids affected the nature of the eHS. Such methods can produce semi-qualitative results about the compounds. The exact nature of these compounds is still unknown.

4.6. References

Abualhaija, M. M., Whitby, H., & van den Berg, C. M. G. (2015). Competition between copper and iron for humic ligands in estuarine waters. Marine Chemistry, 172, 46–56. https://doi.org/10.1016/j.marchem.2015.03.010

Ahner, B.A., Wei, L., Oleson, J.R., Ogura, N., 2002. Glutathione and other low molecular weight thiols in marine phytoplankton under metal stress. Mar. Ecol. Prog. Ser. 232, 93–103.

https://doi.org/10.3354/meps232093

Brand, L.E., Sunda, W.G., Guillard, R.R.L., 1986. Reduction of marine phytoplankton reproduction rates by copper and cadmium. J. Exp. Mar. Bio. Ecol. 96, 225–250. https://doi.org/10.1016/0022-0981(86)90205-4

Courbot, M., Diez, L., Ruotolo, R., Chalot, M., Leroy, P., 2004. Cadmium-responsive thiols in the ectomycorrhizal fungus Paxillus involutus. Appl. Environ. Microbiol. 70, 7413–7417. https://doi.org/10.1128/AEM.70.12.7413-7417.2004

Cutter, G.A., Casciotti, K., Croot, P.L., Geibert, W., Heimbürger, L.-E., Lohan, M., Planquette, H., van de Flierdt, T., 2017. Sampling and Sample-handling Protocols for GEOTRACES Cruises. Version 3, August 2017. Toulouse, France, GEOTRACES International Project Office, 139pp. & Appendices. DOI: http://dx.doi.org/10.25607/OBP-2

Dittmar, T., Paeng, J., 2009. A heat-induced molecular signature in marine dissolved organic matter. Nat. Geosci. 2, 175–179. https://doi.org/10.1038/ngeo440

Donderski, W., Burkowska, A., 2000. Metabolic Activity of Heterotrophic Bacteria in the Presence of Humic Substances and Their Fractions. Polish J. Environ. Stud. 9, 267–271.

Dulaquais, G., Waeles, M., Gerringa, L.J.A., Middag, R., Rijkenberg, M.J.A., Riso, R., 2018. The Biogeochemistry of Electroactive Humic Substances and Its Connection to Iron Chemistry in the North East Atlantic and the Western Mediterranean Sea. J. Geophys. Res. Ocean. 123, 5481–5499. https://doi.org/10.1029/2018JC014211

Dupont, C.L., Ahner, B.A., 2005. Effects of copper, cadmium, and zinc on the production and exudation of thiols by Emiliania huxleyi. Limnol. Oceanogr. 50, 508–515. https://doi.org/10.4319/lo.2005.50.2.0508

Dupont, C.L., Nelson, R.K., Bashir, S., Moffett, J.W., Ahner, B.A., 2004. Novel copper-binding and nitrogen-rich thiols produced and exuded by Emiliania huxleyi. Limnol. Oceanogr. 49, 1754–1762. https://doi.org/10.4319/lo.2004.49.5.1754

Dyrssen, D., 1988. Sulfide complexation in surface seawater. Mar. Chem. 24, 143–153. https://doi.org/10.1016/0304-4203(88)90045-X

Ercal, N., Gurer-Orhan, H., Aykin-Burns, N., 2002. Toxic Metals and Oxidative Stress Part I: Mechanisms Involved in Metal induced Oxidative Damage. Curr. Top. Med. Chem. 1, 529-39. https://doi.org/10.2174/1568026013394831

Fahey, R.C., Buschbacher, R.M., Newton, G.L., 1987. The evolution of glutathione metabolism in phototrophic microorganisms. J. Mol. Evol. 25, 81–88. https://doi.org/10.1007/BF02100044

Ferrari, G.M., Dowell, M.D., Grossi, S., Targa, C., 1996. Relationship between the optical properties of chromophoric dissolved organic matter and total concentration of dissolved organic carbon in the southern Baltic Sea region. Mar. Chem. 55, 299–316. https://doi.org/10.1016/S0304-4203(96)00061-8

Florence, T.M., Stauber, J.L., 1986. Toxicity of copper complexes to the marine diatom Nitzschia closterium. Aquat. Toxicol. 8, 11–26. https://doi.org/10.1016/0166-445X(86)90069-X

Fourrier, P., Dulaquais, G., Guigue, C., Giamarchi, P., Sarthou, G., Whitby, H., Riso, R., 2022. Characterization of the vertical size distribution, composition and chemical properties of dissolved organic matter in the (ultra)oligotrophic Pacific Ocean through a multi-detection approach. Mar. Chem. 240, 104068. https://doi.org/10.1016/j.marchem.2021.104068

Foustoukos, D.I., Seyfried, W.E., 2007. Fluid Phase Separation Processes in Submarine Hydrothermal

Systems. Rev. Mineral. Geochemistry 65, 213–239. https://doi.org/10.2138/rmg.2007.65.7

Gaetke, L.M., Chow-Johnson, H.S., Chow, C.K., 2014. Copper: toxicological relevance and mechanisms. Arch. Toxicol. 88, 1929–1938. https://doi.org/10.1007/s00204-014-1355-y

Gibbon-Walsh, K., Salaün, P., van den Berg, C.M.G., 2012. Pseudopolarography of copper complexes in seawater using a vibrating gold microwire electrode. J. Phys. Chem. A 116, 6609–6620. https://doi.org/10.1021/jp3019155

Giovanelli, J., 1987. Sulfur Amino Acids of Plants: An Overview. Methods Enzymol. 143, 419–426. https://doi.org/10.1016/0076-6879(87)43073-5

Guieu, C., Bonnet, S., 2019. TONGA 2019 cruise, R/V L'Atalante [WWW Document]. https://doi.org/https://doi.org/10.17600/18000884

Guieu, C., Bonnet, S., Petrenko, A., Menkes, C., Chavagnac, V., Desboeufs, K., Maes, C., Moutin, T., 2018. Iron from a submarine source impacts the productive layer of the Western Tropical South Pacific (WTSP). Nat. Sci. Reports 1–9. https://doi.org/10.1038/s41598-018-27407-z

Halliwell, B., Gutteridget, J.M.C., 1984. Oxygen toxicity, oxygen radicals, transition metals and disease Barry 219, 1–14. https://doi.org/10.1042/bj2190001

Harris, D.C., 2003. Quantitative Chemical Analysis, W. H. Freeman. New York. https://doi.org/10.1016/B978-0-444-40826-6.50009-1

Harvey, G. r., Tokar, J. m., Boran, D., Chesal, L.A., 1983. The structure of marine fulvic and humic acids. Mar. Biol. 12, 119–132. https://doi.org/10.1016/0304-4203(83)90075-0

Hawkes, J.A., Hansen, C.T., Goldhammer, T., Bach, W., Dittmar, T., 2016. Molecular alteration of marine dissolved organic matter under experimental hydrothermal conditions. Geochim. Cosmochim. Acta 175, 68–85. https://doi.org/10.1016/j.gca.2015.11.025

Huang, X.G., Li, S. xing, Liu, F.J., Lan, W.R., 2018. Regulated effects of Prorocentrum donghaiense Lu exudate on nickel bioavailability when cultured with different nitrogen sources. Chemosphere 197, 57–64. https://doi.org/10.1016/j.chemosphere.2018.01.014

Kawakami, S.K., Gledhill, M., Eric, P., 2006. Production of phytochelatins and glutathione by marine phytoplankton in response to metal stress 989, 975–989. https://doi.org/10.1111/j.1529-8817.2006.00265.x

Kell, R.G., Montlucon, D.B., Prahlt, F.G., Hedges, J.I., 1994. Sorptive preservation of labile organic maHer in marine sediments. Nature 370, 549–552. https://doi.org/10.1042/bj2190001

Kieber, R.J., Hydro, L.H., Seaton, P.J., 1997. Photooxidation of triglycerides and fatty acids in seawater: Implication toward the formation of marine humic substances. Limnol. Oceanogr. 42, 1454–1462. https://doi.org/10.4319/lo.1997.42.6.1454

Kim, H.J., Kim, J., Pak, S.J., Ju, S.-J., Yoo, C.M., Kim, H.S., Lee, K.Y., Hwang, J., 2016. Geochemical characteristics of sinking particles in the Tonga arc hydrothermal vent field , southwestern Paci fic. Deep. Res. Part I Oceanogr. Res. Pap. 116, 118–126. https://doi.org/10.1016/j.dsr.2016.07.015

Koschinsky, A., Garbe-Schönberg, D., Sander, S., Schmidt, K., Gennerich, H.H., Strauss, H., 2008. Hydrothermal venting at pressure-temperature conditions above the critical point of seawater, 5°S on the Mid-Atlantic Ridge. Geology 36, 615–618. https://doi.org/10.1130/G24726A.1

Laglera, L.M., Battaglia, G., van den Berg, C.M.G., 2007. Determination of humic substances in natural waters by cathodic stripping voltammetry of their complexes with iron. Anal. Chim. Acta. 599,

58–66. https://doi.org/10.1016/j.aca.2007.07.059

Laglera, L.M., Sukekava, C., Slagter, H.A., Downes, J., Aparicio-Gonzalez, A., Gerringa, L.J.A., 2019. First Quantification of the Controlling Role of Humic Substances in the Transport of Iron across the Surface of the Arctic Ocean. Environ. Sci. Technol. https://doi.org/10.1021/acs.est.9b04240

Laglera, L.M., Downes, J., Tovar-Sánchez, A., Monticelli, D., 2014. Cathodic pseudopolarography: A new tool for the identification and quantification of cysteine, cystine and other low molecular weight thiols in seawater. Anal. Chim. Acta. 839, 24-33. https://doi.org/ 10.1016/j.aca.2014.05.026

Laglera, L.M., van den Berg, C.M.G., 2003. Copper complexation by thiol compounds in estuarine waters. Mar. Chem. 82, 71–89. https://doi.org/10.1016/S0304-4203(03)00053-7

Leal, M.F.C., Vasconcelos, M.T.S.D., van den Berg, C.M.G., 1999. Copper-induced release of complexing ligands similar to thiols by Emiliania huxleyi in seawater cultures. Limnol. Oceanogr. 44, 1750–1762. https://doi.org/10.4319/lo.1999.44.7.1750

Lewis, C., Ellis, R.P., Vernon, E., Elliot, K., Newbatt, S., Wilson, R.W., 2016. Ocean acidification increases copper toxicity differentially in two key marine invertebrates with distinct acid-base responses. Sci. Rep. 6, 1–10. https://doi.org/10.1038/srep21554

Longhini, C.M., Mahieu, L., Fabian, S., van den Berg, C.M.G., Salaün, P., Neto, R.R., 2021. Coastal waters contamination by mining tailings: What triggers the stability of iron in the dissolved and soluble fractions? Limnol. Oceanogr. 66, 171–187. https://doi.org/10.1002/lno.11595

Lorenzo, J.I., Nieto-Cid, M., Álvarez-Salgado, X.A., Pérez, P., Beiras, R., 2007. Contrasting complexing capacity of dissolved organic matter produced during the onset, development and decay of a simulated bloom of the marine diatom Skeletonema costatum. Mar. Chem. 103, 61–75. https://doi.org/10.1016/j.marchem.2006.05.009

Luther, G.W., Rozan, T.F., Taillefert, M., Nuzzio B., D., Meo Di, C., Shank M., T., Lutz A., R., Cary Craig, S., 2001. Chemical speciation drives hydrothermal vent ecology. Nature 410, 813–816. https://doi.org/10.1038/35071069

Mann, E.L., Ahlgren, N., Moffett, J.W., Chisholm, S.W., 2002. Copper toxicity and cyanobacteria ecology in the Sargasso Sea. Limnol. Oceanogr. 47, 976–988. https://doi.org/10.4319/lo.2002.47.4.0976

Matrai, P.A., Vetter, R.D., 1988. Particulate thiols in coastal waters: The effect of light and nutrients on their planktonic production. Limnol. Oceanogr. 33, 624–631. https://doi.org/10.4319/lo.1988.33.4.0624

Moriyasu, R., Moffett, J.W., 2022. Determination of inert and labile copper on GEOTRACES samples using a novel solvent extraction method. Mar. Chem. 239, 104073. https://doi.org/10.1016/j.marchem.2021.104073

Navarrete, A., González, A., Gómez, M., Contreras, R.A., Díaz, P., Lobos, G., Brown, M.T., Sáez, ~, Moenne, A., 2019. Copper excess detoxification is mediated by a coordinated and complementary induction of glutathione, phytochelatins and metallothioneins in the green seaweed Ulva compressa. Plant Physiol. Biochem. 135, 423–431. https://doi.org/10.1016/J.PLAPHY.2018.11.019

Omanović, D., Branica, M., 1998. Automation of Voltammetric Measurements by Polarographic Analyser PAR 384B. Croat. Chem. Acta 71, 421–433.

Pernet-Coudrier, B., Waeles, M., Filella, M., Quentel, F., Riso, R.D., 2013. Simple and simultaneous

determination of glutathione, thioacetamide and refractory organic matter in natural waters by DP-CSV. Sci. Total Environ. 463–464, 997–1005. https://doi.org/10.1016/j.scitotenv.2013.06.053

Planquette, H., Gonzalez Santana, D., Sarthou, G., 2023. Particulate trace metals in the vicinity of shallow hydrothermal sources through the Tonga-Kermadec arc (GEOTRACES GPpr14). Front. Mar. Sci. (in prep).

Richards, R., Chaloupka, M., Sanò, M., Tomlinson, R., 2011. Modelling the effects of "coastal" acidification on copper speciation. Ecol. Modell. 222, 3559–3567. https://doi.org/10.1016/j.ecolmodel.2011.08.017

Richon, C., Tagliabue, A., 2019. Insights Into the Major Processes Driving the Global Distribution of Copper in the Ocean From a Global Model. Global Biogeochem. Cycles 33, 1594–1610. https://doi.org/10.1029/2019GB006280

Rossel, P.E., Stubbins, A., Hach, P.F., Dittmar, T., 2015. Bioavailability and molecular composition of dissolved organic matter from a diffuse hydrothermal system. Mar. Chem. 177, 257–266. https://doi.org/10.1016/j.marchem.2015.07.002

Rossel, P.E., Stubbins, A., Rebling, T., Koschinsky, A., Hawkes, J.A., Dittmar, T., 2017. Thermally altered marine dissolved organic matter in hydrothermal fluids. Org. Geochem. 110, 73–86. https://doi.org/10.1016/j.orggeochem.2017.05.003

Sarma, N.S., Kiran, R., Reddy, M.R., Iyer, S.D., Peketi, A., Borole, D. V., Krishna, M.S., 2018. Hydrothermal Alteration Promotes Humic Acid Formation in Sediments: A Case Study of the Central Indian Ocean Basin. J. Geophys. Res. Ocean. 110–130. https://doi.org/10.1002/2017JC012940

Schlitzer, R., 2021. Ocean Data View.

Semeniuk, D.M., Bundy, R.M., Payne, C.D., Barbeau, K.A., Maldonado, M.T., 2015. Acquisition of organically complexed copper by marine phytoplankton and bacteria in the northeast subarctic Pacific Ocean. Mar. Chem. 173, 222–233. https://doi.org/10.1016/J.MARCHEM.2015.01.005

Shaw, T.J., Luther, G.W., Rosas, R., Oldham, V.E., Coffey, N.R., Ferry, J.L., Dias, D.M.C., Yücel, M., Thibault, A., Chanvalon, D., 2021. Fe-catalyzed sulfide oxidation in hydrothermal plumes is a source of reactive oxygen species to the ocean. Proc. Natl. Acad. Sci. U.S.A. 118, 1–7. https://doi.org/10.1073/pnas.2026654118

Steffens, J.C., 1990. The heavy metal-binding peptides of plants. Annu. Rev. Plant Physiol. Plant Mol. Biol. 41, 553–575. https://doi.org/10.1146/annurev.pp.41.060190.003005

Theberge, S.M., Luther, G.W., Farrenkopf, A.M., 1997. On the existence of free and metal complexed sulfide in the Arabian Sea and its oxygen minimum zone. Deep Sea Res. Part II Top. Stud. Oceanogr. 44, 1381–1390. https://doi.org/10.1016/S0967-0645(97)00012-X

Tilliette, C., Gazeau, F., Portlock, G., Bonnet, S., Guigue, C., Leblond, N., Lory, C., Marie, D., Montanes, M., Pulido-, E., Sarthou, G., Tedetti, M., Vorrath, M., Whitby, H., Guieu, C., 2023. Influence of shallow hydrothermal fluids release on the functioning of phytoplankton communities. Front. Mar. Sci. https://doi.org/10.3389/fmars.2023.1082077

Tilliette, C., Taillandier, V., Bouruet-Aubertot, P., Grima, N., Maes, C., Montanes, M., Sarthou, G., Vorrath, M.-E., Arnone, V., Bressac, M., et al., 2022. DFe patterns impacted by shallow hydrothermal sources along a transect through the Tonga-Kermadec arc. Earth Sp. Sci. Open Arch. 43. https://doi.org/10.1029/2022GB007363

Turner, J.A., Abel, R.H., Osteryoung, R.A., 1975. Normal Pulse Polarographic Analysis Based on Mercury

Anodization: Sulfide and Iodide. Anal. Chem. 47, 1343–1347. https://doi.org/10.1021/ac60358a054

Vasconcelos, M.T.S.D., Leal, M.F.C., 2001. Antagonistic interactions of Pb and Cd on Cu uptake, growth inhibition and chelator release in the marine algae Emiliania huxleyi. Mar. Chem. 75, 123–139. https://doi.org/10.1016/S0304-4203(01)00029-9

Vasconcelos, M.T.S.D., Leal, M.F.C., van den Berg, C.M.G., 2002. Influence of the nature of the exudates released by different marine algae on the growth, trace metal uptake and exudation of Emiliania huxleyi in natural seawater. Mar. Chem. 77, 187–210. https://doi.org/10.1016/S0304-4203(01)00087-1

Wang, H., Liu, M., Wang, W., Zhou, H., Ellwood, M.J., Butterfield, D.A., Buck, N.J., Resing, J.A., 2022. Iron ligands and isotopes in hydrothermal plumes over backarc volcanoes in the Northeast Lau Basin, Southwest Pacific Ocean. Geochim. Cosmochim. Acta 336, 341–352. https://doi.org/10.1016/j.gca.2022.09.026

Whitby, H., Bressac, M., Sarthou, G., Ellwood, M.J., Guieu, C., Boyd, P.W., 2020. Contribution of Electroactive Humic Substances to the Iron-Binding Ligands Released During Microbial Remineralization of Sinking Particles. Geophys. Res. Lett. 47, 1–11. https://doi.org/10.1029/2019GL086685

Whitby, H., Posacka, A.M., Maldonado, M.T., van den Berg, C.M.G., 2018. Copper-binding ligands in the NE Pacific. Mar. Chem. 204, 36–48. https://doi.org/10.1016/J.MARCHEM.2018.05.008

Whitby, H., van den Berg, C.M.G., 2015. Evidence for copper-binding humic substances in seawater. Mar. Chem. 173, 282-290. https://doi.org/10.1016/j.marchem.2014.09.011

Williford, T., Amon, R.M.W., Benner, R., Kaiser, K., Bauch, D., Stedmon, C., Yan, G., Walker, S.A., van der Loeff, M.R., Klunder, M.B., 2021. Insights into the origins, molecular characteristics and distribution of iron-binding ligands in the Arctic Ocean. Mar. Chem. 231, 103936. https://doi.org/10.1016/j.marchem.2021.103936

Yang, L., Hong, H., Guo, W., Chen, C.T.A., Pan, P.I., Feng, C.C., 2012. Absorption and fluorescence of dissolved organic matter in submarine hydrothermal vents off NE Taiwan. Mar. Chem. 128–129, 64–71. https://doi.org/10.1016/j.marchem.2011.10.003

Yücel, M., Gartman, A., Chan, C.S., Luther, G.W., 2011. Hydrothermal vents as a kinetically stable source of iron-sulphide-bearing nanoparticles to the ocean. Nat. Geosci. 4, 367–371. https://doi.org/10.1038/ngeo1148

Zhivotovsky, B., 2012. DNA damage-induced cell death. Toxicol. Lett. 211, S7–S8. https://doi.org/10.1016/j.toxlet.2012.03.040

4.7. Supplementary

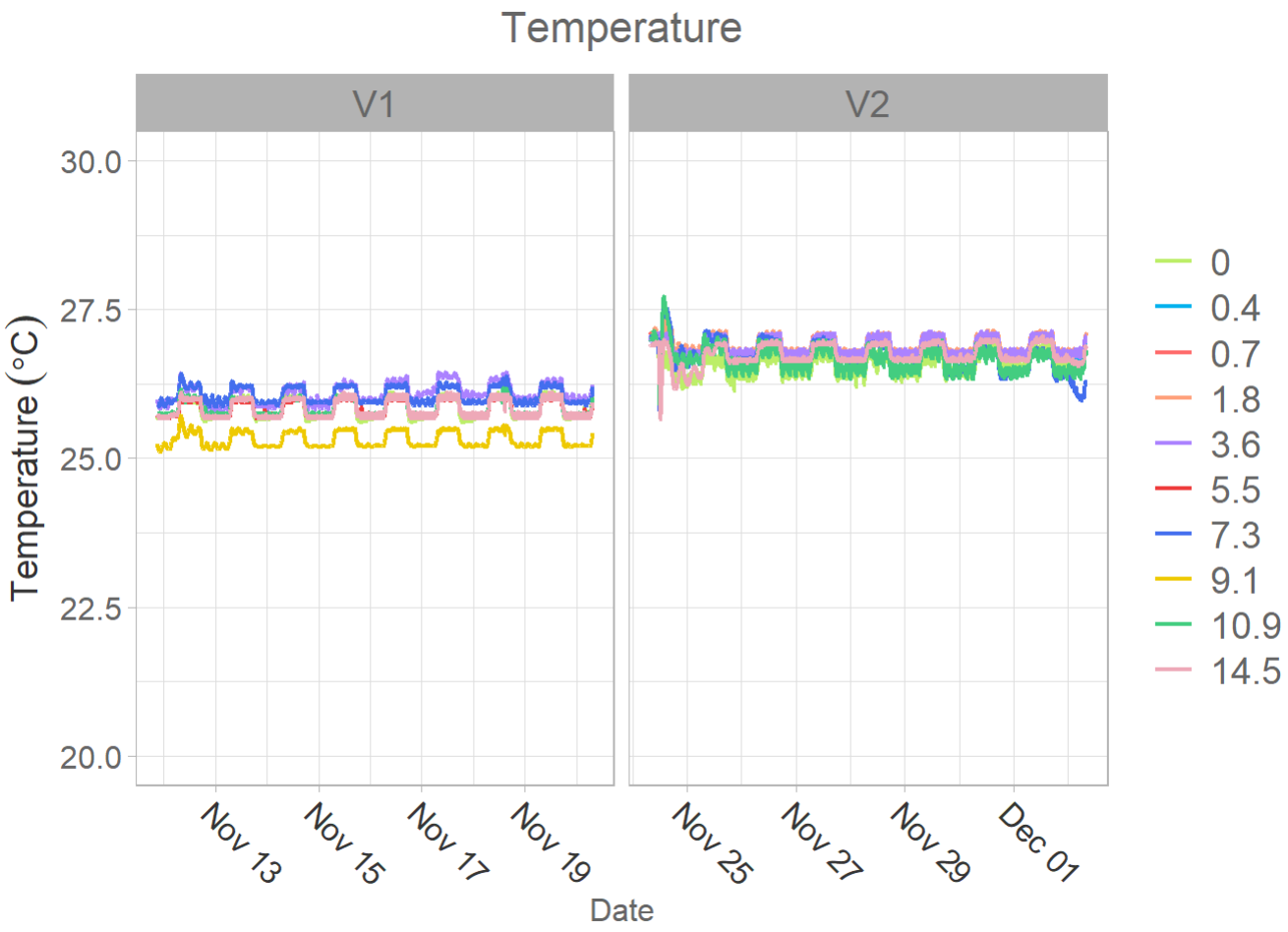

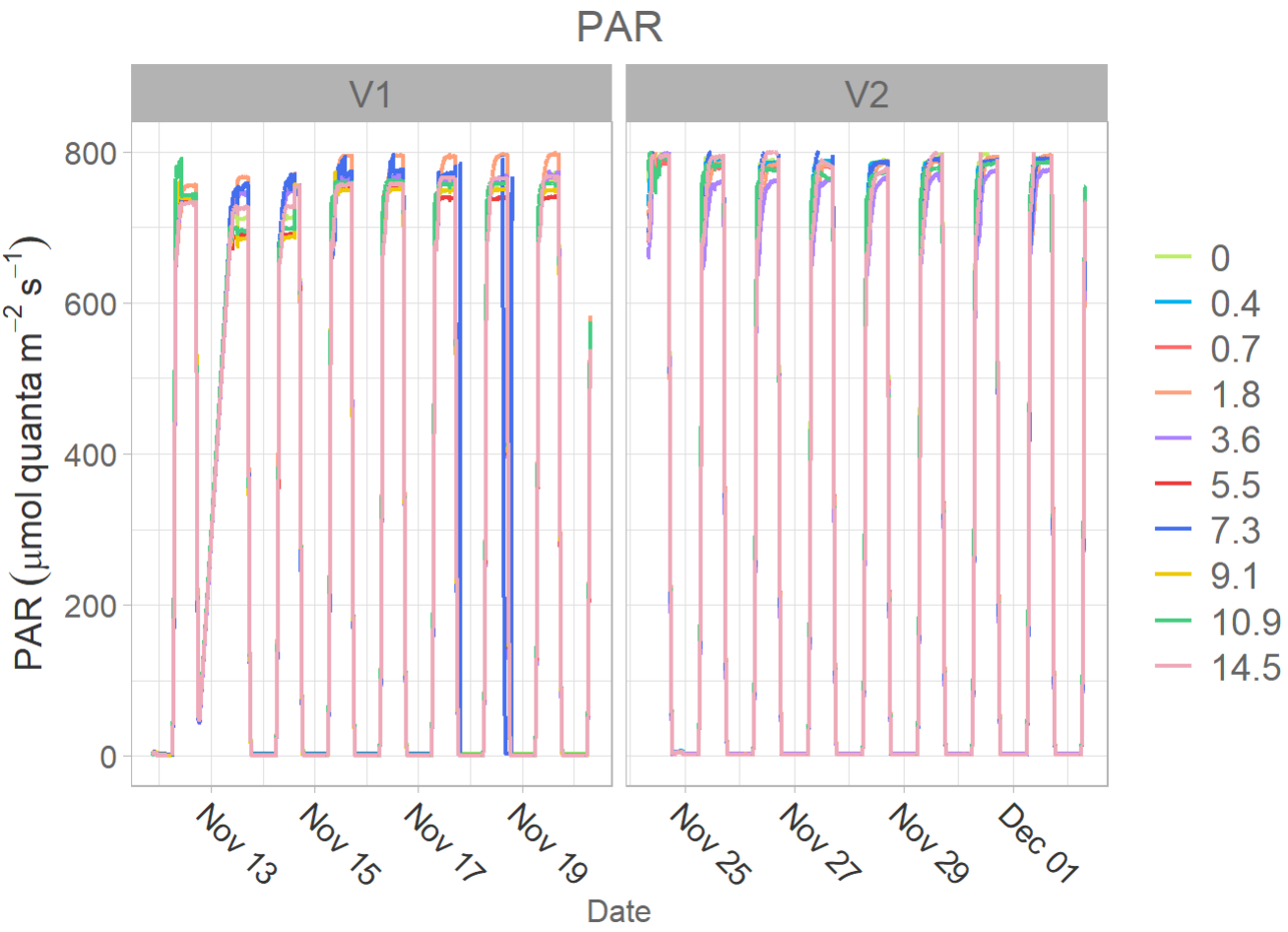

Figure 4S1. *Temperature (°C) of each minicosms tank during both experiments. V1 was 9 days and the temperature ranged from 25.3 °C to 26.1 °C. V2 was 8 days experiment and the temperature ranged from 26.6 °C to 26.9 °C. Photosynthetically active radiation (PAR; µmol photons m^{-2} s^{-1}), was programmed with a 12 h light and dark cycle. A maximum PAR was reached (≈ 735 µE m-² s-1) between 9.30 a.m. and 5 p.m. Figures were obtained from TONGA dataset.*

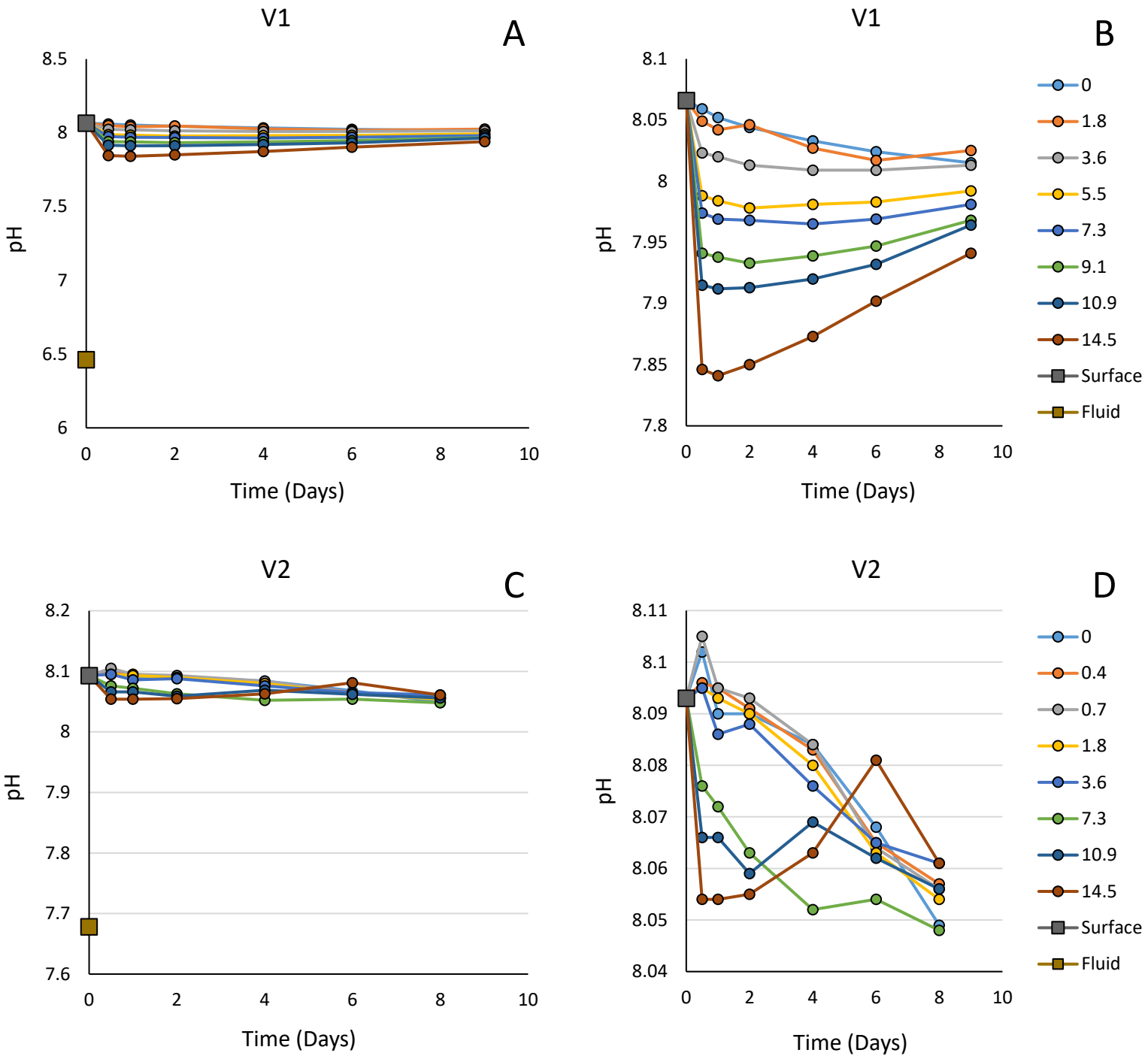

Figure 4S2*. pH of each minicosms tank during both experiments. pH of the end mebers are shown as squares (surface = grey square; hydrothermal fluids = orange square). Hydrothermal fluids used in the V1 experiment were collected from PANAMAX and for V2 hydrothermal fluids were collected from SIMONE. V1 lasted 9 days and V2 lasted 8 days. Numbers in legend represent the % of hydrothermal fluid enrichment.*

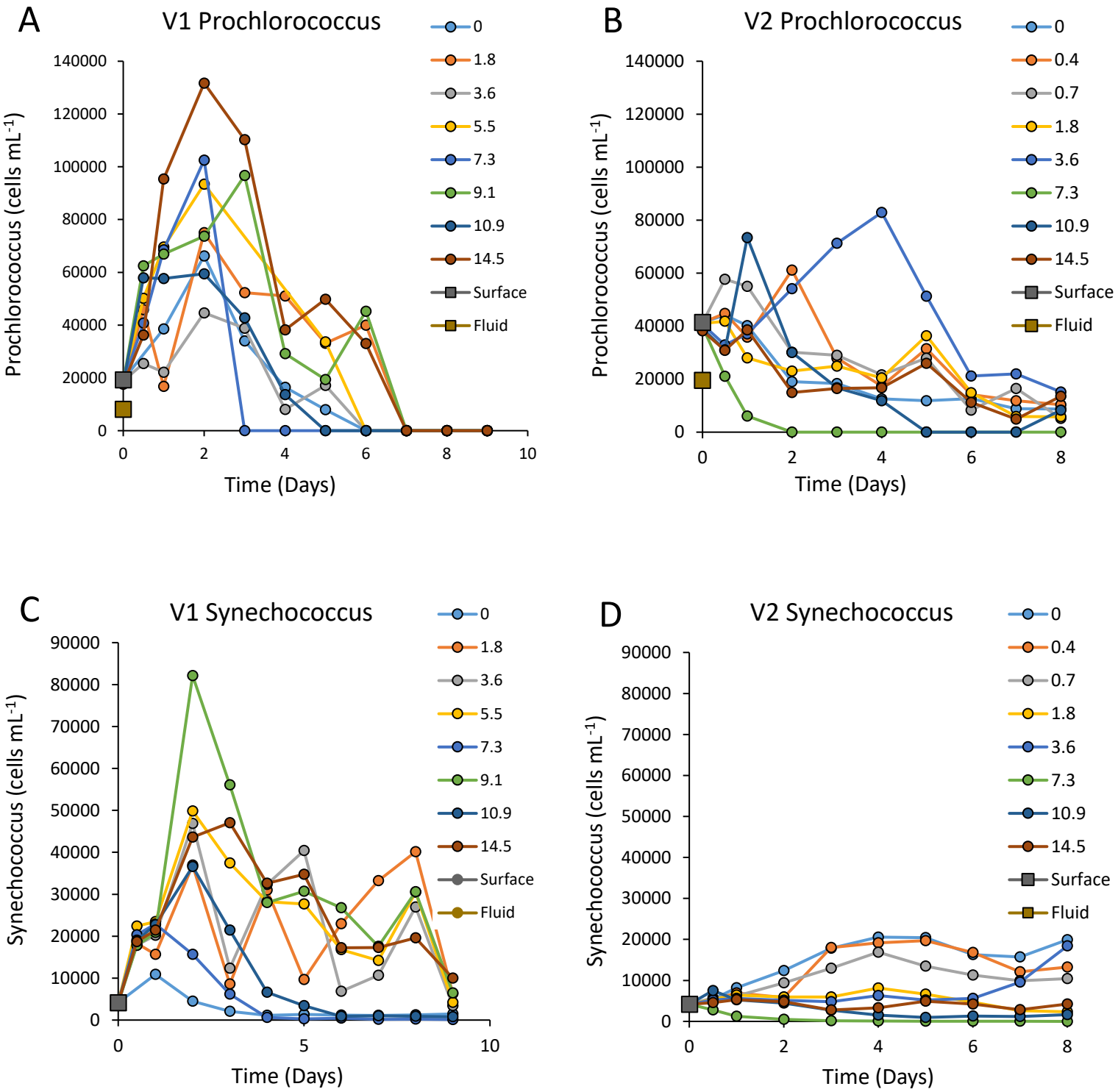

***Figure 4S3**. Abundance of Prochlorococcus (A and B) (cells mL^{-1}) and Synechococcus (C and D) (cells mL^{-1}) during both experiments. Abundance was quantified in the surface (grey square) and fluid (orange square) end members. Hydrothermal fluids used in the V1 experiment were collected from PANAMAX and for V2 hydrothermal fluids were collected from SIMONE. V1 lasted 9 days and V2 lasted 8 days. Numbers in legend represent the % of hydrothermal fluid enrichment.*

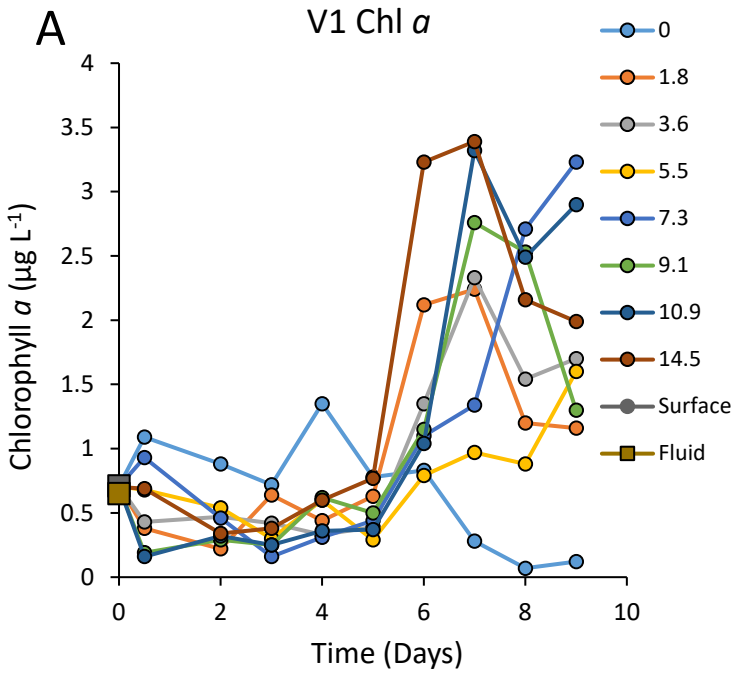
A
V1 Chl a
Chlorophyll a (µg L-1)
Time (Days)
0
1.8
3.6
5.5
7.3
9.1
10.9
14.5
Surface
Fluid

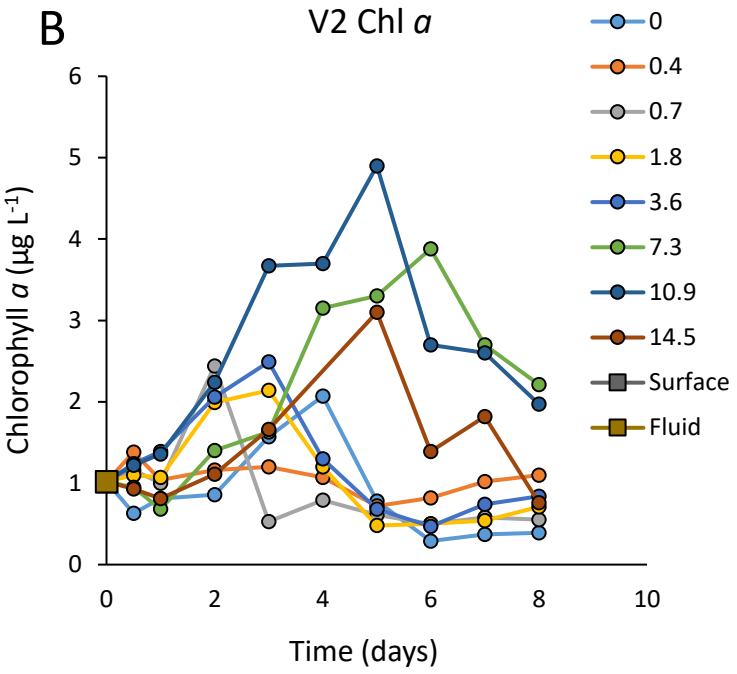
B
V2 Chl a
Chlorophyll a (µg L-1)
Time (days)
0
0.4
0.7
1.8
3.6
7.3
10.9
14.5
Surface
Fluid

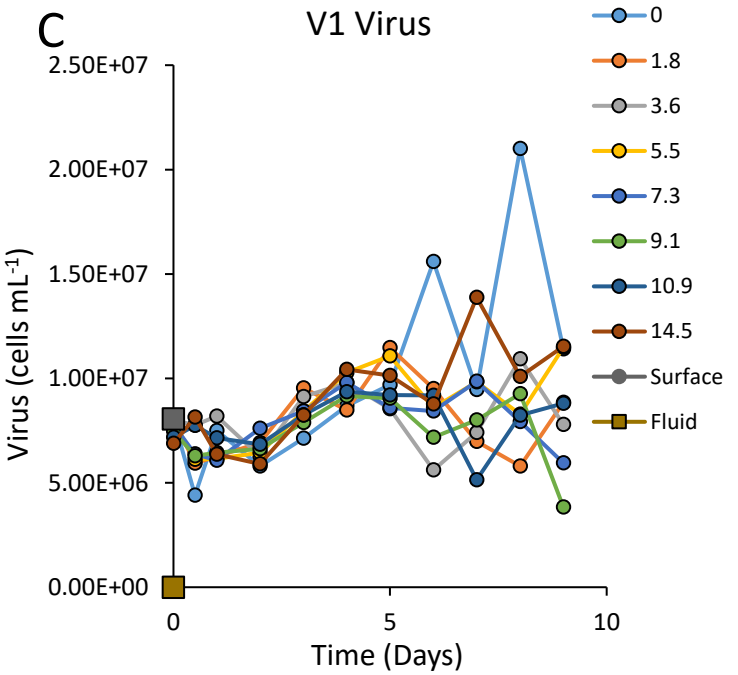
C
V1 Virus
Virus (cells mL-1)
Time (Days)
0
1.8
3.6
5.5
7.3
9.1
10.9
14.5
Surface
Fluid

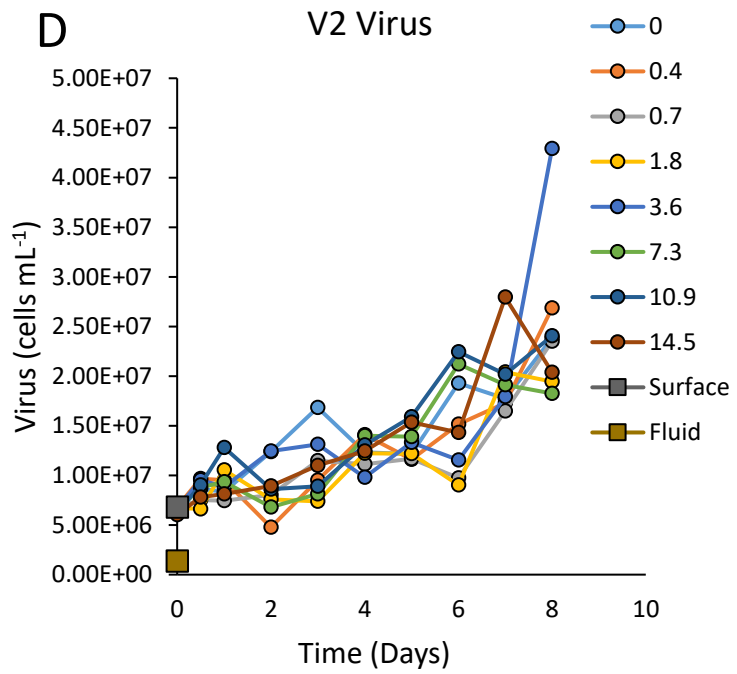
D
V2 Virus
Virus (cells mL-1)
Time (Days)
0
0.4
0.7
1.8
3.6
7.3
10.9
14.5
Surface
Fluid

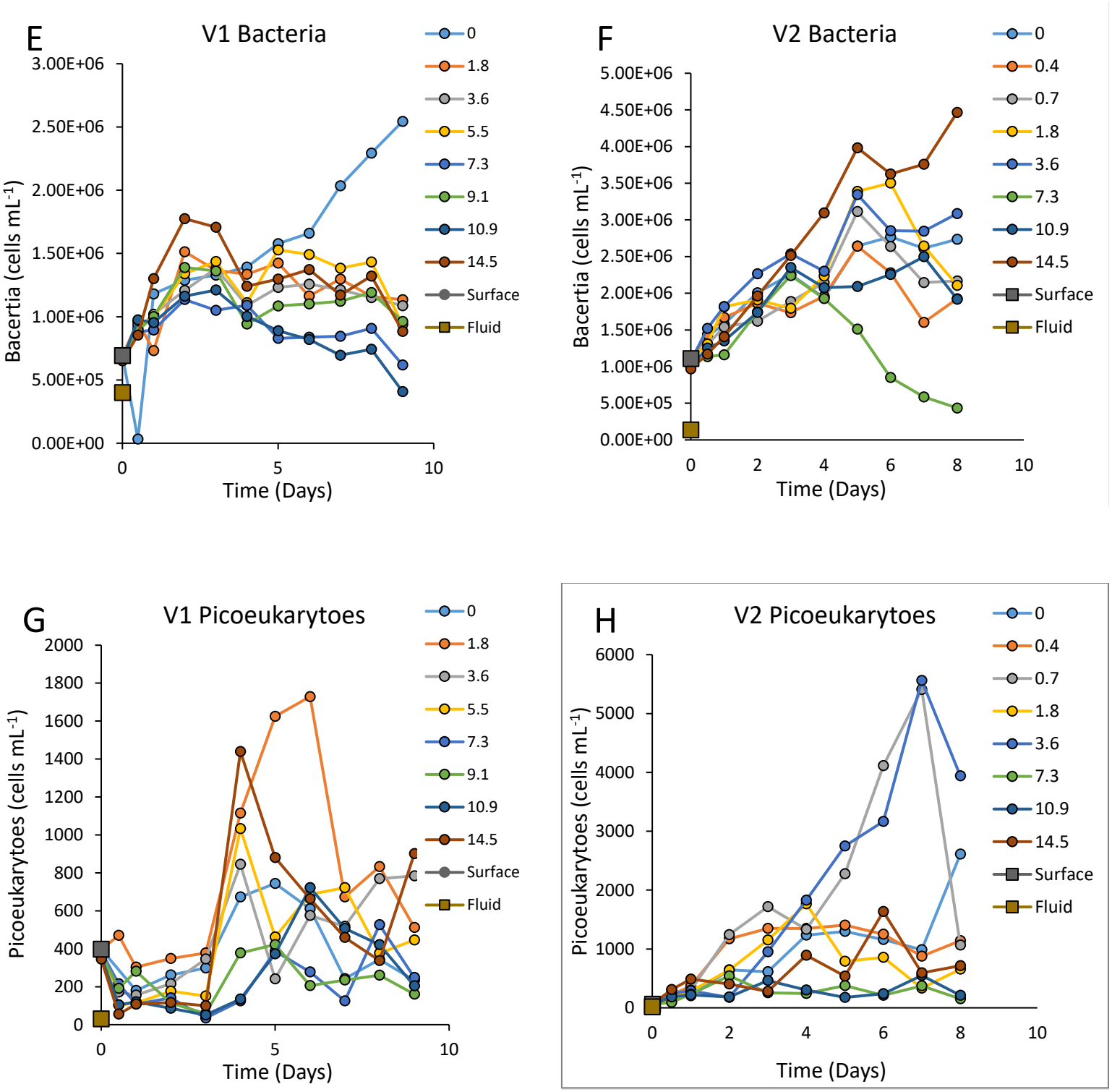

***Figure 4S4**. Abundance of Chlorophyll a (A and B) (cells mL^{-1}), viruses (C and D) (cells mL^{-1}), bacteria (E and F) (cells mL^{-1}) and picoeukarytoes (G and H) (cells mL^{-1}) during both experiments. Abundance was quantified in the surface (grey square) and fluid (orange square) end members. Hydrothermal fluids used in the V1 experiment were collected from PANAMAX and for V2 hydrothermal fluids were*

collected from SIMONE. V1 lasted 9 days and V2 lasted 8 days. Numbers in legend represent the % of hydrothermal fluid enrichment.

Experiment	dFe (nM)	dMn (nM)	dNi (nM)	dCu (nM)	dZn (nM)	dPb (nM)
V1	15.81	430.71	2.46	0.84	7.17	0.01
V2	2.12	2.76	5.10	2.04	68.24	0.03

Table 4S1. *Comparison of the dissolved trace metals in the hydrothermal end member fluids of the V1 and V2 experiments. dFe data obtained provided by Tillette. Other dTM provided by Gonzalez-Sanchez*

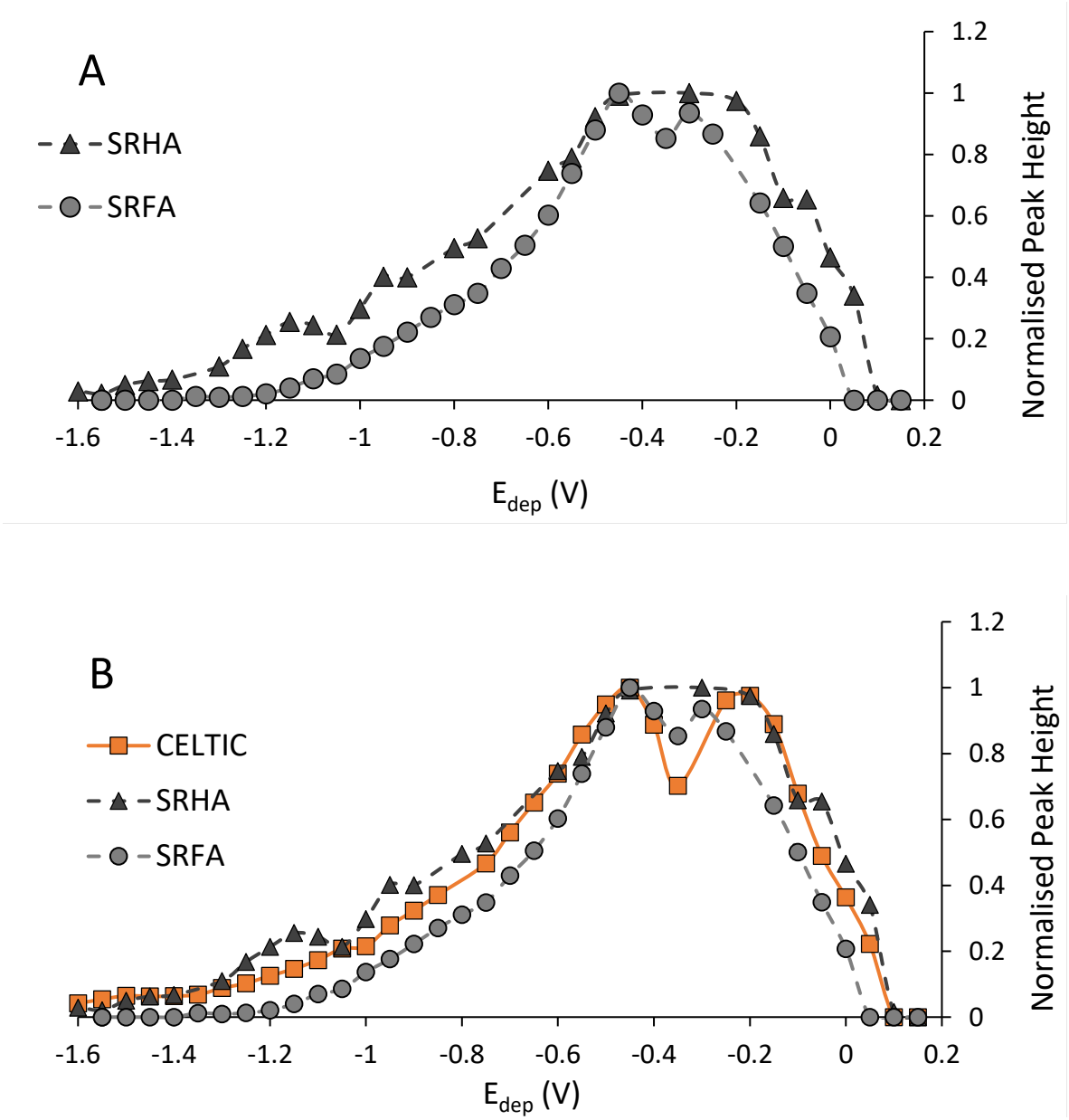

***Figure 4S5**. (A) Pseudopolarograms of 96 µg.L^{-1} of Suwannee River fulvic acid (SRFA) standard and Suwannee River humic acid (SRHA) standard. Standards were added to UV digested seawater. (B) Comparison of pseudopolarograms of eHS in CELTIC water with SRFA and SRHA standards. Measurements were carried out using the method developed by Pernet-Coudrier et al. (2013) with an adsorption time of 150 s. Each point represents the peak height of the eHS signal. Peak height has been normalised to the highest peak value (= peak height/largest peak height). Standards were added to UV digested water. The pH was 2.*

Conclusion

This thesis aimed to assess the role of shallow hydrothermal vents in the supply and cycling of RSS, sulphide and humics, as these compounds have been shown to play essential roles in the cycling of critical trace metals, notably Cu and Fe.

Firstly, an intercomparison was performed of three published cathodic stripping voltammetry (CSV) methods for the quantification of electroactive humic concentrations (eHS) (Chapter 2). These methods were the Mo method (Pernet-Coudrier et al., 2013), the Cu method (Whitby and van den Berg, 2015) and the Fe method (Laglera et al., 2007; Sukekava et al., 2018) between Liverpool and France. This was to see if the different methods were sensitive to the same fraction of HS. A comparison of the three methods was carried out on station 8 from the French GEOTRACES TONGA (shallow hydroThermal sOurces of trace elemeNts: potential impacts on biological productivity and the bioloGicAl carbon pump) cruise. This station was the most representative open ocean sample. At this station, we found good agreement with all three methods, indicating that all three methods are sensitive to the same type of compounds. Two methods (eHS-Mo and eHS-Fe) were then used to compare the rest of the GEOTRACES TONGA transect. The comparison showed discrepancies in the eHS concentrations, but this transect was conducted in a highly dynamic region and is not representative of most oceanographic regions.

Using the three CSV methods, pseudopolarography was perfomed to compare pseudopolarograms of marine eHS to a commonly used terrestrial standard (SRFA). This was to see if it was representative of the eHS in the sample. Using the eHS-Mo method, pseudopolarograms of the natural samples and for SRFA were found to be similar, while using the eHS-Fe and eHS-Cu methods showed differences

between natural samples and SRFA pseudopolarograms. In all methods, pseudopolarograms show differences between the surface and deep sample. The most noticeable differences were observed using the eHS-Fe and eHS-Cu methods and the least noticeable was using the eHS-Mo method, which is in agreement with the structure and composition of eHS changing through remineralisation. This study highlights how the three methods can be used in tandem, along with pseudopolarography, to identify differences in marine humic structure and composition.

In chapter 3, I analysed eHS and species-specific RSS (TA and GSH-like compounds), in samples from the TONGA cruise, which took place in the Western South Tropical Pacific Ocean. The cruise investigated two active shallow (< 500 m) hydrothermal sites, PANAMAX and SIMONE. In the hydrothermal plume at PANAMAX, there were elevated concentrations of both GSH-like and TA-like compounds compared to background waters, suggesting a source of these compounds related to hydrothermal activity. The increased concentrations are likely due to either the formation of RSS from the reaction of CO/CO_2 with sulphide or the production of these RSS from biology, to either help with the uptake or detoxification of metals. Sulphide was also present at PANAMAX. Elevated concentrations of eHS was PANAMAX. At station 2, away from the vents, high concentrations of TA-like compounds were also detected. Pseudopolarography was used to identify the TA-like compounds. A comparison of the station 2 pseudopolarogram and TA standard pseudopolarogram showed discrepancies, indicating that the natural RSS was not identical to TA. The high concentration of RSS and the wide pseudopolarogram indicates the presence of a currently unknown RSS or a RSS-containing compound. Comparison of eHS to dissolved iron suggested that more Fe can bind with HS with depth, in line with previous studies. This was also the case in the hydrothermally influenced Lau Basin compared to samples in the South Pacific Gyre and Melanesian waters.

Finally, the minicosm experiments were two incubation studies that took place during the TONGA 2019 cruise, designed to look at the impact of shallow hydrothermal venting on the plankton communities and biogeochemical functioning (Chapter 4). From these experiments it was found that

the addition of hydrothermal fluids from PANAMAX (V1) into surface waters prompted high production of TA-like compound 12 hours after the initial mixing, indicating a biological response to high levels of toxic trace metals to detoxify the environment. V2 also showed active production of TA-like compounds. GSH-like compounds were not detected immediately but were produced over time, and more were created in V1 than in V2. eHS concentrations in both experiments followed a similar pattern with an initial decrease in concentration and then increase with time. This study also employed pseudopolarography to see how the addition of hydrothermal fluids affected the nature of the eHS.

5.1. Future Perspectives

In marine environments, there are many different types/species of ligands, all with unique chemical structures and functional groups, which affect their ability to bind trace metals. Therefore, understanding the identity, distribution and the production of these ligands is critical to understand the biogeochemical cycles and bioavailability of trace metals accurately.

Below are the areas that I believe are required to advance this field.

Development of a marine humic standard

From Chapter 2, we quantified how much the concentration of eHS varied using different deposition potentials when using any of the 3 CSV methods. This is due to the differences between the analyte in the marine sample and the terrestrial standard being used for quantification. Because of this, the development of a marine humic standard is required to determine eHS accurately.

Database of pseudopolarograms

The idea of a RSS pseudopolarogram database has previously been proposed (Laglera and Tovar-Sánchez, 2012). The findings of this thesis support this idea and also recommend the addition of eHS pseuodpolarograms. There are a variety of different humic and RSS standards that can be purchased for the quantitation. Pseudopolarograms of each of these standards should be uploaded to the database. Individuals running either RSS or eHS analysis can compare pseudopolarograms found in the sample to RSS/eHS standards. Individuals will then be able to pick a standard most representative of their natural sample.

The database could also include pseudopolarograms of marine eHS/RSS found in different oceanic regions. These pseudopolarograms should be coupled with complementary techniques such as the characterization of marine dissolved organic matter DOM (CDOM, FDOM, fluorescence spectroscopy).

Influence of hydrothermal fluids on individual surface communities

The minicosms experiment was a unique experiment to see how shallow hydrothermal fluids affects surface communities. This experiment could use higher ratios of the hydrothermal fluids and if repeated, replicates should be performed at each mixing ratio. It would also be interesting to repeat this experiment where the surface communities are separated (light vs dark for phytoplankton vs bacterial response, for example, etc). This will provide information on the role of each individual community in response to the addition of the hydrothermal fluids. This could also provide more specific understanding of the indirect source of RSS and humic substances to seawater.

5.2. References

Laglera, L.M., Battaglia, G., van den Berg, C.M.G., 2007. Determination of humic substances in natural waters by cathodic stripping voltammetry of their complexes with iron. Anal. Chim. Acta 599,

58–66. https://doi.org/10.1016/j.aca.2007.07.059

Laglera, L.M., Tovar-Sánchez, A., 2012. Direct recognition and quantification by voltammetry of thiol/thioamide mixes in seawater. Talanta 89, 496–504. https://doi.org/10.1016/j.talanta.2011.12.075

Pernet-Coudrier, B., Waeles, M., Filella, M., Quentel, F., Riso, R.D., 2013. Simple and simultaneous determination of glutathione, thioacetamide and refractory organic matter in natural waters by DP-CSV. Sci. Total Environ. 463–464, 997–1005. https://doi.org/10.1016/j.scitotenv.2013.06.053

Sukekava, C., Downes, J., Slagter, H.A., Gerringa, L.J.A., Laglera, L.M., 2018. Determination of the contribution of humic substances to iron complexation in seawater by catalytic cathodic stripping voltammetry. Talanta 189, 359–364. https://doi.org/10.1016/j.talanta.2018.07.021

Whitby, H., van den Berg, C.M.G., 2015. Evidence for copper-binding humic substances in seawater. Mar. Chem. https://doi.org/10.1016/j.marchem.2014.09.011

Annex - Voltammetric detection and speciation of RSS, sulphide and copper in seawater

A.1. Background information

Voltammetry is a powerful and popular technique that offers many benefits such as rapid results, cheap instrumentation, high sensitivity and a relatively simple operation procedure (Zlamalova and Nesmerak, 2016). This annex aims to provide background electrochemical information about the behaviour of different RSS and sulphides present in marine waters when detected at the mercury (Hg) as well as the electrochemical behaviour of copper present in seawater when measured at a gold electrode. A technique used throughout this thesis is stripping scanned voltammetry, also called pseudopolarography when used at the Hg electrode. This technique consists in successive stripping measurements at varying deposition potentials; by plotting the intensity of the peak of interest as a function of E_{dep}, information about its identity, concentration, stability constant and/or possibly origin can be retrieved. Although the term polarography is specific to the Hg electrode, the term pseudopolarography and pseudopolarograms (ip vs E_{dep}) are used consistently, irrespective of the working electrode.

Cathodic pseudopolarography can be used for the detection of RSS and sulphide, which is based on 1- the oxidation of Hg by the sulphur atom of the sulphide/RSS compounds to form an insoluble Hg-sulphide (HgS) complex at the surface of the Hg drop during the deposition step; and 2- the reduction

of the Hg back to Hg^0 during the cathodic stripping scan. Each RSS displays a slightly different pseudopolarogram, even though their stripping signal may look exactly similar, both in terms of position and shape. Comparison of the pseudopolarogram obtained in the natural sample (possibly acidified) with those from well-defined standards help to identify the likely identity of the analyte (Laglera and Tovar-Sánchez, 2012, 2014).

Anodic pseudopolarography is much more popular and can provide an insight into the complexing behaviour of metal such as Cu, Zn, Cd and Pb in seawater (Bi et al., 2013b, 2013a; Croot et al., 1999; Gibbon-Walsh et al., 2012; Luther et al., 2021; Rozan et al., 2003; Tsang et al., 2006) with natural ligands present in seawater. Pseudopolarograms (I vs E_{dep} plots) are created by measuring the peak height of the 'free' metal of interest at various deposition potentials (E_{dep}). When an E_{dep} is applied metal ions can be reduced on the Hg electrode, forming a metal amalgam, M(S). During this step metal-ligand (ML) complexes can be broken (Equation 1):

$$(M^{n+}L)^{p-} + ne- \rightarrow M^0(S) + L^{(n+p)-} \quad \text{Equation 1.}$$

The potential, E, required to break the ML complex and form the M(Hg) is dependent on strength of ML bond, which is related to Gibbs free energy and the thermodynamic stability constant (K_{therm}) (Luther et al., 2021) (Equation 2):

$$\Delta G = -nFE = - (RT) \ln K_{therm} = \Delta H - T\Delta S \quad \text{Equation 2.}$$

$E^0_{(ML)}$ differs from the standard potential of the reversible reduction of the free metal $E^0_{(M)}$ (Equation 3) by a factor dependent on the thermodynamic stability constant K_{therm} (Equation 4) of the complex ML (Equation 5 where {} indicate activities)

$$M^{n+} + ne- \Leftrightarrow M^0(S) \quad \text{Equation 3.}$$

$$E^0_{(ML)} = E^0_{(M)} - 0.059/n. \log(K_{therm}) \quad \text{Equation 4.}$$

$$K_{therm} = \{ML\}/(\{M\}.\{L\}) \quad \text{Equation 5.}$$

The irreversible reduction of a metal complex is indicated by the presence of a sigmoidal reduction wave at a potential $E^{1/2}_{(ML)}$ significantly lower than that of the free metal ion $E^{1/2}_{(M)}$ by possibly several hundreds of mV (e.g. (Gibbon-Walsh et al., 2012). The height of the wave is indicative of the concentration of the complex while the position (along the E_{dep} scale) of the wave is directly correlated to the strength of the complex. By using model ligands with known stability constants, it is possible to derive a so-called "chelate scale" to estimate the stability constants of unknown complexes, such as Cu complexes in marine waters (Croot et al., 1999; Gibbon-Walsh et al., 2012), Zn in seawater (Baars and Croot, 2011) or Cd in freshwater (Tsang et al., 2006).

From the shape of a pseudopolarogram, the presence of one or several electroactive complexes can be visualized from the number of waves. The most positive wave, if at a similar position (few tens of millivolts) than the wave obtained in a non-complexing medium (e.g. UV digested), is due to the reduction of free metal and labile complexes, i.e. complexes that are fast-dissociating species (either organic or inorganic). This wave provides an estimation of the amount of metal that is potentially bioavailable. Other waves, present at lower potentials, indicate the presence of inert complexes (Cu is reduced without prior dissociation of the complex) whose binding strengths are determined using the chelate scale. Not all complexes can be detected and the method is limited by the range of E_{dep} that can be used, defining the upper limit of the detection window. For instance, on gold, deposition at potentials lower than -1.5 V (vs Ag/AgCl) cannot be used because of an interference, imposing an upper limit of K_{therm} for electroactive complexes, On the gold wire electrode, the maximum Cu is log K_{therm} ~ 23 (Gibbon-Walsh et al., 2012).

A.2. Methods and materials

A.2.1. Voltammetric equipment

For RSS and sulphide measurements, the voltammetric system consisted of either a µAutolab type III or Autolab PGStat 10 connected to a Metrohm 663 VA stand through the IME663 interface. The

software NOVA (version 2.1.4) controlled the voltammetric measurements. The working electrode was a hanging mercury drop electrode (HMDE) with a drop size of 0.40 mm^2. The reference electrode was Ag/AgCl with a glass salt bridge filled with 3 M potassium chloride (KCl) solution, and the counter electrode was a glassy carbon rod. Solutions were stirred (setting 4 on the VA stand) during the deposition step by a rotating polytetrafluoroethylene (PTFE) rod. The voltammetric cell was quartz.

For sulphide analysis the majority of the voltammetric equipment stayed the same, however, there were some differences. An Autolab voltammeter (Eco Chemie, Netherlands) was connected to a Metrohm 663 VA stand. The working electrode was with a HMDE or a 25 µm silver amalgam microwire (Goodfellow, UK) fitted in a polypropylene pipette tip and a vibrator as described by by (Bi et al., 2013). Briefly, a 300 µm electrical wire was inserted through a 200 µl pipette tip. The wire was connected to a 25 µm silver wire using a conductive, adhesive silver solution (Leitsilber L100, Maplin, UK). The electrical wire was pulled back leaving only the silver microwire to protrude outside the pipette tip. The tip was then melted to secure the microwire by holding in the mouth of a tubular oven set to 400 °C. The silver microwire was amalgamated with Hg prior to use by plating at −0.5 V (600 s) from an unstirred solution of 4 mM mercury nitrate, acidified to pH 2 with nitric acid. The electrode was stored in MQ overnight. The reference electrode was Ag/AgCl with a salt bridge filled with 3 M KCl, and the counter electrode was a glassy carbon rod. Solutions were stirred during the deposition step by a rotating PTFE rod and the instrument was controlled by the GPES software (version 4.9).

For Cu pseudopolarography, home-made gold wire electrodes were used, fabricated in a similar manner as the silver wire electrode and as previously described (Gibbon-Walsh et al., 2012). The reference electrode and auxiliary electrodes were a Ag/AgCl//KCl (3M) and an iridium wire electrode (150 µm diameter, 5 mm long) respectively. The potentiostat was a µAutolab connected to a IME663 interface and the voltammetric cell was a standalone cell. Measurements were done in presence of oxygen along a similar method as previously described (Gibbon-Walsh et al., 2012). The gold microwire

was vibrated during the deposition step using a small vibrator (1.5 V, 170 Hz) to improve mass transport towards the electrode during the deposition step.

A.2.2. Reagents

All solutions were prepared using ultrapure deionized water (>18 MΩ) from a Milli-Q system (Millipore, UK). Thiourea (TU) (Fluka, UK), thioacetamide (TA) (Fisher Scientific, UK), glutathione (GSH) (reduced, Sigma-Aldrich, UK) and L-cysteine (Sigma-Aldrich, UK) were used as standards for RSS groups (Pernet-Coudrier et al., 2013). Standard were kept in the dark at all times and in the fridge when not in use. A stock solution of 10 mM EDTA (Merck, UK) was prepared in MQ water. A pH buffer of 1 M boric acid (Analytical grade, Fisher Scientific) was prepared in 0.35 M ammonia (trace metal grade, Fisher Scientific) and UV-digested for 45 minutes to remove organic contaminants. It was cleaned from trace metals by the addition of 100 µM MnO_2 (van den Berg, 1982) for several hours followed by filtration (0.2 µm cellulose nitrate membrane, Whatman) on the following day. Hg plating solution was prepared from $Hg(NO_3)_2$ (Fluka, UK) in a 0.1 M sodium nitrate (Fisher, UK) and 10 mM hydrochloric acid (Fisher, UK) solution. A stock solution of 0.1 M NaS was prepared from $Na_2S.xH_2O$ (Aldrich, UK) in 1 mM NaOH (pH 11) to minimise volatilisation. Stock solutions were prepared weekly and dilutions were prepared daily. The stock and the diluted NaS standards were kept in the dark when not in use to avoid photodegradation. All reagents were of analytical grade.

A.2.3. Preparation of UV-seawater

Seawater used for background experiments was filtered Celtic seawater. Seawater was acidified to pH 2 and UV-digested for 45 minutes to remove organic compounds. UV-digestion was carried out using a 125 W high pressure mercury lamp (van den Berg, 2014). The pH was adjusted to 8.1 with addition of ammonia. 100 µL of borate buffer was added to the solution to stop the pH drifting with the addition

of EDTA. EDTA was added to the seawater to suppress the effect of dissolved metals like copper would have on the RSS peak (Laglera and Tovar-Sánchez, 2012). The final pH of the seawater was 8.1.

A.2.4. Electrochemical detection of RSS and sulphide

A.2.4.1. Analytical procedure to detect RSS compounds

The voltammetric method was adapted from Laglera et al., 2012. Briefly, under a laminar flow hood, aliquots of UV-digested seawater (10 mL) were pipetted into an acid-cleaned quartz voltammetric cell. Samples were purged for 300 s with nitrogen (N_2) to remove the interference from the oxygen wave. After discarding 3 mercury drops a deposition potential (E_{dep}) of +0.08 V was applied for up to 60 s. The stirrer was on during the deposition, after which a 9 s quiescence time was imposed. Stripping was done in differential pulse mode, scans initiated at -0.3 V and terminated at -0.85 V. A modulation time of 20 ms, a modulation amplitude of 60 mV, a step potential of 4 mV and an interval time of 0.3 s were used. The intensity of the RSS peak height was measured using the peak height function in the NOVA 2.1. software. After each measurement the voltammetric cell was rinsed with MQ water before loading of the next sample.

A.2.4.2 Analytical procedure to detect sulphide

The voltammetric method for the detection of sulphide is as followed. 20 mL aliquots of UV-digested seawater were pipetted into an acid-cleaned quartz voltammetric cell. Purging was avoided to minimise volatilisation of H_2S. A relatively low E_{dep} was set to -0.4 V for 15 s to avoid detection of RSS. The stirrer was on during the deposition. A 5 s quiescent period was allowed before the potential stripping scan was initiated at -0.3 V and terminated at -0.9 V. The differential pulse technique was used with a step of 6 mV, modulation amplitude of 50 mV, modulation time of 80 ms and an interval time 0.1 s. The sulphide peak derivative was calculated automatically using the GPES software (version 4.9) and has the advantage of being independent of the choice of the baseline, which can be

advantageous when measuring low signals After each measurement the voltammetric cell was rinsed with MQ water before loading of the next sample.

A.2.4.3. Pseudopolarography of RSS and sulphide

Cathodic pseudopolarography for RSS and sulphide standards were carried out. The method was initially published by Laglera et al., (Laglera and Tovar-Sánchez, 2014). Each pseudopolarogram was built up of a series of voltammetric scans where the peak height was measured at various E_{dep}, creating a 'fingerprint' of the RSS compound in the seawater. Pseudopolarograms were initiated at different E_{dep}. For each RSS, the E_{dep} decreased by different increments until the RSS peak was no longer visible. The deposition time was 60 s at each E_{dep}. Pseudopolarograms of standards (thioacetamide, glutathione, GSH, cysteine and thiourea) were carried out in UV-digested seawater (UV-SW). The concentration of standards used were as follows; thiourea = 100 nM, thioacetamide = 100 nM, glutathione = 150 nM, L-cysteine = 300 nM.

For sulphide pseudopolarography, the working electrode was a 25 µM silver amalgam wire instead of the HMDE. Sulphide pseudopolarograms were initiated from -0.9 V with increments of +0.05 V until 0.1 V. The deposition time was 10 s at each E_{dep}. Sulphide standard pseudopolarogram was carried out in 0.6 M NaCl (Fisher Scientific, UK) fixed at pH 9.2 with a borate buffer and the concentration of sulphide was 1 µM.

A.2.5 Copper pseudopolarography

Copper pseudopolarography was run in Celtic seawater using a 10 µm goldwire electrode. Differential pulse anodic stripping voltammetry was used with the following stripping scan parameters: 50 mV amplitude, 6 mV step, 100 ms interval and 10 ms pulse time. The analytical scan consisted in the deposition potential E_{dep} for typically 120 to 300 s, a desorption step at -1.3 V for 2 s, 1 s equilibration time and stripping typically from 0 to 0.55 V. Each analytical scan was immediately followed by a background scan, which was the same as the analytical scan but with a cleaning step at 0.55 V for 10s

instead of the deposition. The background scan was removed from its analytical scan and the Cu peak was quantified on the background-subtracted scan using the peak derivative.

A.3. Results and Discussion

A.3.1. RSS on the Mercury Drop

In marine waters, there is a wide variety of RSS compounds; however, it is hard to distinguish between each RSS because CSV is limited by coalescence. Using CSV techniques, RSS typically produce a peak around -0.55 V. This is associated with the adsorption of the sulphur in the RSS group complexing with the mercury on the HMDE (Al-Farawati and van den Berg, 1997; Laglera and van den Berg, 2003). Figure A1 shows the voltammograms of four common RSS standards.

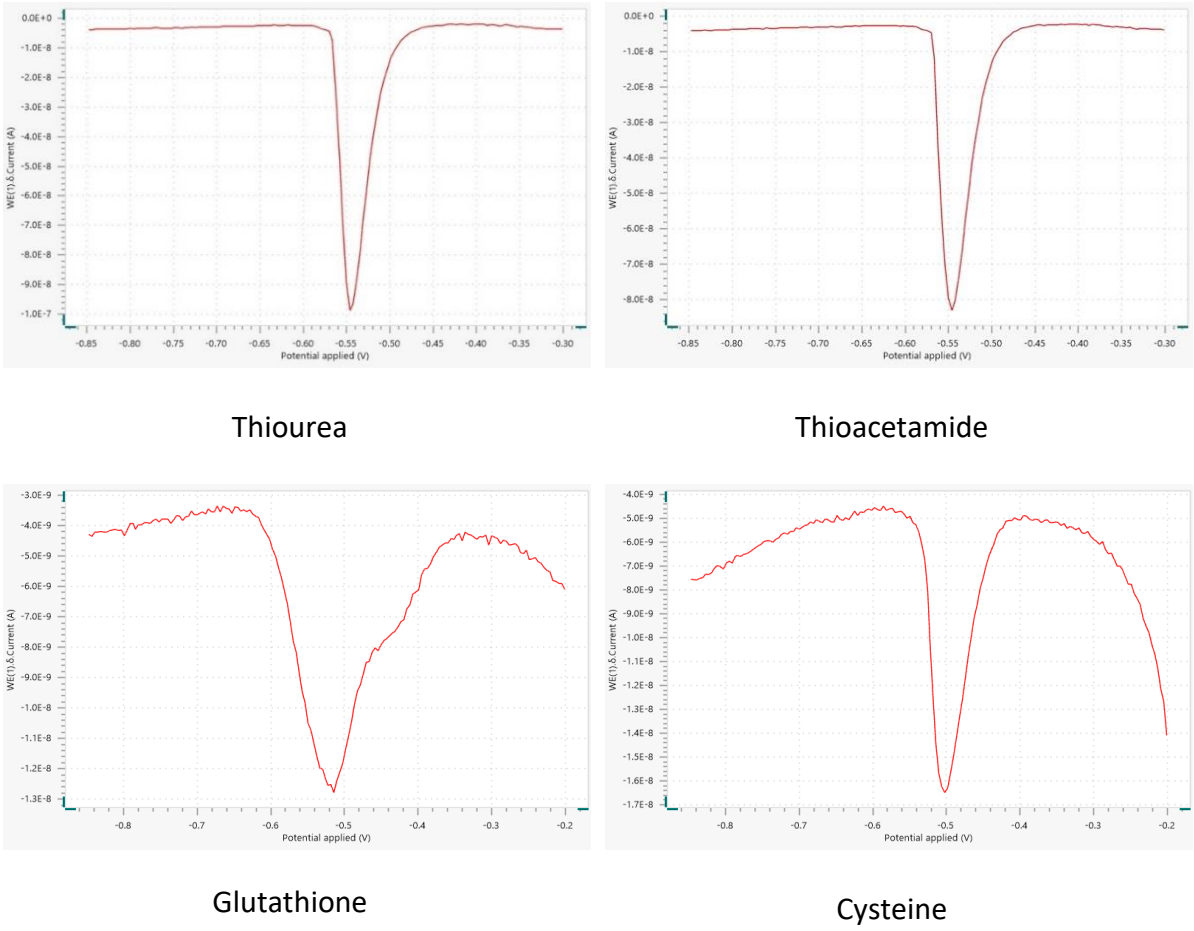

Figure A1. *Voltammograms of 50 nM thiourea (A), 50 nM thioacetamide (B), 150 nM glutathione (C), and 400 nM cysteine in UV-digested seawater. An E_{dep} = +0.08 V was applied for 60 s. For thiourea and thioacetamide, voltammograms were recorded between -0.3 and -0.85 V; glutathione and cysteine voltammograms were recorded between -0.2 and -0.85 V. Standards were added to UV digested water. The pH was 8.1. Scans were obtained from NOVA 2.1.*

There were slight differences in the peak shape and position for the different RSS (Table A1). The peaks for thiourea and thioacetamide were the most similar. They are both sharp and intense peaks that appear at -0.55 V. However, thiourea had a better sensitivity. Glutathione and cysteine appear slightly more positively (-0.51 V and -0.47 V). The peak for glutathione was broader compared to the other RSS.

	Thiourea	Thioacetamide	Glutathione	Cysteine
Peak Position	-0.55 (50nM)	-0.55 (50nM)	-0.51 (160nM)	-0.47 (400nM)

Table A1. *Comparison of voltammetric peak postion for thiourea, thioacetamide, glutathione and cysteine, at pH 8.1. An E_{dep} = +0.08 V was applied for 60 s. Standards were added to UV digested water.*

Even though there are slight differences in the peak position and shape of the RSS, identifying the RSS present would not be possible, especially in waters with a mix of RSS.

The method developed using Mo (Pernet-Coudrier et al., 2013) is carried out at pH 1.95 and can distinguish between the RSS; thiourea, thioacetamide, glutathione, cysteine and N-acetyl-L-cysteine. There is a clear difference between the peak shape and position (Figure A2 and Table A2), providing suitable identification of the RSS present within the sample. Despite this, some RSS could appear in the same position. For example, sulphide and thioacetic acid produce the same signal as thioacetamide. This can make it challenging to identify RSS in seawater, but it provides better information than measuring RSS at pH 8.

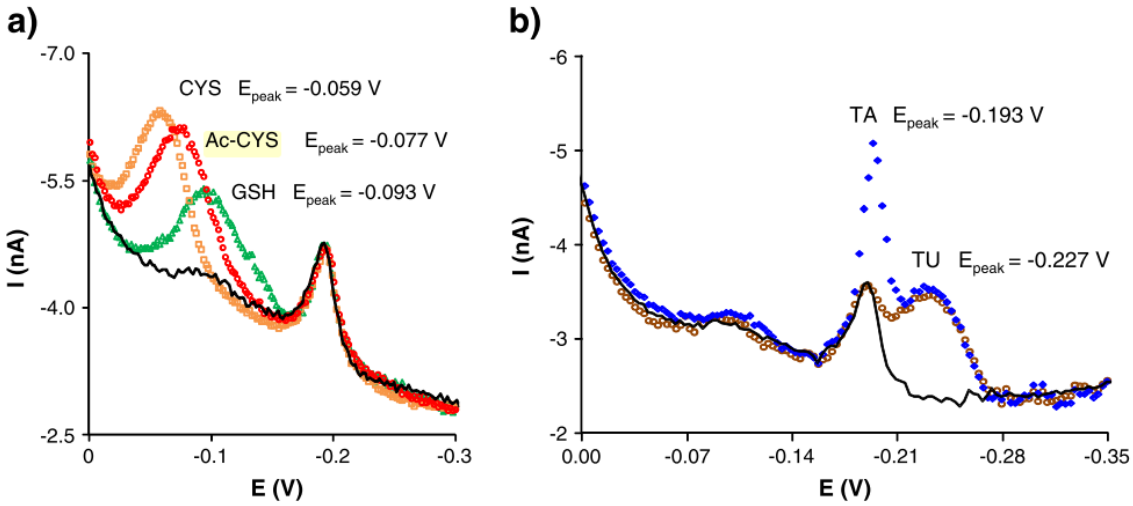

Figure A2. *(A) Voltammogram of coastal seawater containing 5.6 nM of glutathione (black line). In the same water, a single addition of 25 nM of cysteine (orange square), 22 nM, N-acetyl-L-cysteine (red circle) and 15 nM of glutathione (green triangle) were added to the solution. (B) Voltammogram of coastal seawater containing 723 nM of thioacetamide (black line). In the same water, successive additions of 223 nM of thiourea (empty brown circle) and 1.2 µM of thioacetamide (full blue diamond) were added to the solution. The pH of the solution was 1.95. Figure taken from Pernet-Coudrier et al., 2013.*

	Thiourea	Thioacetamide	Glutathione	Cysteine	N-acetyl-L-cysteine
Peak Position	-0.227 V	-0.193 V	-0.093 V	-0.059 V	-0.077 V

Table A2. *Comparison of peak postion for thiourea, thioacetamide, glutathione, cysteine and N-acetyl-L-cysteine at pH 1.95 and E_{dep} = 0 V applied for 60 s. Peak postion values obtained from Pernet-Coudrier et al., 2013.*

A.3.1.1 Detection limit

The limit of detection (LOD) at pH 8.1 was determined for four common RSS standards (Table A3). The E_{dep} varied; thiourea (+0.08 V), thioacetamide (-0.025 V), glutathione (+0.08 V) and cysteine (-0.35 V), but the deposition time remained the same (60 s). E_{dep} was selected for each RSS where the peak height was the highest. RSS standards were added to UV-digested seawater. Seawater was UV-digested to remove any organics in the solution and EDTA was added to complex with trace metals in the solution. LOD's were calculated from 3 times the standard deviation of 11 consecutive measurements.

For thiourea and cysteine, the LODs obtained in this study are lower than previously reported (Table A3), showing the voltammetric conditions are more sensitive than the methods published. For glutathione at pH 2 the LOD is lower than at pH 8.1, indicating that this method is the most sensitive to low concentrations. The most significant difference in the LOD is thioacetamide in natural and acidic conditions. In acidic conditions, the LOD is 29 times higher than at pH 8.1 so even though the Pernet Coudrier et al. (2013) method has the advantage of distinguishing between different RSS and measure humics simultaneously, this is also done at the expense of sensitivity.

Compound	pH	E_{dep}	Limit of detection (nM)	Reference
Thiourea	8.4	+0.07 V (60 s)	3.7 (n = 5)	(Laglera and Tovar-Sánchez, 2012)
Thiourea	8.1	+0.08 V (60 s)	0.18 (n = 11)	This study
Thioacetamide	8.4	−0.02 V (60 s)	1.3 (n = 5)	(Laglera and Tovar-Sánchez, 2012)
Thioacetamide	8.1	-0.025 V (60 s)	2.8 (n = 11)	This study
Glutathione	8.4	−0.3 V (60 s)	4.3 (n = 5)	(Laglera and Tovar-Sánchez, 2012)
Glutathione	8.1	0.08 V (60 s)	2.75 (n = 11)	Thius study
Cysteine	8.4	0.05 V (60 s)	7.5 (n = 5)	(Laglera et al., 2014)
Cysteine	8.1	-0.35 V (60 s)	2.3 (n = 11)	This study
Thioacetamide	1.95	0 V (60 s)	81 (n = 11)	(Pernet-Coudrier et al., 2013)
Glutathione	1.95	0 V (60 s)	1 (n = 11)	(Pernet-Coudrier et al., 2013)

Table A3. *Comparison of the limit of detection (LOD) for thiourea, thioacetamide, glutathione and cysteine, from our study with the LOD published from with Laglera and Tovar-Sánchez (2012) and Pernet-Coudrier et al., (2013). In our study standards were added to UV digested water. The pH was 8.1.*

It was concluded that the Pernet Coudrier et al. (2013) method would be the best method for the quantification of RSS and electroactive humic substances in this thesis.

A.3.1.2. Cathodic pseudopolarography of RSS

Pseudopolarography was developed to provide qualitative information of reduced sulphur substances (Laglera and Tovar-Sánchez, 2014). The technique consists of a series of voltammetric scans where the peak height was measured at various E_{dep}, creating a 'fingerprint' of the RSS compound in the seawater (Figure A3). Each RSS 'fingerprint' range varied, with thiourea having the narrowest pseudopolarogram (-0.05 V to 0.1 V) and cysteine having the widest (-0.6 V to 0.1 V).

Thiourea and thioacetamide behaved similarly, with the maximum peak height around +0.07 V for both RSS, and the peaks vanished rapidly as E_{dep} moved to more negative potentials. However, thioacetamide is easily distinguishable from thiourea as thioacetamide has two peaks at +0.075 V and

-0.025 V, while thiourea only had one at +0.072 V. In contrast, glutathione and cysteine signals are obtained over a much wider range of deposition potentials.

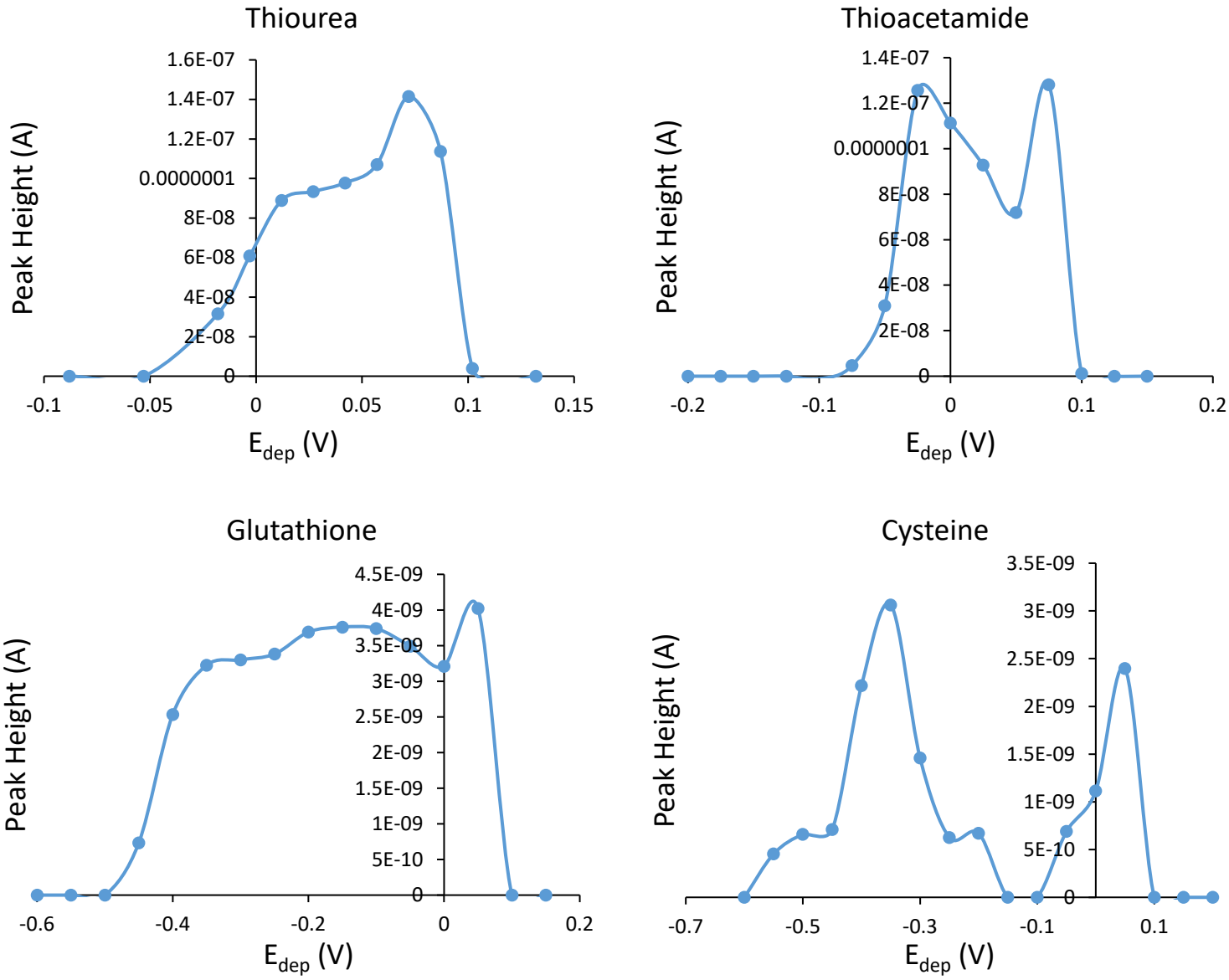

Figure A3. *Pseudopolarograms of 100 nM thiourea (A), 100 nM thioacetamide (B), 150nM glutathione (C), and 300nM cysteine in UV-digested seawater. Deposition time for each E_{dep} was 60 s. Each point represents the peak height of the eHS signal. Standards were added to UV digested water. The pH was 8.1.*

A.3.2. Sulphide

The main problem for the detection of sulphide is related to the instability of the signal: there is a rapid loss of sulphide in seawater samples meaning that it is challenging to preserve sulphide for an

extended period of time and the signal tends to decrease rapidly in the voltammetric cell. Oxidants such as dissolved O_2 (Almgren and Hagström, 1974; Avrahami and Golding, 1968), H_2O_2 (Millero et al., 1989) and IO_3^- (Jia-zhong and Whitfield, 1986) are known to react with sulphide in a matter of hours. O_2 is the primary oxidant of sulphide and has a half-life of 22 hours in seawater (Zhang and Millero, 1993). Purging the sample (with N_2 or Ar) is often required with voltammetric techniques to remove dissolved oxygen. However, this cannot be used because purging can remove free sulphide from the sample.

Al-Farawati and van den Berg (1997) observed that sulphide in seawater did not give a stable peak when a standard voltammetric cell was used with a mercury drop electrode (HMDE). They did not attribute this decrease to O_2, H_2O_2, or IO_3^- but suggested that the sulphide loss was due to metallic mercury (Hg), produced by the mercury drop system, forming an insoluble mercuric sulphide salt. They were able to overcome the loss of sulphide through the use of a flow cell to avoid the solution to be in contact with any mercury before analysis. In comparison, Aumond et al., (2012) investigated the suitability of a vibrating gold microwire electrode for measuring sulphide in seawater. The stability of the sulphide peak was tested in various non-deoxygenated solutions: 0.5 M NaCl, natural coastal seawater (pH 8) and natural coastal seawater at pH 9.6. Solutions were spiked with 13 µM of sulphide, and the solutions were exposed to air during the measurements. For NaCl (0.5 M) and natural seawater (pH ~ 8), the sulphide peak was stable for ~10 minutes, after which a decrease was observed, (rate of loss was 1.8% min^{-1} for NaCl 0.5 M and 2.6% min^{-1} for seawater). When increasing the pH of seawater to 9.6, the sulphide peak was stable for a much more extended period (~1 h). After 2 hours, the initial signal had been lost by 20% (rate of loss was ~0.2% min^{-1}) suggesting that H_2S volatilization is also a factor to consider, in general agreement with another study (Deleon et al., 2012).

The advantage of using the HMDE is that a new and reproducible electrode is created for every measurement. However, there are possibly 2 factors that may affect the stability of the sulphide signal: 1- the amount of mercury is high and 2- the solution is stirred which may favour faster

volatilisation of H_2S. On the other hand, the use of a microwire amalgam electrode presents potential advantages in favour of a stable sulphide signal: 1- limited amount of Hg is needed and 2-vibration of the wire electrode might limit H_2S volatilisation. The drawback of such electrodes is that they are home-made and all different (at least in terms of length), they can break without warning and can be time consuming to prepare. Nevertheless, their potential for sulphide detection has never been looked at. This section therefore aims to report very preliminary results obtained at a silver amalgam electrode for sulphide detection.

A.4.3 Instability of the sulphide signal

Although the sulphide peak potential was present 100 mV more cathodic on the amalgam wire compared to the drop (~ -0.7 and ~ -0.6 V respectively), the peak is similarly sharp and well-shaped on the amalgam electrode. For both electrodes, a decrease of the signal was observed with time in oxygenated UV digested seawater (Figure A4) but the rate of loss (Table A1) was dependent on the sulphide concentration for both electrodes (higher loss at lower concentrations) suggesting that the loss is quantitative, i.e. it is due to a finite amount of oxidant being produced or to a finite amount of Hg^{2+} in the cell (if Hg^{2+} was not the reason). Interestingly, the rate of loss at the wire electrode was significantly smaller than at the HMDE (Table A5). We found that the rate of loss was not influenced by the size of the HMDE drop and that, as previously shown, the effect of oxygen (stability checked in purged and non-purged UV digested seawater), iodate (up to 1 µM) and hydrogen peroxide (up to 1 µM) did not make any difference to the stability. The only difference that was noticed was stirring: when running successive measurements (15 s deposition at -0.4 V) with a 30 s interval between each measurement, a 30% faster decrease was obtained when the solution was stirred during the intervals, suggesting a loss by volatilisation that also occur during the voltammetric deposition step. From those experiment, we concluded that the detection of sulphide is best achieved at an amalgam wire electrode without stirring of the solution but instead, vibration of the electrode in an attempt to minimise the instability of the signal.

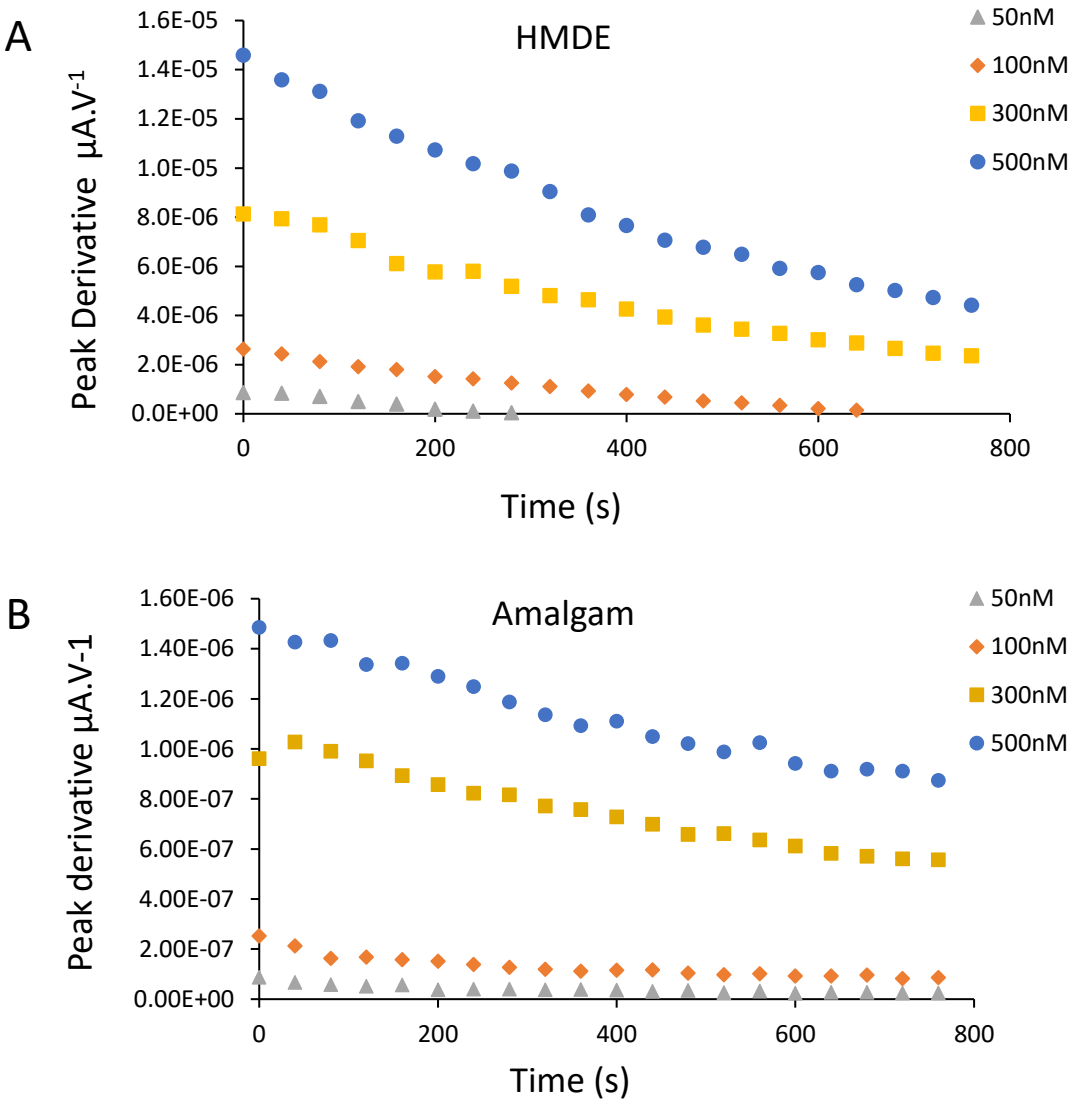

Figure A4. Sulphide *peak instability over time with various concentrations of sulphide. Standards were added to UV-digested seawater, and the pH was set to 8. Each point represents the peak derivative of the sulphide signal. (A) shows the instability with a HMDE electrode, and (B) shows the instability with a silver amalgam wire electrode. An* E_{dep} *of -0.4 V was applied for 15 s.*

Parameter	HMDE (%. s^{-1})	Silver Amalgam (%. s^{-1})
Sulphide Concentration		
50nm	0.32	0.09
100nm	0.15	0.08
300nm	0.09	0.06
500nm	0.09	0.06

Table A5. *Comparison of the sulphide rate of loss per second (%.* s^{-1}*) with a HMDE and a silver amalgam wire electrode. Sulphide standard was added to UV digested seawater, and the pH was 8. An* E_{dep} *of -0.4 V was applied for 15 s.*

A.3.4. Cathodic Pseudopolarography of sulphide

An example of the pseudopolarogram of sulphide obtained at the HMDE electrode is shown in Figure A5. The experiment was done in 0.6 M NaCl at pH 9.2 to avoid instability of the signal. The pseudopolarograms had a 50 mV E_{dep} resolution, starting from -0.8 V up to 0 V. It can be clearly seen that the sulphide pseudopolarogram is different to the RSS pseudopolarogram. Sulphide displays a strong signal at a more negative E_{dep} than the RSS (see Figure A3) and suggest that using a low deposition potential like -0.6 V should all the sole detection of sulphide.

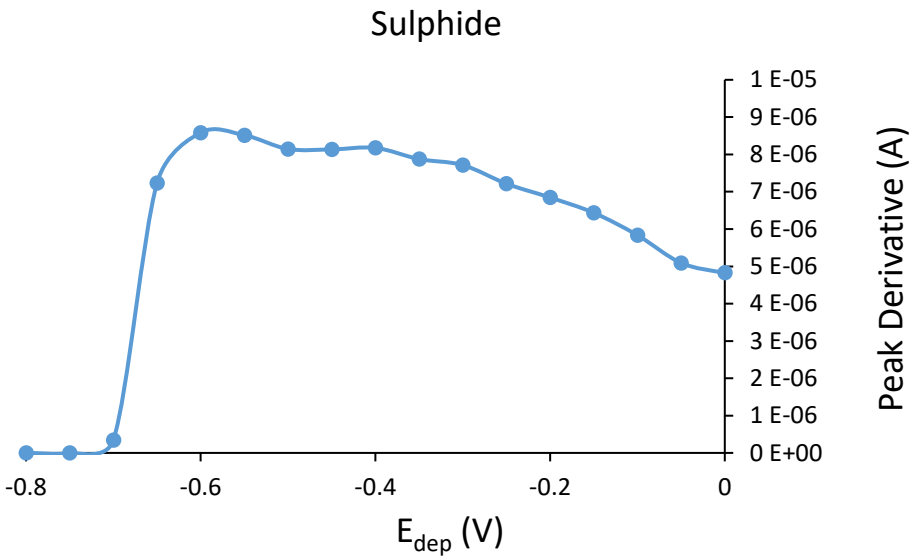

Figure A5. *Pseudopologram of sulphide standard (1µM) in 0.6M NaCl. Solution was buffered to pH 9.2 with borate buffer and ammonia. Deposition time for each E_{dep} was 10 s. Each point represents the the peak derivative of the sulphide signal.*

A.3.5. Copper speciation on gold electrode in seawater:

A.3.5.1. Electrode conditioning and analytical parameters:

Detection of Cu in seawater by anodic stripping voltammetry can be achieved sensitively on the gold microwire electrode. Before use and when new, the electrode requires a conditioning step which consists in the imposition of a low E_{dep} (-2 V) for 10-15 s in 0.5 M H_2SO_4. It is believed that the imposition of such low deposition potential results in the desorption of interfering compounds

adsorbed on the surface of the electrode. Once conditioned, the electrode can be used without any further conditioning but this very much depends on the type of solution being analysed; in coastal seawater of Liverpool bay, regular conditioning (daily) was needed while in open ocean seawater, the electrode could be used for a long time (weeks) without any.

Detection of Cu is best achieved using anodic stripping voltammetry. In seawater, the Cu peak is present on a large bump (Figure A6) which is due to the adsorption of chloride and bromide on the gold electrode (Salaün and van Den Berg, 2006). The presence of this bump hides the Cu peak at low concentrations which can only be resolved using background subtraction (Figure A6). With background subtraction, the Cu peak is well-shape (half-wdith of ~ 54-60 mV), is located at around 0.25 V (vs Ag/AgCl//3M KCl) and its detection is sensitive. Detection limit at a 10 µm diameter gold wire electrode was in 10 mM HCl and determined as 50 pM for 300 s deposition, in general agreement with previously reported value (Salaün and van Den Berg, 2006).

Figure A6 also shows the presence of a Hg peak at ~ 0.38 V. The presence of a Hg peak could not be avoided during preliminary testing as VA663 stands had previously been used with the Hg drop electrode. The Hg peak would increase with time, therefore interfering with the Cu peak. This would then interfere with the recording of a pseudopolarograms, as pseudopolarography experiments can take hours to complete, depending on the deposition time being required. If the solution was purged than the effect Hg signal was even more drastic. To avoid these problems, a stand-alone voltammetric cell was used and the samples were not purged.

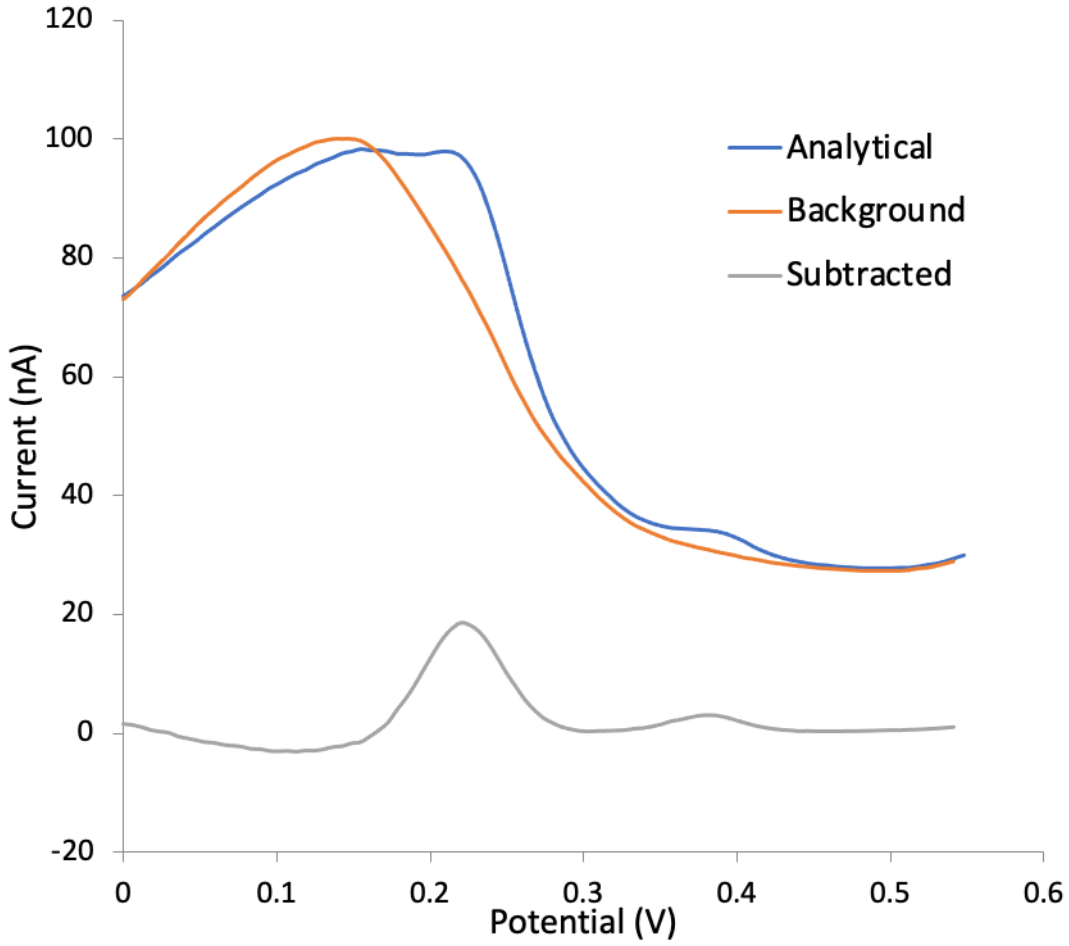

Figure A6. *Example of an analytical, background and background subtracted scans using a gold electrode. An E_{dep} of -1.3 V was applied for 120 s. Water used was coastal seawater from Liverpool Bay. The pH was 8.*

A.3.6. Pseudopolarography of copper:

Pseudopolarograms were ran automatically in seawater using the Project option of the GPES software together with a specific executable file that allows the automatic change of the deposition potential with any specific resolution. In this work, a resolution of 50 mV was always used and deposition potential were generally varied from -1.3 to 0.3 V. Figure A7 shows 2 examples of typical pseudopolarograms of Cu obtained at the gold electrode. One of them was obtained in UV digested, acidified to pH 2 coastal water from Liverpool Bay and the second one was obtained in non-treated same sample. The UV digested samples, acidified, is a non-complexing and only one wave is observed

at a potential of ~ 0.2 V, which corresponds to the inorganic wave and the reduction of Cu from inorganic complexes (Cu chloride). In the natural sample, 3 different waves can be observed with a half-wave potential $E^{1/2}$ at ~ 0.15 V, ~ -0.25 V and ~ -0.9 V. The most positive wave at 0.15 V is close to the inorganic wave and is due to the reduction of Cu(II) released from fast-dissociating copper complexes; this wave is also called the labile wave. The waves at -0.25 V and -0.9 V represent the presence of 2 types of Cu complexes whose stability can be estimated from the position of the reduction waves. The complex at -0.25 V had a stability constant that was less than the complex at -0.9 V. Using the chelate scale determined previously at the gold electrode (Gibbon-Walsh et al., 2012) (equation 1), the thermodynamic stability constants corresponding to a half-wave potential of -0.25 V and -0.9 V can be estimated to log Ks of 12.2 and 19.4 respectively.

$$\text{Log } K_{therm} = (0.85 - E^{1/2}_{(ML)})/0.09 \qquad \text{Equation 5.}$$

At deposition potentials below -1 V in the natural seawater sample, a decrease of the signal was often observed. It is unclear why such decrease is occurring.

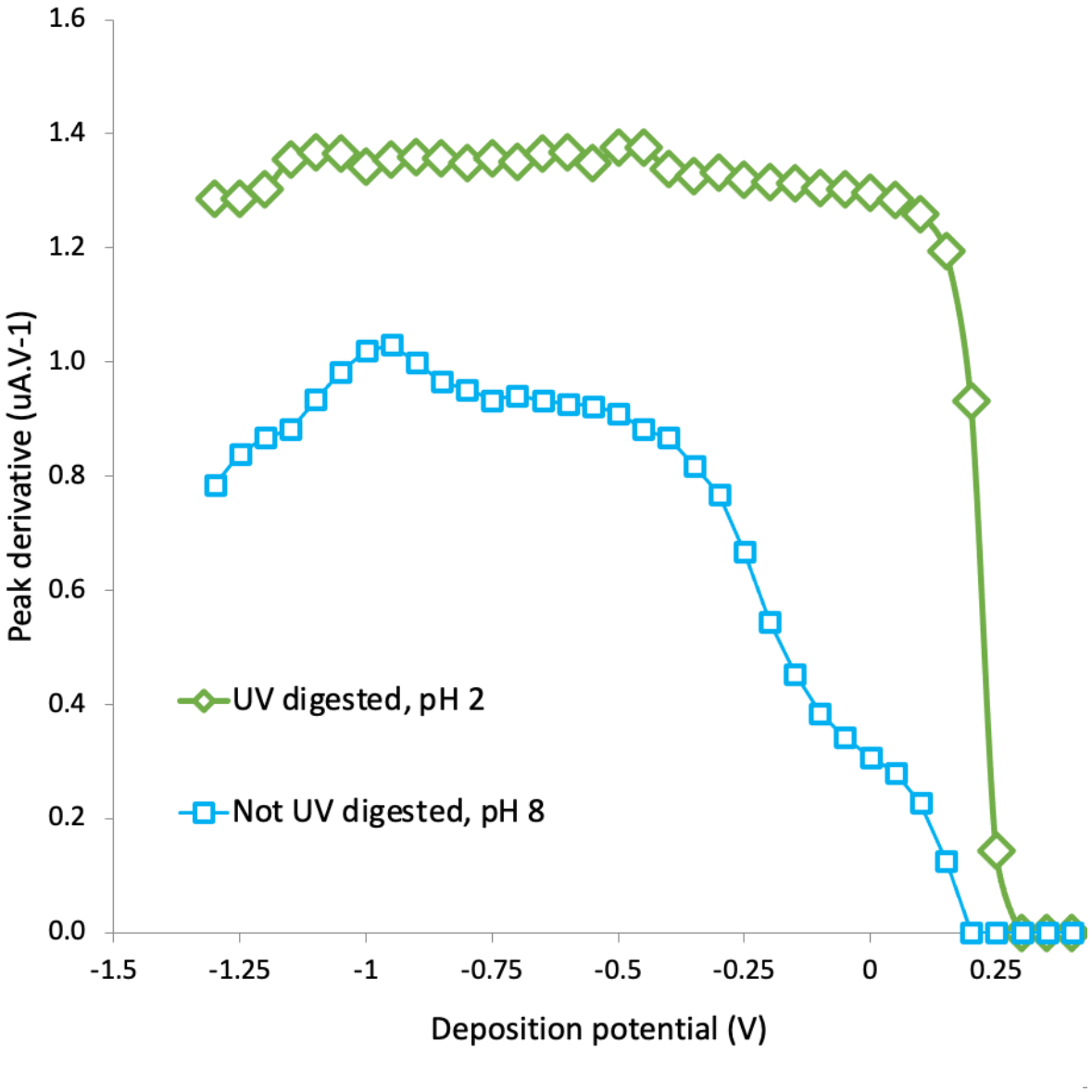

Figure A7*. Comparison of UV digested and non-UV digested Cu pseudopolarograms. The pH of UV digested seawater was 2 and the pH of non-UV digested seawater was 8. Water used was coastal seawater from Liverpool Bay. Each point represents the peak derivative of the Cu signal.*

A.3. References

Al-Farawati, R., van den Berg, C.M.G., 1997. The determination of sulfide in seawater by flow-analysis with voltammetric detection. Mar. Chem. 57, 277–286. https://doi.org/10.1016/S0304-4203(97)00014-5

Almgren, T., Hagström, I., 1974. The oxidation rate of sulphide in sea water. Water Res. 8, 395–400. https://doi.org/10.1016/0043-1354(74)90069-4

Avrahami, M., Golding, R.M., 1968. The oxidation of the sulphide ion at very low concentrations in

aqueous solutions. J. Chem. Soc. A Inorganic, Phys. Theor. 0. 647-651. https://doi.org/10.1039/J19680000647

Baars, O., Croot, P.L., 2011. The speciation of dissolved zinc in the Atlantic sector of the Southern Ocean. Deep. Res. Part II 58, 2720–2732. https://doi.org/10.1016/j.dsr2.2011.02.003

Bi, Z., Salaün, P., van den Berg, C.M.G., 2013a. Determination of lead and cadmium in seawater using a vibrating silver amalgam microwire electrode. Anal. Chim. Acta 769, 56–64. https://doi.org/10.1016/j.aca.2013.01.049

Bi, Z., Salaün, P., Van Den Berg, C.M.G., 2013b. The speciation of lead in seawater by pseudopolarography using a vibrating silver amalgam microwire electrode. Mar. Chem. 151, 1–12. https://doi.org/10.1016/j.marchem.2013.02.003

Croot, P.L., Moffett, J.W., Luther, G.W., 1999. Polarographic determination of half-wave potentials for copper-organic complexes in seawater. Mar. Chem. 67, 219–232. https://doi.org/10.1016/S0304-4203(99)00054-7

Deleon, E.R., Stoy, G.F., Olson, K.R., 2012. Passive loss of hydrogen sulfide in biological experiments. Anal. Biochem. 421, 203–207. https://doi.org/10.1016/j.ab.2011.10.016

Gibbon-Walsh, K., Salaün, P., van den Berg, C.M.G., 2012. Pseudopolarography of copper complexes in seawater using a vibrating gold microwire electrode. J. Phys. Chem. A 116, 6609–6620. https://doi.org/10.1021/jp3019155

Jia-zhong, Z., Whitfield, M., 1986. Kinetics of inorganic redos reaction in seawater: I. The reduction of iodate by bisulphide. Mar. Chem. 19. 2. 121-137. https://doi.org/10.1016/0304-4203(86)90044-7

Laglera, L.M., Downes, J., Tovar-Sánchez, A., Monticelli, D., 2014. Cathodic pseudopolarography: A new tool for the identification and quantification of cysteine, cystine and other low molecular weight thiols in seawater. Anal. Chim. Acta 836, 24–33. https://doi.org/10.1016/j.aca.2014.05.026

Laglera, L.M., Tovar-Sánchez, A., 2012. Direct recognition and quantification by voltammetry of thiol/thioamide mixes in seawater. Talanta 89, 496–504. https://doi.org/10.1016/j.talanta.2011.12.075

Laglera, L.M., van den Berg, C.M.G., 2003. Copper complexation by thiol compounds in estuarine waters. Mar. Chem. 82, 71–89. https://doi.org/10.1016/S0304-4203(03)00053-7

Lewis, B.L., Holt, P.D., Taylor, S.W., Wilhelm, S.W., Trick, C.G., Butler, A., Luther, G.W., 1995. Voltammetric estimation of iron (III) thermodynamic stability constants for catecholate siderophores isolated from marine bacteria and cyanobacteria. Mar. Chem. 50, 179–188. https://doi.org/10.1016/0304-4203(95)00034-O

Luther, G.W., Mullaugh, K.M., Hauser, E.J., Rader, K.J., Di Toro, D.M., 2021. Determination of ambient dissolved metal ligand complexation parameters via kinetics and pseudo-voltammetry experiments. Mar. Chem. 234. https://doi.org/10.1016/j.marchem.2021.103998

Millero, F.J., LeFerriere, A., Fernandez, M., Hubinger, S., Hershey, J.P., 1989. Oxidation of H2S with H2O2 in Natural Waters. Environ. Sci. Technol. 23, 209–213. https://doi.org/10.1021/es00179a012

Pernet-Coudrier, B., Waeles, M., Filella, M., Quentel, F., Riso, R.D., 2013. Simple and simultaneous determination of glutathione, thioacetamide and refractory organic matter in natural waters by DP-CSV. Sci. Total Environ. 463–464, 997–1005. https://doi.org/10.1016/j.scitotenv.2013.06.053

Rozan, T.F., Luther, G.W., Ridge, D., Robinson, S., 2003. Determination of Pb complexation in oxic and sulfidic waters using pseudovoltammetry. Environ. Sci. Technol. 37, 3845–3852. https://doi.org/10.1021/es034014r

Salaün, P., Van Den Berg, C.M.G., 2006. Voltammetric detection of mercury and copper in seawater using a gold microwire electrode. Anal. Chem. 78, 5052–5060. https://doi.org/10.1021/ac060231+

Tsang, J.J., Rozan, T.F., Hsu-Kim, H., Mullaugh, K.M., Luther, G.W., 2006. Pseudopolarographic determination of Cd2+ complexation in freshwater. Environ. Sci. Technol. 40, 5388–5394. https://doi.org/10.1021/es0525509

van den Berg, C., 2014. UV digestion apparatus. [WWW Document]. URL http://pcwww.liv.ac.uk/~sn35/Site/ UV_digestion_apparatus.html

van den Berg, C.M.G., 1982. Determination of copper complexation with natural organic ligands in seawater by equilibration with MnO2 II. Experimental procedures and application to surface seawater. Mar. Chem. 11, 323–342. https://doi.org/10.1016/0304-4203(82)90029-9

Zhang, J.-Z., Millero, F.J., 1993. The products from the oxidation of H2S in seawater. Geochim. Cosmochim. Acta 57, 1705–1718. https://doi.org/10.1016/0016-7037(93)90108-9

Zlamalova, M., Nesmerak, K., 2016. Recent Advances in Electrochemical Detection of Important Sulfhydryl- Recent advances in electrochemical detection of important sulfhydryl-containing compounds. Monatsh Chem 147, 1331–1338. https://doi.org/10.1007/s00706-016-1757-z